University of Bath

PHD

Development of a novel hollow fibre membrane for use as a tissue engineered bone graft scaffold

Ellis, Marianne Jane

Award date:
2005

Awarding institution:
University of Bath

Link to publication

General rights
Copyright and moral rights for the publications made accessible in the public portal are retained by the authors and/or other copyright owners and it is a condition of accessing publications that users recognise and abide by the legal requirements associated with these rights.

- Users may download and print one copy of any publication from the public portal for the purpose of private study or research.
- You may not further distribute the material or use it for any profit-making activity or commercial gain
- You may freely distribute the URL identifying the publication in the public portal ?

Take down policy
If you believe that this document breaches copyright please contact us providing details, and we will remove access to the work immediately and investigate your claim.

Download date: 13. May. 2019

DEVELOPMENT OF A NOVEL HOLLOW FIBRE MEMBRANE FOR USE AS A TISSUE ENGINEERED BONE GRAFT SCAFFOLD

Marianne Jane Ellis

A thesis submitted for the degree of Doctor of Philosophy

University of Bath

Department of Chemical Engineering

April 2005

COPYRIGHT

Attention is drawn to the fact that copyright of this thesis rests with its author. This copy of the thesis has been supplied on condition that anyone who consults it is understood to recognise that its copyright rests with its author and that no quotation from the thesis and no information derived from it may be published without the prior written consent of the author.

This thesis may be made available for consultation within the University Library and may be photocopied or lent to other libraries for the purposes of consultation.

UMI Number: U193731

All rights reserved

INFORMATION TO ALL USERS
The quality of this reproduction is dependent upon the quality of the copy submitted.

In the unlikely event that the author did not send a complete manuscript
and there are missing pages, these will be noted. Also, if material had to be removed,
a note will indicate the deletion.

UMI U193731
Published by ProQuest LLC 2013. Copyright in the Dissertation held by the Author.
Microform Edition © ProQuest LLC.
All rights reserved. This work is protected against
unauthorized copying under Title 17, United States Code.

ProQuest LLC
789 East Eisenhower Parkway
P.O. Box 1346
Ann Arbor, MI 48106-1346

UNIVERSITY OF ALBERTA
LIBRARY
75-4 AUG 2005
PL-D.

ABSTRACT

The most successful therapy for repairing bone defects is currently the autograft. Autografts have several disadvantages associated with their use including a limited availability per patient, donor site morbidity and deformity, and the graft itself can be resorbed before osteogenesis is complete. Production of a synthetic bone graft, using tissue engineering principles, to overcome these drawbacks would be a significant step forward for orthopaedic surgery.

The aim of this thesis was to develop a scaffold to address the mass transfer limitations of autografts and current synthetic scaffolds that are used for treating bone defects. A novel PLGA hollow fibre membrane scaffold was created using a poly(lactic-co-glycolic acid) - N-methyl pyrrolidinone -water (PLGA-NMP-water) system by immersion precipitation. NMP was selected as the solvent due to the resulting asymmetric macroporous structure of the membrane that had interconnecting finger-like pores. The entire range of PLGA containing the racemic mix of PLLA and PDLA was found to be soluble in NMP with PDLLA:PGA ratio 45:55 to 100:0. PLLA and PGA did not dissolve in NMP between 15-30°C, 10-40% (w/w). PLGA with the PLLA:PGA ratio of 75:25 (75L:25) was found to be soluble in NMP at 10% (w/w) across the temperature range tested. The hollow fibre membranes were spun using PDLLA:PGA ratios of 50:50 and 75:25 at 20 %(w/w) and 25 %(w/w) polymer concentrations, 0 mm and 30 mm air gaps, and 5.5 m/min and 7.7 m/min take-up rates. The structure was found to be optimal for use as a bone tissue engineering scaffold in the range of conditions tested when spun using a 20% (w/w) polymer solution with a zero air gap at a take up rate of 5.5 m/min. This resulted in a fibre with typical outer diameter of 700 μm and wall thickness of approximately 150 μm. The porous outer skin had pores of around 1 μm diameter for both 50:50 and 75:25. 50:50 was seen to have a relatively less dense outer skin at a given set of conditions. 70% ethanol was found to be a suitable sterilising agent, if not optimal due to its effect on the membrane morphology. It was also found that residual solvent could be reduced to 4 ppm after 7 days by soaking in water. The osteoblastic cell line 560pZIPv.neo (pZIP) and human bone derived cells (HBDC) were cultured on 100:0, 75:25, 50:50 and 75L:25 PLGA flat sheet membranes to assess the suitability of the membranes as a scaffold in comparison to tissue culture polystyrene (TCP). 75:25, 50:50 and 75L:25 were not significantly different to the TCP ($P<0.05$) for both cells types during a 6 hour attachment period, 100:0 had significantly fewer HBDC after 6 hours but showed a comparable number of pZIP. After the 7-day proliferation study, the four membranes showed a similar number of pZIP to the TCP. 50:50 and 75:25 had significantly lower HBDC compared to TCP. HBDC showed osteogenic function (alkaline phosphatase activity and mineralisation) on all membranes after 3 weeks, but significantly less compared to TCP. 75:25 hollow fibre membranes were bedded into a hollow fibre module and seeded with pZIP. An in situ rotating seeding method was used over a 6 hour period and was found to be 4 times more efficient that traditional static seeding. The number of pZIP was significantly lower compared to the TCP control following a counter current fed perfusion set up for 7 days. The work in this thesis has shown that the PLGA hollow fibre membrane scaffold has the potential to address the current problems associated with autologous bone grafts and traditional tissue engineered scaffolds.

ACKNOWLEDGEMENTS

I especially thank Professor Julian Chaudhuri whose ability to supervise with the perfect balance of guidance and freedom that allowed this project to develop. Thanks also to Dr Jon Beresford whose great ideas were priceless and to Karina and Julie, whose knowledge and expertise were invaluable. Thanks to Semali, Chin-Chih, and May Ling Yeow. I am also grateful to the members of the Tissue Engineering Group in Bath; Moreica, Marcus, Andy and Holly, and the enthusiasm of the undergraduates who have contributed to the work; the staff in the Department of Chemical Engineering especially Roger, Tony, Mac, Bob and Fernando; Ursula Potter, Hugh Perrott and Ann O'Reilly for the help with the electron-optic studies; Adrian Bowyer, Barry Chapman and Sue Wonnacott whose kindness in allowing me the use of their equipment was invaluable; Pete whose workshop skills allowed my designs to be realised.

I gratefully acknowledge the funding of this work by the EPSRC.

Infinite thanks to my Mum, Nana and Grandad who have always believed in my academic abilities which gave me the belief I can achieve whatever I put my efforts into; to Dad and Granny for their support and inspiration throughout. Thanks to Kate for listening and laughing and seeing me through the highs and lows, to Debbie, Nikki and Claire who remind me what's important in life, Beth and Justin for keeping my most treasured friend safe and well, Angharad who is the best tea-buddy, and to Riley who has kept me sane during the depths of writing up.

> *"Every day you may make progress. Every step may be fruitful. Yet there will stretch out before you an ever-lengthening, ever-ascending, ever-improving path. You know you will never get to the end of the journey. But this, so far from discouraging, only adds to the joy and glory of the climb."*
>
> **Sir Winston Churchill (1874 - 1965)**

TABLE OF CONTENTS

	Page
ABSTRACT	I
ACKNOWLEDGEMENTS	II
TABLE OF CONTENTS	III
LIST OF FIGURES	XII
LIST OF TABLES	XVIII
NOMENCLATURE	XXI
CHAPTER ONE: INTRODUCTION	**1**
1.1 THE NEED FOR BONE TISSUE ENGINEERING	1
1.2 AIM OF THE RESEARCH	2
1.3 OUTLINE OF THE THESIS	2
CHAPTER TWO: BONE REGENERATION USING A SYNTHETIC SCAFFOLD AND BIOREACTOR	**6**
2.1 INTRODUCTION	6
2.2 BONE BIOLOGY, DISEASES AND TREATMENTS	6
2.2.1 Biology of Bone	6
2.2.2 Osteogenesis, Disease and Regeneration	15
2.3 STATUS OF BONE TISSUE ENGINEERING	17
2.3.1 Cell Types and Sources	17
2.3.2 Media and Growth Factors for In Vitro Culture of Bone Cells	18
2.3.3 Culture Substrates and Scaffolds	18

2.3.4 Culture Systems and Bioreactors 33

2.4 NEW SOLUTIONS FOR BONE TISSUE ENGINEERING USING MEMBRANE TECHNOLOGY 41

2.4.1 Properties of Membranes 41

2.4.2 Membrane Synthesis and Manufacture 42

2.4.3 Membrane Characterisation 46

2.4.4 Membrane Bioreactor Configurations for Tissue Engineering 46

2.4.5 Membrane Bioreactor Configuration for Bone Tissue Engineering 48

2.7 CONCLUSIONS 50

2.8 AIM & OBJECTIVES 51

CHAPTER THREE: MATERIALS & METHODS 52

3.1 INTRODUCTION 52

3.2 MATERIALS 52

3.2.1 Materials Supplier Listings 52

3.2.2 Source of Cells 56

3.3 EXPERIMENTAL METHODS 56

3.3.1 Obtaining Human Bone Derived Cells from Bone Reamings 56

3.3.2 Freezing Down and Raising Cells from Cryostorage 57

3.3.3 Cell Culture and Maintenance 57

3.3.4 Cell Culture on Flat Sheet Membranes 58

3.3.5 Cell Culture on Hollow Fibre Membranes 58

3.3.6 Membrane Preparation 59

3.4 CULTURE SYSTEM & BIOREACTOR DESIGN AND MANUFACTURE 61
3.4.1 Flat Sheet Membrane Culture Chamber Design and Manufacture 61
3.4.2 Hollow Fibre Bioreactor Design and Manufacture 64

3.5 ANALYTICAL METHODS 65
3.5.1 Cell Number 65
3.5.2 Cell Morphology 67
3.5.3 Mineralisation and Alkaline Phosphatase Activity 67
3.5.4 Polymer Solution Characterisation 68
3.5.6 Membrane Characterisation 68

3.6 STATISTICAL METHODS 70
3.6.1 Data Representation 70
3.6.2 Comparative Statistics 70

CHAPTER FOUR: PLGA MEMBRANE SCAFFOLD DESIGN I-FLAT SHEETS 71

4.1 INTRODUCTION 71
4.1.1 Selecting the Ternary System Components for Phase Inversion Membrane Casting 72
4.1.2 Properties of Casting Dopes 73
4.1.3 Structural Properties of Membrane Scaffolds 74

4.2 RESULTS 74
4.2.1 Polymer-Solvent Selection 74
4.2.2 PLGA Flat Sheet Membrane Fabrication 86

4.3 DISCUSSION 93
4.3.1 Solubility 94
4.3.2 Viscosity 94
4.3.3 Morphology 96

4.4 CONCLUSIONS 98

CHAPTER FIVE: PLGA MEMBRANE SCAFFOLD DESIGN II-HOLLOW FIBRES **100**

5.1 INTRODUCTION 100
5.1.1 Polymer Concentration in the Spinning Dope and its Effect on Fibre Characteristics 101
5.1.2 Air Gap and its Effect on Fibre Characteristics 101
5.1.3 Take-Up Rate and its Effect on Fibre Characteristics 102
5.1.4 Fibre Characteristics and the Relation to Their Use as a Scaffold 102

5.2 RESULTS 103
5.2.1 Effect of Polymer Solution Concentration on Hollow Fibre Structure 103
5.2.2 Effect of Air Gap on Hollow Fibre Structure 108
5.2.3 Effect of Take-Up Rate on Hollow Fibre Structure 114
5.2.4 Hollow Fibre Characterisation 119

5.3 DISCUSSION 120
5.3.1 Polymer Solution Concentration 120
5.3.2 Air Gap 121
5.3.3 Take-Up Rate 122
5.3.4 Hollow Fibre Characterisation 123

5.4 CONCLUSIONS 123

CHAPTER SIX: MEMBRANE SURFACE TREATMENT AND MODIFICATION FOR CELL CULTURE 125

6.1 INTRODUCTION 125
6.1.1 Solvent Removal From Scaffolds 125
6.1.2 Degradation of PLGA Scaffolds 126
6.1.3 Sterilising Scaffolds For Cell Culture 127
6.1.4 Affect of Fixatives and Lysing Agents on PLGA Scaffolds 128
6.1.5 Surface Modification of PLGA Membrane Scaffolds 128

6.2 RESULTS 129
6.2.1 Solvent Removal 129
6.2.2 Degradation of PLGA Membranes in Cell Culture Media 131
6.2.2 Effect of Sterilisation Agents on PLGA Flat Sheet and Hollow Fibre Membranes 135
6.2.3 Effect of Fixing and Lysing Agents on PLGA Membranes 141
6.2.4 Surface Modification of PLGA Membranes 148

6.3 DISCUSSION 149
6.3.1 Solvent Removal 150
6.3.2 Degradation 151
6.3.3 Sterilisation 152
6.3.4 Fixing and Lysing 153
6.3.5 Surface Modification 154

6.5 CONCLUSIONS 154

CHAPTER SEVEN: HUMAN BONE DERIVED CELLS AND CELL LINE CULTURE ON PLGA FLAT SHEET MEMBRANE SCAFFOLDS **156**

7.1 INTRODUCTION 156
7.1.1 Cell Attachment 156
7.1.2 Cell Proliferation 157
7.1.3 Cell Function 158

7.2 RESULTS 159
7.2.1 Osteoblast Cell Line Attachment and Proliferation on PLGA Membranes 159
7.2.2 HBDC Attachment, Proliferation and Function on PLGA Membranes 166

7.3 DISCUSSION 174
7.3.1 Attachment 175
7.3.2 Proliferation 177
7.3.3 HBDC Function 178

7.4 CONCLUSIONS 179

CHAPTER EIGHT: CELL CULTURE IN A PLGA HOLLOW FIBRE BIOREACTOR **181**

8.1 INTRODUCTION 181
8.1.1 The Rationale of Selecting a Hollow Fibre Membrane Bioreactor Configuration for Bone Tissue Engineering 181
8.1.2 Seeding Methods of Hollow Fibre Bioreactors 182
8.1.3 Cell Numbers in Hollow Fibre Bioreactors Compared to Traditional Systems 183

8.2 PLGA HOLLOW FIBRE BIOREACTOR DESIGN AND OPERATION 183
8.2.1 Module Design and Preparation 183
8.2.2 Bioreactor System Design 184

8.3 RESULTS 185
8.3.1 Seeding and Six-Hour Attachment of 560pZIPv.neo to PLGA Hollow Fibre Membranes in the Hollow Fibre Bioreactor 185
8.3.2 Proliferation of 560pZIPv.neo on PLGA Hollow Fibre Membranes in the Hollow Fibre Bioreactor 189

8.4 DISCUSSION 190
8.4.1 Seeding 191
8.4.2 Proliferation 191

8.5 CONCLUSIONS 193

CHAPTER NINE: CONCLUSIONS AND FUTURE WORK 194

9.1 INTRODUCTION 194

9.2 CONCLUSIONS 194

9.3 IMPLICATIONS OF THE FINDINGS ON BONE TISSUE ENGINEERING 198

9.4 FUTURE WORK 200
9.4.1 Short Term 200
9.4.2 Long Term 202

REFERENCES **205**

APPENDIX A: REAGENT PREPARATION **236**

A.1 MEDIA REAGENTS 236

A.2 PASSAGING REAGENTS 241

A.3 ANALYSIS REAGENTS 242

A.4 MEDIA PREPARATION 247

A.5 SIMULATED BODY FLUID PREPARATION 248

APPENDIX B: EQUIPMENT AND CONSUMABLES **249**

APPENDIX C: DEVELOPMENT OF CELL CULTURE AND ANALYSIS METHODS **253**

C.1 PICOGREEN ASSAY BUFFER SELECTION 253

C.2 QUANTITATIVE CELL NUMBER ASSAY SELECTION 255

C.3 ATTACHMENT KINETICS 258

C.4 CELL MORPHOLOGY STAIN SELECTION 260

APPENDIX D: PHYSICAL PROPERTIES OF POLYMERS AND SOLVENTS **262**

D.1 SOLVENT PROPERTIES 262

D.2 POLYMER PROPERTIES 264

APPENDIX E: CALIBRATION DATA **266**

E.1 CALIBRATIONS FOR HOLLOW FIBRE SPINNING 266
E.1.1 Take-Up Rate 266
E.1.2 Polymer Solution Flow Rate 269
E.1.3 Bore Flow Rate 272
E.1.4 Air Gap Residence Time 272

E.2 OTHER CALIBRATIONS 276

APPENDIX F: SAMPLE RAW DATA AND RELATED CALCULATIONS **281**

F.1 EXAMPLE OF VISCOSITY RAW DATA 281

F.2 SAMPLE CALCULATION FOR THE PICOGREEN ASSAY 283

F.3 EXAMPLE STATISTICS 286

F.4 MEAN PORE SIZE CALCULATION METHOD 287

LIST OF FIGURES

Figure	Title	Page
Figure 1.1	Summary of the work carried out in each of the results chapters.	5
Figure 2.1	The structure of bone.	7
Figure 2.2	The structure of cortical bone.	8
Figure 2.3	Sketch of an osteoclast degrading mineralised bone.	9
Figure 2.4	Postulated steps in the osteoblast lineage implying recognisable stages of differentiation.	9
Figure 2.5	Partially resorbed extracellular matrix.	10
Figure 2.6	Sketch of a cross-section of an osteon showing areas of bone fluid.	11
Figure 2.7	Blood supply of a long bone.	12
Figure 2.8	Different stress-strain curve configurations for cortical bone depending on loading.	13
Figure 2.9	Frost's mechanostat theory.	14
Figure 2.10	Endochonral bone formation.	16
Figure 2.11	Phase inversion scaffolds used for bone tissue engineering.	25
Figure 2.12	A tubular scaffold prepared from the poly(phosphoester) P(BHET-EOP/TC) using dipcoating.	26
Figure 2.13	Tubular scaffolds prepared from X using injection moulding.	27
Figure 2.14	A range of glass-ceramic products currently in orthopaedic clinical use.	28
Figure 2.15	Hydroxyapatite scaffold macro-architectures.	29
Figure 2.16	Apatite coating on various materials.	30
Figure 2.17	A composite scaffold; PLGA coated gelatin.	31
Figure 2.18	Flat bed bioreactors.	36
Figure 2.19	A Traditional stirred tank for cell culture-the Stirrer Flask.	36
Figure 2.20	Rotating wall bioreactors.	37
Figure 2.21	Schematic drawing of a packed bed bioreactor.	38
Figure 2.22	A bone tissue engineering-specific 'Flow Perfusion Bioreactor System' which uses 6 parallel packed beds.	39
Figure 2.23	Oscillating perfusion bioreactor.	40

Figure 2.24	Schematic drawing of a fluidised bed bioreactor.	41
Figure 2.25	Binary mixture phase diagram.	43
Figure 2.26	Ternary system phase diagram.	44
Figure 2.27	Schematic of a spiral-wound membrane module.	47
Figure 3.1	Spinning set up.	60
Figure 3.2	Nucleation (left) and growth (right) of apatite on organic polymer substrate.	61
Figure 3.3	Photograph of flat sheet membrane culture chamber.	62
Figure 3.4	Engineering drawings of flat sheet membrane culture chamber.	63
Figure 3.5	Schematic of PLGA hollow fibre bioreactor.	64
Figure 3.6	Photograph of hollow fibre membrane bioreactor.	65
Figure 4.1	Viscosity profiles of PLGA polymers dissolved in NMP at different concentrations and temperatures.	80
Figure 4.2	Detail of viscosity profiles of PLGA polymers dissolved in NMP at different concentrations and temperatures.	81
Figure 4.3	Viscosity profiles of PLGA polymers dissolved in dioxane at different concentrations and temperatures.	83
Figure 4.4	Detail of viscosity profiles of PLGA polymers dissolved in dioxane at different concentrations and temperatures.	84
Figure 4.5	Spinning dope profiles for 75:25 and 75L:25 in the temperature range 20°C - 30°C.	85
Figure 4.6	Top surface of flat sheet membranes cast using NMP.	88
Figure 4.7	Bottom surface of flat sheet membranes cast using NMP.	89
Figure 4.8	Top surface of flat sheet membranes cast using dioxane.	90
Figure 4.9	Bottom of flat sheet membranes cast using dioxane.	91
Figure 4.10	Cross-section of flat sheet membranes cast using NMP.	92
Figure 4.11	Cross-section of flat sheet membranes cast using dioxane.	93
Figure 5.1	Cross-section of hollow fibre membranes at different polymer concentrations.	104
Figure 5.2	Outer edge of cross-section of hollow fibre membranes at different polymer concentrations.	105
Figure 5.3	Inner edge of cross-section of hollow fibre membranes at different polymer concentrations.	106

Figure 5.4	Outer surface of hollow fibre membranes at different polymer concentrations.	107
Figure 5.5	Inner surface of hollow fibre membranes at different polymer concentrations.	108
Figure 5.6	Cross-section of hollow fibre membranes at different air gaps.	109
Figure 5.7	Outer edges of the hollow fibre membranes at different air gaps.	111
Figure 5.8	Inner edges of the hollow fibre membranes at different air gaps.	112
Figure 5.9	Outer surface of hollow fibre membranes at different air gaps.	113
Figure 5.10	Inner surface of hollow fibre membranes at different air gaps.	114
Figure 5.11	Cross-section of hollow fibre membranes at different take up rates.	115
Figure 5.12	Outer edge of cross-section of hollow fibre membranes at different take up rates.	116
Figure 5.13	Inner edge of cross-section of hollow fibre membranes at different take up rates.	117
Figure 5.14	Outer surface of hollow fibre membranes at different take up rates.	118
Figure 5.15	Inner surface of hollow fibre membranes at different take up rates.	119
Figure 6.1	75:25 flat sheet membrane surface immediately after precipitation.	130
Figure 6.2	75:25 flat sheet membrane after 1 week in water, post-fabrication.	130
Figure 6.3	NMP removal from the 75:25 flat sheet membrane.	131
Figure 6.4	Surface images of flat sheet membranes maintained in media at 15°C (A-D) and 37°C (E-H).	133
Figure 6.5	Average surface roughness of 75:25 flat sheet membrane maintained in media over 26 days.	134
Figure 6.6	Maximum surface roughness of 75:25 flat sheet membrane maintained in media over 26 days.	134
Figure 6.7	Cumulative generation of lactic and glycolic acid in the media in which the 75:25 flat sheet membranes were maintained.	135

Figure 6.8	Top surface of flat sheet membranes after 30min in 70% ethanol.	137
Figure 6.9	Top surface of untreated flat sheet membranes.	138
Figure 6.10	Bottom surface of flat sheet membranes after 30min in 70% ethanol.	139
Figure 6.11	Comparison of untreated PLGA hollow fibres and 70% ethanol treated hollow fibres.	140
Figure 6.12	Chart showing normalised surface area of PLGA flat sheet membranes after sterilising with ethanol.	141
Figure 6.13	Chart showing normalised thickness of PLGA flat sheet membranes after sterilising with ethanol.	141
Figure 6.14	Top surface of flat sheet membranes after 15min in NBF.	143
Figure 6.15	Bottom surface of flat sheet membranes after 15min in NBF.	144
Figure 6.16	Top surface of flat sheet membranes after 10min in 90% ethanol.	145
Figure 6.17	Bottom surface of flat sheet membranes after 10min in 90% ethanol.	146
Figure 6.18	Chart showing normalised surface area of PLGA flat sheet membranes after exposure to fixing agents.	147
Figure 6.19	Chart showing normalised thickness of PLGA flat sheet membranes after exposure to fixing agents.	148
Figure 6.20	Hydroxyapatite coating of 75:25 hollow fibres at different time points during the growth phase.	149
Figure 7.1	Schematic illustration of receptors in the cell plasma membrane that link to the cytoskeleton for force transmission.	157
Figure 7.2	Normalised number of 560pZIPv.neo attached to PLGA membranes 6h post-seeding.	160
Figure 7.3	Distribution of 560pZIPv.neo attached to PLGA membranes 6h post-seeding.	161
Figure 7.4	Morphology of 560pZIPv.neo attached to PLGA membranes 6h post-seeding.	162
Figure 7.5	Number of 560pZIPv.neo on PLGA membranes 1 week post-seeding.	163

Figure 7.6	Distribution of 560pZIPv.neo cultured on PLGA membranes 1 week post-seeding.	164
Figure 7.7	Morphology of 560pZIPv.neo cultured on PLGA membranes 1 week post-seeding.	165
Figure 7.8	Number of HBDC attached to PLGA membranes 6h post-seeding.	166
Figure 7.9	Distribution of HBDC attached to PLGA membranes 6h post-seeding.	168
Figure 7.10	Morphology of HBDC attached to PLGA membranes 6h post-seeding.	169
Figure 7.11	Number of HBDC on PLGA membranes 1 week post-seeding.	170
Figure 7.12	Distribution of HBDC cultured on PLGA membranes 1 week post-seeding.	171
Figure 7.13	Morphology of HBDC cultured on PLGA membranes 1 week post-seeding.	172
Figure 7.14	Typical morphology of mineralised nodule.	173
Figure 7.15	Mineralisation of extra cellular matrix laid down by HBDC after 21 days in culture.	174
Figure 8.1	Schematic diagram of different potting-gaskets used.	184
Figure 8.2	Hollow fibre bioreactor set up for the proliferation of 560pZIPsv.neo on PLGA hollow fibre membranes.	185
Figure 8.3	Schematic of the method used to seed the PLGA hollow fibre membrane bioreactor	186
Figure 8.4	560pZIPsv.neo attached to PLGA membranes 6h post-seeding.	187
Figure 8.5	Normalised number of 560pZIPsv.neo attached to PLGA hollow fibre membranes 6h post-seeding in the hollow fibre bioreactor.	188
Figure 8.6	Normalised number of 560pZIPsv.neo attached to PLGA hollow fibre membranes 7 days post-seeding in the hollow fibre bioreactor.	190
Figure 9.1	Future Work model for the clinical application of the PLGA hollow fibre membrane bioreactor system.	204
Figure C.1	Comparison of buffers for the picogreen assay.	254

Figure C.2	Comparison of cell number quantitative assays.	256
Figure C.3	Attachment kinetics of the osteoblast cell line 560pMT1.	259
Figure C.4	Comparison of haematoxylin and methylene blue stains for morphology visualisation.	261
Figure E.1	Schematic of the take up reel showing the diameter (d_r).	266
Figure E.2	Calibration graph for spinning rate based on take up rate.	268
Figure E.3	Schematic of spinneret showing dimensions of diameter of exit port (d_o)and bore needle (d_n).	269
Figure E.4	Calibration graph for polymer flow rate based on take up rate.	271
Figure E.5	Calibration graph for bore flow rate of water as a function of bore setting.	274
Figure E.6	Calibration graph for air gap residence time as a function of take up rate.	275
Figure E.7	Calibration chart for peristaltic pump used in the bioreactor system.	277
Figure E.8	Calibration chart for HPLC for NMP concentration.	278
Figure E.9	Calibration chart for HPLC for the degradation of 75:25 in media.	279
Figure E.10	Calibration chart for Picogreen assay using ATM buffer.	280
Figure F.1	Rheometer readings for 10% 7525DL in NMP.	282
Figure F.2	Graph of normalised HBDC cell number for different polymers.	285
Figure F.3	Plot of gas permeability versus mean pressure.	291

LIST OF TABLES

Table	Title	Page
Table 2.1	Mean values for human bone material parameters.	13
Table 2.2	Cell types commonly used in bone tissue engineering.	19
Table 2.3	Growth factors for bone culture.	20
Table 2.4	Scaffold materials and their common macro-architectures and dimensions.	21
Table 2.5	Scaffold materials and their structures.	23
Table 2.6	Properties of culture systems.	34
Table 2.7	Size classification of tubular membranes.	47
Table 2.8	Adherent-dependent cell microenvironments utilized in hollow fibre bioreactors.	49
Table 2.9	Common design considerations for membrane bioreactors.	50
Table 3.1	Alphabetical list of materials used for cell culture.	52
Table 3.2	Alphabetical list of materials used for cell culture analysis.	53
Table 3.3	Alphabetical list of materials used for scaffold preparation, modification and analysis.	54
Table 3.4	Alphabetical list of flat sheet membrane culture chamber and hollow fibre bioreactor components.	55
Table 3.5	Concentrations and volumes of solutions for the picogreen assay standards.	67
Table 3.6	Parameter settings for HPLC analysis.	69
Table 4.1	Properties of solvents commonly used in scaffold preparation.	73
Table 4.2	Solubility of various PLGA polymers in NMP at different temperatures and polymer concentrations.	76
Table 4.3	Solubility of various PLGA polymers in dioxane at different temperatures and polymer concentrations.	77
Table 4.4	Minimum and maximum pore sizes of the top surface of polymer-NMP flat sheet membranes.	87
Table 4.5	Minimum and maximum pore sizes of the top surface of polymer-dioxane flat sheet membranes.	90

Table 5.1	Mean pore diameter and effective surface porosity.	120
Table 6.1	Roughness values of 75:25 flat sheet membranes at the start and end point of solvent removal studies.	130
Table 6.2	Minimum and maximum pore sizes of the top surface of polymer-NMP flat sheet membranes untreated and sterilised in 70% ethanol.	136
Table 6.3	Minimum and maximum pore sizes of the top surface of polymer-NMP flat sheet membranes untreated and fixed in 90% ethanol.	142
Table 7.1	Alkaline phosphatase activity shown by extent of fast red staining.	174
Table 8.1	Number of cells added to the bioreactor at t = 0 h and the number of cells removed from the bioreactor at t = 6 h.	188
Table 8.2	Cell concentrations in the PLGA hollow fibre membrane bioreactor after a 7-day culture period.	190
Table A.1	Preparation of 100 ml human bone derived cell media.	247
Table A.2	Preparation of 100 ml 560PMT1 media.	247
Table A.3	Preparation of 100 ml 560PzipU19 media.	248
Table A.4	Preparation of '1SBF' for the apatite coating nucleation phase.	248
Table A.5	Preparation of '1.5SBF' for the apatite coating growth phase.	248
Table B.1	Consumables used during project.	249
Table B.2	Equipment used in project.	251
Table D.1	Physical properties of selected solvents.	262
Table D.2	Polymers and their specifications used in this work.	264
Table D.3	PLGA-NMP solution concentration ranges suitable for spinning at various temperatures.	264
Table D.4	PLGA-dioxane solution concentration ranges suitable for spinning at various temperatures.	265
Table E.1	Rotational take-up rate and corresponding linear take-up rate.	267
Table E.2	Polymer solution flow rate as a function of take-up a rate and spinning rate.	270
Table E.3	Bore liquid pump settings and corresponding bore flow rates for water.	272

Table E.4	Air gap residence times as a function of spinning rates at a selection of different air gaps.	273
Table E.5	Calibration data for peristaltic pumps.	276
Table E.6	Calibration data for HPLC degradation readings.	276
Table E.7	Calibration data for HPLC NMP release readings.	276
Table E.8	Calibration data for picogreen assay.	276
Table F.1	Raw data for 20% 75:25 in NMP.	281
Table F.2	Fluorospectrometer readings for the seeded membranes.	283
Table F.3	Fluorospectrometer readings for the unseeded membranes.	283
Table F.4	Fluorospectrometer readings for the unseeded membranes.	283
Table F.5	Cell number calculations.	284
Table F.6	Descriptives for the normalized cell numbers.	286
Table F.7	Multiple Comparisons for the Dependent Variable, the normalised cell number using Tukey post hoc tests.	286
Table F.8	Conversions and constants used in the calculation of the mean pore size and effective surface porosity.	287
Table F.9	Raw data and mean volumetric gas flow rate.	287
Table F.10	Mean molar flow rate.	288
Table F.11	Surface area for permeation.	289
Table F.12	Gas permeability.	289
Table F.13	Mean pressure.	290
Table F.14	The gradient and intercept.	291
Table F.15	Mean pore diameter of fibre.	292
Table F.16	Effective porosity of fibre.	292

NOMENCLATURE

NOMENCLATURE

ABBREVIATION	*FULL NAME*
1°	Primary
2D	Two-dimensional
3D	Three-dimensional
A	Area
AFM	Atomic force microscope
ALP	Alkaline phosphatase
ANOVA	Analysis of variants
ATM	Alkaline buffer solution/ Triton X-100 /MilliQ water
BGA	Blood gas analyser
CFU-f	Colony forming unit-fibroblasts
CO_2	Carbon dioxide
d	Diameter
d-	Dexorotary stereo isomer
d,l-	Racemic mix of the levorotary and dexorotary stereo isomers
dioxane	1,4-dioxane
DMEM	Dulbecco's modified Eagle's medium
DMSO	Dimethyl sulphoxide
DNA	Deoxyribonucleic acid
Dx	Dexamethasone
EDTA	Ethylenediamine tetra-acetic acid
EDX	Energy dispersive X-ray
EtOH	Ethanol
FCS	Foetal calf serum
g	Acceleration due to gravity
HA	Hydroxyapatite
HAPEX	Hydroxyapatite-reinforced high-density polyethylene
HBDC	Human bone derived cells

HPLC	High performance liquid chromatography
IGF-I	Insulin like growth factors-1
J	Gas permeability
l-	Levorotary stereo isomer
L_p	Effective pore length
Max	Maximum
MESm	Minimum effective strain causing matrix deposition and bone formation
MESr	Maximum effective strain causing bone resorption
Min	Minimum
M_{N2}	Molecular mass of nitrogen
MSC	Mesenchymal stem cells
MTT	Thiazol blue (3-[4,5-dimethyl-2-yl]-2,5-diphenyltetrazolium bromide)
n	Number of samples (statistics)
n	Number of mols
NASA	National Aeronautical and Space Administration
NBF	Neutral buffered formalin
NEAA	Non-essential amino acids
NMP	N-methyl pyrrolidinone
NSTM	N-succinimidyl tartrate monoamine
P	Probability
P	Pressure
P/S	Penicillin/streptomycin solution
PBS	Phosphate buffered saline
PCL	Polycaprolactone
PDLLA	Poly-d,l-lactic acid
PE	polyethylene
PET	Poly(ethylene glycol)
PGA	Poly(glycolic acid)
PLA	Poly(lactic acid)
PLGA	Poly(lactic-co-glycolic acid)
PLLA	Poly-l-lactic acid

PLL-g-PLGA	poly(L-lysine)-with grafting chains of-poly(D,L- lactic-co-glycolic acid)
PPF	poly(propylene fumerate)
PTFE	polytetrafluoroethylene
PVA	Poly vinyl acetate
PVDF	polyvinylidene fluoride
Pzip	560pZIPv.neo
r	Radius
R	Universal gas constant
RGD	Arginine-glycine-aspartic acid amino acid sequence
RNAse	Ribonuclease
ROBS	Rotating oxygen-permeable bioreactor system
rpm	Revolutions per minute
RWB	Rotating wall bioreactor
SBF	Simulated body fluid
SD	Standard deviation
SEM	Scanning electron microscope
T	Temperature
TCP	Tissue culture polystyrene
TE	Tris-HCl/ EDTA
TGF-β	Transforming growth factor-β
Ti	Titanium
TIPS	Thermally induced phase separation
UV	Ultra-violet light
v	Volume
V	Volumetric flowrate
VP	Vinylpyrrolidone
w	Weight
XRD	X-ray diffraction
β-GP	β-glycerophosphate

SYMBOLS

SYMBOL	*DEFINITION*
Φ	Concentration
ε	Porosity/Strain
μ	Viscosity
π	Pi
ρ	Density
ω	Angular velocity

SUBSCRIPT

SYMBOL	*DEFINITION*
0	Time = 0
A	Absolute
c	Critical
i	Instantaneous (velocity)
m	Mean
o	Terminal (velocity)
t	Time = t

CHAPTER ONE
INTRODUCTION

1.1 THE NEED FOR BONE TISSUE ENGINEERING

The ability to aid the regeneration of bone by using tissue engineering principles to prepare a synthetic bone graft in vitro would help to treat problems such as trauma injuries, osteoporosis, arthritis and bone cancers (Porter *et al.* 2000; Rose and Oreffo 2002). An increasing ageing population means degenerative diseases are becoming more common, in addition to work and recreation related injuries. In the mean time fractures occur frequently in the elderly, often resulting in loss of function or replacement. The present cost of skeletal defects is high both to the patient and the medical institutions (Rose and Oreffo 2002). In the UK there are around 50,000 hip replacements, costing £250 million a year, up to half of which will need revision (Green *et al.* 2002). The USA recorded around 280,000 hip fractures, 700,000 vertebral fractures and 250,000 Colle's fractures in 2000, costing $10billion (Hollinger *et al.* 2000). Vertebral and Colle's fractures usually lead to a loss of normal function, particularly in the elderly whose bone has lost the ability to regenerate normally. Surgery for trauma injuries often involves fixation with stainless steel implants. Due to the rigidity of the stainless steel, the bone is not loaded sufficiently during the healing process and has a tendency to fracture when the implant is removed (Middleton and Tipton 2000). If the implant is not removed, in time it can become loose or irritate the surrounding tissue to an extent function is only partially restored, particularly to the extent required by an athlete. Such patients are often discharged, the surgery deemed a success due to the state of the injury site being 'suitable for every day use'. A severe fracture may reduce the range of use of a joint and weaken the affected limb such that the patient is prevented from returning to a physical job such as manual labour or elite sport. Since the first approved biodegradable sutures in the 1960's, orthopaedic devices made out of biodegradable polymers have been used. These have a number of advantages over the stainless steel devices; a second surgical operation is not required for removal, they can be tailored to degrade at a rate to allow the transfer of load to the healing bone, they can be used

to deliver drugs to aid the healing process (Middleton and Tipton 2000). It may be necessary to use a bone graft for cases where the defect is of a critical size across which the tissue cannot heal itself. Autografts from the patients femur are the most common graft but this secondary operation can result in problems including donor site morbidity and deformity, and there is a limited supply per patient (Kokubo *et al.* 2003a). In large defects the bone may be resorbed before osteogenesis is complete, and since the graft is avascular it is diffusion dependent so the size of the defect and its location can limit their application (Burg *et al.* 2000). There is also a chance that even if the operation is successful, the treated area will not return to its original healthy state and need further attention, and that the donor site takes longer to heal than the injury site (Eddy 2004).

1.2 AIM OF THE RESEARCH

In 1993, Langer and Vacanti defined tissue engineering as "an interdisciplinary field that applies the principles of engineering and life sciences toward the development of biological substitutes that restore, maintain or improve tissue or organ function" (Langer and Vacanti 1993) and it is the ultimate aim of this research to use these tissue engineering principles to address the shortcomings associated with the use of bone grafts. Through combining cell biology, materials science and chemical engineering principles, this thesis presents a novel PLGA hollow fibre scaffold to support bone cell culture in a 3D structure that allows good mass transfer throughout the construct. The scaffold was specifically designed for use in a hollow fibre bioreactor. The scaffold structure is such that it has the potential to form large constructs that will give better tissue regeneration than autografts, allowing angiogenesis throughout the structure leading to complete regeneration of bone once implanted.

1.3 OUTLINE OF THE THESIS

This thesis is divided into nine chapters, including this chapter, which presents the need for the research carried out in this thesis as well as a general thesis overview.

Chapter Two reviews the literature on bone tissue engineering to date. Some bone biology is given to show what the bone tissue engineer is working towards, along with current scaffold materials and structure, and bioreactors that have been utilised in the field. There is also an explanation of the phase inversion process, which was used in the project to fabricate the membrane scaffolds. At the end of Chapter Two, the aims and objectives of the research are laid out. Chapter Three is the Materials and Methods and details the reagents and techniques used to carried out the research. Chapters Four to Eight detail the results, each chapter presenting a discussion on those results. Figure 1.1 summarises the work carried out in these chapters.

Chapters Four and Five are concerned with the fabrication and characterisation of the PLGA hollow fibre membrane scaffold. Chapter Four investigates the most appropriate solvent but considering the viscosity of the polymer-solvent solutions and the pore structure. Chapter Five investigates the fabrication of PLGA hollow fibre membranes and the effect of the spinning conditions on the resulting structure, with the aim of selecting the most appropriate conditions to give the best scaffold structure.

Chapter Six assesses the effect of the methods used to process the scaffold prior to and post-culture. This chapter was written using contributions from student projects, the names of who are mentioned where appropriate. The effects of the sterilisation, fixing and lysing agents on scaffold structure are investigated. In addition to these treatments, solvent removal and degradation are assessed using high performance liquid chromatography (HPLC) analysis and the effects on topography are also analysed, using atomic force microscopy (ATM) (Tingting Yue). The ability for a scaffold surface to be modified with bioactive ceramics is recognised as a potential method to improve osseointegration because they spontaneously bind to bone hydroxyapatite (Kokubo *et al.* 2003b). Kokubo's method for hydroxyapatite coating of the PLGA hollow fibres is also investigated (Eduardo Hernandez).

Chapters Seven and Eight take the PLGA membrane scaffolds selected based on the results in Chapters Four and Five and culture an osteoblastic cell line and human bone derived cells (HBDC) to assess the ability of the membranes to support bone cell cultures. Chapter Seven investigates different PLA:PGA ratios and their effect

on attachment and proliferation of the osteoblastic cell line and human bone derived cells, and osteoblastic function of the HBDC. Based on these results, Chapter Eight assesses an in situ seeding method for the hollow fibre bioreactors and its ability to support a bone-like cell culture on the PLGA hollow fibre membranes.

Chapter Nine summarises the findings of the results chapters, links these findings to each other and suggests the future work to take the PLGA hollow fibre membrane towards a clinically viable synthetic bone graft. By considering the results as a whole, the implications on the field of bone tissue engineering are also presented.

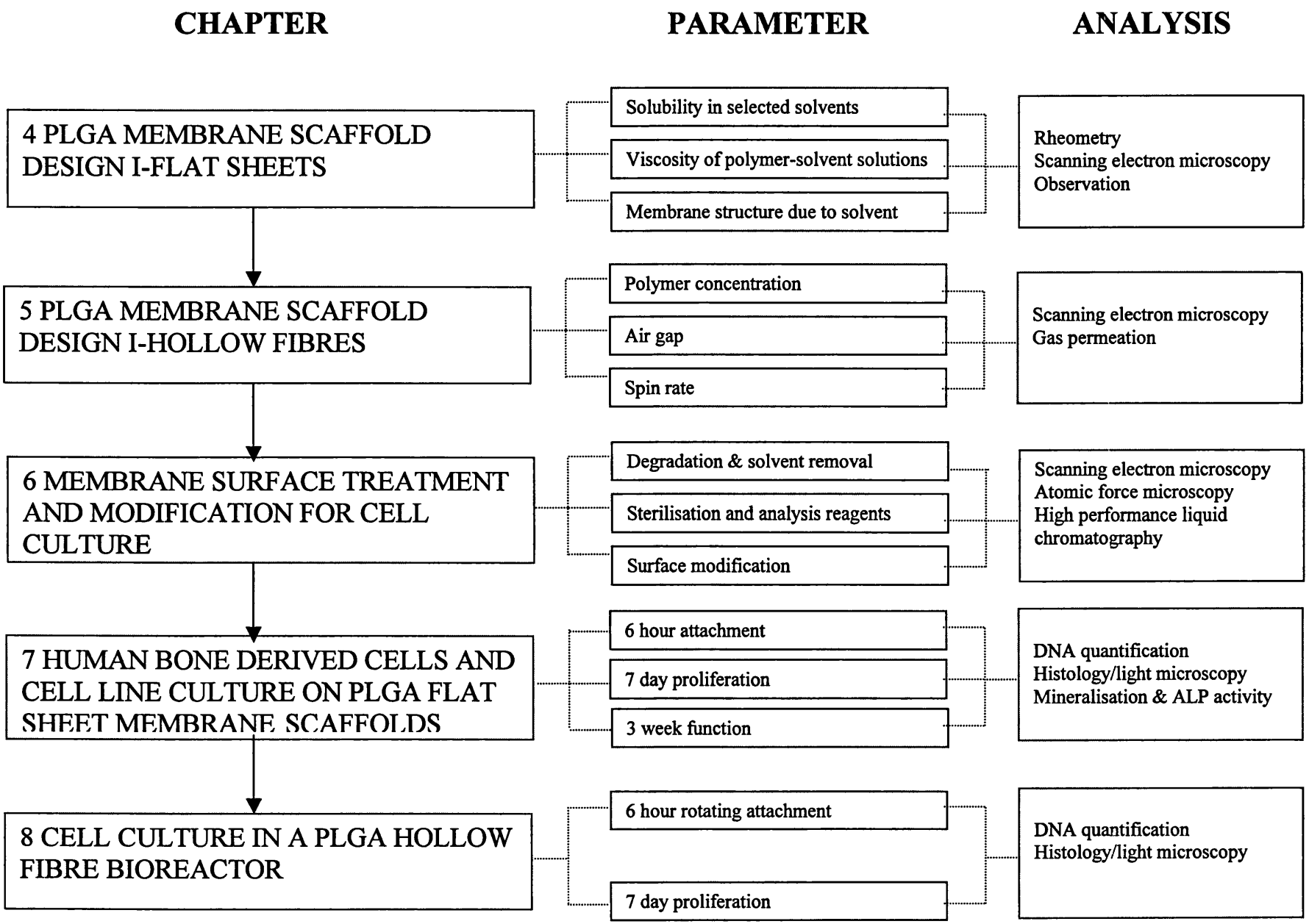

Figure 1.1. Summary of the work carried out in each of the results chapters.

CHAPTER TWO
BONE REGENERATION USING A SYNTHETIC SCAFFOLD AND BIOREACTOR

2.1 INTRODUCTION

This chapter begins with an outline of the biology of bone and the major diseases associated with the tissue, as well as common treatments for the diseases (Section 2.2). The next section (Section 2.3) describes the current state of bone tissue engineering from the cells and media to the scaffold and culture systems used to develop ways of bone regeneration. Section 2.4 leads the way to the basis of this project by discussing membrane technology and its use in designing a scaffold and bioreactor for bone tissue engineering. A summary of the current state of bone tissue engineering is given in Section 2.5 and the aims and objective of the project are shown in Section 2.6.

2.2 BONE BIOLOGY, DISEASES AND TREATMENTS

2.2.1 BIOLOGY OF BONE

The regeneration of bone requires an understanding of how bone is formed, its structure and components, and how it functions as a living tissue.

Types of Bone

There are two forms of bone, namely cortical (compact) and cancellous (spongy or trabecular) which differ in morphology due to their different primary functions (Figure 2.1). Cortical bone has 10% porosity whereas cancellous bone has 50-90% (Buckwalter *et al.* 1996; Currey 1984). Adult skeleton consists of 80% cortical and 20% cancellous bone, proportions vary at different locations in the skeleton.

Cortical bone gives mechanical support and protection to internal organs, where as cancellous bone provides the environment for metabolic functions such as blood

production (Marks and Hermey 1996). The highly porous cancellous bone contains bone marrow which supports the hematopoietic process system.

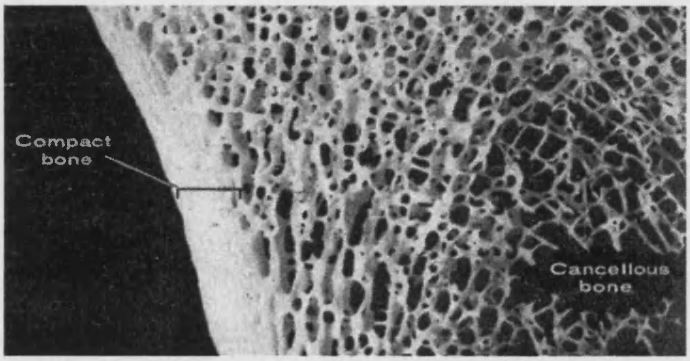

Figure 2.1. The structure of bone.
The two types of bone, compact and cancellous are shown.

The Structure of Cortical Bone

Mature cortical bone is made up of units called osteons, these are cylindrical structures made up of annular layers of bone called lamellae which surround a central Haversian canal. The Haversian canal contains the blood and nerve supply to the osteon, and are connected through Volkmann's canals. The lamellae are made of calcified matrix; interstitial lamellae are found between osteons and are the remains of remodelled osteons. Osteoblasts and MSCs are found on the periosteal and endosteal surfaces as well as the lining of Haversian canals.

In lamellae, osteocytes are housed in lacunae within the matrix; these mature bone cells were osteoblasts that remained in the matrix and further differentiated during osteon formation (Figure 2.2). Osteocytes form contacts with other osteocytes via long processes, through small channels called canaliculi, which allow them to form a 3-dimensional network (Burger and Klein-Nulend 1999; Schirrmacher *et al.* 1992). Osteons are skirted by a cement line across which canaliculi do not pass and so osteocytes do not communicate.The morphology and positioning of the osteocytes in bone suggest they are the most likely recipients of signals created by mechanical forces.

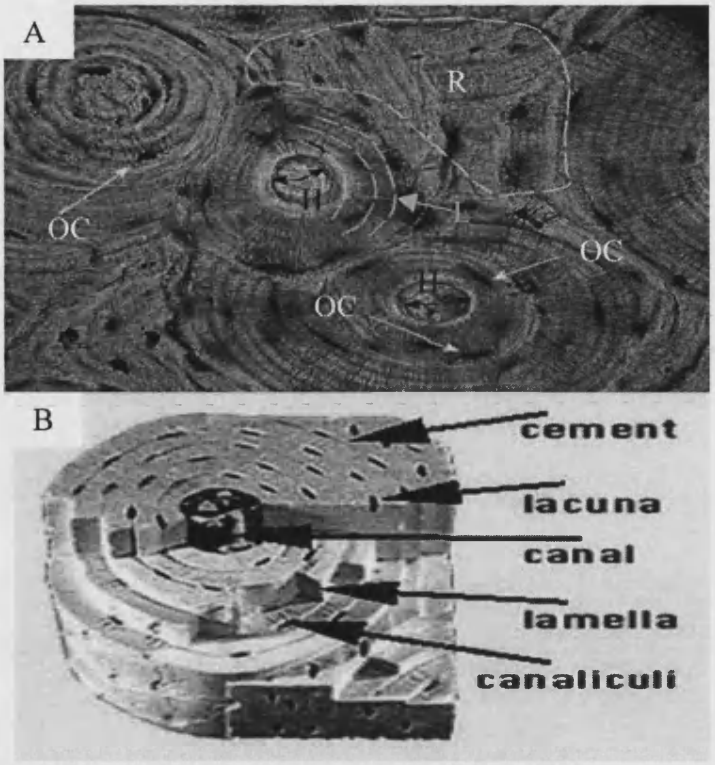

Figure 2.2. The structure of cortical bone.
(A) Cross-section of cortical bone. Circle marked OS shows an osteon, dashed lines marked L show lamellae, double headed arrows marked H show Haversian canal, OC mark osteocytes, area marked R shows old bone that has been partially resorbed and replaced with new osteons, (B) sketch of an osteon.

The Cells Found in Bone

There are several cells involved in bone formation; osteoblasts are the bone forming cells; osteoclasts and phagocytes are also present and necessary for matrix remodelling, (Figure 2.3) and once vascularisation begins the cells for this process, such as endothelial cells, are also present (Caplan and Boyan 1994; Buckwalter *et al.* 1996; Caplan and Bruder 1997). Bone lining cells are present on the outer surface of the bone (Marks and Hermey 1996). Osteoblasts and bone lining cells are thought to be derived from the marrow stroma cell lineage, (Figure 2.4) whereas osteoclasts and phagocytes are thought to be derived from part of the hematopoietic lineage.

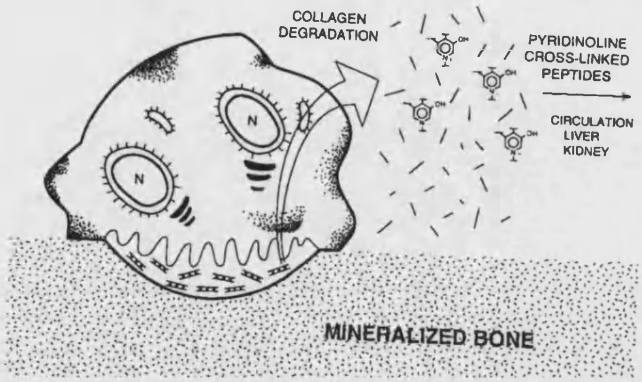

Figure 2.3. Sketch of an osteoclast degrading mineralised bone.
(Eyre 1996).

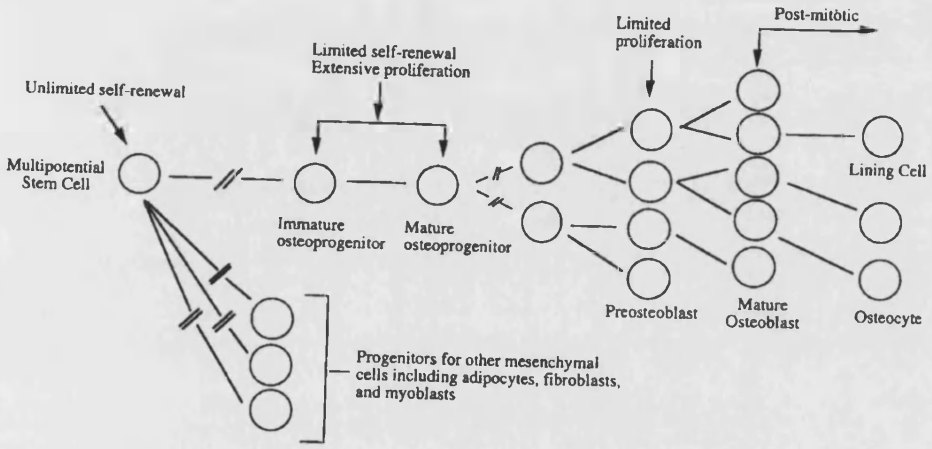

Figure 2.4. Postulated steps in the osteoblast lineage implying recognisable stages of differentiation.
Decreasing proliferation and increasing differentiation from left to right. (Aubin 1996).

The Extracellular Matrix

The matrix provides structure, guides restructuring, maintains inter-cellular distances that permit diffusion, transmits tissue-specific mechanical forces (Marler *et al.* 1998), regulates proliferation and differentiation (Tabata 2001) and transmits information to the attached cells (Damsky *et al.* 1997). Cancellous bone has a matrix consisting of mainly proteins and is softer than the densely packed, largely mineralised matrix of cortical bone. The main component of the bone matrix is collagen I, but there are several other components including other collagen types,

other proteins, and non-organic constituents such as hydroxyapatite (Marks and Hermey 1996). Mineralisation of the collagen is shown in Figure 2.5 below.

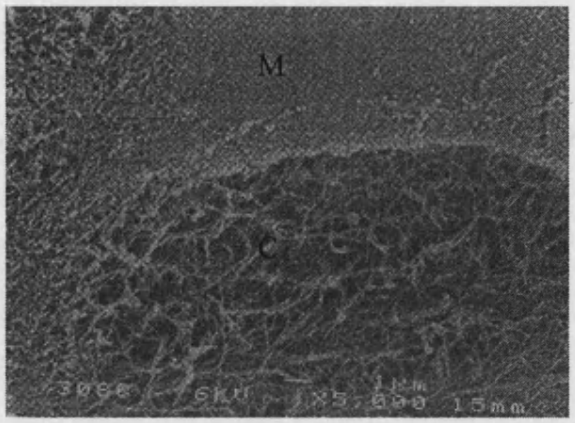

Figure 2.5. Partially resorbed extracellular matrix.
Part of the mineralisation, M has been resorbed, exposing the collagen, C. (Aubin 1996; Eyre 1996; Vaananen 1996)

Bone Fluid and Blood Supply

Bone tissue fluid, also called interstitial fluid, exists between osteogenic tissue and the mineral surface, and also possibly in the vascular connective spaces between the endothelial walls of the blood capillaries and the bone surfaces of the Haversian canals (Owen and Melick 1973) (Figure 2.6). It is thought that the fluid is continuous in the canniculi, osteocyte lunacae and the vascular connective spaces. The composition is unique, differing from plasma and extracellular fluids, and may in fact differ at different sites in the bone (Owen and Melick 1973; Triffitt and Owen 1973). The role of the bone tissue fluid is to deliver nutrients; the flow of the fluid also has a role in cell function and bone remodelling (Hillsey and Frangos 1994). Further explanation of the flow of the interstitial fluid and its role in bone signalling is given in below in the sub-section entitled 'Properties of Bone'.

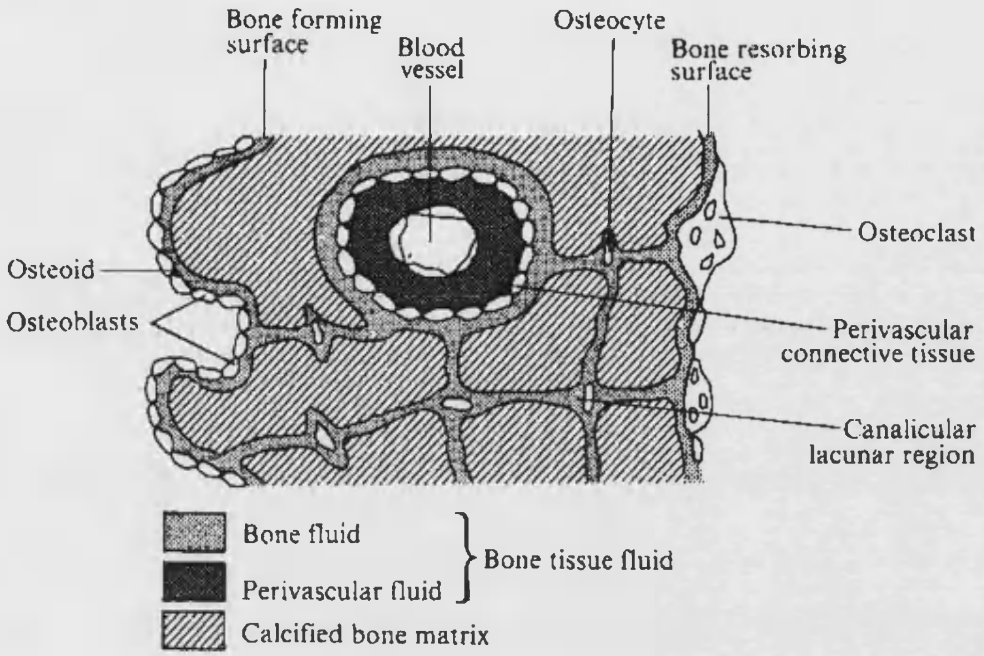

Figure 2.6. Sketch of a cross-section of an osteon showing areas of bone fluid. (Owen and Melick 1973).

In simple terms, the blood supply has three functions: nutrient supply, waste removal and transport of cells and other products manufactured, or stored in bone, for use else where, e.g. blood cells and calcium. A long bone, as shown in Figure 2.6, has three basic blood supplies: the nutrient artery, the metaphyseal combined with the epiphyseal arteries (after closure of the growth plate), and the periosteal arterioles (Vaughan 1975).

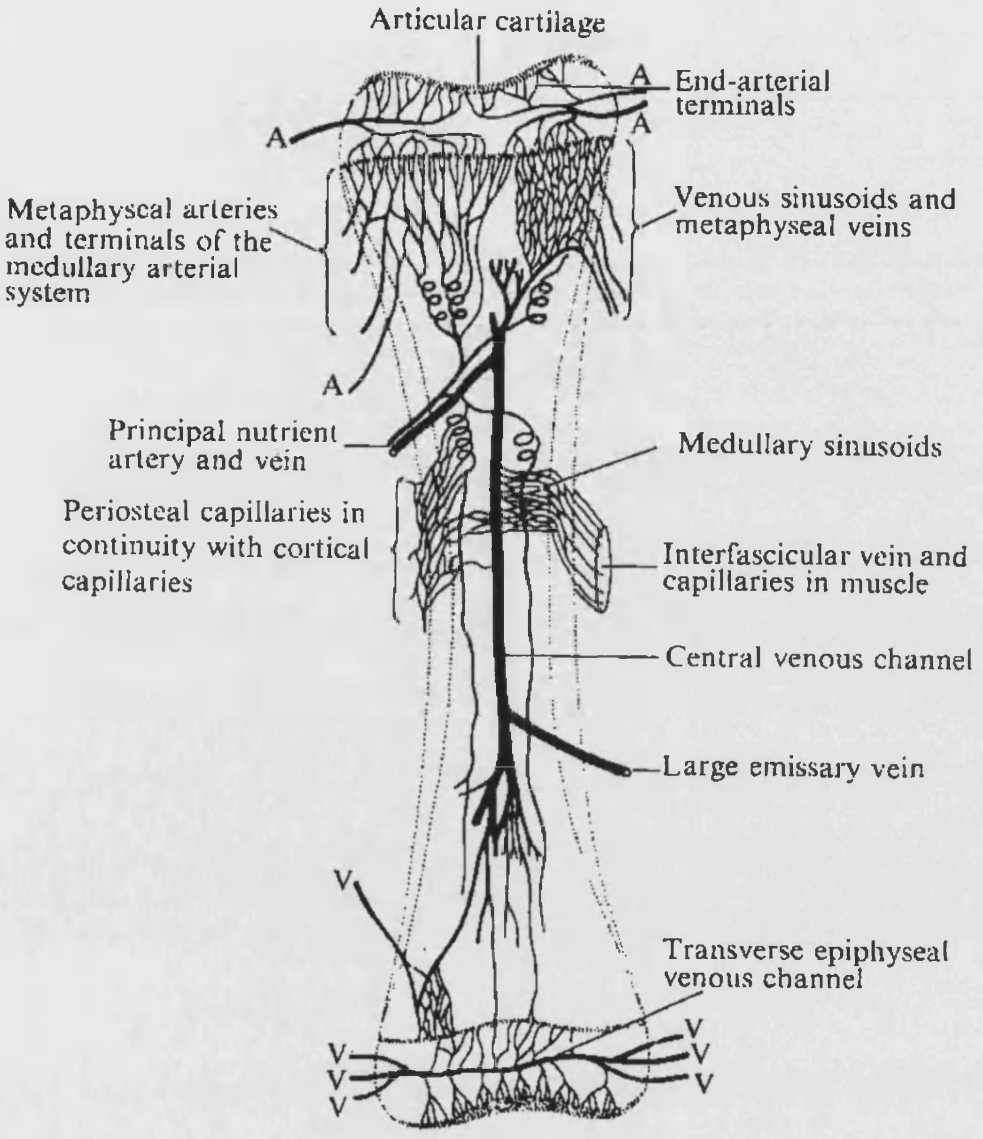

Figure 2.7. Blood supply of a long bone.

(Vaughan 1975).

Properties of Bone

Mechanically, bone is highly anisotropic, nonlinear and viscoelastic. These characteristics, coupled with the fact bone continually remodels to adapt to its mechanical environment, makes it hard to put values on its physical properties (Einhorn 1996); values can be approximated as shown in Figure 2.8 and Table 2.1.

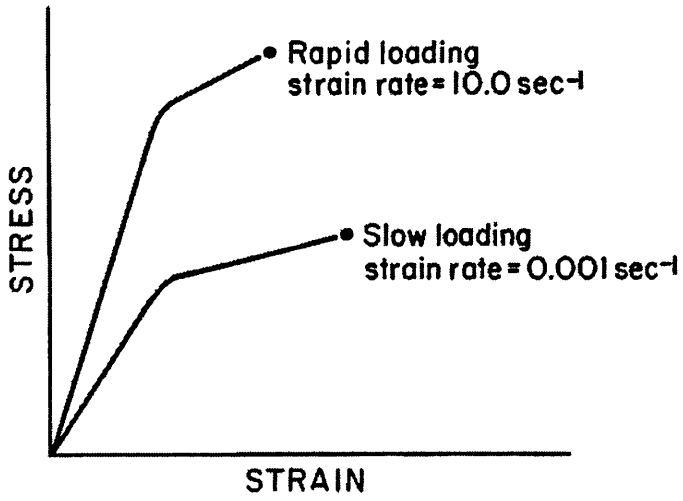

Figure 2.8. Different stress-strain curve configurations for cortical bone depending on loading.
(Einhorn 1996).

Table 2.1. Mean values for human bone material parameters.

Type of Bone	*Direction and type of load*	*Apparent density (g/cm^3)*	*Ultimate strength*	*Modulus of elasticity (10^6 MPa)*
Cortical (mid-femur)	Longitudinal tension	1.85	133	17,000
	Longitudinal compression	1.85	193	17,000
	Longitudinal shear	1.85	68	3,000
	Transverse tension	1.85	51	11,500
Trabecular (vertebral	Transverse compression	1.85	33	11,500
body)	Compression	0.31	6	76

Data from (Einhorn 1996)

It is necessary for bone to constantly remodel itself in order to adapt to its situation so that it can maintain the appropriate mechanical support (Vaughan 1975). It is known that exercise leads to an increase in bone mass (Nillson and Westlin 1971) and the atrophy effects of weightlessness and bed rest where there is no loading, is also well recognised (Arnaud *et al.* 1992; Donaldson *et al.* 1970; Roer and Dillaman 1990; Schneider and McDonald 1984; Whedon 1984; Vaughan 1975). In both cases the extent of loading leads to the cells receiving signals to remodel the bone to cope

with the mechanical forces being applied. Frost's mechanostat theory (Figure 2.9) describes the effect of strain on bone. For strains between 200 με and 2500με there is no net change in bone formation, this is the basal, or physiological level of strain. Strain below 200 με is considered as disuse and results in net bone loss, strain between 2500 με and 5000 με is overuse and causes net bone formation, strain over 5000 με is pathological and results in periosteal woven bone formation in the area of maximum stress (Basso and Heersche 2002).

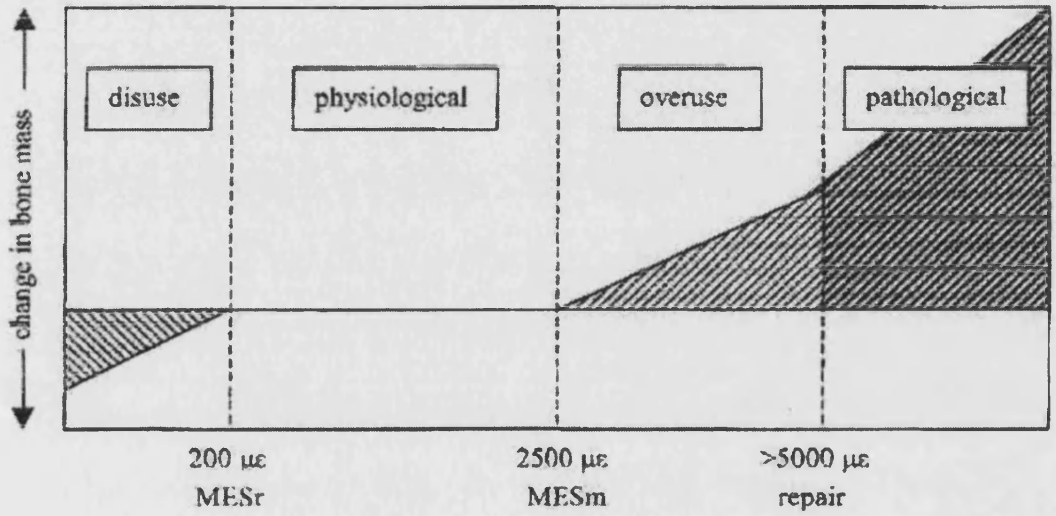

Figure 2.9. Frost's mechanostat theory.
(Basso and Heersche 2002).

It is generally accepted that mechanical loading causes a deformation of the matrix which, in turn, creates pressure gradients that drive interstitial fluid flow (Hillsey and Frangos 1994; Cowin *et al.* 1995; Klein-Nulend *et al.* 1995; Knothe-Tate *et al.* 1998; Weinbaum *et al.* 1994; Dillaman *et al.* 1991; McAllister and Frangos 1999; Qin *et al.* 1999). It is possible that flow through any of the three levels of porosity-vascular, lacunar-canalicular, or collagen-hydroxyapatite porosity-may play a part, but it is likely that lacunar-canalicular porosity has the primary role in fluid flow due to mechanical loading (Weinbaum *et al.* 1994).

Mechanotransduction is the means by which cells communicate via detection of fluid flow due to mechanical force. How the flow is actually detected by the cells is not yet established; an early view still held is that the transduction of mechanical to electrical signals is the most likely mechanism (Vaughan 1975). Basset (1966) suggested that deformation-based piezo-electric, solid-state (p-n junction, between apatite crystals and collagen fibrils), and streaming potentials, as well as non-deformation based electrical signals including those generated in vessels by cardiac and skeletal muscle pumps, and electrical flow in the peripheral nervous system were involved. More recent work has shown that piezoelectric potentials are insignificant compared with streaming potentials (Banes *et al.* 1990; Tjandrawwinata *et al.* 1997). Further work has backed up the streaming potential theory suggesting the positively charged surface becomes the site of increased resorption and the negatively charged surface the site of increased bone formation (Brighton and McCluskey 1986; Ferrier *et al.* 1986). If streaming potentials are involved in mechanotransduction, it is then important for the scaffold to exhibit the same electrochemistry as the extracellular matrix. Ligand-receptor affinity ultimately comes down to electrochemical bonds; the work carried out by Rocha *et al.* (2002) with an anionic collagen matrix showed promising results for use in bone healing.

It has also been reported that the mechanical forces per se are related to bone development. Osteocytes respond to increased strain by increasing nitrogen oxide production, which inhibits osteoclast resorption and promotes the production of prostaglandins which stimulate osteoblast formation (Cowin *et al.* 1991; Klein-Nulend *et al.* 1995; Ajubi *et al.* 1996). Another view is that increased fluid flow due to increased mechanical loading increases nutrient and waste transport which has been hypothesised to result in osteoblast recruitment (Burger and Klein-Nulend 1999). It is suggested however, that flow stimulation of osteoblasts is mainly by the shear stress and not the increase in nutrient and waste transport (Sikavitsas *et al.* 2001).

2.2.2 OSTEOGENESIS, DISEASE AND REGENERATION

A brief overview of bone formation, regeneration and disease is given here. The reader is pointed towards bone biology literature including Beresford (1984); Bilezikian *et al.* (1996); Caplan and Bruder (1997); Beresford and Owen (1998);

Russell *et al.* (1998) for more detail. Bone is a complex organ made up of osseous, cartilaginous, fibrous and hematopoietic tissue (Russell *et al.* 1998). The majority of bone formation during skeletal growth is due to endochondral bone formation (Figure 2.10). This involves the maturation of cartilage in which the matrix eventually calcifies and is invaded with blood vessels.

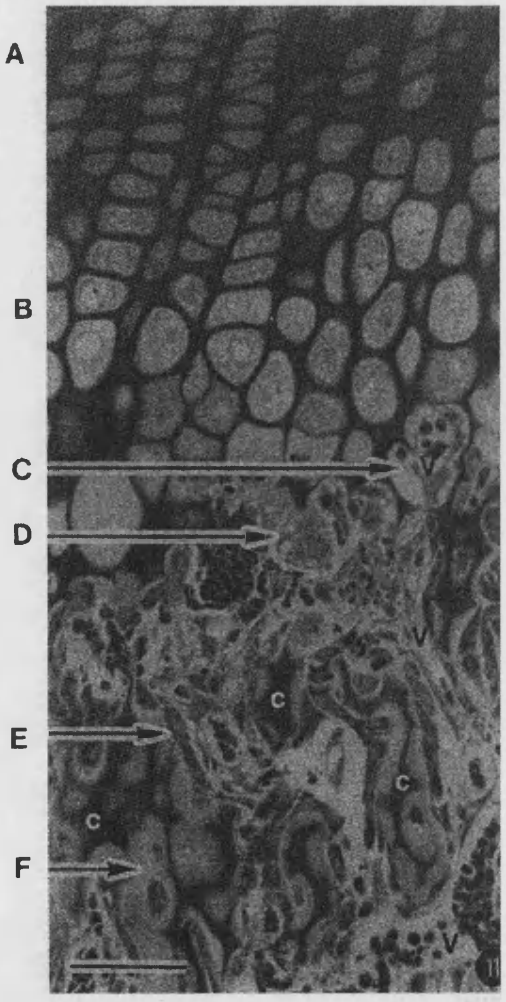

Figure 2.10. Endochonral bone formation.
(A) chondrocyte proliferation, (B) chondrocyte hypertrophy, in columns supported by a mineralised longitudinal matrix. (C) vascularisation of eroded cartilage matrix by (D) osteoclasts. (E and F) bone formation by osteoblasts (Marks and Hermey 1996). Scale bar 50 μm.

When bone is fractured the healing process is a similar process to the bone formation process and virtually no sign injury will remain. Neonatal and postnatal bone is known to be able to heal without scarring (Russell *et al.* 1998). Disorders arise because the normal healing mechanisms cannot occur, for example due to non-union in which the gap to be bridged is too large (critical sized defect), osteoporosis when the bone formation process does not keep pace with the resorption process (Bilezikian *et al.* 1996), or the process itself is defective as is the case with achondroplasia (Russell *et al.* 1998) the short limbed dwarfism related to the overexpression of the growth factor FGFR-3 (Bilezikian *et al.* 1996) (Section 2.3.2).

2.3 STATUS OF BONE TISSUE ENGINEERING

2.3.1 CELL TYPES AND SOURCES

The cells used for in vitro tissue engineering models fall into one of two categories; primary cells, or cell lines in bone tissue engineering. Osteoblastic cell lines are the least complex as the population is homogeneous whereas primary cell populations are heterogeneous. There are advantages and disadvantages to both categories. A heterogeneous population means data cannot be localised to a single cell type, however more typical behaviour is likely to be seen as bone contains several cell types which continuously interact and so bone formation mechanisms are likely to take place during culture. Immortalised cell lines have been developed to proliferate rapidly while maintaining a normal phenotype and have the ability to proliferate many more times than primary cells. However, the cells may adapt to in vitro culture conditions and the transfection may affect cell behaviour. Greater detail can be found in (Russell *et al.* 1998).

Primary cells types can be subdivided according to their maturity; mesenchymal stem cells (MSC) and the more mature osteoblasts. The marrow stroma (supporting environment of hematopoeisis) contain an adherent population of colony forming unit-fibroblasts (CFU-f). Within the CFU-f population a subset of cells have the potential to differentiate into any of the cell types found in the stroma; it is these cells that are the MSC. The MSC can be selected using antibodies, they are then expanded, and differentiated, and eventually give rise to bone-like cultures.

Osteoblasts are differentiated stem cells obtained from mineralised bone samples. Explants are cultured and, under particular conditions, osteoblasts from the bone will proliferate. Primary cells are sometimes named depending on the age of the source tissue, e.g. neonatal, postnatal or adult. Table 2.2 shows the cell types used by bone tissue engineering groups. Osteosarcoma cell lines are common because of their useful adaptation to the in vitro environment making them easy to culture while being widely available. Rat osteoblasts are the most used primary cells, although human cells are also popular due to the obvious benefits in their use since the end product is for human use. It should be noted that while some groups state that they have used homogeneous osteoblast populations, in practice these are likely to be mixed populations of bone derived cells and show osteoblast-like behaviour.

2.3.2 MEDIA AND GROWTH FACTORS FOR IN VITRO CULTURE OF BONE CELLS

While the basic media for bone cell culture is the same for cell lines and primary cells (Section 3.3.3), different growth factors can be added depending on the required outcome of the culture. In vivo, growth factors are either delivered to the cells via blood or produced by the cells themselves. They have specific roles in development and will only be present when they are required. Growth factors can be added into the media in vitro. A list of some of the growth factors important for bone is shown in Table 2.3.

2.3.3 CULTURE SUBSTRATES AND SCAFFOLDS

An understanding of the structure and properties of bone should be kept in mind when choosing a scaffold material and structure; both the overall macro-architecture and the micro-architecture - pore size and shape and topography. Surface characteristics and topography, surface chemistry and treatment, and degradation characteristics all affect bone cell viability, attachment and spreading (Sikavitsas *et al*, 2001). For this reason surface modification can improve cell culture or even allow growth on materials otherwise unsuitable. Scaffolds should have mechanical strength for creation of a macroporous scaffold that retains its structure after implantation (Yang *et al*, 2001). It should also behave like the bone and mimic the natural extracellular matrix produced by the osteoblasts it is replacing in order to relay the correct signals involved in mechanotransduction. In addition to this, it must be processable and reproducible, and easily shaped.

Table 2.2. Cell types commonly used in bone tissue engineering.

Cell type	Referenced cell type name	Reference
Primary Cells		
1° osteoblast-like cells	Rat calvarial osteoblasts	(Gray *et al.* 1996)
	1° human osteoblasts	(Mankani *et al.* 2000; Yang *et al.* 2001; Dalby *et al.* 2002; Elias *et al.* 2002; Borden *et al.* 2003; El-Amin *et al.* 2003)
	1° rat bone marrow derived cells	(Holy *et al.* 2000)
	1° rat osteoblasts	(Goldstein *et al.* 2001)
	Neonatal rat osteoblasts	(Ishaug-Riley *et al.* 1998)
	Stromal osteoblast-like rat cells	(Wake *et al.* 1998)
Stem cells	BMSSCs (human postnatal bone marrow stromal stem cells)	(Shi *et al.* 2002)
	hMSCs (human marrow stromal cells)	(Simosen *et al.* 2002)
	HMSF (human marrow stromal fibroblasts)	(Kuznetsov *et al.* 1997)
	Neonatal rat bone marrow cells MSCs	(Yoshimoto *et al.* 2003)
Cell Lines		
Osteosarcoma cell line	MC3T3-E1	(Webb *et al.* 2000; Stephansson *et al.* 2002)
	MG-63	(Shieh 2000; Lee *et al.* 2003)
	SAOS-2	(Ciapetti *et al.* 2003)
Transfected, immortalized cell line	PMT	Unpublished
	pZIP	Unpublished

Table 2.3. Growth factors for bone culture.

Growth Factor	Description & Role
Bone morphogenic proteins (BMP)	Family of cytokines. Stimulates proliferation of both chondrocytes and osteoblasts. Induces MSC differentiation
Fibroblast growth factors (FGF)	Family of growth factors. Stimulates proliferation of MSCs, chondrocytes and osteoblasts. Angiogenic properties
Insulin like growth factors (IGF)	Family of growth factors. Stimulates proliferation chondrocytes and osteoblasts. Induces matrix secretion
Platelet derived growth factor (PDGF)	A growth factor. Stimulates proliferation of chondrocytes and osteoblasts. Implicated in bone resorption
Transforming growth factor-β (TGF-β)	A growth factor. Causes differention of MSC to chondrocytes and osteoblast proliferation. Enhances bone resorption
Epidermal growth factor (EGF)	A growth factor. Stimulautes chondrocyte proliferation, decreases cells' ability to synthesize matrix components
Parathyroid hormone (PTH)	Single chain polypeptide. Causes release of calcium. Induces osteoblast differentiation
Estrogen	A hormone. Effects to decrease bone resorption
Dexamethasone	A corticosteroid. Promotes events early in differentiation of chondrocytes
Thyroxin	A thyroid hormone. Stimulates osteoclastic bone resorption
Prostaglandins	A family of fatty acids. Linked to proliferation and differention of osteoclasts
Interleukin-1 (IL-1)	stimulates proliferation of osteoclast precursors
Vitamin D	Possibly regulates synthesis of other molecules e.g. osteopontin, osteonectin.

Data from (Caplan and Boyan 1994; Rosen and Thies 1995; Buckwalter *et al.* 1996)

Materials and Macro-Architecture

2D scaffolds provide a basic understanding of cell culture on a particular material and many groups have used monolayer culture in the study of bone tissue regeneration (Calvert *et al.* 2000; Ishaug *et al.* 1994, Karp *et al.* 2002). Traditional cell culture systems use a modified polystyrene commonly known as tissue culture plastic (TCP). This is the standard culture material and is used as a control to compare other scaffold materials. However, since the construct will ultimately need to be 3D to function in vivo such architecture, and the culture techniques associated with it, need to be examined prior to implantation.

There is a range of potential material that the bone tissue engineering scaffold can be made from, including natural and synthetic polymers, ceramics & glasses, metals, hydrogels and combinations of these materials (Yang *et al.* 2001), (Gibson 2003). These materials can take on a variety of macro-architectures. Table 2.4 shows some common macro-architecture and the maximum dimensions that the scaffolds can be to support cell growth throughout the construct.

Table 2.4. Common scaffold macro-architectures and dimensions.

Macro-architecture	***Dimensions (m)***
Films	10^{-5} – 10^{-4} thick, unlimited surface area
Porous foams/sponges	10^{-2} cubed (Kokubo *et al.* 2003)
Electrospun nonwoven sheets	10^{-2} cubed
Microspheres	10^{-4} diameter (Botchwey *et al.* 2001)
Dipcoating tubes	10^{-5} – 10^{-3} diameter
Non-hollow fibres	10^{-4} diameter (Williamson and Coombes 2004)
Hollow fibres	10^{-4} diameter
Porous particles	10^{-4} diameter (Jin *et al.* 2000).
Extruded channelled-blocks	10^{-3} diameter

The most common, well studied and successful materials used in bone tissue engineering is hydroxyapatite and the range of poly(alpha-hydroxy acids); poly(lactic acid) (PLA), poly(glycolic acid) (PGA) and the copolymer of the two, poly(lactic-co-glycolic acid) (PLGA). These polymers can be further copolymerised with other polymers (Hasirci *et al.* 2001; Hacker *et al.* 2003; Jeong *et al.* 2003; Kempen *et al.* 2004; Oh *et al.* 2003) or blended with other materials such as hydroxyapatite (Ambrosio *et al.* 2001; Dalby *et al.* 2002; Kim *et al.* 2004). Other materials used in bone tissue engineering include alginate hydrogels (Alsberg *et al.* 2001), carbon nanofibres (Elias *et al.* 2002), cellulose sponge (Martson *et al.* 1998), anionic collagen (Rocha *et al.* 2002), and peptide-amphiphile self-assembling nanofibres (Hartgerink *et al.* 2001).

Polymers

The range of polymers, both natural and synthetic, is vast. Natural polymers, such as collagen and starch, closely simulate native cellular milieu but have large batch to bath variations. Synthetic polymers have properties that are more easily controllable including degradation time and physical properties, but have the potential to cause an immune response and consequently be rejected (Yang *et al.* 2001). Biodegradable scaffolds reduce the potential long-term effects of a implanting a foreign body since they are removed via the bodies normal waste paths once their role is complete (Middleton and Tipton 2000).

The range of synthetic polymers used on bone tissue engineering is shown in Table 2.5. Of these the most commonly used for scaffolds are the poly(α-hydroxy acids) and polyhydroxybutyrates both of which degrade by hydrolysis (Hasirci *et al.* 2001). The poly(α-hydroxy acids) are particularly widely used since due to their approval for use in the human body by the US Food and Drug Administration (FDA) (Middleton and Tipton 2000).

Table 2.5. Scaffold materials and their structures.

Material	Structure	Reference
Synthetic Polymers		
PCL	Film coatings on glass slides	(Calvert *et al.* 2000)
	porous foams	(Ciapetti *et al.* 2003)
	nanofibrous nonwoven sheets	(Yoshimoto *et al.* 2003)
	nonhollow fibres	(Williamson and Coombes 2004)
	microtubles	(Ma and Zhang 2001)
PLA	In situ forming scaffold	(Burdick *et al.* 2003)
	membrane	(Gugala and Gogolewski 1999)
	Microtubles	(Ma and Zhang 2001)
PLGA	Microspheres	(Borden *et al.* 2003), (Botchwey *et al.* 2001)
	Film coatings on glass slides	(Calvert *et al.* 2000), (Ishaug *et al.* 1994), (Karp *et al.* 2002)
	Porous foams	(Holy *et al.* 2000), (Holy and Yakubovich 2000), (Karp *et al.* 2002), (El-Amin *et al.* 2003), (Goldstein *et al.* 2001), (Hu *et al.* 2002), (Ishaug *et al.* 1996; Ishaug *et al.* 1997; IshaugRiley *et al.* 1997; Ishaug-Riley *et al.* 1998), (Partridge *et al.* 2002; Terai *et al.* 2002) (Sikavitsas *et al.* 2002)
	nanofibrous nonwoven sheet	(Li *et al.* 2002)
PPF	Porous foam	(Vehof *et al.* 2002)
PVDF	Polymer films	(Klee *et al.* 2003)
Natural Polymers		
cellulose	Viscose cellulose sponge	(Martson *et al.* 1998)
collagen	Ionic collagen matrix	(Rocha *et al.* 2002)
starch	foam	(Gomes *et al.* 2002)
Polymer Blends		
Chitosan and soybean protein isolate	Solvent cast membranes	(Silva *et al.* 2004)
NSTM PEG-block-PLGA	foam	(Hacker *et al.* 2003) (Tessmar *et al.* 2003)
PLGA-PPF-VP	foam	(Hasirci *et al.* 2001)
PLL-g-PLGA	Self-assembling micelle structure	(Jeong *et al.* 2003)
PPF/PLGA	microspheres	(Kempen *et al.* 2004)
PLGA coated gelatin	Sponge	(Kokubo *et al.* 2003)

Fabrication methods for synthetic polymer scaffolds for bone tissue engineering are varied the most common being phase inversion. This process involves dissolving the polymer in a solvent, forming it with a mould as a liquid then removing the solvent to leave a porous solid structure; more detail on this process can be found in Section 2.4. Solvent evaporation where the polymer is dissolved in a volatile solvent and left exposed to the air allowing the solvent to evaporate is the simplest and most common. 2D films can be cast onto glass coverslips in this way (Calvert *et al.* 2000; Ishaug *et al.* 1994; Karp *et al.* 2002; Klee *et al.* 2003). 3D structures can also be formed using solvent evaporation by simply pouring the solution alone into a mould (El-Amin *et al.* 2003) or combined with particle leaching. Particle leaching involves adding a salt or glucose to the polymer-solvent solution then washing the particles out with water after the solvent has been removed. This creates macro pores the size of the particle, for example 150 μm to 710 μm when sieved sodium chloride is used (Ciapetti *et al.* 2003; Ishaug *et al.* 1997), and 300 μm to 1.5 mm using glucose crystals (Figure 2.11 B) (Terai *et al.* 2002; Holy *et al.* 2000;, Holy and Yakubovich 2000; Karp *et al.* 2002). El-Amin *et al.* (2003) produced porous foams from solvent casting and moulding with dimensions 4 mm thick and 15 mm in diameter. Combining solvent casting and particulate leaching can produce thicker scaffolds due to the larger pores obtained than when using solvent casting alone. Ishaug *et al.* (1996-1998) produced porous foams 8-10 mm thick and 10 mm x 10mm (Ishaug *et al.* 1996; Ishaug *et al.* 1997; IshaugRiley *et al.* 1997; Ishaug-Riley *et al.* 1998; Terai *et al.* 2002). Karp *et al.* (2002) produced scaffolds that were cut into cubes 6 x 6 x 6 mm^3. Nanofibres can be formed using electrospinning in which a polymer-solvent solution stream is ejected from a charged capillary towards a grounded collector plate, the solvent evaporates as the stream moves down so forming a charged nonwoven mesh (Figure 2.11 A) (Yoshimoto *et al.* 2003), (Li *et al.* 2002). Another phase inversion process, immersion precipitation, has also been used to fabricate scaffolds. Instead of a volatile solvent being allowed to evaporate a third component, the nonsolvent, is used. The solvent is miscible with the solvent but not the polymer so on addition of the nonsolvent to the polymer-solvent solution the polymer precipitates to form a porous structure. Structures formed include membranes, (Gugala and Gogolewski 1999; Ma and Zhang 2001) fibres (Williamson and Coombes 2004) (Figure 2.11 D) and microspheres typically forming with diameters

in the range 200-900 μm (Figure 2.11 C) (Borden *et al.* 2003; Botchwey *et al.* 2001). Other techniques include compression moulding (Goldstein *et al.* 2001) and photocuring both in vitro (Vehof *et al.* 2002) or in situ (Burdick *et al.* 2003). (Goldstein *et al.* 2001) produced PLGA scaffolds 6 mm thick using a combination of solvent casting, compression moulding and solvent leaching.

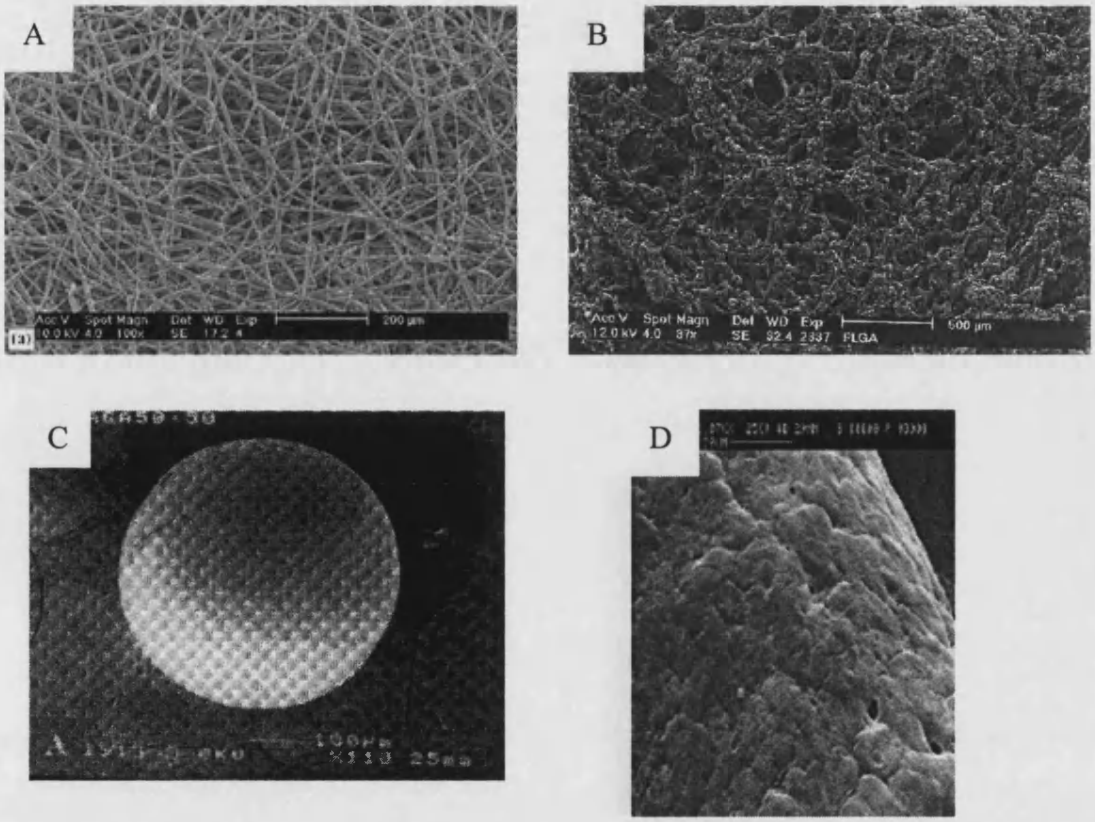

Figure 2.11. Phase inversion scaffolds used for bone tissue engineering. (A) electrospun nanofibrous nonwoven sheet (Yoshimoto *et al.* 2003), (B) solvent cast & moulded porous foam (Terai *et al.* 2002), (C) microsphere (Botchwey *et al.* 2001), (D) surface of an immersion precipitation spun fibre (Williamson and Coombes 2004).

The scaffolds formed using the techniques above typically create a construct shaped as either a sheet or a block. Macro-architecture of scaffolds should mimic that of the tissue; bone, ligament, tendon, nerve, blood vessel, muscle, liver and intestine all have tubular or fibrous structure. Synthetic polymer tubular scaffolds have been well reported particularly for nerve (Den Dunnen *et al.* 1998; Luciano *et al.* 2000; Sundback *et al.* 2003) (Evans *et al.* 1999; Oudega *et al.* 2001; Evans *et al.* 2002) and

blood vessel regeneration (Mooney *et al.* 1996). Poly(a-hydroxy acid) are the most common polymer used, as well as poly(caprolactone) and blends which incorporate other polymers such as urethane and poly(orthoesters) (Borkenhagen *et al.* 1998) (Wan *et al.* 2001; Wang *et al.* 2001). Dipcoat ing (Figure 2.12)(Wan *et al.* 2001; Wang *et al.* 2001; Den Dunnen *et al.* 1998; Luciano *et al.* 2000) or wrapping a nonwoven mesh around a PTFE mandrel (Kim *et al.* 2000; Oudega *et al.* 2001; Mooney *et al.* 1996) has been used with various polymers by several groups. Dimensions of the scaffolds resulting from dipcoating are dependant on the dimensions of the guide and the number of coats but internal diameter of 1 mm with a wall thickness of a few hundred micron are common. Luciano *et al.* (2000) used needles 0.7-1.3 mm diameter, a 1.27 mm Teflon mandrel was used by Wang *et al.* (2001). Wrapped mesh tubes tend to be larger; 2mm internal diameter and thickness 0.5-2 mm depending on the thickness of the mesh. Smaller dimensions are achieved with injection moulding with internal diameter 60μm- 500μm (Figure 2.13) (Hadlock *et al.* 2000).

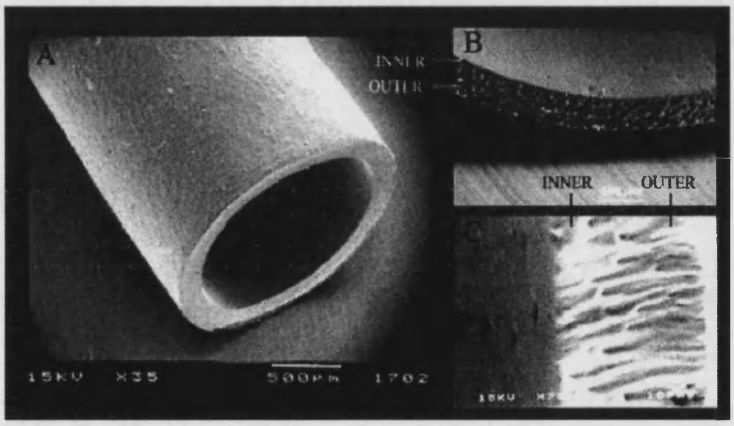

Figure 2.12. A tubular scaffold prepared from the poly(phosphoester) P(BHET-EOP/TC) using dipcoating.
(A) cross section, (B) cross-section of conduit showing distinct coating layers, (C) cross-section close up showing finger-like cavities (Wan *et al.* 2001).

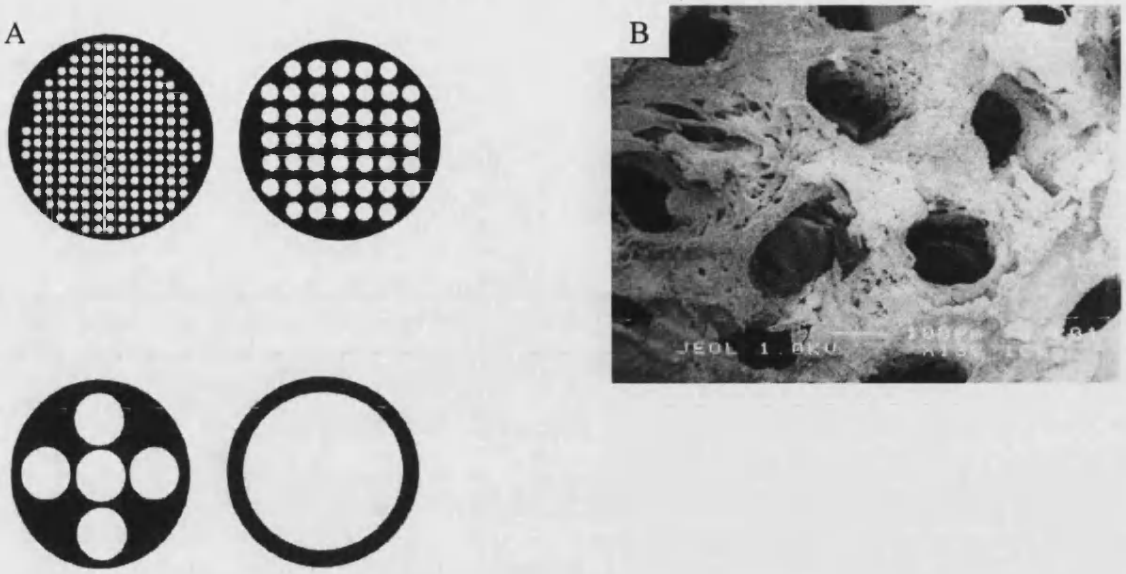

Figure 2.13. Tubular scaffolds prepared from PLGA using injection moulding. (A) schematic of cross sectional appearance of the conduit (black) with 183-, 45-, 5- or 1-channel structure, (B) detail of a 45-channel conduit. (Hadlock *et al.* 2000).

Hydrogels

Hydrogels have the advantage of being able to be injected to fill a cavity, and contain cells and growth factors (Alsberg *et al.* 2001). Alginate and poly(ethylene glycol have been used and modified with RGD to improve cell attachment (Alsberg *et al.* 2001; Burdick and Anseth 2002), however, hydrogels by their nature, have poor mechanical properties. Lee *et al.* (2001) used a hydrogel made of poly(aldehyde guluronate) and adipic acid dihydrazide which has controllable mechanical properties and degradation rates. The next stage on from this is an injectable scaffold that cross links or 'self-assembles' in situ, so filling the defect and allowing ingrowth from the surrounding bone (Salem *et al.* 2003). Jeong *et al.* (2000) carried out a similar process using PEG-PLGA-PEG, which is a liquid at room temperature but becomes a gel once in situ.

Ceramics

A number of ceramics have been developed and used in the treatment of bone disease and are now being used as scaffolds to further aid the efficiency of repair and regeneration. These ceramics are known as bioactive ceramics because they spontaneously bind to bone so preventing their isolation due to fibrous tissue

encapsulating in vivo (Kokubo *et al.* 2003) - the body's natural response to a foreign body. The main group of bioactive ceramics clinically used are Bioglass®, sintered hydroxyapatite, sintered β-tricalcium phosphate, hydroxyapatite/ β-tricalcium phosphate bi-phasic ceramic and glass-ceramic (Kokubo *et al.* 2003; Jin *et al.* 2000; De Oliveira *et al.* 2003). Hydroxyapatite is found naturally in the calcified matrix of bone and so fills many criteria of a scaffold. Hydroxyapatite scaffold architecture is typically prepared by cutting the solid material or extruding a paste. Naturally occurring ceramic such as coral has also been utilised as a scaffold (Petite *et al.* 2000). Ceramic structures are typically formed by mechanical means; the resulting structures can be porous or nonporous, articulate or blocks (Kokubo *et al.* 2003) (Figure 2.14). Hydroxapatite structures specifically designed as scaffolds have also been developed (Figure 2.15). Despite the success of ceramics used, they are often crystalline in nature as opposed to apatite that is found naturally in bone which is a 'poorly crystalline carbonated phosphate system (Ambrosio *et al.* 2001). The use of a noncrystalline carbonated calcium phosphate as developed by Ambrosio *et al.* (2001) may further increase the benefits of ceramics used in tissue engineering.

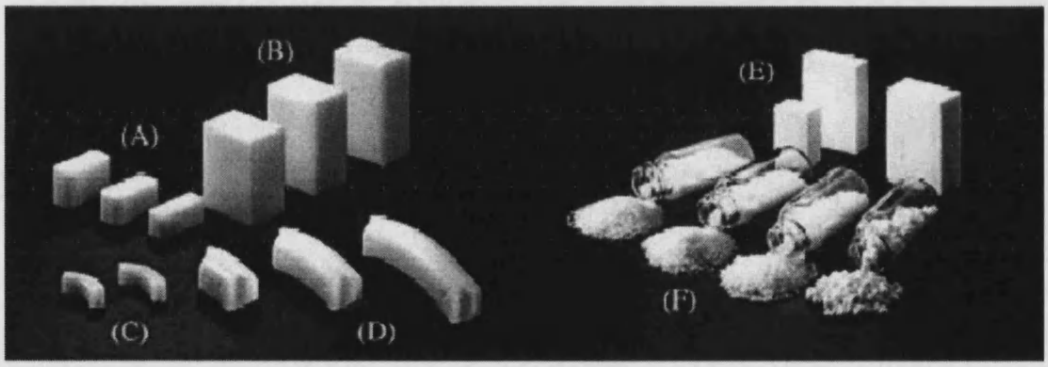

Figure 2.14. A range of glass-ceramic products currently in orthopaedic clinical use.
(A) intervertebral discs, (B) artifcial vertebrae, (C) spinal spacer, (D) iliac crests, (E) porous spacer, (F) bone filler. (Kokubo *et al.* 2003)

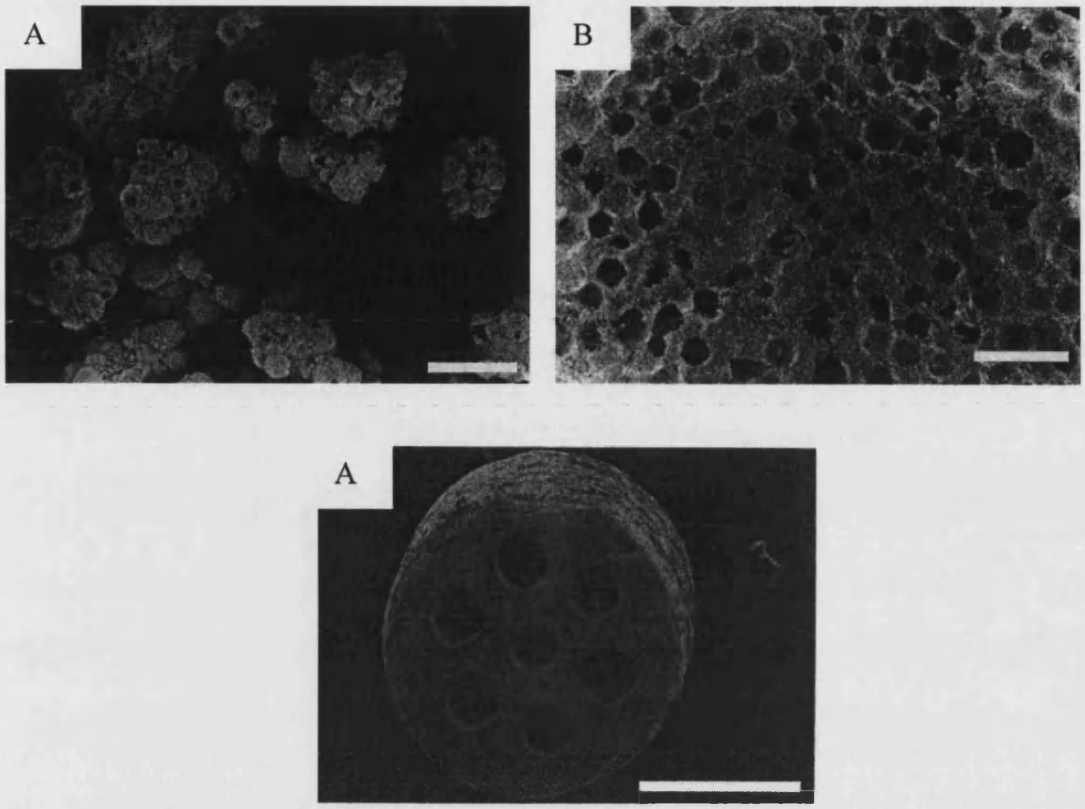

Figure 2.15. Hydroxyapatite scaffold macro-architectures.
(A) porous particles, (B) porous block, (C) honeycomb (Jin *et al.* 2000). Scale bar is 360 μm.

Composites

Composite scaffolds allow the properties of different materials to be combined. For example, copolymerisation of poly(α-hydroxy acids) with PET or PVA increases hydrophilicity so making the surface better for cell attachment (Koegler and Griffith 2004). The copolymer (N-succinimidyl tartrate monoamine poly(ethylene glycol)-block-poly(D,L-lactic acid)) has the ability to covalently immobilize proteins on their surfaces (Tessmar *et al.* 2003). The addition of amporphous calcium phosphate ceramics, including hydroxyapatite acts as a buffer to compensate for the potentially harmful release of acidic byproducts of poly(α-hydroxy acids) (Schiller and Epple 2003). Furthermore, polymer-hydroxyapatite composite scaffolds combine the processablility of the polymer with the bioactivity of hydroxyapatite. The bioactiviy of hydroxyapatite means it can improve the biocompatibility of other scaffold materials. It can be coated onto polymers (Figure 2.16) (Murphy *et al.* 2000; Kokubo *et al.* 2003b; Costantini *et al.* 2002), collagen, and metal (Zhang *et al.* 2002; Merolli

et al. 2003; Hong *et al.* 2003; Lavos-Valereto *et al.* 2002) or added into polymer-solvent solutions prior to phase inversion casting such as polycaprolactone-hydroxyapatite (PCL-HA) composite filaments materials (Yang *et al.* 2002), PLGA microspheres with hydroxyapatite (Ambrosio *et al.* 2001) or as with the commercially available HAPEX™, combined with polyethylene by screw extrusion and compression moulding (Dalby *et al.* 2002). Wei and Ma (2004) incorporated nano-particle hydroxyapatite into the pore walls of PLLA foams fabricated using TIPS (thermally induced phase separation). Polymer coatings have also been successfully utilised, such as PLGA on gelatin sponges (Kokubo *et al.* 2003a) (Figure 2.17).

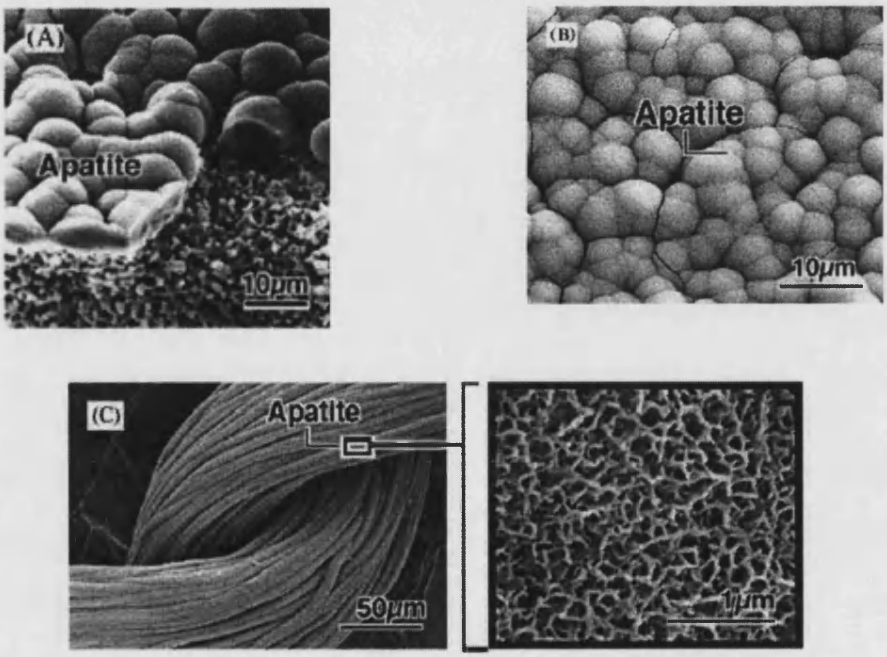

Figure 2.16. Apatite coating on various materials.
(A) silica gel, (B) titanium, (C) EVOH polymer fibres (Kokubo *et al.* 2003b).

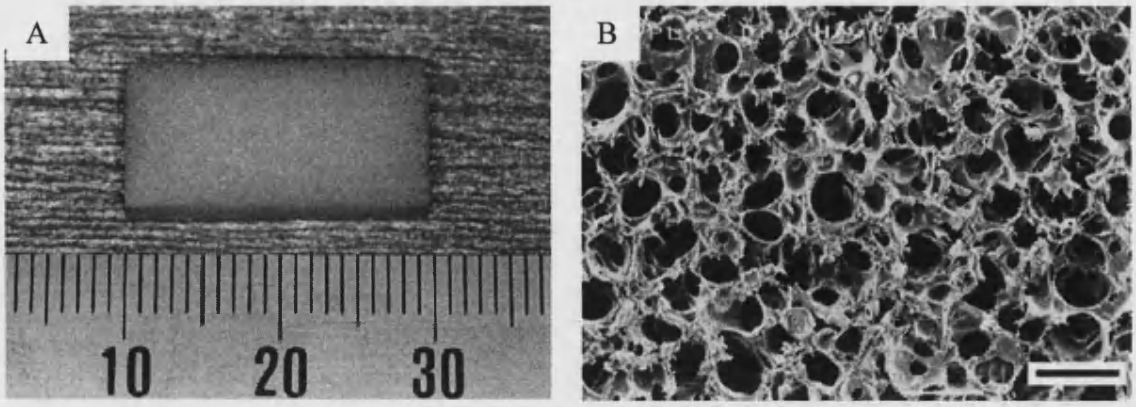

Figure 2.17. A composite scaffold; PLGA coated gelatin.
(A) complete scaffold, (B) cross section. Scale bar is 500 μm. (Kokubo *et al.* 2003a).

Micro-Architecture and Topography

Regeneration in traditional porous scaffolds is dependent on pore size and porosity. A large surface area favours cell attachment and growth, while a large pore volume is required to accommodate and deliver a large enough cell mass for tissue repair, and a highly porous structure is necessary for diffusion (Yang *et al.* 2001). One important aspect is vascularisation and the fact that cells are no further than 150 μm from a blood supply. Cells more than approximately 200 μm are either metabolically inactive or necrotic due to low oxygen tension (Colton 1995). Whang *et al.* (1999) reported that optimum pore size is 40-100 μm for osteoid ingrowth on bioabsorbable scaffolds, and 100-350 μm for regeneration of bone (Klawitter and Hulbert 1971) on porous ceramics. It has also been reported by Hulbert *et al.* (1970) that 50-150 μm induces osteoid formation, and 150-500 μm leads to mineralized bone. However, Holy *et al.* (2000) reported bone formation in vitro on PLGA with pores ranging from 1.5-2.2 mm. Jin *et al.* (2000) reported bone formation after 3 weeks in vivo in honeycomb hydroxypatite scaffolds with tunnels 110 μm diameter. Whether bone can grow in a wide range of pore sizes, or other factors are controlling the growth is not clear at present. Another consideration is the change in pore size with degradation (Cohen *et al.* 1991) and cell invasion.

The surface topography of the material also effects bone growth. Microporosity due to the molecular structure of the material as well as well grooves and roughness

appear to affect bone growth (Boyan *et al.* 1996; Schwartz *et al.* 1999; Schwartz *et al.* 2001). Dalby *et al.* (2002) showed that initial attachment of osteoblasts is dependent on the topography of the material. The comparison used was between machined and alumina roughened HAPEX™, and thermanox tissue culture control coverslips. While the more regular topography of the roughened surface proved to be better for initial attachment compared with the machined sample (the coverslips however were superior to both), the roughened surface also had more hydroxyapatite (HA) exposed. It was previously shown that a greater HA/PE ratio lead to greater initial cell adhesion (Silvio *et al.* 2002), whereas an early paper (Dalby *et al.* 2000) concluded the topography also affected osteoblast attachment and proliferation. Gray *et al.* (1996) studied rat osteoblast cultures on Phyester dentine, either intact or with a grid of grooves cut into it. The results showed that the topography affects the siting, timing and extent of new bone formation, and also orientation (osteocyte lacunae were often aligned along the axis of the groove or the edge of the dish or slab of tissue). However, Wan *et al.* (2005) studied the effect on osteoblast-like cells of PLA with pit and island topography and concluded that the patterned surfaces did not significantly enhance cell proliferation compared to the smooth controls.

Surface Modification of Scaffolds

Surface modification allows cellular functions to be enhanced and manipulated to improve tissue development on bioactive materials, and the potential use of materials with good scaffold properties but poor cell culture properties, albeit temporary if the scaffold itself is biodegradable (Yang *et al.* 2002). It has been observed that for a given adhesion protein the underlying substrate substantially effects its effectiveness (Klee *et al.* 2003). Stephansson *et al.* (2002) found that different substrates coated with fibronectin showed no differences with adhesion, proliferation or morphology, but significant differences with differentiation, shown by alkaline phosphatase activity and mineralisation. The substrates treated with fibronectin that supported differentiated cultures (shown in order of the greatest differentiation first) were collagen-coated tissue culture polystyrene > tissue culture polystyrene > untreated polystyrene.

Scaffold surfaces can be modified by using composite materials, as described above or with the use of adherence proteins. Fibronectin is an extracellular matrix protein

and has successfully been used to enhance bone cell attachment and proliferation on PLGA, PLA and PVDF (Yang *et al.* 2001; Klee *et al.* 2003). Fibronectin, along with other matrix proteins, carry the amino acid sequence arginine-glycine-aspartic acid (RGD) which cells bind to using integrins (Klee *et al.* 2003). Another extracellular matrix-associated protein, pleiotropin, known to act as a target for the deposition of new bone, was found to promote adhesion, migration, proliferation and differentiation of osteoporgenitor cells when coated onto PLGA (Yang *et al.* 2003). Another method of surface modification is plasma treatment which involves using nonpolymerising gases to create reactive sites on polymers (Wan *et al.* 2003). Cell retention on PLA under fluid shear forces was improved with plasma treatment, suggesting that the process improves the surface for adhesion (Wan *et al.* 2003).

2.3.4 CULTURE SYSTEMS AND BIOREACTORS

Tissue culture systems for adherent cells have traditionally been 2D such as the T-flask and well-plate. The cells are grown in a static environment and nutrients given semi-batch. These static systems have limitations that arise from their non-homogeneous nature. Without mixing, concentration gradients of pH, nutrients, toxins, gases and growth factors will occur in the culture medium (Collins *et al.* 1998). This will give rise to different cell behaviour in different spatial locations in the culture and reduce culture reproducibility. It has been documented that the behaviour of cells in 2D can be very different in 3D culture (Abbott 2003) and this has important implications for the in vitro generation of functional human tissues (Ellis *et al.* 2005).

The main bioreactor configurations are stirred tanks, fixed beds, packed beds, fluidised beds and membrane bioreactors. Below are examples of each configuration that have been used, or could potentially be used, in bone tissue engineering. Examples of membrane bioreactors can be found in Section 2.4.4.

Table 2.6 below summarises some important properties of the most common bioreactor configurations.

Table 2.6. Properties of culture systems.

Culture system	Media change	Mixing/Shear	Tissue development	Culture dimensions	Reactor size needed to grow a functional unit*	Reactor size needed to grow an organ**
Tissue culture flask	Batch	Poorly mixed No shear Diffusion	2D sheet	†290 cm^2/L †1 x 10^5 cell/ml	1-10 ml	10-1000 L
Stirred tank bioreactor	Batch or continuous	Well mixed Turbulent Convection	2D or 3D	†2,800 cm^2/L †5 x 10^5 cell/ml	0.2-2 ml	2-200 L
Packed bed bioreactor	Continuous feed (perfusion)	Well mixed Convection Laminar flow	3D	†18,000 cm^2/L †2.5 x 10^6 cell/ml	40-400 µl	0.4-40 L
Fluidised bed bioreactor	Continuous feed (perfusion)	Well mixed Convection Laminar flow	3D	†25,000-70,000 cm^2/L †5-6 x 10^6 cell/ml	20-200 µl	0.2-20 L
Membrane bioreactor	Continuous feed	Well mixed Laminar flow convection and solution diffusion	3D	100,000-200,000 cm^2/L †2 x 10^8 cell/ml	0. 5-5 µl	0.005-0.5 L

† (Scragg 1991)

*A typical functional subunit contains 10^2-10^3 cells (Palsson 2000)

**A typical organ contains a few hundred million subunits or 10^9-10^{11} cells

Flat Bed

Flat bed cell culture bioreactors are typically a number of 2D plates which are seeded with cells and placed in a module, the media is then passed over the plates. Traditional cell culture plates can be thought of as batch fixed bed bioreactors (Figure 2.18 A). The CellCube is a disposable bioreactor for anchorage-dependent cell culture, the configuration resembles a plate and frame arrangement with 26 polystyrene plates stacked 1 mm apart (Figure 2.18 B). Despite a large surface area:volume ratio typical of such a configuration, it was found that cell distribution was not uniform due to the fluid dynamics that arose from the operating conditions (Aunins *et al.* 2003).

Stirred Tank

A stirred tank consists of a vessel of media that is continuously mixed with a mechanical agitator. A stirred tank can be operated as batch or continuous and are particularly suited for reactions where good mass transfer is required since the agitation is controllable (Sinnott 1998) and media within the vessel is well mixed. A traditional cell culture bioreactor is the stirrer flask (Figure 2.19). Either the construct itself is fixed onto the agitator and rotated, or the media is mixed, for example with a magnetic flea. Roller bottles are another example of stirred tanks; they have cells attached over the entire wall and the rotation of the vessel allows media to reach all the cells. Modifications to traditional stirred tanks include the Wave Bioreactor™ which contains a disosable CellBag™ in which nonadherent cell, or potentially micorcoarriers, are housed, the media is mixed by a rocking motion (Weber *et al.* 2002). Qi *et al.* (2003) developed a membrane aeration device using silicon tubular membranes in a stirred tank. The most common and well known stirred tank bioreactor in bone tissue engineering and tissue engineering in general is the rotating wall bioreactors (RWB). RWB were first developed by NASA (Granet *et al.* 1998) (Figure 2.20 C), they are now commercially available, marketed by Synthecon (Houston, TX, USA) and modifications have also been devised such as the rotating oxygen-permeable bioreactor system (ROBS) (Terai *et al.* 2002) (Figure 2.20 A & B). The principle is based on a stirred tank with the centrifugal force creating an environment with only microgravitational forces due to the movement of the media with the wall (Granet *et al.* 1998).

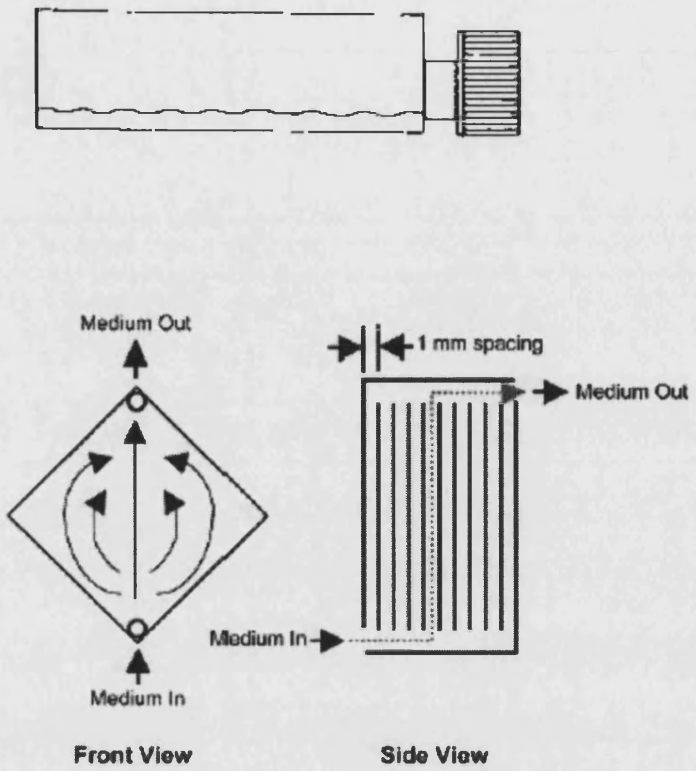

Figure 2.18. Flat bed bioreactors.
(A) Tissue culture polystyrene flask (Scragg 1991). (B) Schematic of the CellCube disposable bioreactor. Front view shows general features of fluid flow patterns in the bioreactor, side view shows bulk fluid movement through bioreactor (Aunins *et al.* 2003).

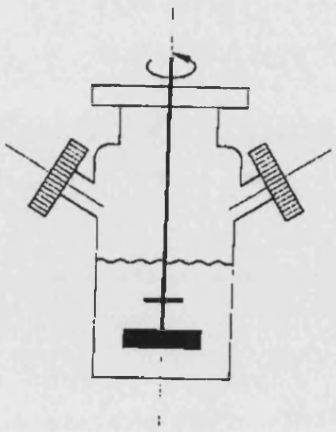

Figure 2.19. A Traditional stirred tank for cell culture-the Spinner Flask.
(Scragg 1991).

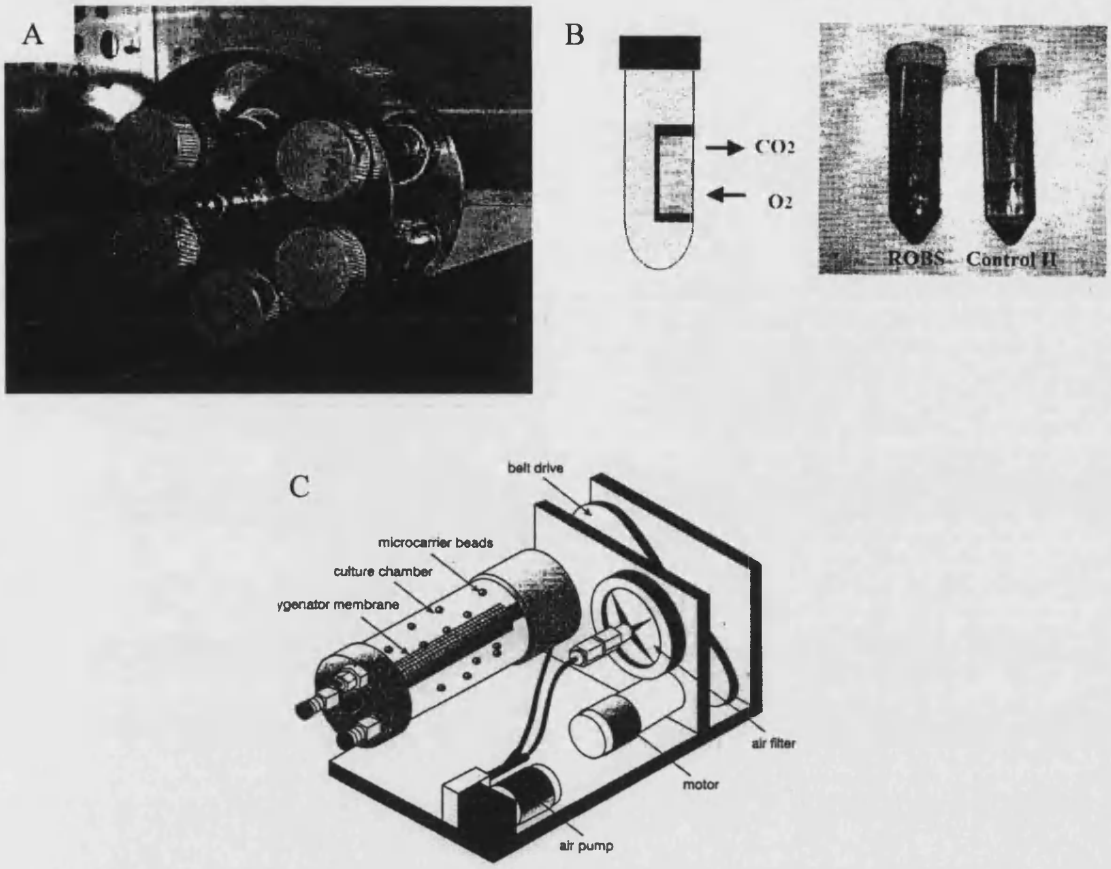

Figure 2.20. Rotating wall bioreactors.

(A) ROBS system, (B) ROBS module, (Terai *et al.* 2002), (C) The original RWB (Granet *et al.* 1998).

Sikavitsas *et al.* (2002) compared proliferation and differentiation towards the osteoblastic lineage of MSC in 75:25 foam scaffolds. The scaffolds were seeded and then maintained in either static culture, a spinner flask or a rotating wall vessel. Enhanced proliferation and differentiation was found in the spinner flask compared to the other culture systems. Despite this, cells and mineralisation were concentrated near the surface of the scaffolds suggesting the likelihood of concentration gradients within the construct.

Packed Bed

A packed bed bioreactor (sometimes known as a fixed bed bioreactor (Coulson *et al.* 1996)) contains a bed of multiple particles or a single porous block. Media is fed into the bioreactor and passes through the packing (Figure 2.21). A packed bed bioreactor

system designed specifically for bone tissue engineering was developed by Bancroft *et al.* (2003) (Figure 2.22). The bioreactor system was previously used by Goldstein *et al.* (2001) and compared to static culture, a rotary vessel and a spinner flask. Osteoblastic cells were seeded drop-wise onto the porous 75:25 PLGA foam scaffold then placed into the culture systems the following day. Cell numbers were found to be similar in all three systems after 7 and 14 days, however, a more uniform distribution and higher ALP activity was found in the flow systems.

A packed bed that allows oscillating perfusion was developed by Wendt *et al.* (2003). Instead of a traditional peristaltic pump, an oscillatory pump was used, allowing dynamic seeding as well as perfusion through the scaffolds (Figure 2.23).

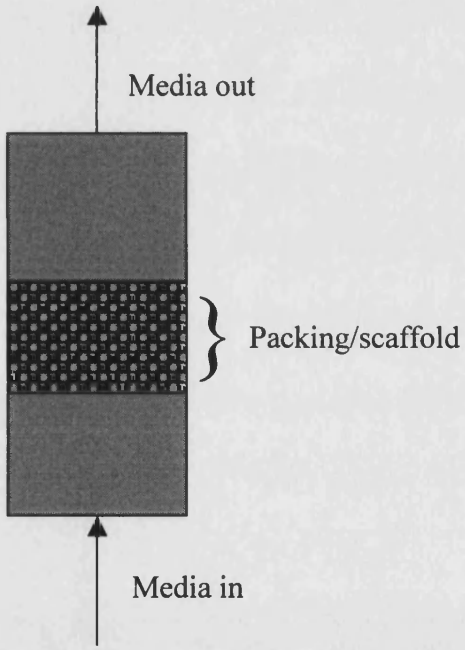

Figure 2.21. Schematic drawing of a packed bed bioreactor.

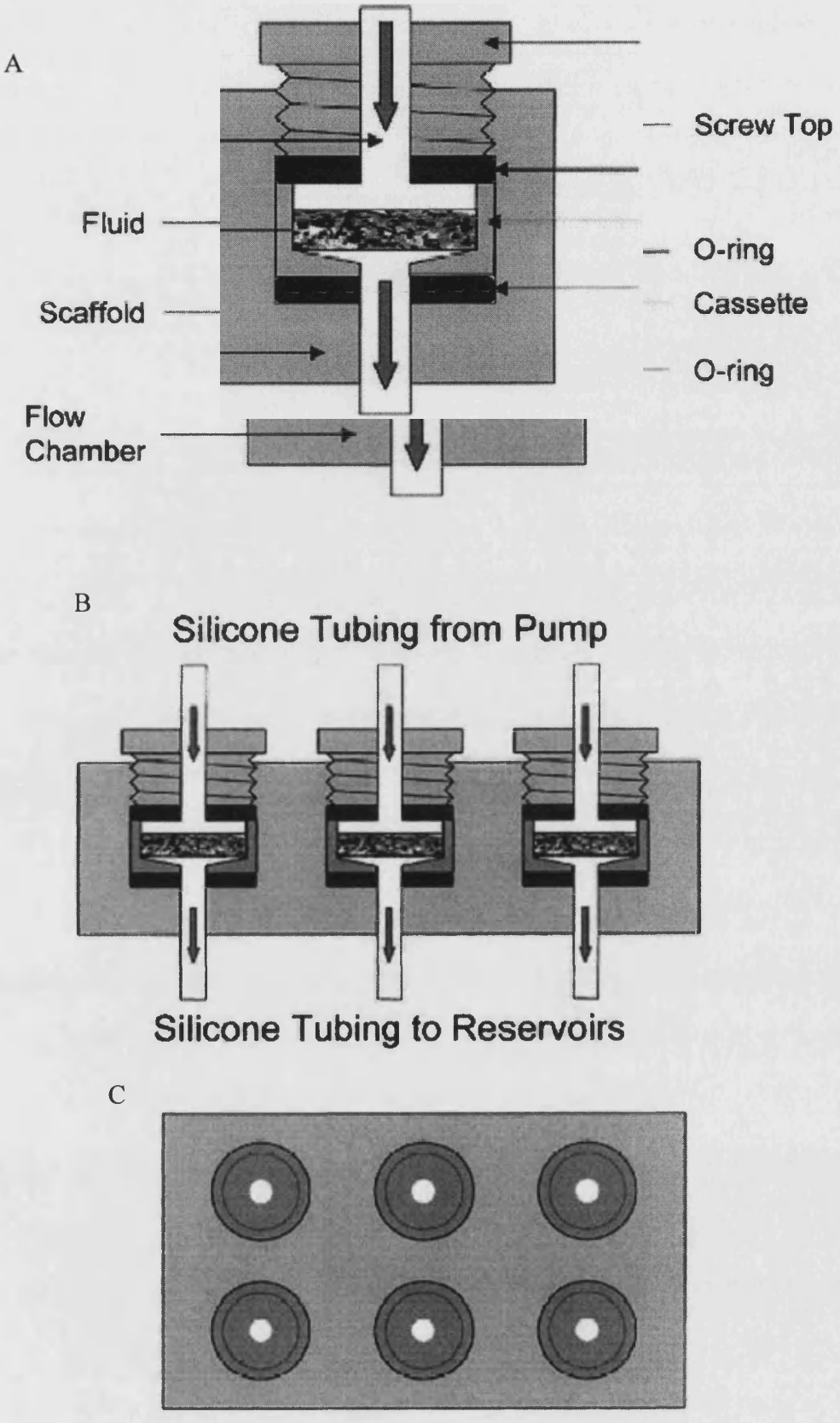

Figure 2.22. A bone tissue engineering-specific 'Flow Perfusion Bioreactor System' which uses 6 parallel packed beds.
(A) module detail, (B) side view, (C) top view. (Bancroft *et al.* 2003).

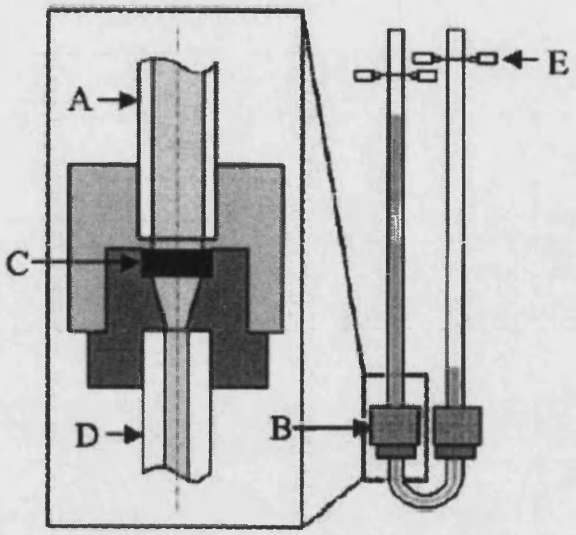

Figure 2.23. Oscillating perfusion bioreactor.
The cell suspension oscillates between the two glass columns (A), flowing through the sample chamber (B), scaffold (C), and U-tube (D). The direction of flow reverses when the cell suspension reaches the level of the sensors (E). (Wendt *et al.* 2003).

Fluidised Bed

A fluidised bed bioreactor contains particles that are suspended by the upward flow of the media (Figure 2.24). This promotes good mixing and high rates of mass transfer (Sinnott 1998). Fluidised beds can only be used with relatively small particles, such as microspheres, otherwise the media flow rate would be high leading to increased shear and operating costs.

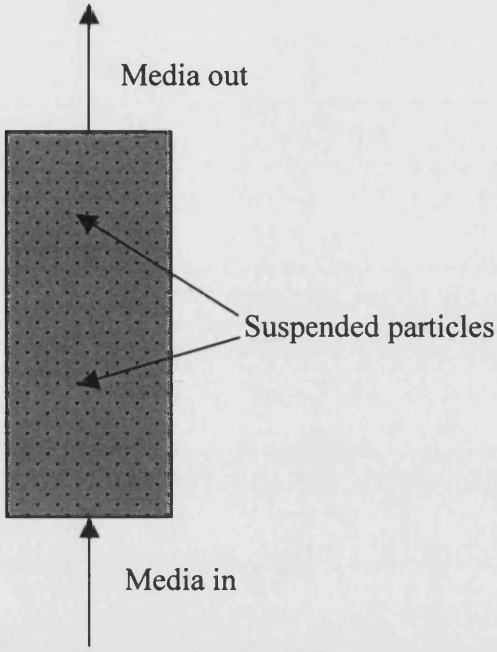

Figure 2.24. Schematic drawing of a fluidised bed bioreactor.

2.4 NEW SOLUTIONS FOR BONE TISSUE ENGINEERING USING MEMBRANE TECHNOLOGY

A membrane is defined as a selective barrier so is ideal as a scaffold; the cells are 'retained' on the surface while nutrients and waste products can pass freely across the membrane. The maximum pore size is 5 μm as cells can enter spaces larger than this (Beresford 2002) while the largest molecules required to pass across the membrane are approximately 150 kDa (Kumar *et al.* 2004) (0.1 μm ~ 1000 kDa (Planchamp *et al.* (2003)).

2.4.1 PROPERTIES OF MEMBRANES

Membranes can be classified in a number of ways and have a variety of structures to which the properties are directly related. A brief description is given here while for a more detailed discussion on membrane classification and structure the reader is referred to Mulder (1992).

Membrane materials can be biological or synthetic; biological membranes can be living or non-living, synthetic membranes can be organic or inorganic. Membrane

structure can be symmetric or asymmetric; symmetric membranes can be cylindrical porous, porous or homogeneous, asymmetric membranes can be porous, porous with a dense top layer or composite which have a dense top layer made of one material and a porous sublayer of another material. The material and its properties, the membrane morphology and pore size as well as the driving force will determine the application. Typically porous membranes are used for micro- and ultra-filtration, nonporous (dense) membranes for gas separation and pervaporation and liquid membranes for carrier-mediated transport.

2.4.2 MEMBRANE SYNTHESIS AND MANUFACTURE

There are many synthetic membrane fabrication techniques and the material determines their suitability. Techniques include sintering, stretching, track-etching, coating and phase inversion (Mulder 1992). Phase inversion casting allows a wide variety of morphologies to be obtained and is the most common method used to produce commercially available membranes (Mulder 1992). The process involves a polymer in the liquid state becoming a solid state; this can be done by a number of techniques including solvent evaporation, thermally induced phase separation (TIPS) and immersion precipitation (Mulder 1992).

Immersion Precipitation

Phase inversion membrane casting by immersion precipitation involves three components; the polymer, the solvent and the nonsolvent. The polymer is dissolved in the solvent to form a solution, called the 'casting-' or 'spinning dope'. The nonsolvent is a liquid that is miscible with the solvent but immiscible with the polymer. Casting involves a polymer-solvent solution being fed into a nonsolvent bath. The solvent moves into the nonsolvent and the nonsolvent into the polymer-solvent solution. Once phase inversion is complete, a solid-phase membrane will be present in a solution rich in nonsolvent. The resulting structure of the membrane depends on the mechanism of membrane formation, which in turn depends on the interactions of the three components of the ternary system.

Mechanisms and Resulting Structure of Membrane Formation by Phase Inversion

In simple terms, phase inversion involves dissolving a solid polymer in a solvent to form a liquid solution, then in the case of immersion precipitation, adding a

nonsolvent which causes the polymer to precipitate out of solution to form a solid structure. While membrane design evolves around modifying the structure to suit the application, the exact mechanisms of formation are still not fully understood. Park *et al.* (1999) and Xu and Qusay (2004) reference a number of publications that describe the theories of membrane formation by phase inversion. The porous structure of membranes is generally believed to arise from liquid-liquid demixing, by either nucleation and growth or spinodal decomposition, or a combination of both. The rate of the demixing mechanism leads to either an asymmetric cross section with finger-like pores or a sponge-like structure (Mulder 1992).

Liquid-liquid demixing can be described with the aid of a phase diagram which relates solution composition, temperature and solution state. A phase diagram can be 2D if the system contains 2 components (Figure 2.25) or 3D if the system contains 3 components (Figure 2.26).

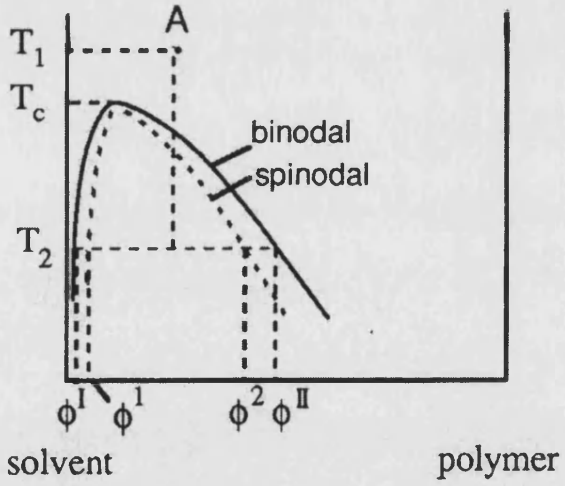

Figure 2.25. Binary mixture phase diagram.
The diagram shows how demixing can occur by decreasing the temperature (Mulder 1992).

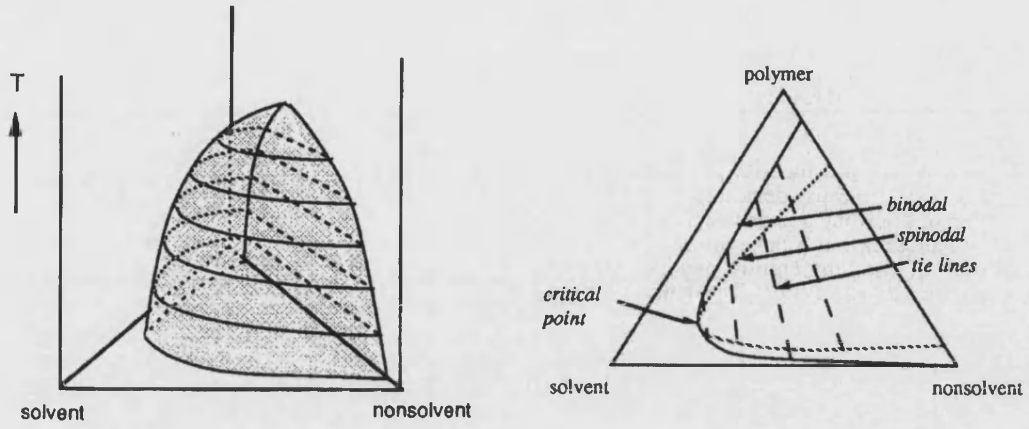

Figure 2.26. Ternary system phase diagram.
3D phase diagram showing binodal surface at different temperatures (T) on the left, and 2D, isothermal phase diagram on the right (Mulder 1992).

Liquid-liquid demixing of a solution will occur when the binodal is reached. The binodal can be reached either by a drop in temperature (Figure 2.25), or by the addition of another component, the nonsolvent (Figure 2.26). Above a critical temperature T_c a solution containing any concentration of polymer and solvent will be completely miscible, such as Solution A at temperature T_1 (Figure 2.25). If the temperature of Solution A is lowered from T_1 to T_2, the binodal will eventually be reached and the solution will demix into two liquid phases, one rich and one poor in polymer. This process is called liquid-liquid demixing. The temperature at which the binodal is reached is dependant on the polymer concentration in the solvent. Similarly, if a ternary system is used, the polymer, solvent and nonsolvent will be miscible in any combination of concentrations above the critical temperature (Figure 2.26). When the binodal is reached, either by a drop in temperature or change in concentration combination, liquid-liquid demixing occurs and two liquid phases are formed, again one rich and one poor in polymer. The composition of these two phases at temperature T_2 are linked by a tie line.

For concentrations Φ where $\Phi^1<\Phi<\Phi^2$, where Φ^1 and Φ^2 lie on the spinodal, the solution is thermodynamically unstable. If the solution is thermodynamically unstable, it will demix spontaneously into very small interconnected regions with fluctuating composition. The amplitude of these fluctuations increases with time and

results in a 'lacy' structured membrane; this is spinodal decomposition and solution A will undergo this type of liquid-liquid demixing at T_2.

For concentrations Φ where $\Phi^{I}<\Phi<\Phi^{1}$ and $\Phi^{2}<\Phi<\Phi^{II}$, the solution is metastable. A metastable solution is stable with respect to small fluctuations and does not spontaneously demix, but demixing occurs when a stable nucleus has formed. This will occur near compositions Φ^{I} and Φ^{II}. The nucleus grows by downhill diffusion, this is nucleation and growth, the final structure will depend on the initial polymer-solvent concentration. a dilute polymer solution will form a 'latex' type structure whereas an open porous structure is likely to form with a high polymer concentration (Mulder 1992).

The structure is also governed by whether the liquid-liquid demixing is delayed or instantaneous. Instantaneous demixing leads to a porous top layer whereas delayed mixing leads to a dense top layer. Exposure to air will induce a separate demixing mechanism at the surface, and while this does not affect the type of demixing once the nonsolvent is added, the morphology will be altered because of the formation of the top layer. Instantaneous demixing often results in membranes containing macrovoids (Mulder 1992; Li *et al.* 2004). Macrovoids are large teardrop shaped pores extending from the top layer through a large section of the membrane wall, able to form due to a stable polymer solution underneath the nuclei so no new nuclei form allowing the top nuclei to continue to grow down. Li *et al.* (2004) suggest that macrovoids are a transition stage between a sponge-like and finger-like structure, the transition being dependent on membrane thickness (Li *et al.* 2004). Although macrovoids are generally not favourable as they can be weaknesses in the structure (Mulder 1992), they pose no resistance to mass transfer and may be beneficial in some applications because of this.

The transport properties of porous membranes formed by immersion precipitation are dependent on the solvent-nonsolvent combination, unlike nonporous membranes cast using the same process where the chemical structure of the polymer is important (Mulder 1992).

2.4.3 MEMBRANE CHARACTERISATION

The methods used to characterise membranes are largely dependent on whether the structure is porous or nonporous. Porous membrane separation process involve a sieving mechanism, meaning the most important properties are the pore size, pore size distribution and pore geometry. The main characterisation techniques used are scanning electron microscopy (SEM), bubble-point measurements, mercury porometry and permeation measurements (Mulder 1992). For membranes used as scaffolds, atomic force microscopy (AFM) allows the surface topography to be characterised.

2.4.4 MEMBRANE BIOREACTOR CONFIGURATIONS FOR TISSUE ENGINEERING

Membrane bioreactors are considered the best configuration to increase biological performance of cell-based systems (Mercier-Bonin *et al.* 2001). Due to the separation of the cell population and the media feed stream, no cell mass is unnecessarily lost from the system (Mercier-Bonin *et al.* 2001). Other benefits of membrane bioreactors, compared to stirred bioreactors and those which are aerated by micro-sparging with a gas stream, are that the high rates of agitation and oxygen delivery which can damage the cells are avoided; the agitation increases shear forces as does the bubble break-up (Millward *et al.* 1996; Qi *et al.* 2003).

Membrane bioreactor configurations can be based on flat sheets or tubular membrane structures. Flat sheet membrane configurations can be 'plate-and-frame' or 'spiral-wound' (Figure 2.27). Flat sheet bioreactors contain modules in which membranes sheets are separated by a spacer. Spiral-wound bioreactors contain modules with a plate and frame set up wrapped around a pipe for permeate collection. Tubular configurations are classed based on the tube diameter as shown in Table 2.7.

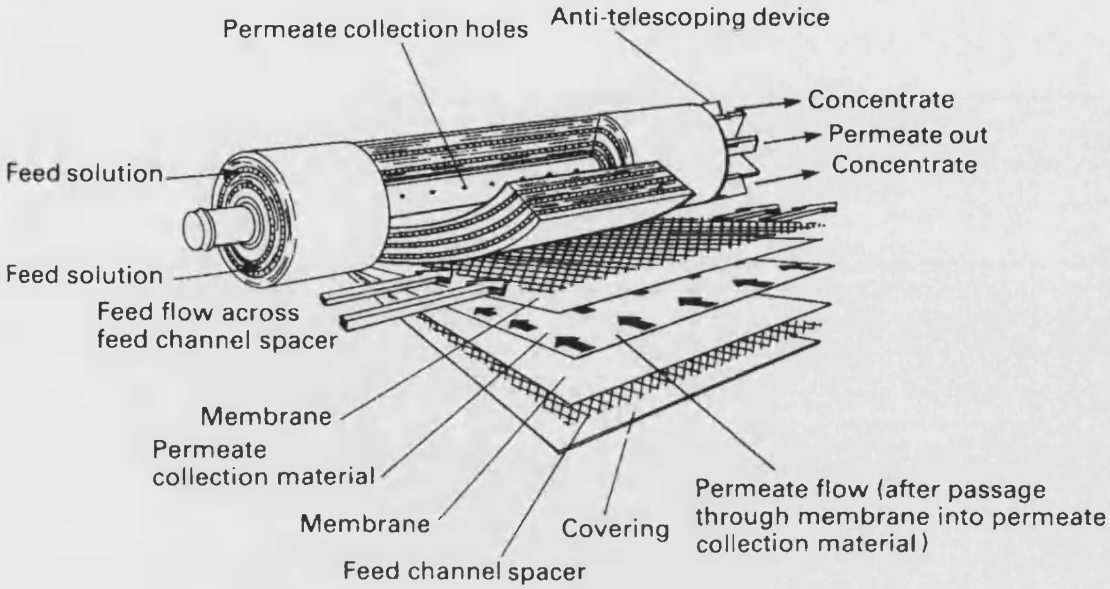

Figure 2.27. Schematic of a spiral-wound membrane module.
(Coulson et al. 1996).

Table 2.7. Size classification of tubular membranes.

Configuration	Diameter (mm)
Tubular	> 10.0
Capillary	0.5-10.0
Hollow fibre	< 0.5

Data from (Mulder 1992).

Tubular modules contain supported tubes with the feed flowing through the tube, the permeate flowing across the tube wall into the module housing. Capillary and hollow fibre modules contain unsupported tubes and feed can flow through the lumen with permeate passing into the module housing, or vice versa. The tendency for fouling of hollow fibre bioreactors is high for typical applications, including artificial liver by the media in vitro, or blood and plasma in vivo (MacDonald *et al.* 2001; Mercier-Bonin *et al.* 2001). Despite this, hollow fibre bioreactors have been extensively used for enzyme, yeast and bacteria cultures as well as mammalian cell culture (Brotherton and Chau 1996). With regards to tissue engineering, the use of membrane bioreactors have only been widely used in liver tissue engineering. Haemodyalisis machines,

which have been in use for many years, are hollow fibre bioreactors, this configuration along with sprouted bed and flat bed configurations have been implemented for liver tissue engineering (Bader *et al.* 1995). Hollow fibre bioreactors are the most common configuration for tissue engineered liver and the review by Planchamp *et al.* (2003) provides an excellent overview of this application. Interestingly, the methods of seeding vary; seeding hepatocytes in the lumen of the fibre, usually combined with embedding of the cells for example in collagen gel is common (Nyberg *et al.* 1993). Seeding directly onto the shell side of the fibres has also been used (Moussy 2003). Like osteoblasts, hepatocytes are anchorage dependent so attachment improves their activity and viability (Planchamp *et al.* 2003). The chemical and physical properties and intrinsic structure of the membranes are recognized to affect the hepatocyte culture, different materials and coatings have been used in an attempt to optimise the hollow fibres. A comparison of the different microenvironments utilized in hollow fibre bioreactors is summarised in Table 2.8.

2.4.5 MEMBRANE BIOREACTOR CONFIGURATION FOR BONE TISSUE ENGINEERING

In the case of bone, a 3D tubular structure would most closely resemble that of the tissue. Whereas bone has osteons as functional units in which the Haversian c anal feeds nutrients to and removes waste products from the surrounding tissue, the lumen supplies and removes the nutrients to and waste products from the cells on the shell-side surface of the hollow fibre membrane. As for all tissue engineering applications, a large surface area: volume ratio, also known as the packing density, not only provides the more efficient culture system but allows a relatively greater cell population to develop. It can be seen in Table 2.8 than a hollow fibre bioreactor has a very high packing density compared to the other configurations and is, of course, tubular. In addition, the cost is low for both capital investment and operation.

Table 2.8. Adherent-dependent cell microenvironments utilized in hollow fibre bioreactors.

Cell microenvironment	Advantage	Disadvantage
Cell suspension / aggregates	▪ Quick and simple ▪ Loading can be done with high cell numbers ▪ Represents a homogeneous population with cellular density, activity and function comparable to in vivo	▪ The isolation causes loss of polarity leading to structural and functional operations. This limits in functionality and viability to a few hours of culture only.
Cell adhesion	▪ Improves viability and function ▪ Nutrients and waste products are immediately taken to and from the cells*	▪ Relatively low cellular density dependent on surface area of membrane
Gel embedding	▪ Increased surface area for cell support yields a higher cell density with improved functionality	▪ Steep concentration gradients (limited mass transfer of nutrients and accumulation of toxic metabolites) can occur in the gel layer resulting in necrosis
Microcarriers	▪ Increase surface area compared to membrane attachment alone ▪ Cell-microcarrier constructs can be cryopreserved	▪ Volume taken up by microcarriers*
Microencapsulation	▪ Increase surface area compared to membrane attachment alone ▪ Cell-microcarrier constructs can be cryopreserved	▪ Mass transfer limitations for high-molecular-weight substances such as secreted plasma proteins

Data is based on examples for hepatocytes in Planchamp *et al.* (2003) except those marked with an astrix*.

Table 2.9. Common design considerations for membrane bioreactors.

	Packing density	Fouling tendency	Investment	Operating cost
Plate-and-frame	100-400 m^2/m^3	Low	High	High
Spiral-wound	300-1000 m^2/m^3	Medium	Medium	Medium
Tubular	<300 m^2/m^3	Very low	Very high	Very high
Capillary	600-1200 m^2/m^3	High	Low	Low
Hollow fibre	Up to 30,000 m^2/m^3	Very high	Very low	Very low

Data from (Mulder 1992).

2.7 CONCLUSIONS

A vast number of materials and fabrication methods have been used to manufacture scaffolds for bone tissue engineering, PLGA foams being the most common. There are also a variety of bioreactors available, the packed bed and the rotating wall bioreactor configurations being having the widest use. While there have been many advancements in the field of tissue engineering, there has been no scaffold designed in conjunction with a specific bioreactor configuration, and the mass transfer limitations found with constructs of a useful clinical size have not yet been overcome.

2.8 AIM & OBJECTIVES

The aim of the thesis was to address the issue of mass transfer limitations of current scaffolds used in tissue engineering by designing, manufacturing and evaluating a novel scaffold which was also designed with a bioreactor configuration in mind. It was hypothesised that a PLGA hollow fibre membrane scaffold and a hollow fibre bioreactor would meet this aim.

The work carried out was designed to meet the following objectives.

- Selection of a PLGA-solvent-nonsolvent system to spin hollow fibre membranes.
- Manufacture the hollow fibre membrane scaffold and optimise the spinning conditions to give characteristics suitable for cell culture.
- Assess the suitability of PLGA membranes with the processing methods required for a scaffold.
- Assess the ability of the PLGA membranes with regards to bone-like cell culture.
- Evaluate the potential of the PLGA hollow fibre membrane bioreactor to support bone-like cell cultures.

CHAPTER THREE
MATERIALS & METHODS

3.1 INTRODUCTION

This chapter details the materials and methods used for the experimental work carried out in this thesis. The information in this chapter is generic to all the experimental work. Further details of reagent preparation can be found in Appendix A, and a list of equipment and consumables can be found in Appendix B.

3.2 MATERIALS

3.2.1 MATERIALS SUPPLIER LISTINGS

The materials used have been grouped into four subsections: cell culture; cell culture analysis; scaffold preparation and analysis; and flat sheet culture chamber and hollow fibre bioreactor components.

Table 3.1 Alphabetical list of materials used for cell culture

Material	Supplier	Catalogue number
ascorbate-2-phosphate	Sigma-Aldrich Company Ltd, Gillingham, UK	A8960
cadmium sulphate ($CdSO_4$)	Sigma-Aldrich	C3266
calcium chloride	Sigma-Aldrich	C3881
collagenase	Sigma-Aldrich	C0773
dexamethasone	Sigma-Aldrich	D4902
DMSO	Sigma-Aldrich	D2650
DNAse	Sigma-Aldrich	D4263

dulbecco's modification of minimum essential medium (DMEM) (glutamax)	InVitrogen Ltd, Paisley, UK	32430-027
fetal calf serum	Sigma-Aldrich	F7524
geneticin (G418)	Sigma-Aldrich	G9516
isopropanol	Sigma-Aldrich	I9516
non-essential amino acid (NEAA)	Sigma-Aldrich	M7145
penicillin/streptomycin solution (P/S)	Sigma-Aldrich	P0906
phosphate buffered saline (PBS)	Sigma-Aldrich	D8537
sodium pyruvate	InVitrogen Ltd	11360-039
trypsin-EDTA solution	Sigma-Aldrich	T4174
zinc sulphate ($ZnSO_4$)	Sigma-Aldrich	Z0251
β-glycerophosphate	Sigma-Aldrich	G9891

Table 3.2 Alphabetical list of materials used for cell culture analysis

Material	**Supplier**	**Catalogue number**
AMP (Alkaline buffer solution)	Sigma-Aldrich	221
boric acid	BDH Laboratory Supplies, Poole, BN15 1TD	27410
ethanol	Fisher Scientific UK Ltd, Loughbourough, UK	E/0600/17
fast red TR salt	Sigma-Aldrich	F2768
formalin	Sigma-Aldrich	F1635
Bostik Fast-Tak		
hydrochloric acid (HCl_{aq})	Sigma-Aldrich	H7020
methanol	Sigma-Aldrich	M3641
methylene blue	Sigma-Aldrich	M4159
MTT	Sigma-Aldrich	M2128
N,N-dimethylformamide (DMF)	Fluka (Sigma-Aldrich)	40240

sodium hydroxide (NaOH)	Sigma-Aldrich	S0899
napthol AS-MX	Sigma-Aldrich	N4875
pico green assay kit	Molecular Probes (InVitrogen Ltd)	P7589
picric acid	Sigma-Aldrich	925-40
p-nitrophenol standard solution	Sigma-Aldrich	104-1
p-nitrophenyl phosphate (pNPP)	Sigma-Aldrich	N4645
PNP standard	Sigma-Aldrich	104-1
sigma 104®	Sigma-Aldrich	104-100
sirius red (direct red)	Sigma-Aldrich	36554-8
sodium chloride (NaCl)	Sigma-Aldrich	S9888
triton X-100 (TX-100)	Sigma-Aldrich	T9284
trizma ® Hydrochloric acid (tris-HCl)	Sigma-Aldrich	T7149
trypan blue	InVitrogen Ltd	15250-061
von kossa reagent	Fluka (Sigma-Aldrich)	85193

Table 3.3 Alphabetical list of materials used for scaffold preparation, modification and analysis

Material	Supplier	Catalogue number
1,4-dioxane	Sigma-Aldrich	27,053-9
1-methyl-2-pyrrolidinone (NMP)	Acros Organics (Fisher Scientific UK Ltd, Loughbourough, UK)	12763-0025
ethanol	Fisher Scientific UK Ltd	E/0600/17
fibronectin	Sigma-Aldrich	F2006
glacial acetic acid	Acros Organics	124040025
penicillin/streptomycin solution (P/S)	Sigma-Aldrich	P0906
phosphate buffered saline (PBS)	Sigma-Aldrich	D8537
poly(lactic-co-glycolic acid)	Alkermes, Inc.	

(PLGA)	6960 Cornell Road Cincinnati, Ohio 45242, USA	
sodium chloride	Sigma-Aldrich	S9888
sodium bicarbonate	Sigma-Aldrich	S6014
potassium chloride	Sigma-Aldrich	P9666
potassium hydrogen phosphate trihydrate	Sigma-Aldrich	221317
magnesium chloride hexahydrate	Sigma-Aldrich	M0250
calcium chloride dihydrate	Sigma-Aldrich	C3881
sodium sulphate	Fluka (Sigma-Aldrich)	71959
hydrochloric acid	Sigma-Aldrich	H7020
sodium hydroxide	Sigma-Aldrich	S0899
acetonitrile	Sigma-Aldrich	27,071-7
glycolic acid	Sigma-Aldrich	G8284
lactic acid	Sigma-Aldrich	L6402
sulphuric acid	Fissons	1830

Table 3.4. Alphabetical list of flat sheet membrane culture chamber and hollow fibre bioreactor components

Material	Supplier	Catalogue number
polycarbonate	Goodfellow Cambridge Ltd, Huntingdon, UK	593-123-92 (25 mm) 972-237-77 (5 mm)
silocone elastomer	Goodfellow Cambridge Ltd	947-690-83 (1 mm)
Araldite® Rapid (apoxy resin)	B&Q Ltd	Not applicable
hepa-vent filter disk >3um	Fisher Scientific UK Ltd	FDP-540-030X

3.2.2 SOURCE OF CELLS

The cell lines 560pMT1 and 560pZIPv.neo was produced and kindly donated by Dr Jon Beresford of the University of Bath, UK. The cell lines used were named based on the convention ###(donor)pXYZ(plasmid)SV.neo+. Hence 560pMT1SV.neo+ indicates that the cells were obtained from donor 560 and were transfected with the pMT1 plasmid that confers neomycin resistance and inducible expression of large T antigen under the control of a synthetic repeat of the mouse metallothionein promoter. + indicates that these cells are cultured in the presence of 10nM Dx as a standard supplement. 560pZIPv.neo are an sv40 transformed bone marrow stromal cell line generated in Jon Beresford's laboratory, from primary bone marrow stromal cells cultured in osteogenic medium (unpublished). The sv40 gene 'immortalises' the cell and they remain in the proliferation stage of the cell cycle. The names 560pMT1 and 560pZIPv.neo, denoting the donor and plasmid, are commonly used; in this project they are abbreviated to pMT and pZIP respectively. Primary osteoblasts were obtained from bone reamings donated by consenting elective surgery patients undergoing hip replacement at Southmead Hospital, Bristol.

3.3 EXPERIMENTAL METHODS

Experimental methods have been split into experimental and analytical, and these have been further divided into cell culture and scaffold subsections. The methods given are general, with specifics given in the relative results chapters (Chapters Four to Eight).

3.3.1 OBTAINING HUMAN BONE DERIVED CELLS FROM BONE REAMINGS

The bone reamings containing the human bone derived cells (HBDC) were obtained in 5 ml DMEM already finely chopped and washed in DMEM. Using a bone scoop, the bone reamings were divided into approximately 0.5 g aliquots, and placed into T75 tissue culture flasks along with 15 ml primary media (Section 3.3.3). The media was changed weekly until cells were visibly migrating from the bone chips; the media was then changed twice weekly. Once the cells were confluent, the cultures were passaged and maintained as detailed in Section 3.3.3 below. The cell lines were obtained as frozen samples having been stored in liquid nitrogen (Section 3.3.2).

3.3.2 FREEZING DOWN AND RAISING CELLS FROM CRYOSTORAGE

Cells were stored in liquid nitrogen until required for use. This was done by passaging and resuspending the cells at 5-10 x10^6 cells/500µl in 500 µl FCS. This cells suspension was aliquoted into cryovials to which 500 ml/vial of 40% (v/v) DMSO in DMEM was added drop-wise. The cryovials were then placed in a freezing container filled with isopropanol and placed into a –80 °C freezer immediately. The cryovials were then transferred to liquid nitrogen after 24 hours. When needed, a cryovial was removed from the liquid nitrogen and thawed under a running hot tap, shaking gently to distribute the heat. Once thawed, the content of the cryovial was added to a T75 tissue culture flask in 15 ml media. The media was changed after 6 hours to remove the DMSO in the solution and any dead cells. The cells were then maintained as detailed below in Section 3.3.3.

3.3.3 CELL CULTURE AND MAINTENANCE

Media Preparation

HBDC media contained DMEM Glutamax, supplemented with 10% (v/v) heat inactivated foetal calf serum (FCS), 1 mM sodium pyruvate, 100 µM Ascorbate-2-phosphate, 1% (v/v) non essential amino acid (NEAA) and 1% (v/v) pen/strep antibiotic. For 560pZIPv.neo culture, 10^{-8} M dexamethasone, and 50 µg/ml geneticin was also added. 560pMT1 media also contained 200 µm zinc sulphate and 1 µm cadmium sulphate. Details for how to make up 100 ml of media for each of the cell types can be found in Appendix A.

Cell Culture Procedures

Cell culture methods for the three cell types are the same, differing only in the media used. The following is based on procedures described in Beresford and Owen (1998) for a single T75 flask; for other culture vessels, volumes were altered according to the surface area of the substrate. Volumes of reagents given below are based on the stock solutions, details of which can be found in Appendix A.

The cultures were rinsed twice in DMEM then 5 ml collagenase solution (25 units/ml containing 2 mM filtered calcium chloride in DMEM) was added to the cells for 1 hour. The collagenase solution was removed and the cells rinsed twice

with PBS before adding 4 ml trypsin-EDTA for 5-10 minutes. The tryspin action was stopped by rinsing the T75 three times with 5ml DMEM into a flacon tube containing 100 µl DNase and 100 µl medium. The suspension was centrifuged at 200G for 5 minutes. The supernatant was aspirated off the resulting cell pellet. The tube was gently flicked to loosen the cells before adding 5 ml DMEM and further separating the cells with a needle and 5 ml syringe. Any remaining clumps were removed by then passing the solution through a cell filter into a fresh falcon tube. Cells were then seeded at a density of 20,000 or 25,000 cells/cm^2 for cell proliferation and maintained in a humidified environment at 37 °C and 5% CO_2. Media was changed twice a week and the cultures passaged after one week.

Mineralisation

Cells were cultured as above until day 7. β-glycerophosphate was added to the media at a concentration of 10 mM from day 7; the media continued to be changed twice weekly for a further two weeks.

3.3.4 CELL CULTURE ON FLAT SHEET MEMBRANES

Flat sheet membranes were prepared as detailed in Section 3.3.6. They were sterilised by submerging in 70% ethanol for 30 minutes, then rinsed twice with PBS. The chamber was then assembled and the membranes left to soak in complete media for 20-30 minutes (for chamber design see Section 3.4.1).

Cells were passaged and prepared as described in Section 3.3.3. Prior to seeding, 0.5ml fresh complete media was added to each membrane. The required number of cells was added to each membrane in 1 ml of complete media. The cells were maintained in a humidified environment at 37 °C and 5% CO_2 for 6 hours (attachment), 1 week (proliferation) or 3 weeks (mineralisation); media was changed twice weekly for the proliferation and mineralisation studies.

3.3.5 CELL CULTURE ON HOLLOW FIBRE MEMBRANES

Hollow fibre membranes were prepared as detailed in 3.3.6. They were sterilised by submerging in penicillin/streptomycin (P/S) solution overnight then rinsed twice with DMEM. The bioreactor was then assembled and the membranes left to soak in

complete media for 20-30 minutes. Cells were passaged and prepared as described in Section 3.3.3. When the membranes were ready to be seeded, the required number of cells was added to the bioreactor through a side port in 8 ml of complete media. The seeding solution was removed after 6 hours and fresh media was added to the bioreactor before connecting into the bioreactor system (Section 3.4.2).

3.3.6 MEMBRANE PREPARATION

Poly(lactide-co-glycolide) (PLGA) was used in a range of lactide:glycolide ratios. All polymers were GMP grade except PLLA, which was experimental grade. The solvents used were 1-methyl-2-pyrrolidinone (NMP) and 1,4-dioxane (dioxane), which were reagent grade and HPLC grade respectively.

Solution Preparation

The polymers were added to NMP or dioxane in airtight containers then placed in a water bath at 40°C. Once the solution temperature had equilibrated, they were moved onto a roller mixer and left overnight. The solutions were then placed back into the water bath at 40°C. This process was repeated until the polymer had completely dissolved and the solution appeared homogeneous by eye.

Flat Sheet Fabrication

The membranes were cast by pouring approximately 2 ml polymer solution onto a flat glass sheet (10 cm x 15 cm) and spreading it with a glass rod kept at a height of 200 μm from the glass sheet using 200 μm wire wrapped around a 1 cm diameter rod. The coated glass sheet was then submerged in deionised water at 25 °C. The water was changed at 6 hours and 24 hours after initial immersion to remove residual solvent.

Hollow Fibre Fabrication

Hollow fibres were prepared using a method based on that described in Wang *et al.* (1996) using the rig shown in Figure 3.1. The polymer was degassed under a vacuum for 1 hour to remove air bubbles. The coagulation bath and wash bath were filled with the nonsolvent, water, the temperature of the coagulation bath was set to 25°C. The spinning rig was set up with the holding tank and spinneret (needle 0.3 mm

outer diameter, bore 0.5 mm inner diameter) in place (Figure 3.1). The polymer solution was then added to the holding tank sealed with the 'O' ring and lid. The air supply to the holding tank was slowly increased to a pressure of 1.5 barg; the pressure required to cause the solution to flow is dependent on the viscosity of the solution. The take-up reel was wetted and started at a low rate of 20rpm (4.84 m/min). The polymer solution valve was gently opened by 45° and once the solution was flowing freely from the spinneret, the internal coagulant valve was released. The polymer solution and internal coagulation streams were allowed to settle before setting the take-up and internal coagulant rates. As the polymer solution valve was opened, both the internal coagulant and take-up rates were increased. Altering the height of the spinneret above the coagulation bath set the air gap. Calibrations for the spinning rig can be found in Appendix E.

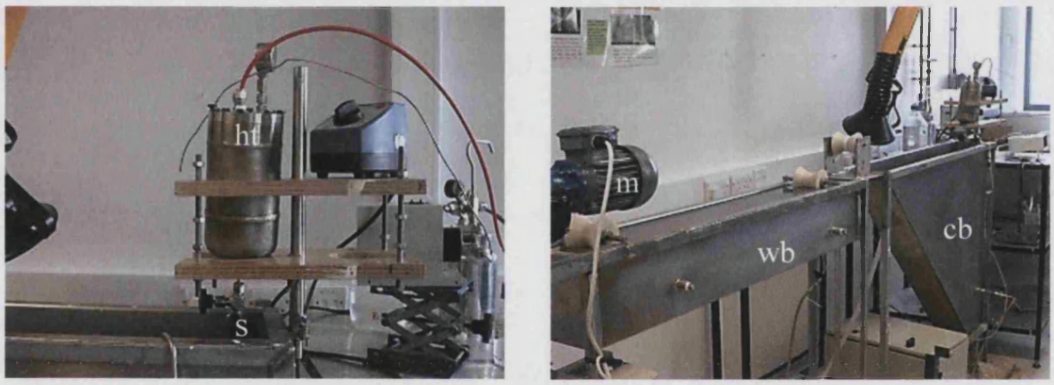

Figure 3.1. Spinning set up.
Holding tank (ht) and spinneret (s), coagulation bath (cb), wash bath (wb) and take-up reel motor (m).

Membrane Surface Modification

Simulated body fluid (SBF) was prepared at two concentrations (see Appendix A); '1SBF' for the nucleation phase and '1.5SBF' for the growth phase, and adjusted to pH 7.25 (Miyaji *et al.* 1999; Gomes *et al.* 2001). The SBF was filtered and steam sterilised at 121 °C and 1.5 barg for 20 minutes. Bioactive glass was crushed to a fine powder and steam sterilised at 121 °C and 1.5 barg for 20 minutes. Once cooled, glass was added to 6-well plates in a thin layer covering the base of the well to act as

the nucleating agent. Membrane samples were cut to 4 cm^2 and placed into the 6-well plates, held in place with transwell® inserts then 2 ml of 1SBF was added to each well. The nucleation phase was 1 day and maintained at 37 °C and 5% CO_2. After day 1, the glass was removed and 1.5SBF was added to the samples and changed twice a day (Figure 3.2). Growth was allowed to persist for 10 days maintained at 37 °C and 5% CO_2; samples were analysed at 2, 4, 6 and 10 days.

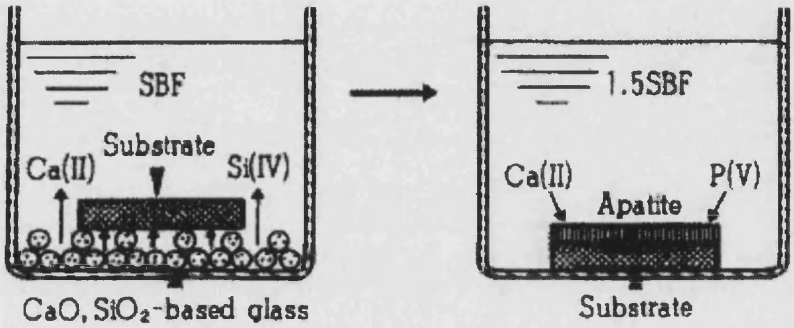

Figure 3.2. Nucleation (left) and growth (right) of apatite on organic polymer substrate.
(Kokubo 1998).

3.4 CULTURE SYSTEM & BIOREACTOR DESIGN AND MANUFACTURE

3.4.1 FLAT SHEET MEMBRANE CULTURE CHAMBER DESIGN AND MANUFACTURE

Cell culture on flat sheet membranes was carried out in a specially designed culture chamber (Figure 3.3), which held the membranes flat, exposing a specific culture surface of know area (3.83 cm^2). This surface area size was chosen as it is comparable with standard 12-well tissue culture polystyrene plates.

The chambers were made from polycarbonate and consisted of two parts connected with screw and sealed with a silicon rubber gasket. Once the chamber had been assembled, seeding and feeding could be carried out through the port which was sealed using a hepa-vent filter disk. All chamber components were steam sterilised in a Boxer autoclave (1.5 barg, 20 minutes, 121 °C).

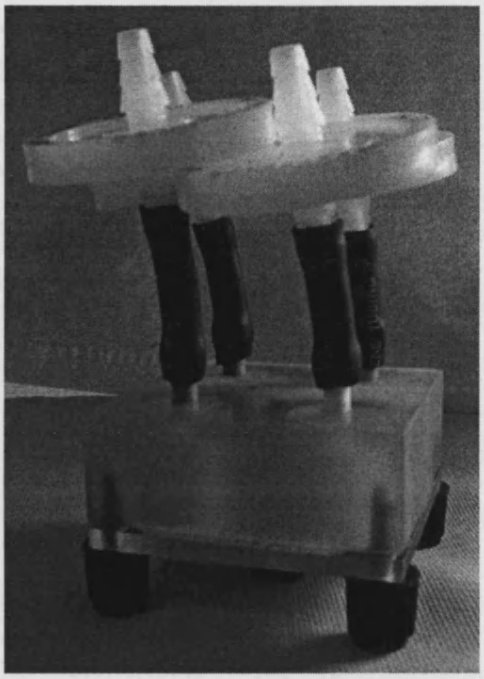

Figure 3.3. Photograph of flat sheet membrane culture chamber.

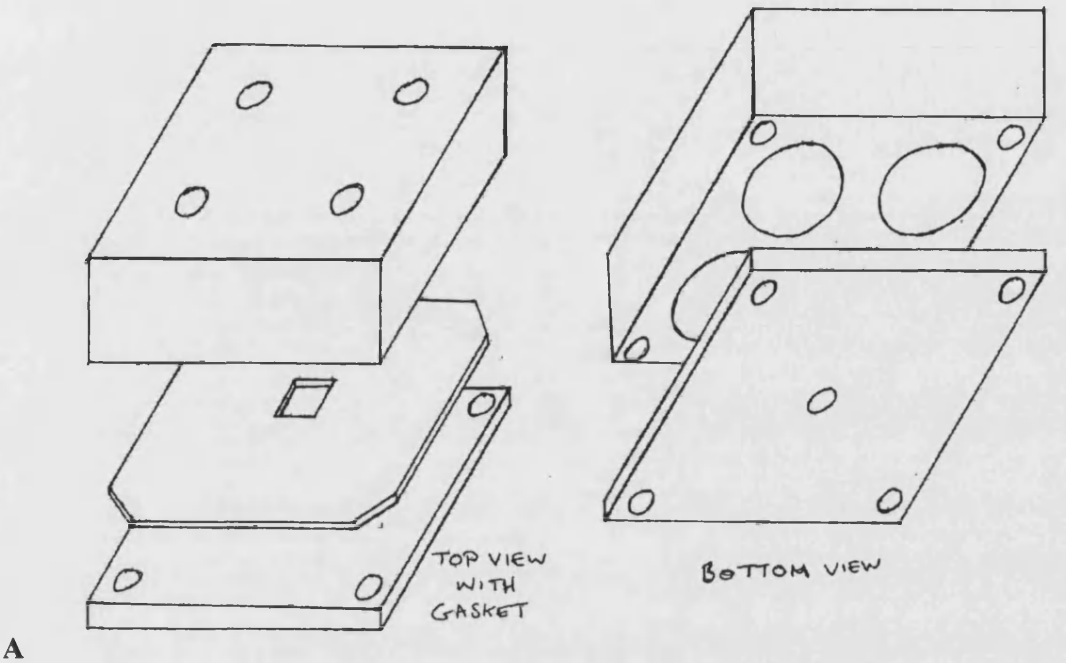

A

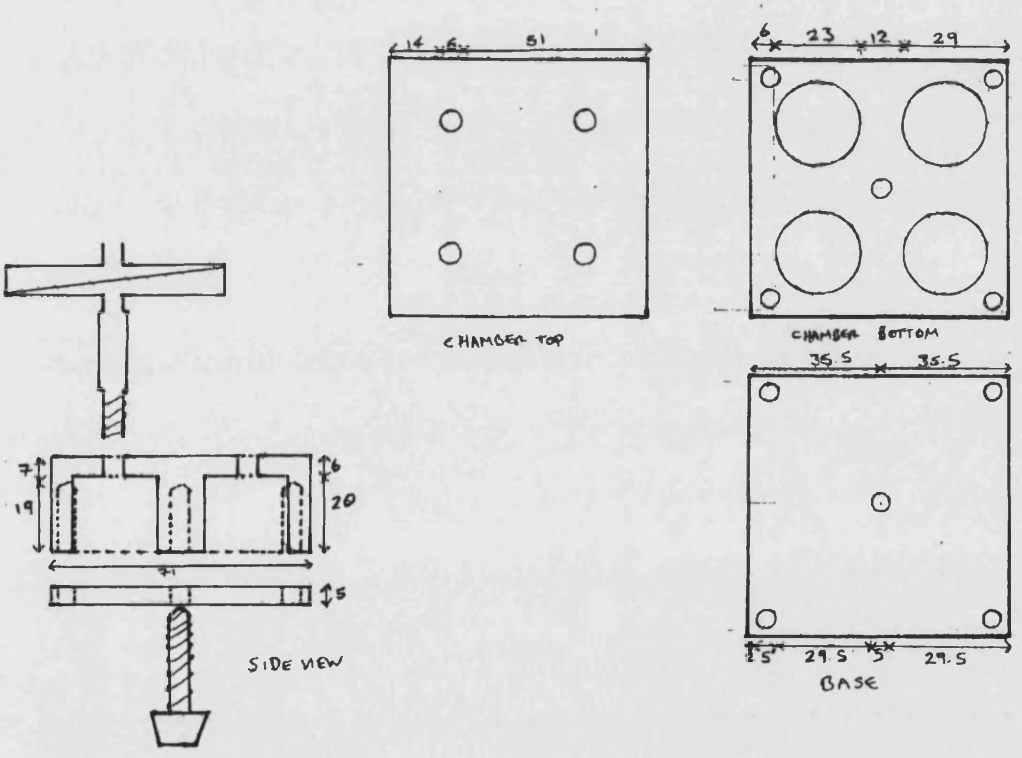

B

Figure 3.4. Engineering drawings of flat sheet membrane culture chamber.
(A) Exploded view, (B) Side and Plan views showing measurements.

3.4.2 HOLLOW FIBRE BIOREACTOR DESIGN AND MANUFACTURE

Cell culture on the hollow fibre membranes was carried out in a hollow fibre bioreactor. The module was made from glass with two side ports for seeding, and optional addition of media to the ablumenal surface side of the fibres. The fibres were held in position by use of silicon gaskets and epoxy resin. All bioreactor components were steam sterilised at 1.5 barg and 121 °C for 20 minutes.

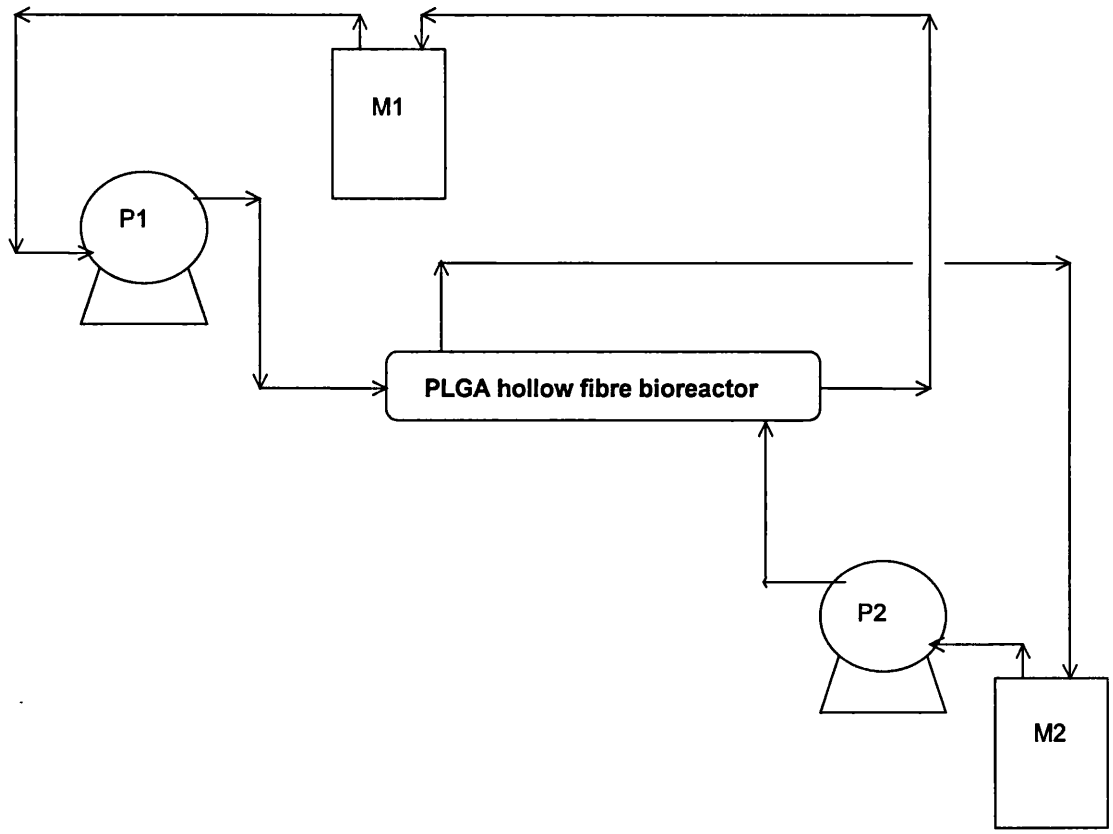

Figure 3.5. Schematic of PLGA hollow fibre bioreactor.
Media supply to lumen (M1), media supply to shell side (M2), peristaltic pump for lumen feed (P1), peristaltic pump for shell side feed (P2).

Figure 3.6. Photograph of hollow fibre membrane bioreactor.

3.5 ANALYTICAL METHODS

3.5.1 CELL NUMBER

Cell Counts

In addition to cell suspension cell count, several proliferation assays were compared and the most appropriate selected to calculate cell number (see Appendix C). Cells were counted using a haemacytometer. To allow detection of live and dead cells, the cell solution sample was diluted 9:1 with trypan blue. The 16-square (4 x 4) grid is equal to 10^{-4} ml. To calculate the total number of cells: (cell count) x (dilution due to trypan blue (10/9)) x (10,000) x (number of ml of cell suspension).

Methylene Blue

Samples were rinsed in PBS then fixed with 10% NBF for 15 minutes in the fridge. They were then rinsed with distilled water. Methylene blue was added so as to cover the samples for 10 minutes then rinsed with tap water until it ran clear, soaked twice in borate buffer for 10 minutes. The samples were allowed to air dry. To elute the dye, 1% acidified ethanol (0.5 ml for 12-well and 24-well samples) was added to the sample and left for 10 minutes with gentle agitation. Aliquots (100 µl) were taken from each sample and absorbancy read at 650 nm. Results were compared with a standard curve and the cell number calculated (cells/cm^2).

MTT

MTT was added four hours before the endpoint of the experiment at a concentration of 0.05 mg/ml. For example, consider 10 wells of cells seeded in 12-well plates with 0.5 ml media. 10 ml of MTT solution containing 100 µl MTT storage solution (5 mg/ml) was made up in media. 0.5 ml of the MTT-in-media solution was added to each well. At the endpoint of the experiment the media was aspirated off and the cells were left to air dry. The samples were then stored in the fridge wrapped in foil (MTT is light sensitive) until reading. 0.5 ml DMSO was added to each well and left for 5 minutes with gentle agitation. Aliquots (100 µl) were taken from each sample and absorbency read at 550 nm. Results were compared with a standard curve and the cell number calculated (cells/cm^2).

PicoGreen

The Picogreen assay was carried out using the Molecular Probes picogreen assay kit. At the end of the experiment, cells were washed with PBS before adding ATM lysis buffer (see Appendix C for lysis buffer selection). To assist the lysis, samples underwent freeze-thaw by placing into the –80 °C freezer then thawing at 37 °C. Standards were then prepared using the ATM lysis buffer and DNA solution; Table 3.5 shows the concentrations of the standards. TE buffer was made up in RNAse free water at a 1 in 20 dilution for the picogreen reagent. Picogreen reagent was made up in TE buffer at a 1 in 200 dilution and kept in a foil wrapped falcon tube. Standards and samples were aliquoted (100 µl) into 96-well plates and read in a fluorospectrometer at 480nm excitation and 520 nm reading. Results were compared with the standard curve and the cell number calculated (cells/cm^2).

Table 3.5. Concentrations and volumes of solutions for the picogreen assay standards.

Concentration ng/ml	DNA solution µl	ATM µl
Using 20ng/ml DNA solution		
0	0	400
0.5	20	380
1.0	40	360
5.0	200	200
Using 2µg/ml DNA solution		
10	4	396
50	20	380
100	40	360
500	200	200
1000	400	0

3.5.2 CELL MORPHOLOGY

Cells on TCP were observed under a transmitted light microscope and photographed. Cells on membranes were routinely observed using a reflected light microscope, and photographed. To improve contrast, cultures were fixed with 10% NBF then stained with 1% methylene blue solution for 10min. Samples were then rinsed with tap water until it ran clear then soaking twice in borate buffer for 10min (see Appendix C for stain selection analysis). The samples were allowed to air dry before gluing to a glass microscope slide for observation.

3.5.3 MINERALISATION AND ALKALINE PHOSPHATASE ACTIVITY

After the three-week culture, samples were rinsed twice in PBS before being fixed in 95% ethanol for 10 minutes. The ethanol can be left on samples until staining if well sealed and stored in a fridge. The ethanol was removed and the samples allowed to air dry. Cells were stained with fast red, to detect alkaline phosphatase activity, for 10-20 minutes until the colour is noticeable. The samples were then rinsed under tap water and any excess was aspirated off. Von Kossa's reagent was then added to the

samples for 30 minutes in direct sunlight or under a UV lamp. The solution was removed, samples rinsed under tap water and left to air dry.

3.5.4 POLYMER SOLUTION CHARACTERISATION

Solubility

The polymers were added to NMP and dioxane at 30% (w/w) polymer concentration to a total weight of 5 g. The bottles were then placed in the water bath at 40 °C. The solutions were left in the bath overnight then observed for signs of polymer granules. If there were no polymer granules visible, the polymer was deemed soluble at 40 °C and 30% concentration. If granules were visible, the polymer was placed on the roller mixer for up to 48 hours to see if the granules dissolved. If, after this time, there were still granules visible, the polymer was deemed insoluble at 40 °C and 30% concentration. The polymer solutions were then placed in a 25 °C water bath over night and the same procedures followed as at 40 °C. Similarly, the 30% solutions were tested at 20 °C and 15 °C. Solutions made to 25, 20 and 10% polymer concentration were also tested.

Viscosity

The PLGA made using various PLA:PGA was dissolved in NMP and dioxane at 20-, 25- and 30% (w/w) concentrations. The polymer solutions were measured for viscosity using a plate and cone rheometer at a constant temperature of 20°C, 25 °C and 30°C.

3.5.6 MEMBRANE CHARACTERISATION

Morphology

The surfaces and cross section structures of the flat sheet and hollow fibre membranes were studied using scanning electron microscopy. The fresh hollow fibres were cut into small pieces of approximately 50 mm and the flat sheet membranes were trimmed into small stripe of approximately 4-5 mm wide for the ease of handling. The samples were dipped in liquid nitrogen and then freeze fractured using forceps and a scalpel blade. The fractured fibre or sheet was adhered on a special aluminium dish using a conductive pad and placed in a silica gel container overnight to ensure thorough removal of moisture from the membrane

pores. A thin layer of gold coating was then deposited using a sputter coater prior to the morphological examination using a scanning electron microscope. Images were taken using the camera attached.

Topography

The topography of the membranes was analysed using atomic force microscopy (AFM). The samples were allowed to air dry for 24 hours then in a desicattor for 24 hours. Samples were mounted onto sample disks and analysed using tapping mode over a 10 μm x 10 μm area at a rate of 1-2 Hz.

Solvent Release and Degradation

Solvent release and degradation was analysed using high performance liquid chromatography (HPLC). Calibration curves were plotted (Appendix E) and samples analysed using the parameter settings shown in Table 3.6.

Table 3.6. Parameter settings for HPLC analysis.

Parameter	NMP	LA/GA
Column	Synergy I 4u Polar-RP 80A Column (C18)	Polypor H
Mobile Phase	50% Acetonitrile in Water	0.01 N Sulphuric Acid
Reference time	3.5-3.8 min	13.78-14.65 min
Flow rate	1 ml/min	0.2 ml/min
Analysis time for each loop	7 min	30 min
Detector	UV 210 nm	UV 210 nm
Peak width	0.50 min-1 min	0.5 min –1 min
Peak sensitivity	0.5%-1%	0.5%-1%

Mean Pore Size and Effective Surface Porosity

Mean pore size and effective surface porosity were calculated using measurements obtained by gas permeation. A representative single fibre section was glued into a module and connected into a gas permeation circuit. Air was passed into the module, through the lumen, and exited through the fibre wall. The fibre was given time to stabilise at the set air pressure before a bubble meter was used to measure the volumetric flow rate of air through the fibre. Measurements were taken for a range of air pressures.

Mean pore size and effective surface porosity were calculated using the method described in (Li *et al.* 1999), a full example of which can be found in Appendix F. Gas permeability was calculated using J = nA/P and plotted against mean pressure. The gradient P_0 and intercept K_0 were calculated and used in the following equations to find the mean pore radius, r (m), and the effective porosity ε/L_p (m^{-1}):

$$r = (16/3) \times (P_0/K_0) \times (8RT/\pi M_{N2})^{0.5}$$

$$\varepsilon/L_p = 8\mu RTP_0/r^2$$

3.6 STATISTICAL METHODS

3.6.1 DATA REPRESENTATION

Data was plotted on a Normal probability plot to test for normal or skewed distribution. In addition to this, the mean and median were calculated. Normal data was plotted as mean values, ± one standard deviation (SD). The number of samples was 9 (n=9) unless otherwise stated. For example, for the picogreen assay (Section 3.5.1), three membrane disks were seeded per PLA:PGA ratio then lysed using ATM buffer. Three samples of the lysis was taken from each disk and measured to calculated the DNA content, so for each PLA:PGA ratio, n = 9.

3.6.2 COMPARATIVE STATISTICS

One way analysis of variance (one way ANOVA) with Tukey post hoc tests was used to assess the significance difference ($P<0.05$) between 3 or more independent samples; the independent samples were for instance the different PLA:PGA ratios. A type two (unpaired) two-tailed Student's t-test was used for comparison between two samples, also with significant difference $P<0.05$.

CHAPTER FOUR
PLGA MEMBRANE SCAFFOLD DESIGN I-FLAT SHEETS

4.1 INTRODUCTION

Phase inversion membranes were initially considered as potential scaffolds because of their link with efficient mass transfer. This chapter discusses the evaluation and consequent selection of suitable PLGA-solvent-water ternary systems for eventual hollow fibre spinning (Chapter 5). In general, the mechanisms of formation for flat sheets are related to that for hollow fibres from the same ternary system (Cabasso 1980; Cabasso *et al.* 1977). PLGA can be made up of any molar ratio of PLA:PGA. A range of PLGA compositions, containing monomers at different ratios, were evaluated alongside two solvents, NMP and dioxane.

Prior to preparing hollow fibres, it was necessary to select suitable ternary systems for the required membrane structure (Section 2.4.2). For bone cell culture the membrane should allow easy mass transfer of molecules up to 150kDa (Kumar *et al.* 2004) (0.1 μm ~ 1000 kDa (Planchamp *et al.* (2003)) whilst the maximum pore size is 5μm as cells can enter spaces larger than this (Beresford 2002). The topography is also an important consideration and a rough surface at a nanometre scale is beneficial for cell adhesion (Section 2.3.3). A highly porous structure will improve mass transfer and is therefore desirable.

Polymers were named according to their poly(lactic acid) (PLA) and poly(glycolic acid) (PGA) content. 100:0 is 100 mol% PDLLA, 75L:25 is 75 mol% PLLA, 25 mol% PGA. DL and L indicates a mixture of *d*- and *l*- or pure *l*-isomers of lactic acid respectively. Polymer concentrations in polymer-solvent solutions are shown as weight percent of polymer in the solution. The choice of PLA:PGA ratios selected for the work was based on the most common and readily available (Spencer 2003).

4.1.1 SELECTING THE TERNARY SYSTEM COMPONENTS FOR PHASE INVERSION MEMBRANE CASTING

There are many potential solvents that will dissolve PLGA, and that have been used for scaffold preparation by various techniques. Examples include methylene chloride (Widmer *et al.* 1998) or methyl chloride (Luciano *et al.* 2000), for high temperature extrusion and dip coating, glacial acetic acid for low temperature (and pressure) injection moulding (Hadlock *et al.* 2000; Sundback *et al.* 2003), and chloroform for extrusion and solvent evaporation and dip coating and immersion precipitation (Kivalo *et al.* 1999; Wan *et al.* 2001; Wang *et al.* 2001; Yoshimoto *et al.* 2003). The extensive studies by Ishaug *et al.* (1996-1998) into osteoblast culture on PLGA films used chloroform to cast the scaffolds by solvent evaporation (Ishaug *et al.* 1996; Ishaug *et al.* 1997; IshaugRiley *et al.* 1997; Ishaug-Riley *et al.* 1998).

Due to the nature of solvents, many are harmful and hazardous (Table 4.1). N-methyl pyrrolidinone (NMP) is considered relatively harmless and has been used in animal models and shown to increase bone formation (Weber *et al.* 2004a; Weber *et al.* 2004b). Volatile solvents not only increase the chance of user exposure but can also effect the solution composition as a function of time. Chloroform and methyl chloride are poorly miscible with water so are of no use in a ternary system where water is used as the nonsolvent. Dioxane and NMP are common solvents for hollow fibre preparation so data is relatively easy to obtain on the solvent-water interactions, which is important for predicting and assessing the hollow fibre structure and performance. Further solvent properties can be found in Appendix D.

When a solvent-nonsolvent combination with a high mutual affinity is used, instantaneous demixing occurs and a porous membrane will be obtained. If the combination has low mutual affinity, delayed demixing will proceed and a dense, nonporous membrane will form (Section 2.4.2). Dioxane-water and NMP-water both have high mutual affinities so porous structures are expected to form. Chloroform and methylene chloride cannot be paired with water but methanol, ethanol or propanol, are suitable nonsolvent alternatives. Still, the mutual affinity is low and a nonporous structure will result (Mulder 1992) and a porous membrane is desirable to allow diffusion of the relatively large nutrient molecules. For these reasons, NMP and dioxane were chosen as the two solvents to be used in this study.

Table 4.1. Properties of solvents commonly used in scaffold preparation.

	chloroform	**methyl chloride**	**dioxane**	**NMP**
Toxicity	Irritant and probable carcinogen. Can be fatal on ingestion or inhalation	Irritant and probable carcinogen. Known mutogen	Irritant and probable carcinogen	skin, eye and respiratory irritant
Volatility	volatile	volatile	volatile	non volatile at STP[1]
Flammability		highly flammable	highly flammable	
Misciblity with water	not miscible	slightly soluble in water[2]	miscible	miscible

Data from Oxford University MSDS unless otherwise stated.
[1]STP is standard temperature pressure; 273K and 1atm.
[2](Sadek).

4.1.2 PROPERTIES OF CASTING DOPES

The viscosity of the solution will affect the shear experienced in the spinneret and will influence the structure (see Chapter 5 for more detail on the effect of shear). More fundamental than this is to have a solution with a viscosity that is low enough to allow the solution to flow, but high enough to 'hold' the solution together until precipitation has occurred. The viscosity range used for spinning varies between groups; Eenink and Feijen (1987) selected spinning dopes with viscosities in the range 20-100 Pas where as Tai *et al.* (2005) found that viscosities between 8-15 Pas were ideal. In the study by Eenink and Feijen (1987), a minimum polymer concentration of 10% (w/w) was regarded as necessary to obtain a suitable hollow fibre. Below this concentration, there would not be enough polymer to form a continuous structure. Polymer concentration can affect the porosity of the membrane. A higher volume fraction of polymer will give a less porous structure. A higher initial concentration means a higher concentration at the film interface so leading to a less porous top layer, which will reduce the flux (Mulder 1992).

4.1.3 STRUCTURAL PROPERTIES OF MEMBRANE SCAFFOLDS

The pore size and number of pores is related to how fast the demixing occurs, the type of polymer, its molecular weight and the solvent used (Tai *et al.* 2005). Both flat sheet and hollow fibre membranes exhibit similar performance, the process of the formation differs since for flat sheet membranes demixing occurs from one side only while it occurs from the bore and shell side during hollow fibre membrane formation (Tai *et al.* 2005).While no data is available for PLGA-solvent-water systems, more common systems for ultra- and microfiltration membranes prepared with NMP or dioxane and water can be used with confidence.

4.2 RESULTS

A range of PDLLA:PGA ratios from 45:55 to 100:0, the PLLA:PGA ratios 75:25 and 100:0, and 0:100 (PGA) were tested for their solubility in NMP and dioxane. Those that dissolved were tested and rheological data were analysed to find the polymer solution concentrations with viscosities suitable for spinning. Membranes were cast as flat sheets from three PDLLA:PGA ratios, 50:50, 75:25, 100:0 and PLLA:PGA ratio 75:25 (75L:25), the structure of which was assessed to aid the choice of ternary system to use for spinning hollow fibre membranes.

4.2.1 POLYMER-SOLVENT SELECTION

The structure and hence properties of a phase inversion membrane are dependent on the interactions of the tertiary system. It is therefore important to select a solvent that dissolves the polymer and is completely miscible with the nonsolvent. The rheological properties of the polymer-solvent solution govern whether the solution is suitable to spin hollow fibres.

Solubility of PLGA in Different Solvents

The polymer must dissolve in the solvent to form a homogeneous liquid that can be used for membrane casting. It was necessary to test if such a mixture could be obtained using PLGA of various PLA:PGA ratios and the two selected solvents, NMP and dioxane. Varying solubility was observed over a range of temperatures and polymer concentrations in NMP (Table 4.2) and dioxane (Table 4.3).

The entire range of PLGA compositions containing the DL-isomer of PLA dissolved at all temperatures and polymer concentrations tested in both NMP and dioxane. The highly crystalline PGA and PLLA did not dissolve in either NMP or dioxane. 75L:25 dissolved completely in a 10% polymer concentration solution and appeared to gel at higher polymer concentrations in both solvents.

Table 4.2. Solubility of various PLGA polymers in NMP at different temperatures and polymer concentrations.

Temperature		15°C				20°C				25°C				40°C			
Polymer concentration (w/w%)		10%	20%	25%	30%	10%	20%	25%	30%	10%	20%	25%	30%	10%	20%	25%	30%
Polymer	100:0	✓	✓	✓	✓	✓	✓	✓	✓	✓	✓	✓	✓	✓	✓	✓	✓
	85:15	✓	✓	✓	✓	✓	✓	✓	✓	✓	✓	✓	✓	✓	✓	✓	✓
	75:25	✓	✓	✓	✓	✓	✓	✓	✓	✓	✓	✓	✓	✓	✓	✓	✓
	65:35	✓	✓	✓	✓	✓	✓	✓	✓	✓	✓	✓	✓	✓	✓	✓	✓
	50:50	✓	✓	✓	✓	✓	✓	✓	✓	✓	✓	✓	✓	✓	✓	✓	✓
	45:55	✓	✓	✓	✓	✓	✓	✓	✓	✓	✓	✓	✓	✓	✓	✓	✓
	100L:0	×	×	×	×	×	×	×	×	×	×	×	×	×	×	×	×
	75L:25	✓	gel	gel	gel	✓	gel	gel	gel	✓	gel	gel	gel	✓	gel	gel	gel
	PGA	×	×	×	×	×	×	×	×	×	×	×	×	×	×	×	×

Concentrations are shown as weight percent of polymer in the solution. Further physical properties can be found in Appendix C. ✓ denotes the polymer did dissolve in the solvent, × denotes the polymer did not dissolve in the solvent, gel denotes a gel formed.

Table 4.3. Solubility of various PLGA polymers in dioxane at different temperatures and polymer concentrations.

Temperature		15°C				20°C				25°C				40°C			
Polymer concentration (w/w%)		10%	20%	25%	30%	10%	20%	25%	30%	10%	20%	25%	30%	10%	20%	25%	30%
Polymer	100:0	✓	✓	✓	✓	✓	✓	✓	✓	✓	✓	✓	✓	✓	✓	✓	✓
	85:15	✓	✓	✓	✓	✓	✓	✓	✓	✓	✓	✓	✓	✓	✓	✓	
	75:25	✓	✓	✓	✓	✓	✓	✓	✓	✓	✓	✓	✓	✓	✓	✓	✓
	65:35	✓	✓	✓	✓	✓	✓	✓	✓	✓	✓	✓	✓	✓	✓	✓	✓
	50:50	✓	✓	✓	✓	✓	✓	✓	✓	✓	✓	✓	✓	✓	✓	✓	✓
	45:55	✓	✓	✓	✓	✓	✓	✓	✓	✓	✓	✓	✓	✓	✓	✓	✓
	100L:0	✗	✗	✗	✗	✗	✗	✗	✗	✗	✗	✗	✗	✗	✗	✗	✗
	75L:25	✓	gel	gel	gel	✓	gel	gel	gel	✓	gel	gel	gel	✓	gel	gel	gel
	PGA	✗	✗	✗	✗	✗	✗	✗	✗	✗	✗	✗	✗	✗	✗	✗	✗

Concentrations are shown as weight percent of polymer in the solution. Further physical properties can be found in Appendix C. ✓ denotes the polymer did dissolve in the solvent, ✗ denotes the polymer did not dissolve in the solvent, gel denotes a gel formed.

Viscosity of PLGA-Solvent Solutions

Wet and wet/dry hollow fibre spinning (see Chapter 5 for further details on these processes) require a solution with a viscosity low enough to flow through the spinneret yet not too low that the solution cannot hold its annular shape until phase inversion reaches such a stage that the solid phase can support its structure. While different groups consider different viscosity ranges suitable, preliminary results showed that viscosities as low as 1 Pas are suitable for spinning and up to 10 Pas for ease of solution handling. These results are confirmed by the viscosity data for the polysulphone-solvent system described by Tai *et al.* (2005).

The viscosities of the polymer-solvent solutions were measured at three different temperatures; 20°C, 25°C, 30°C. The viscosity data for all polymer solutions at given PLA concentrations are shown in Figures 4.1 to 4.4. Figure 4.1 shows the viscosity profiles of the polymer-NMP solutions on the same scale, Figure 4.2 shows viscosity profiles in more detail with appropriate scales. Similarly, Figure 4.3 shows the viscosity profiles for polymer-dioxane solutions on the same scale and Figure 4.4 shows the viscosity profiles in more detail with appropriate scales. An example of the casting solution profiles for the conditions tested is shown in Figure 4.5.

The viscosity of the PLGA-NMP solutions increased as PLA content increased from 45 mol% to 65 mol%, then decreases as PLA content is further increased from 65 mol% to 100 mol% (Figures 4.1 and 4.2). At any given PLA content and solution concentration, the viscosity decreased with increasing temperature.

A polymer concentration of 10% is too low for spinning in the case of all the polymer solutions tested, all being below 0.12 Pas (Figure 4.1 A and 4.2 A). The viscosity of the 10% 45:55 solution was too low to be read with the cone and plate rheometer. At 20% polymer concentration, 85:15, 75:25, 65:35 and 50:50 were within the ideal spinning range at all three temperatures (Figure 4.1 B and 4.2 B). 100:0 and 50:50 were just below the minimum ideal spinning viscosity of 1 Pas, but potentially suitable for spinning. 45:55 had a very low viscosity in the temperature range tested, so was regarded as unsuitable for spinning at 20% polymer concentration. At 25% polymer concentration, all PLGA-NMP solutions except 45:55-NMP were within the ideal spinning range at all three temperatures (Figure 4.1 C and 4.2 C). This

concentration offers the best range of spinning solutions. At 30% polymer concentration, 100:0, 85:15 and 50:50 were all within the ideal spinning range at the three temperatures (Figure 4.1 D). 75:25 was within the range at the higher temperatures of 30°C and 25°C but was above the ideal range at 20°C with a viscosity of around 12 Pas. 6515DL was above the ideal range at all temperatures, but it is likely that the viscosity of 12 Pas at 30°C would be suitable to spin with since it is not far above the ideal spinning viscosity range. 45:55 had very low viscosity at all three temperatures.

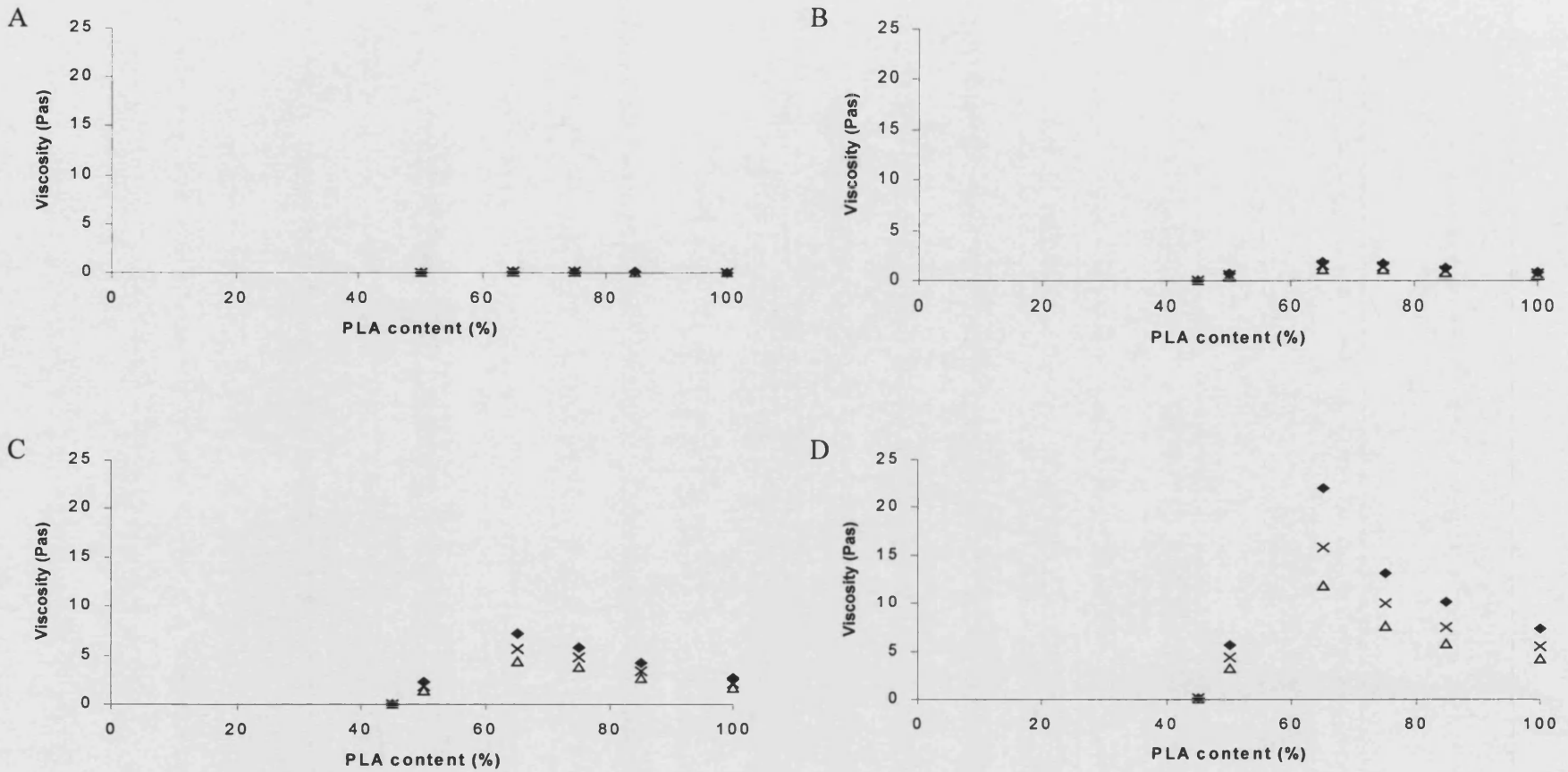

Figure 4.1. Viscosity profiles of PLGA polymers dissolved in NMP at different concentrations and temperatures.
(A) 10%, (B) 20%, (C) 25%, (D) 30% polymer concentration in solvent, (w/w%). PLA content is mol%. ◆ 20°C, × 25°C, △ 30°C.

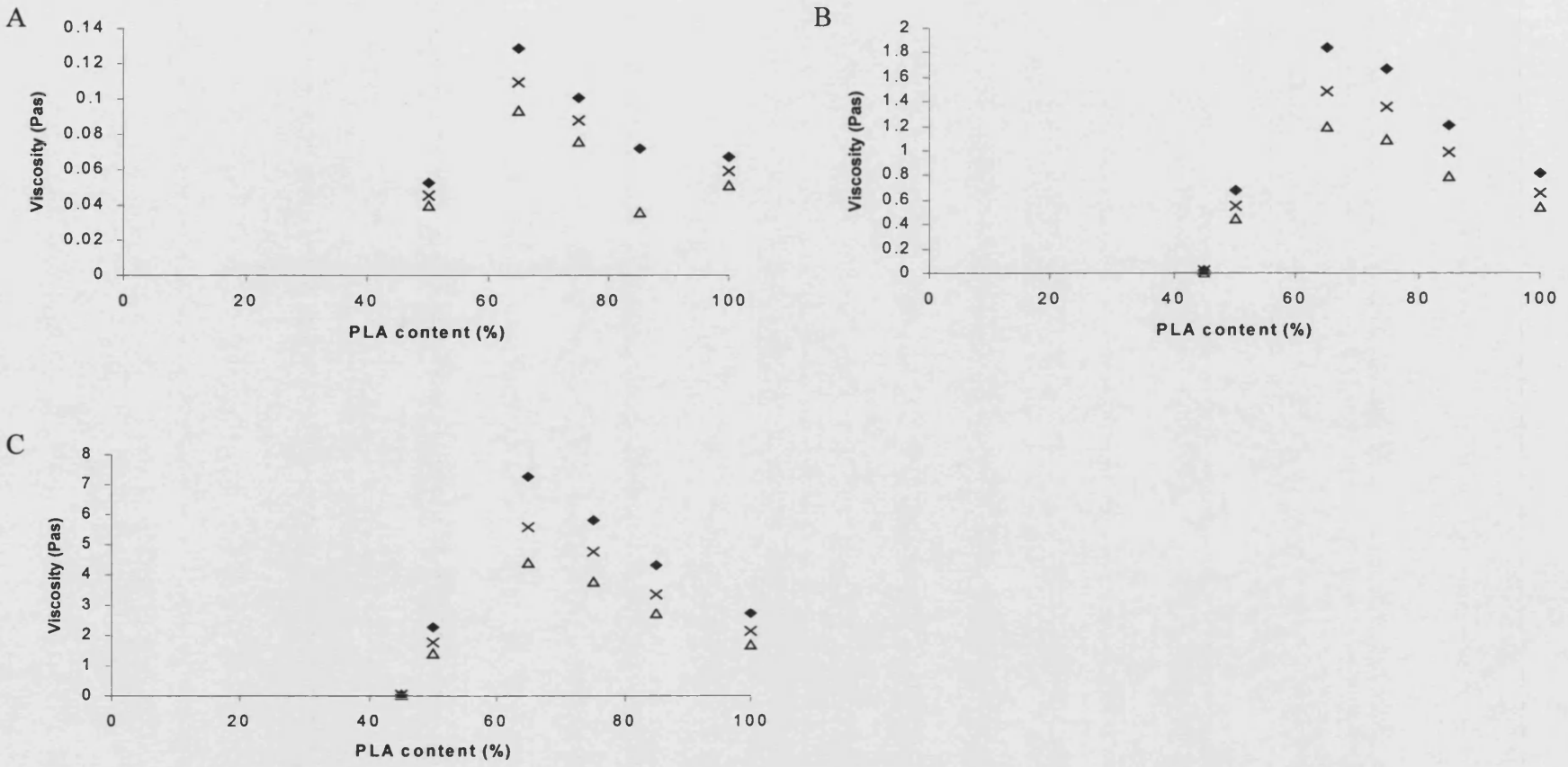

Figure 4.2. Detail of viscosity profiles of PLGA polymers dissolved in NMP at different concentrations and temperatures.
(A) 10%, (B) 20%, (C) 25%, polymer concentration in solvent, (w/w%). PLA content is mol%. ◆ 20°C, × 25°C, △ 30°C.

The viscosity of PLGA-dioxane solutions generally increased as PLA content increased, up to a maximum of between 65 mol% and 75 mol% PLA, then decreased as PLA content increased to 100 mol%. The relationship between viscosity and temperature appeared somewhat erratic, which is likely to be due to experimental error.

A polymer concentration of 10% is too low for spinning in the case of all the polymer solutions tested, all being below 0.15 Pas (Figure 4.3 A and 4.4 A). The viscosity of the 10% 45:55 solution was too low to be read with the cone and plate rheometer. At 20% polymer concentration, all PLGA-dioxane solutions except 45:55-NMP and 50:50 at 30°C, with a reading of 0.6 Pas, were within the ideal spinning range at all three temperatures (Figure 4.3 B and 4.4 B), allowing for experimental error. This concentration offers the best range of spinning solutions. At 25% polymer concentration 85:15, 75:25 and 50:50 are within the ideal spinning viscosity range and suitable for spinning at the three temperatures tested. 65:35 has viscosities within range at 25°C and 30°C (Figure 4.3 C and 4.4 C). 45:55 had very low viscosities unsuitable for spinning across the entire temperature range tested. At 30% polymer concentration all but 50:50 at 30°C were above the ideal spinning range and not suitable for spinning (Figure 4.3 D and 4.4 D). 100:0, 75:25 and 65:35 could not be measured at 20°C due to extremely high viscosity. 45:55 had very low viscosities unsuitable for spinning.

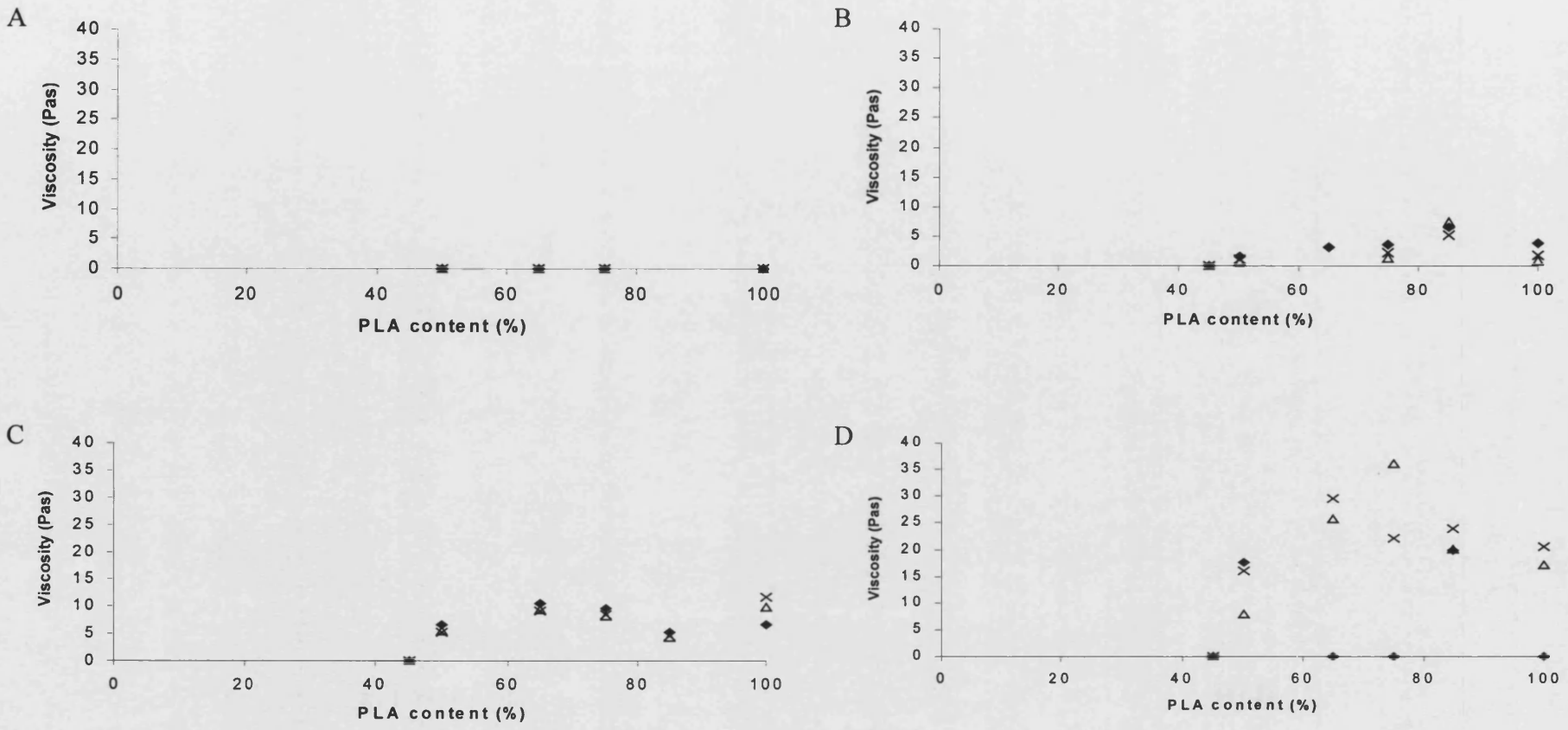

Figure 4.3. Viscosity profiles of PLGA polymers dissolved in dioxane at different concentrations and temperatures.
(A) 10%, (B) 20%, (C) 25%, (D) 30% polymer concentration in solvent, (w/w%). PLA content is mol%. ◆ 20°C, × 25°C, △ 30°C.

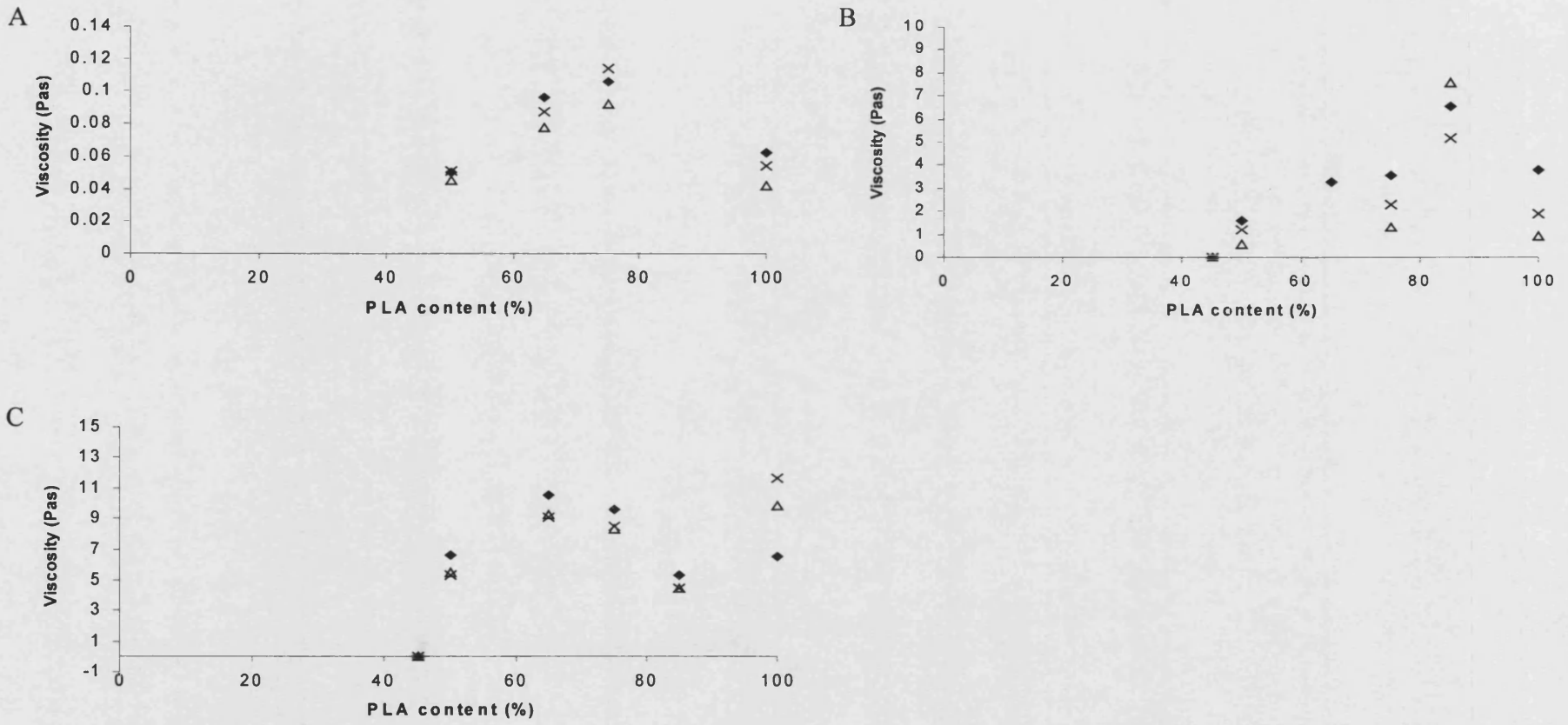

Figure 4.4. Detail of viscosity profiles of PLGA polymers dissolved in dioxane at different concentrations and temperatures.
(A) 10%, (B) 20%, (C) 25%, (w/w%). PLA content is mol%. ◆ 20°C, × 25°C, △ 30°C.

The viscosity data can be used to prepare a spinning dope profile for particular temperature ranges. Two examples of spinning dope profiles are shown in Figure 4.5. A summary of the data for each PLGA blend is shown in Tables D.3 and D.4 in Appendix D. Each dashed border shows the range of polymer concentrations and related viscosities of spinning dopes suitable between 20°C and 30°C. Ties lines join the horizontal boundaries and represent the suitable spinning dopes at a specific temperature. As temperature is increased, the polymer concentration must also be increased to obtain a given viscosity.

The polymer-NMP solutions with the lowest polymer concentrations that are suitable for spinning were 65:35 (18%), 75:25 (18%) and 85:15 (19%), at 20°C. Polymer-dioxane solutions tested could be used for spinning at concentrations as low as 8% (65:35). On the whole, solutions containing 25% polymer was near the maximum ideal spinning viscosity. Higher concentrations tended to cause gelling or poor mixing and are not suitable for spinning; 50:50 was an exception and a 25% solution was near the middle of the ideal viscosity range.

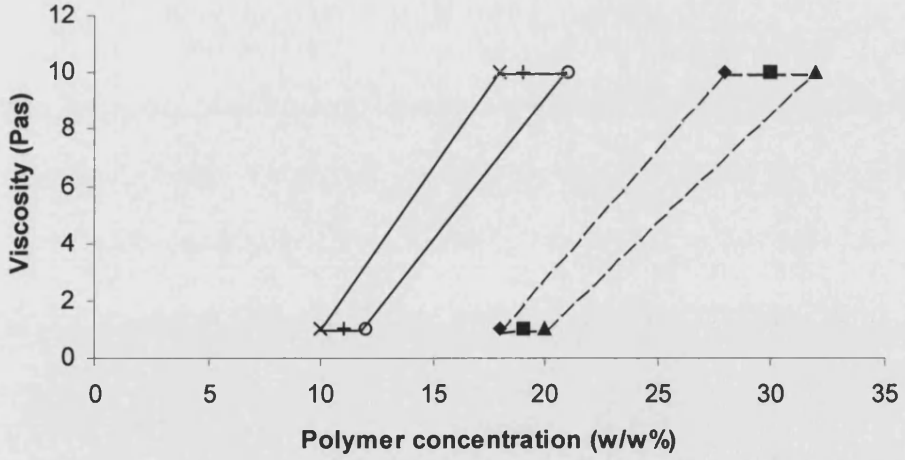

Figure 4.5. Casting solution profiles for 75:25 and 75L:25 in the temperature range 20°C - 30°C.

▪ ▪ ▪75:25, — 75L:25. ×715:25 20°C, + 75L:25 25°C, ○ 75L:25 30°C, ◆ 75:25 20°C, ■75:25 25°C, ▲ 75:25 30°C.

Comparing the Effect of the d,l- and l-Isomers of PLA on the Viscosity of PLGA in NMP and Dioxane

The effect of the PLA isomer was studied using 75:25 ratio PLGA. PLGA is commonly made with a mixture of the natural *l*-isomer and the manufactured *d*-isomer, denoted DL. The viscosity of 75:25 was compared to 75L:25.

The effect of the isomers on viscosity of the isomers can be seen in Figure 4.5. The spinning dope containing only the *l*-isomer (75L:25) requires a much lower polymer concentration to achieve a given viscosity. 75L:25 has viscosities suitable for spinning between 10%, at 20°C and 21%, at 30°C. Such low suitable spinning concentrations are not seen with 75:25 which requires a minimum of around 18% polymer concentration, at 20°C, and can be spun with concentrations up to 32%, at 30°C. Similarly with dioxane solutions, the 75L:25 had much larger relative viscosities compared with 75:25. Because of the generally higher viscosities seen with dioxane, solutions of between approximately 6% and 12% could be used for spinning with 75L:25, and 12% to 26% for 75:25.

4.2.2 PLGA FLAT SHEET MEMBRANE FABRICATION

Flat sheets are cast by the process of phase inversion, described in Section 4.1.2, by the movement of solvent into a nonsolvent, which forms a binary liquid phase solution and a solid-phase porous membrane. The flat sheet membrane were made to test the suitability of a polymer-solvent-nonsolvent system because they are quick and easy to produce, requiring a small polymer solution volume, small area of work and little time. They also have a similar top surface (surface exposed to water; bottom surface is that in contact with glass sheet) and cross section structure as the hollow fibre that would result if spun, as the phase inversion will involve the same mechanism (Eenink and Feijen 1987). For these reasons, flat sheet membranes were used for initial morphological assessment and to test the PLGA membranes for cell culture suitability (Chapter 7).

Flat sheet membranes were made from four PLGA polymers; 100:0, 75:25, 50:50 and 75L:25. The polymers were dissolved in NMP and dioxane at 20%, except 75L:25 which was dissolved at 10%. These concentrations were chosen because they

are at the lower limit of the ideal spinning viscosity range so would use less polymer, making the process more cost efficient, and were expected to give the greatest free volume which would give rise to a higher nutrient flux.

PLGA Flat Sheet Membrane Morphology

The micrographs in this section show the top and bottom surfaces and the cross section of the PLGA membranes cast from both PLGA-NMP and PLGA-dioxane solutions. Macrotopography and pore size can be determined from the top and bottom surface images. The pore structure of the membranes cast with the different solvents can be seen from the cross section images.

Surface Structure of Phase Inversion Cast Membranes

The top surface is that exposed to water and is the surface used or cell culture, the bottom surface is that in contact with the glass during fabrication.

NMP-cast membranes have small pores size ranges. 75L:25 has both a wider pore size range compared to the PLGA containing both the D-, and L-isomers, and also has relatively larger pores (Table 4.4). The surface of the 50:50 membrane shows the presence of ridges, unlike the other flat sheets which had no ridges visible on the micrographs (Figure 4.6). The morphology of the 75L:25 top surface is very open and the structure below the surface is visible. 75L:25 has the most porous bottom surface (Figure 4.7 D) with pores around 1 μm where as 100:0 (Figure 4.7 A), 75:25 (Figure 4.7 B) and 50:50 (Figure 4.7 C) have a dense film on the bottom surface with only a few, yet large, pores 1 to 2 μm in diameter.

Table 4.4. Minimum and maximum pore sizes of the top surface of polymer-NMP flat sheet membranes.

Polymer	Min pore size μm	Max pore size μm
100:0	0.2	0.5
75:25	0.2	0.5
50:50	0.3	0.8
75L:25	0.5	1.0

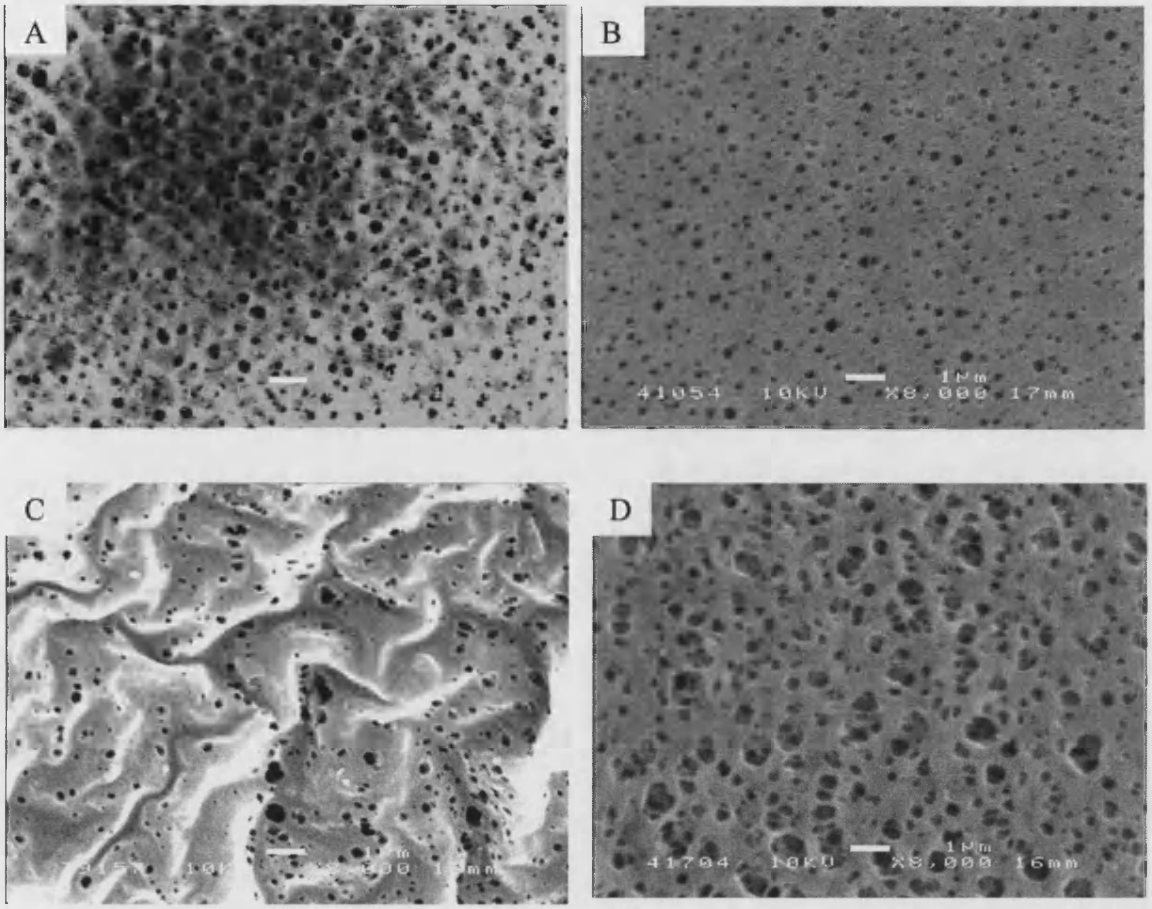

Figure 4.6. Top surface of flat sheet membranes cast using NMP.
Membranes were cast from polymer-NMP solutions at 20 w/w% polymer concentration, except 75L:25 which was cast at 10 w/w% polymer concentration. (A) 100:0, (B) 75:25, (C) 50:50, (D) 75L:25. Scale bar 1 μm.

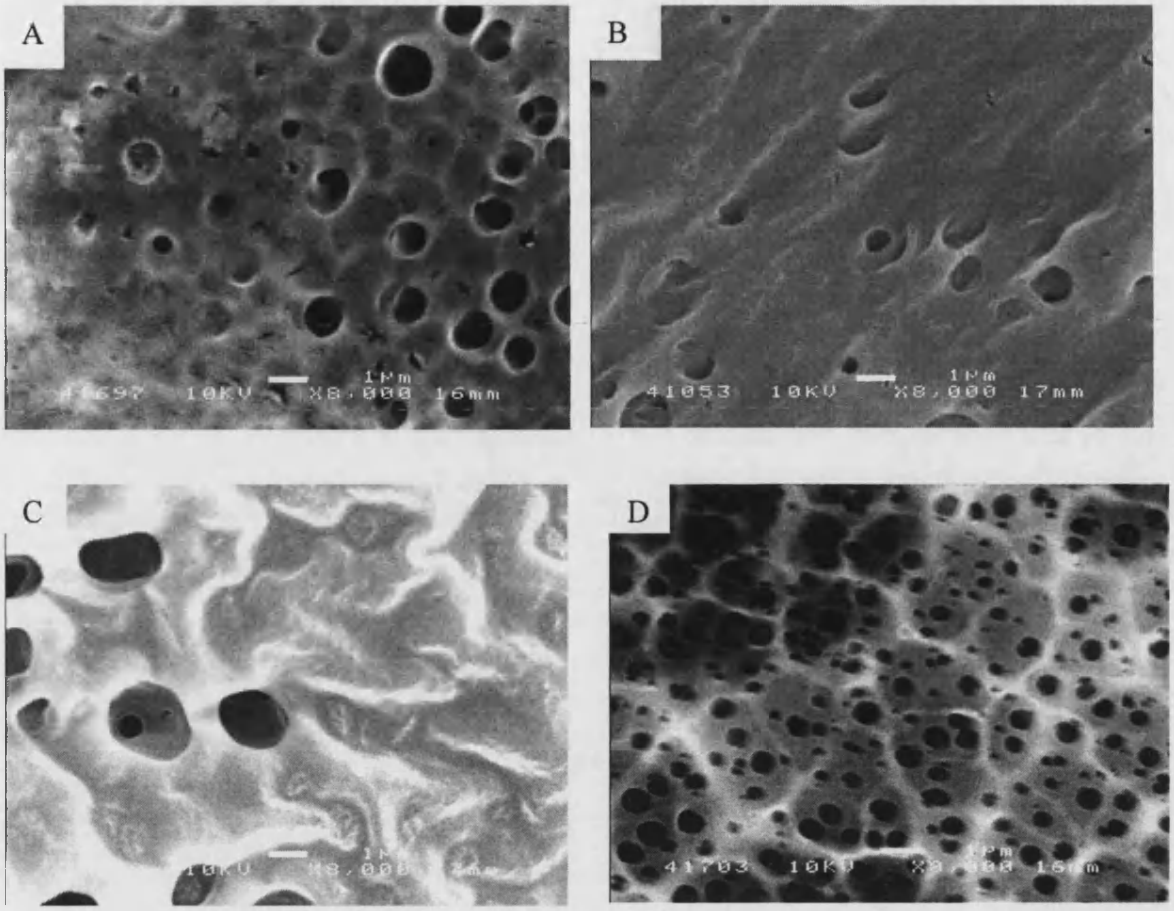

Figure 4.7. Bottom surface of flat sheet membranes cast using NMP.
Membranes were cast from polymer-NMP solutions at 20 w/w% polymer concentration, except 75L:25 which was cast at 10 w/w% polymer concentration. (A) 100:0, (B) 75:25, (C) 50:50, (D) 75L:25. Scale bar 1 μm.

Dioxane-cast membranes of 100:0 have the greatest pore size range and also the largest pores. 75L:25 has the smallest pore size range (Table 4.5). 75:25 has the roughest top surface, 50:50 appears the smoothest with large nonporous areas across the surface (Figure 4.8). The bottom surfaces are a dense film, with the exception of 75L:25 (Figure 4.9 D) which has a few very large crater-like pores up to 5 μm in diameter.

Table 4.5. Minimum and maximum pore sizes of the top surface of polymer-dioxane flat sheet membranes.

Polymer	Min pore size μm	Max pore size μm
100:0	0.2	2.0
75:25	0.2	1.4
50:50	0.1	1.6
75L:25	0.4	1.2

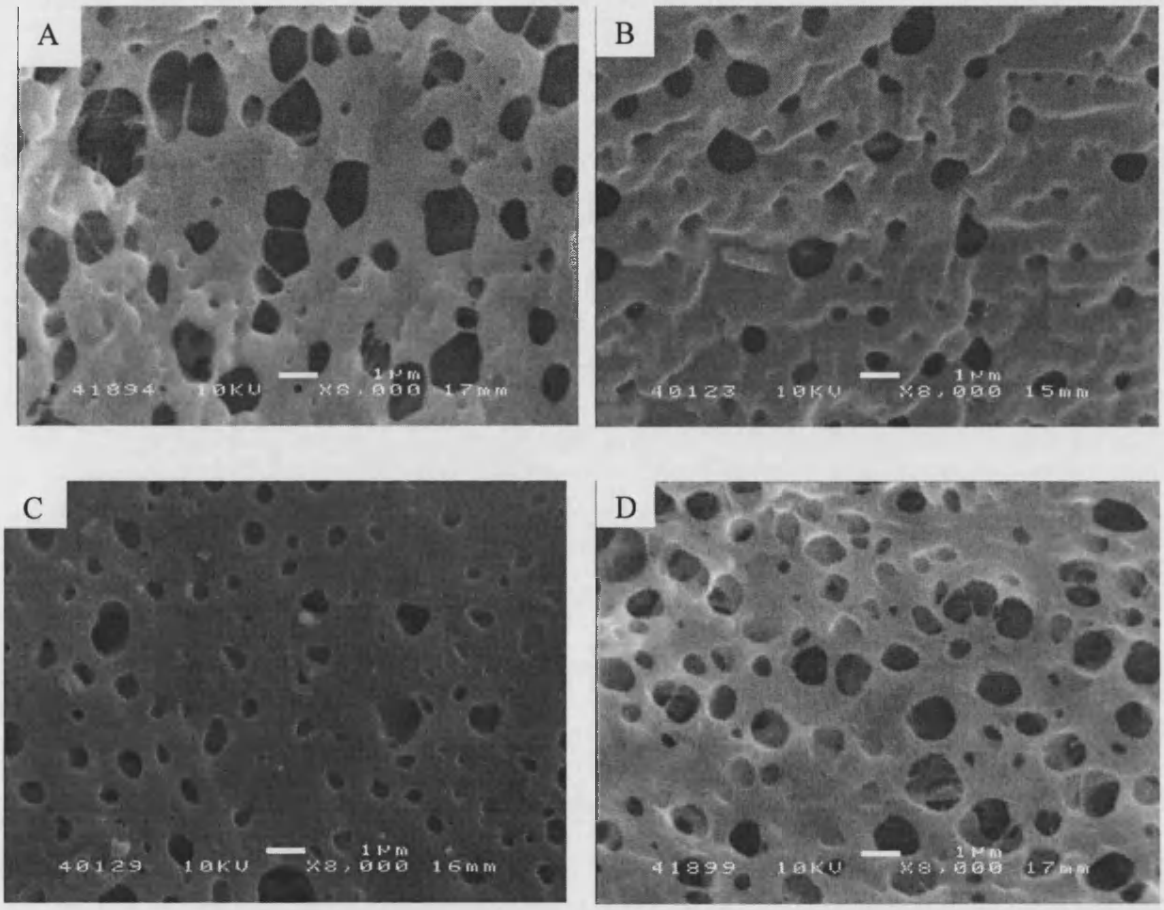

Figure 4.8. Top surface of flat sheet membranes cast using dioxane.
Membranes were cast from polymer-dioxane solutions at 20 w/w% polymer concentration, except 75L:25 which was cast at 10 w/w% polymer concentration. (A) 100:0, (B) 75:25, (C) 50:50, (D) 75L:25. Scale bar 1 μm.

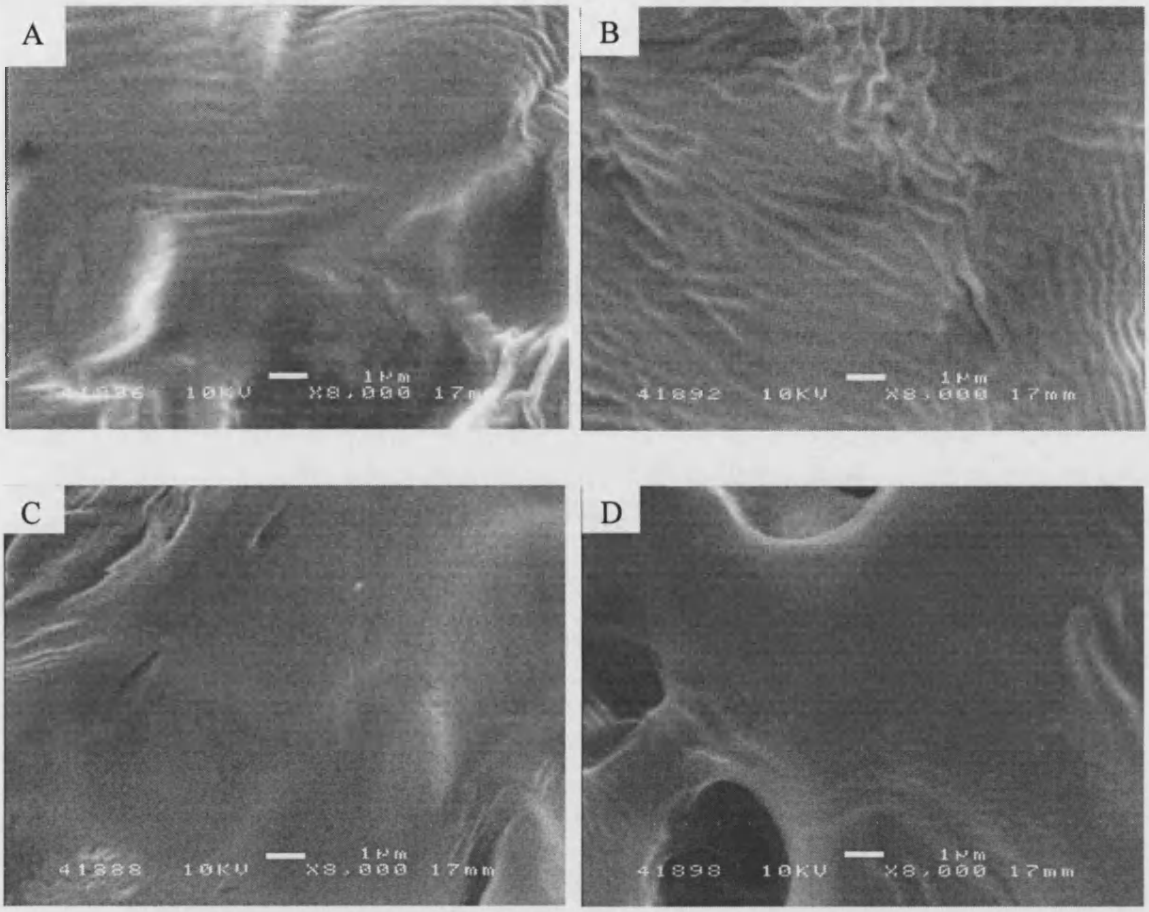

Figure 4.9. Bottom surface of flat sheet membranes cast using dioxane. Membranes were cast from polymer-dioxane solutions at 20 w/w% polymer concentration, except 75L:25 which was cast at 10 w/w% polymer concentration. (A) 100:0, (B) 75:25, (C) 50:50, (D) 75L:25. Scale bar 1 μm.

Cross Section Structure of Phase Inversion Cast Membranes

While all flat sheets were cast with the same 200μm depth of solution, the resulting membranes cast using polymer-NMP solutions have different thicknesses. 75L:25 was the thinnest at 40 μm (Figure 4.10 D), being less than half the thickness of the other membranes cast. 100:0 had a thickness of 100 μm (Figure 4.10 A), 75:25 of 80 μm (Figure 4.10 B). 50:50 had a thickness of 230 μm (Figure 4.10 C). The greater thickness of the 50:50 membrane is accompanied by a more open porous structure compared to the two other *d,l*- polymers. All membranes have an asymmetric pore structure with finger-like shaped pores running perpendicular between surfaces. 100:0 appeared to have a dense layer at its top surface.

The resulting flat sheets from the polymer-dioxane solutions have thicknesses of 40μm for 100:0 (Figure 4.11 A), 50 μm for 75:25 and 50:50 (Figure 4.11 B and C respectively), and 20 μm for 75L:25 (Figure 4.11 D). The pore structure is sponge-like with dense films surrounding each pore with no interconnection between pores.

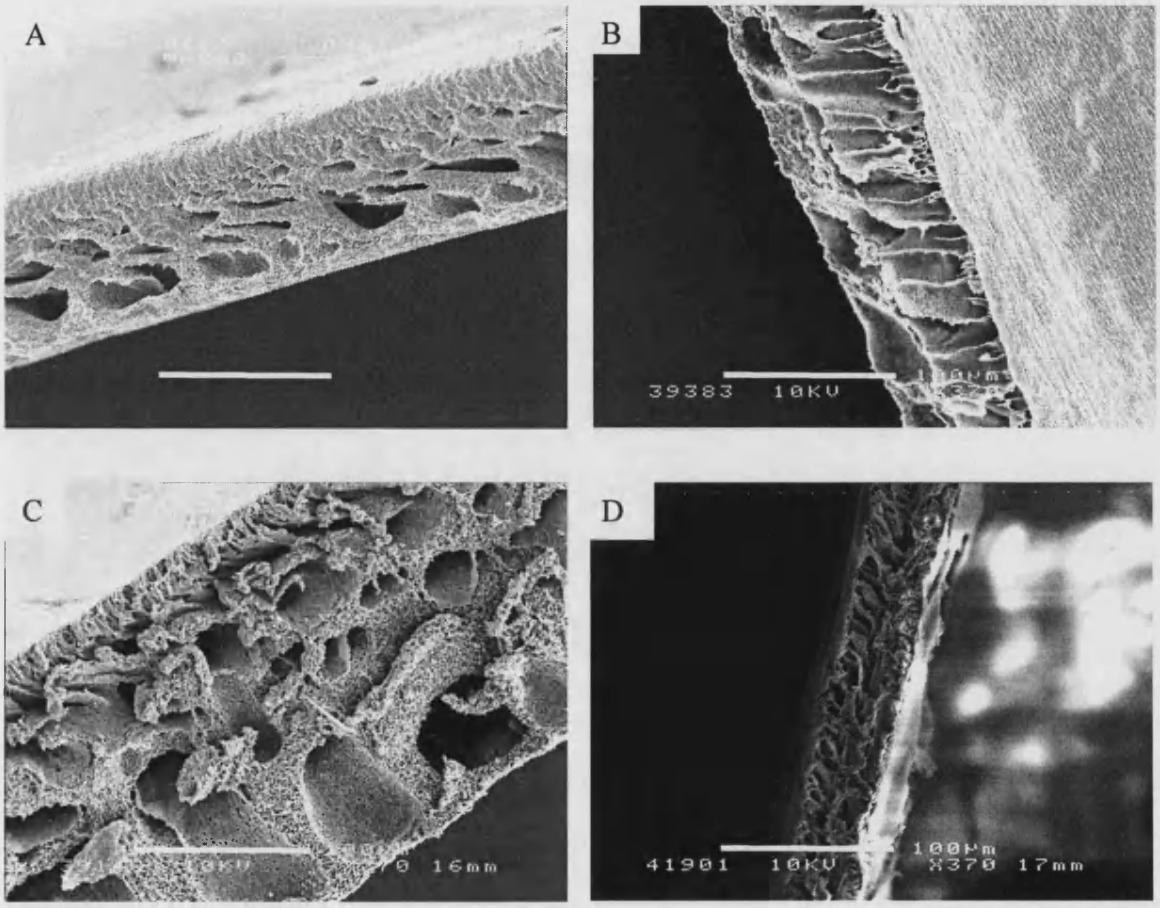

Figure 4.10. Cross-section of flat sheet membranes cast using NMP.
Membranes were cast from polymer-NMP solutions at 20 w/w% polymer concentration, except 75L:25 which was cast at 10 w/w% polymer concentration. (A) 100:0, (B) 75:25, (C) 50:50, (D) 75L:25. Scale bar 100 μm.

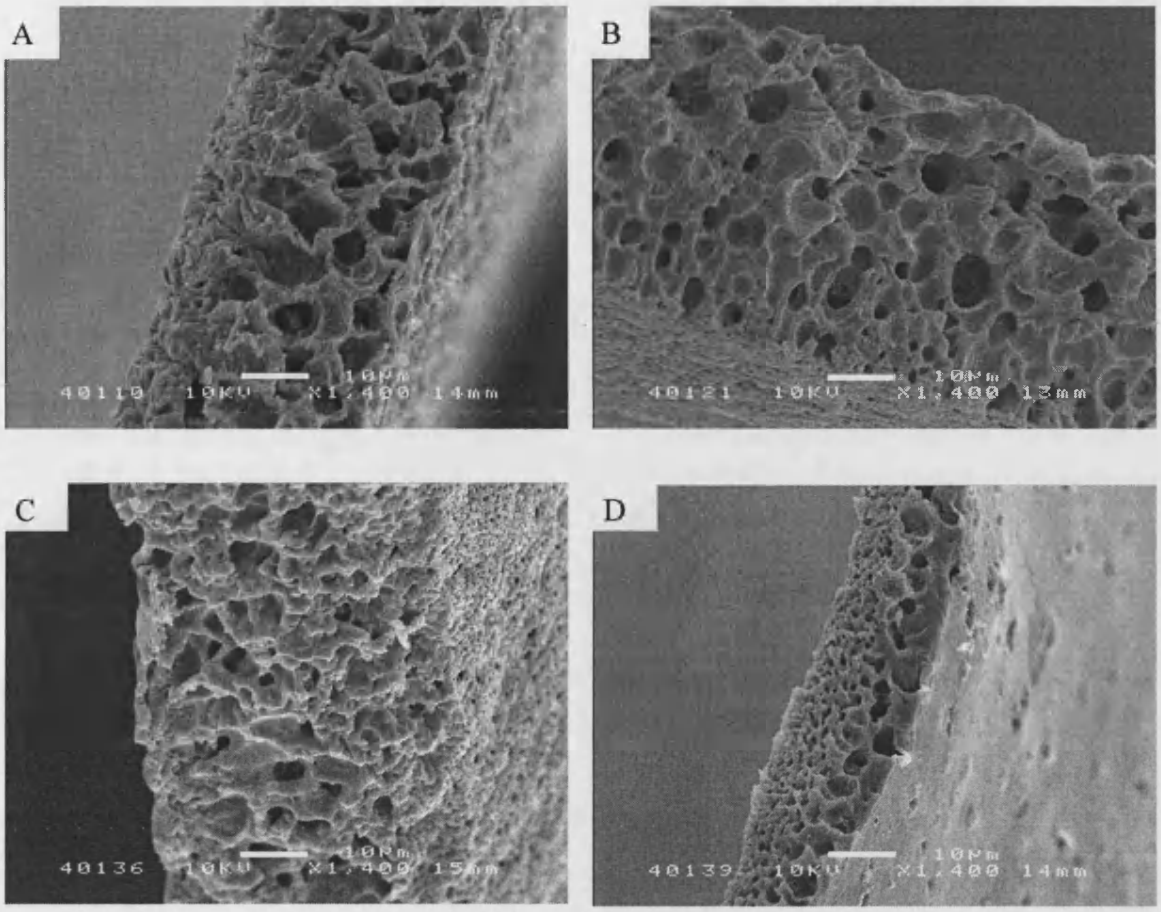

Figure 4.11. Cross-section of flat sheet membranes cast using dioxane.
Membranes were cast from polymer-dioxane solutions at 20 w/w% polymer concentration, except 75L:25 which was cast at 10 w/w% polymer concentration. (A) 100:0, (B) 75:25, (C) 50:50, (D) 75L:25. Scale bar 10 μm.

4.3 DISCUSSION

The results in this chapter can be used as a selection process for polymer solutions suitable for spinning. By analysing their viscosity and pore structure, the data presents a simple and fast method of solution selection.

A prerequisite to phase inversion membrane casting is the ability of the polymer to be dissolved in a solvent, which can be linked with a suitable nonsolvent. The solvent should be safe to use and, to minimise eventual manufacturing costs and complications, ambient preparation conditions are desirable. While many groups (see Section 4.1.1) use solvents to prepare scaffolds, they are often harmful and

additional steps for removal of residue would be required. NMP has been successfully used in animal models (Weber *et al.* 2004; Weber *et al.* 2004). Regarding the resulting structure, two main factors govern the selection of the ternary system to cast PLGA membranes by phase inversion; the cross-sectional pore structure and top surface pore size. The morphology is important such that it allows nutrients to pass freely across the membrane wall while. The pore size should be less than 5 μm to prevent cells migrating through the scaffold yet large enough to minimise resistance to nutrient transfer of molecules in the order of 150 kDa.

4.3.1 SOLUBILITY

All PLGA polymers containing the DL-isomer of PLA dissolved under all conditions tested in both NMP and dioxane. It is likely that the crystallinity of the polymers caused the differences in solubility. The highly crystalline PGA and PLLA did not dissolve in either NMP or dioxane. It was shown by Eenink and Feijen (1987) that PLLA will dissolve in NMP at 80°C, however, maintaining this temperature is costly and not practical.

75L:25 is semi-crystalline and can be viewed as an 'intermediate' between the crystalline homopolymers of PLLA and PGA, and the amorphous DL copolymers. The 75L:25 polymer dissolves in both NMP and dioxane at 10% polymer concentration but exhibits gel-like appearance at higher concentrations. Gels are fluids of infinite viscosity common with such semi-crystalline polymers (Mulder 1992). They form due to either chemical or physical cross-linking and do not flow, and hence are not suitable for membrane casting by phase inversion.

4.3.2 Viscosity

PLGA-NMP solutions where seen to exhibit Newtonian fluid behaviour since the shear stress increased linearly with shear rate (Coulson *et al.* 1997) (Appendix F). The viscosities increased with decreasing temperature and also with increasing polymer concentration. The viscosity showed a maximum at 65 mol% PLA. 100:0 had a viscosity similar to 50:50. Considering this and the fact that PGA is insoluble yet 45:55, the copolymer with the greatest content of PGA, had the lowest viscosity

shows that viscosity is not proportional to the increase in PGA content. This suggests that copolymerising the two acids involves a change at the molecular level.

Dioxane and NMP have different chemical structures and so interact differently with the polymers (Appendix D). NMP has both a methyl and an oxygen side group, as does PLGA. The similarity in structure allows interaction and increases the solubility. The dioxane solutions all had higher viscosities relative to the corresponding NMP solutions, 20% polymer concentration gave the largest range of PLGA-dioxane solution conditions available to spin with compared with 25% polymer concentration for PLGA-NMP solutions. This means that a lower polymer concentration could be used to achieve a given viscosity if dioxane was used as opposed to NMP. If a lower concentration can be used to achieve the same suitable spinning viscosity, a more open structure with high free volume will result which is beneficial for larger nutrient fluxes (Mulder 1992). 75L:25 solutions are suitable for spinning at polymer concentrations as low as 8% (in dioxane) and 10% (in NMP). These lower suitable concentrations would reduce cost and give a more open structure. However, it is not necessarily desirable to spin at a very low concentration as, although the free volume is greater, the mechanical integrity will be reduced so increasing the possibility of scaffold collapse. Typical polymer concentrations for spinning dopes are 18 w/w% (Xu and Qusay 2004), to 30 w/w% (Chung and Hu 1997) polyethersulphone in NMP both for spinning at 25°C; 20 w/w% being commonly used (Torrestiana-Sanchez *et al.* 1999; Li *et al.* 2004). When Eenink and Feijen (1987) prepared PLLA-NMP and PLLA-dioxane dopes, 10 and 15 w/w% solutions were prepared and maintained at 80 °C and 50 °C respectively to prevent premature coagulation. The viscosities were 180 Pas at 60 °C for PLLA-NMP and 40 Pas at 50 °C for PLLA-dioxane. The higher viscosity of PLLA-NMP does not support the relationship found between polymer-NMP and polymer-dioxane viscosities found in this study, NMP solutions being relatively less viscous.

Several of the PLGA-dioxane solutions had higher readings at 25°C (85:15, 65:35 and 50:50) or even 30°C (75:25) suggesting non homogeneity, a homogeneous mixture being harder to achieve with the higher viscosity of dioxane, solutions or gelling, or possibly evaporation of the solvent during measurement since dioxane is quite volatile (see Appendix D).

These phenomena would help to explain the inability to obtain some readings for dioxane solutions and the lack of trends with temperature and polymer concentration as seen with PLGA-NMP solutions. The large variation in data makes it somewhat difficult to fully assess the dioxane solutions, although the fact that solution is not so user friendly should be considered when selecting the solvent.

4.3.3 MORPHOLOGY

Flat sheet membranes formed with NMP and dioxane differ in both top and bottom surface structure; differences are also seen between membranes made with the same solvent. The top surfaces of the membranes made using NMP have a greater number of smaller pores than their dioxane counter parts. The bottom surfaces of the dioxane flat sheets are less porous with a smoother morphology compared to those made with NMP. The NMP-cast membranes were seen to form faster than the dioxane-cast membranes. 75L:25 was seen to form the fastest in both cases. 75L:25 lifted of the glass immediately ($t<2$ sec) when NMP was the solvent. 100:0 and 75:25 lifted off within 10 sec. 50:50 was noticeably the slowest in the NMP system, taking a matter of minutes to fully coagulate. There was no distinguishable difference between 100:0, 75:25 and 50:50 in the dioxane system, all of which were still stuck to the glass after several hours. This observed rate of membrane formation is a direct consequence of the rate of demixing. The rate of the demixing leads to either an asymmetric cross section with finger-like pores or a sponge-like structure (Mulder 1992) (Section 2.4.4). Instantaneous demixing leads to a porous top structure and an asymmetric cross section as seen with the PLGA-NMP membranes.

The rate at which coagulation occurred and the finger-like structure of NMP-cast membranes and the sponge-like structure of the dioxane-cast membranes suggest that the NMP-cast membranes underwent instantaneous demixing whereas the dioxane-cast membranes were formed by delayed demixing. The pores with dense skins of the dioxane-cast membranes would only allow molecular diffusion and would prevent the flow of the larger proteins found in media; such membranes are commonly used for gas separation processes (Ismail *et al.* 2003). Both these solvents commonly undergo instantaneous demixing (Mulder 1992) suggesting that the polymer has a relatively high affinity for dioxane.

PLGA-NMP-water forms membranes with finger-like pores whereas the PLGA-dioxane-water system forms a sponge-like structure. When coagulation occurs rapidly, this finger-like structure as seen in the NMP system is generally found (Xu and Qusay 2004; Mulder 1992; Li *et al.* 2004), and delayed demixing tends to form the sponge-like structure seen with the dioxane-cast membranes (Mulder 1992). Qin *et al.* (2001) found that in a PES-NMP-water system, a finger-like structure was seen with the 30% polymer concentration solution but at 37% there were no finger-like pores observed. The higher concentration would also have a higher viscosity so such polymer-solvent interactions may affect the phase separation mechanism. Li *et al.* (2004) also recently reported a critical structure-transition thickness above which macrovoids appear and finger-like structures are seen, while below, sponge-like structure are seen.

The porous structure of the NMP-cast membrane is conducive with instantaneous demixing, however, the large pores seen on the top surface of the dioxane-cast membranes are not conducive with the dense membrane structure seen with delayed demixing (Mulder 1992). It could be that the surface coagulation is in fact rapid with slower demixing underneath this film. The smooth nonporous bottom layer of the membrane cast with both solvents is due to the delayed demixing which is further delayed as water must diffuse through the membranes to reach the polymer solution in contact with the glass.

50:50 has the roughest surface of the NMP-cast membranes as observed on the micrographs and is likely to be preferred by the cells to the smoother surfaces of the other membranes (Section 2.3.3). Polymer-dioxane cast membranes have much larger surface pores. All four membranes appear to have a rougher surface compared to the NMP cast membranes. The porous top structure of the membranes formed with both NMP and dioxane are suitable to test for cell culture, as the pores do not exceed 5μm. The porous surface seen shows that despite being exposed to air for up to 5 sec before being placed into the water bath, no dense film formed.

The 75L:25 membranes made with both NMP and dioxane have larger pores and a higher top and bottom surface porosity compared to the other. This is expected considering that the membrane lifts off the glass almost immediately. The lower initial concentration of 10% means a lower concentration at the film interface so leading to a more porous top layer (Mulder 1992).

The membranes cast from polymer-dioxane solutions have thinner cross sections than their polymer-NMP counter parts despite being cast from solutions of the same concentration and being prepared with the same depth of solution on the glass.

A decrease in size from the initial solution thickness of 200 μm is due to a greater outflow of solvent than influx of water. The net flow from the membrane must be dependent on either polymer-solvent or polymer-nonsolvent interaction, or a combination of both.

The solubility of the PLGA in both NMP and dioxane, and the viscosities suggest that both polymer-solvent combinations are suitable for spinning. The surface structure of the flat sheets formed with both solvents are also suitable for cell culture, the larger pores seen with polymer-dioxane cast membranes appear better for mass transfer. However, the cross section is the deciding factor since it must be highly porous for the diffusion of the large molecules found in media. The sponge-like structure of the polymer-dioxane cast membranes is unsuitable for this purpose. For static or simple perfusion two-dimensional cell culture the choice of solvent is greater as the internal structure of the polymer is not critical other than to give mechanical support.

4.4 CONCLUSIONS

Since PLGA was soluble in NMP and dioxane, PLGA-NMP and PLGA-dioxane solutions could both be used to spin hollow fibre membranes. However, NMP was selected as the solvent of choice for spin casting PLGA hollow fibre membranes. The decision was based on the combined results for solution viscosity and

macrostructure of the polymers tested. The polymer concentration in NMP required to give a suitable viscosity for spin casting was between 19% and 30% at 25°C which is the suggested concentration range (Xu and Qusay 2004). Furthermore, the macro-structure was open finger-like and interconnected pores as required for good nutrient mass transfer. Surface pore size ranged from 0.2 to 0.8 μm for the different polymer-NMP combinations. This pore size range is adequate to retain cells, which can migrate through pores down to 5 μm diameter, on the membrane surface while allowing nutrient and waste molecules of up 150 kDa to permeate. In addition, NMP has a low toxicity and volatility making the solvent more user friendly than dioxane.

The following chapters use the PLGA-NMP-Water system to prepare the membrane scaffolds.

CHAPTER FIVE
PLGA MEMBRANE SCAFFOLD DESIGN II-HOLLOW FIBRES

5.1 INTRODUCTION

Novel hollow fibre asymmetrical membranes were selected as the scaffold structure due to the structural similarities with cortical bone (Section 2.2.1). Once placed into a hollow fibre bioreactor (HFB) this structure has two other major advantages; a large surface area to volume ratio beneficial for obtaining large cell numbers, and relatively consistent mass transfer across the membranes and subsequently the tissue construct. Once the construct is implanted, the lumen of the fibres can act as guides for angiogenesis and are proposed to function in a similar role to the Haversian canal until remodelling occurs and the scaffold is replaced with mature bone.

The mechanism of membrane formation by phase inversion is described in Section 2.4.2. In the case of hollow fibre membrane spinning, both the outer and inner surfaces of the membrane are exposed to the nonsolvent so demixing occurs from both surfaces, whereas with flat sheet membrane casting only the top surface is exposed to the nonsolvent so demixing occurs from one side only. Chapter 4 showed that a PLGA-NMP-water system formed membranes with an asymmetric porous structure. All PDLLA:PGA ratios tested, except 45:55, were suitable for spinning at 25°C when dopes were at least 19 w/w% polymer so having a viscosity of at least 1 Pas. The data in this chapter shows the effects of changing the spinning conditions on the characteristics of the hollow fibre membranes. Polymer concentration in the spinning dope, air gap (the distance between the spinneret and the coagulation bath) and take-up rate (rate at which the hollow fibre is collected) were investigated and assessed for optimal settings for the desired structure. 50:50 and 75:25 were selected for the studies; 50:50 required the largest polymer concentration (22%) to achieve the minimum spinning viscosity of 1 Pas and 75:25 required the lowest polymer concentration (19%) to achieve the same viscosity.

As described in Chapter 4, the maximum pore size of the cell culture surface-the outer skin of the hollow fibres-is 5μm as cells can enter spaces larger than this (Beresford 2002). The minimum pore size must allow the passage of gas, nutrients and waste products which have a molecular mass of up to 150 kDa, Kumar *et al.* (2004). The cross-section structure should provide support to maintain the shape of the fibre and should be highly porous with interconnecting pores to provide a low resistance to mass transfer for nutrients.

5.1.1 POLYMER CONCENTRATION IN THE SPINNING DOPE AND ITS EFFECT ON FIBRE CHARACTERISTICS

Originally, Flory and Huggins who developed the expression for the free enthalpy of mixing of a polymer-solvent-nonsolvent system, thought that it was independent of concentration, however it has since been shown that the interaction parameters are dependent on the composition (Mulder 1992). Since the rate of demixing is determined by the nonsolvent flux into and the solvent flux out of the polymer-solvent solution, which in turn is a function of the free energy of mixing, polymer concentration in the spinning dope is an important consideration.

5.1.2 AIR GAP AND ITS EFFECT ON FIBRE CHARACTERISTICS

The work by Chung and Hu (1997) showed that different precipitation paths were taken with dry-wet and wet spinning. The former initially involved a moisture-induced phase separation that gave skins with "long-range random unorientated chains with a loose structure". Wet spun fibres were formed by an almost instantaneous phase separation resulting in a "short-range random, compact and a slightly orientated or stretched structure" which gave a greater free volume. With the introduction of, and by increasing the air gap, the group found that the finger-like structure was reduced as was permeance. An air gap also introduces elongation stress due to gravity (take-up rate set to the free falling velocity to prevents additional elongational stresses), which can have an effect on the resulting structure depending on the magnitude of the stress (Chung and Hu 1997).

5.1.3 TAKE-UP RATE AND ITS EFFECT ON FIBRE CHARACTERISTICS

Several papers including Chung *et al.* (1998); Qin and Chung (1999); Chung *et al.* (2000); Wang and Chung (2001) have described the effect of shear within the spinneret, but it is accepted as hard to decouple these effects from other parameter effects. The orientation due to shear in the spinneret is thought to be maintained in wet spinning (Qin and Chung 1999), but when an air gap is introduced, the molecules may experience die swell and relax (Chung *et al.* 2000) and loose this orientation which will effect the wall structure of the hollow fibre as well formation of a dense skin seen with exposure to air with dry, wet spinning (Chung and Hu 1997). The flow rate of the dope from the spinneret affects the shear rate within the spinneret. Qin and Chung (1999) found that a higher dope rate resulted in a fibre with a smaller pore size and a denser skin due to greater molecular orientation. Interestingly, the fibres formed at a higher shear rate had a larger Young's modulus and tensile strength that would be beneficial for a scaffold to maintain its structure.

It should also be noted that polymer solutions with a critical low viscosity will not be able to balance out the stresses due to rapid solvent exchange in wet spinning (see Section 5.1.2) which results in a double finger-like structure in which the finger-like voids penetrate from both the inner and outer edges of the fibre cross-section (Chung and Hu 1997). It can be hypothesised that the PLGA solutions made up at lower concentrations and hence having lower viscosities will show this double finger-like structure.

5.1.4 FIBRE CHARACTERISTICS AND THE RELATION TO THEIR USE AS A SCAFFOLD

The fibre morphology, namely the pore size and free volume govern the mass transfer characteristics. Permeability would be lower for smaller pores, as would flux which would also be lower with a low free volume. However, smaller pores and less free volume would be expected to increase tensile strength and Young's modulus based on previous findings (Qin and Chung 1999; Chung *et al.* 2000).

The topography of the cell culture surface can also be highly influential on the final success of the scaffold. Both surface roughness and surface microgrooves have been shown to effect osteoblast and osteoblast-like cell culture, further details of which are discussed in Section 2.3.3.

5.2 RESULTS

It was shown in Chapter Four that asymmetric membranes could be made from the PLGA-NMP-water ternary system. A range of suitable PLGA compositions, solution concentrations and operating temperatures was also selected based on solubility, viscosity and resulting membrane morphology.

For the experiments to investigate the properties of PLGA hollow fibres, 50:50 and 75:25 were chosen to look for differences between PLGA compositions and NMP was the solvent. Both 20% and 25% polymer concentrations were examined, 0 mm and 30 mm air gap and 5.5 m/min and 7.7 m/min take-up rate were also examined. The basal spinning conditions were a 20% polymer concentration, 0 mm air gap and 7.7 m/min take-up rate. Hollow fibres were spun at 25°C and water was used as the nonsolvent in all cases. The hollow fibres are analysed using SEM and gas permeation; comparisons were made for morphology, topography, pore size, porosity and dimensions.

5.2.1 EFFECT OF POLYMER SOLUTION CONCENTRATION ON HOLLOW FIBRE STRUCTURE

The polymer concentration affects the structure of the membrane. A higher volume fraction of polymer will give a less porous structure. A higher initial concentration means a higher concentration at the film interface so leading to a less porous skin top layer, which will reduce the flux (Mulder 1992).

Based on the results in Chapter 4, 20 w/w% and 25 w/w% polymer concentration were selected to investigate the effect of polymer concentration on hollow fibre structure.

The macro-structure of the fibres made from 20% polymer concentration solutions (Figure 5.1 C & D) are more open than those made from 25% (Figure 5.1 A & B). 20% 50:50 shows a collapsed central section. Long finger-like pores were seen in the cross-section of 75:25 fibres made from a 25% solution. Shorter finger-like pores were seen in fibres made from a 20% solution, with large round macrovoids in the central section protruding from the inner edge.

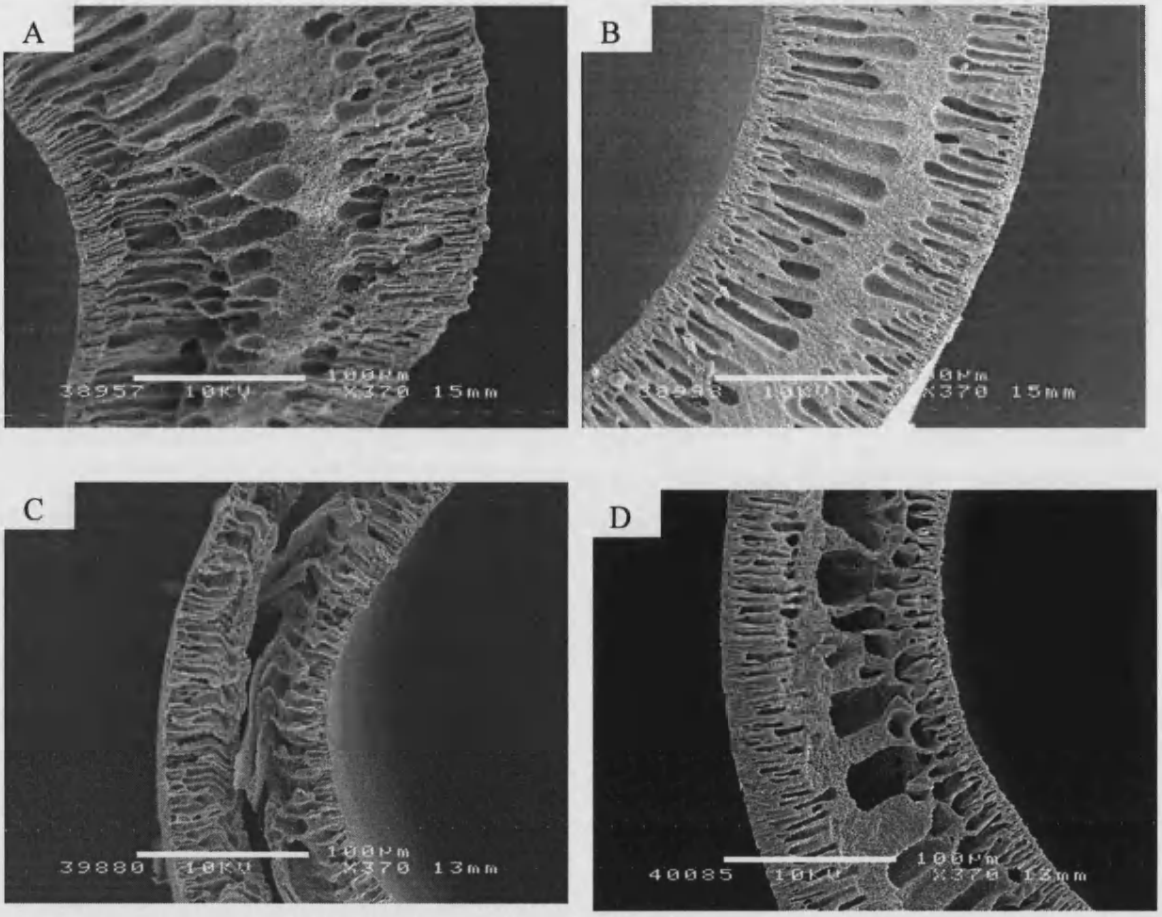

Figure 5.1. Cross-section of hollow fibre membranes at different polymer concentrations.
(A) 25% 50:50, (B) 25% 75:25, (C) 20% 50:50, (D) 20% 75:25. Scale bar 100 μm.

The finger-like pores perpendicular to and in contact with the outer and inner edges can be seen in more detail in Figures 5.2 and 5.3 respectively. The hollow fibres made from 25% polymer solutions have finger-like pores perpendicular to the outer surface, up to 20μm in length for 50:50 and 5μm for 75:25 (Figure 5.2 A and B respectively). The hollow fibres made from 20% polymer solutions have finger-like pores perpendicular to the outer surface, up to 15 μm in length for 50:50 (Figure 5.2 C). There is a dense film of around 5μm in contact with the surface for 75:25 (Figure 5.2 D).

At the inner edge, finger-like pores up to 15μm in length are seen for 50:50, and 10 μm for 75:25 for fibres made with 25% polymer concentrations (Figure 5.3 A and B

respectively). The hollow fibres made from 20% polymer solutions have finger-like pores perpendicular to the inner surface up to 10 μm in length for 75:25 (Figure 5.3 D). At the inner edge of the 20% 50:50 fibres, the pores are less finger-like and more rounded (Figure 5.3 C).

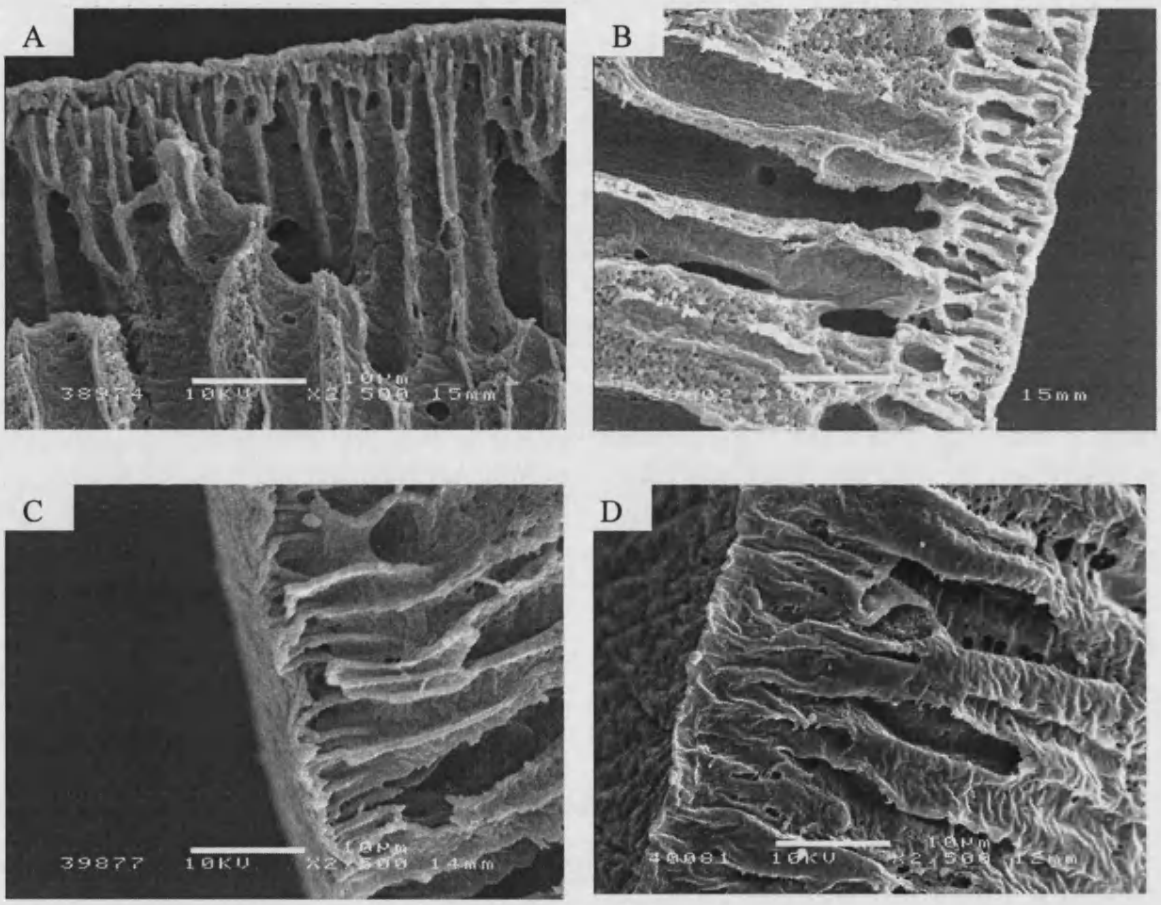

Figure 5.2. Outer edge of cross-section of hollow fibre membranes at different polymer concentrations.
(A) 25% 50:50, (B) 25% 75:25, (C) 20% 50:50, (D) 20% 75:25. Scale bar 10 μm.

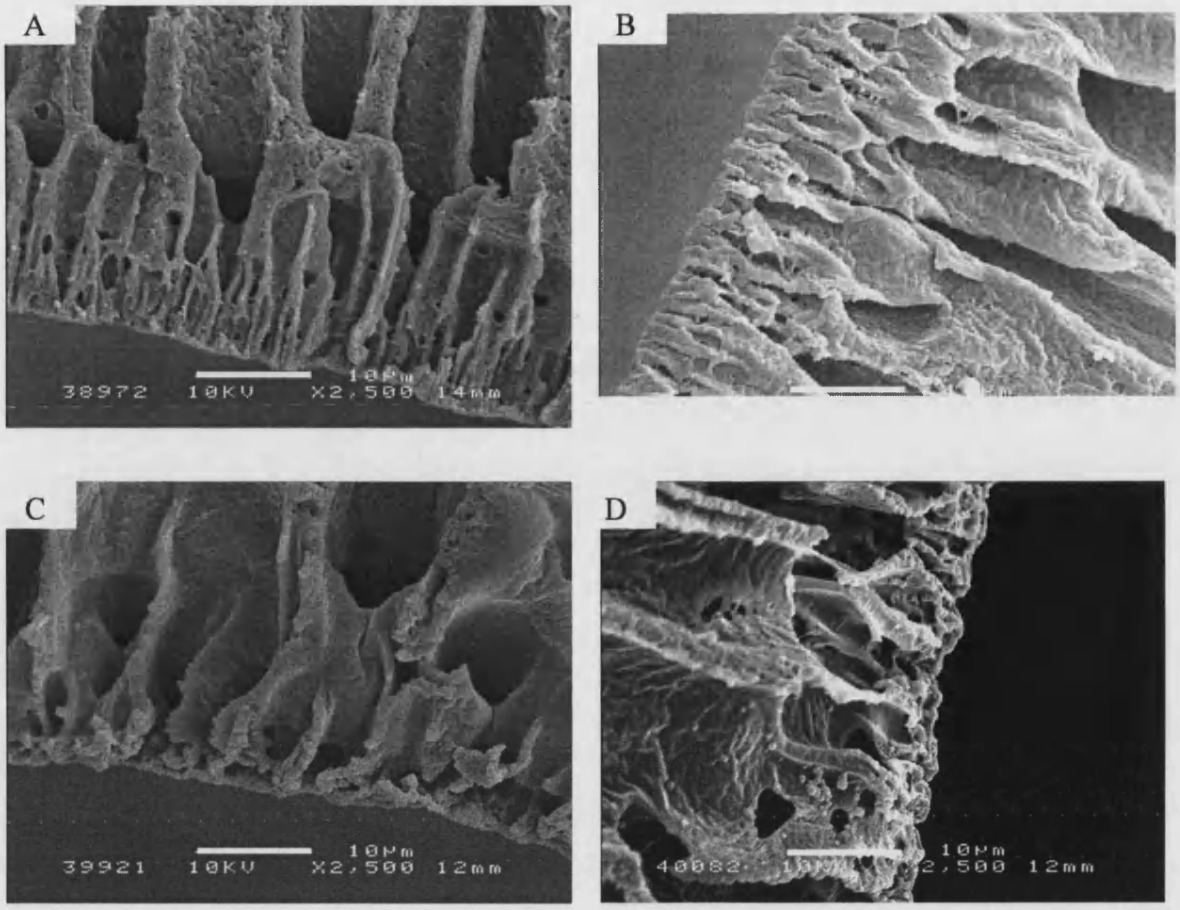

Figure 5.3. Inner edge of cross-section of hollow fibre membranes at different polymer concentrations.
(A) 25% 50:50, (B) 25% 75:25, (C) 20% 50:50, (D) 20% 75:25. Scale bar 10 μm.

The polymer concentration also affects the surface structures, which differ both with polymer concentration and PLA content (Figure 5.4 and 5.5). 50:50 had a relatively more porous surface structure compared with 75:25 for both the polymer solution concentrations tested (Figure 5.4). The pore size range for 50:50 is 0.1 – 0.5 μm at both 20% and 25% polymer concentration, however, the outer surface of the 50:50 fibres is more porous at 20% than 25% (Figure 5.4 A & C). 75:25 has a more undulating surface than 50:50 at both polymer solution concentrations, but it was more dense.

The inner surfaces (Figure 5.5) are both highly porous with pores in the size range 0.2 – 1 μm. This pore size is larger than those on the surface of 50:50, which are in

the range 0.1 – 0.5 μm. The surfaces are grooved and the pores aligned in the direction of flow from the spinneret.

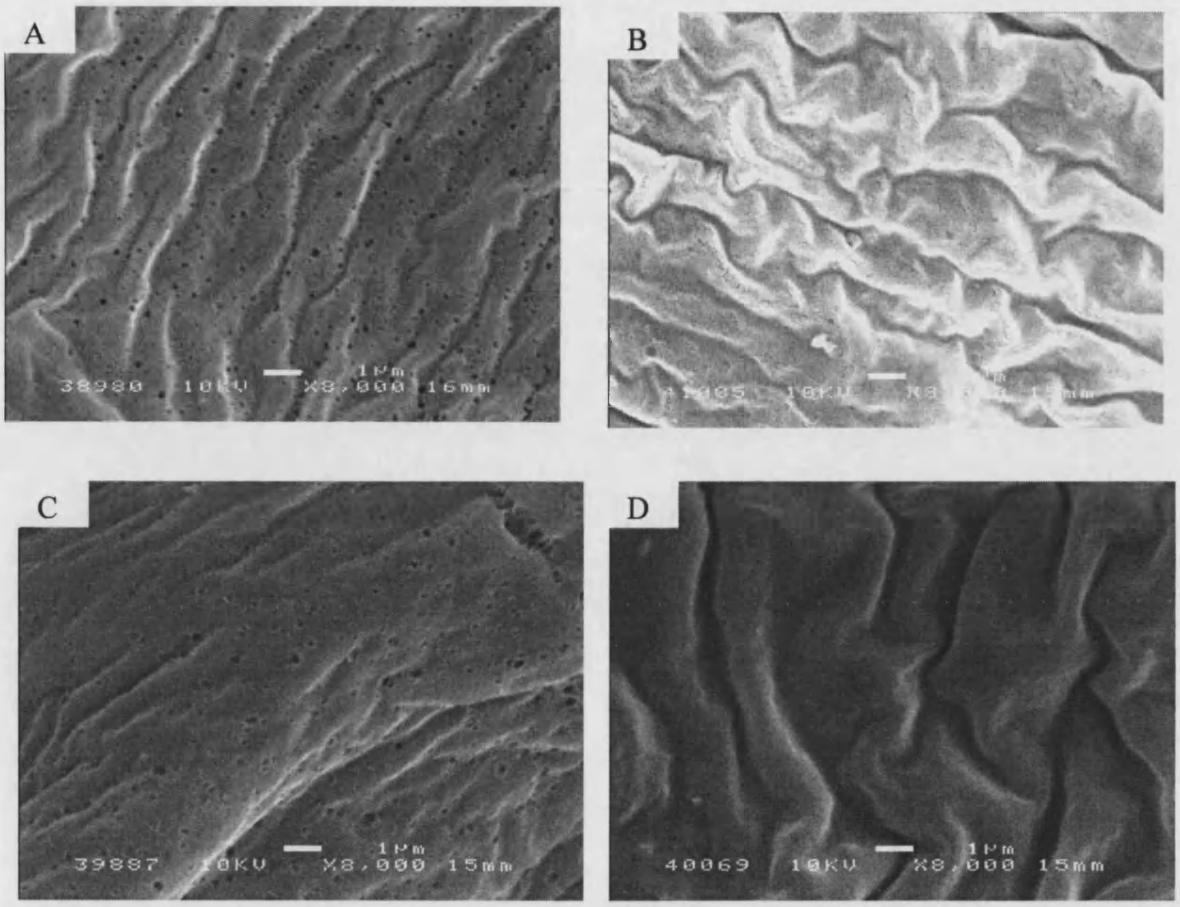

Figure 5.4. Outer surface of hollow fibre membranes at different polymer concentrations.

(A) 25% 50:50, (B) 25% 75:25, (C) 20% 50:50, (D) 20% 75:25. Scale bar 1 μm.

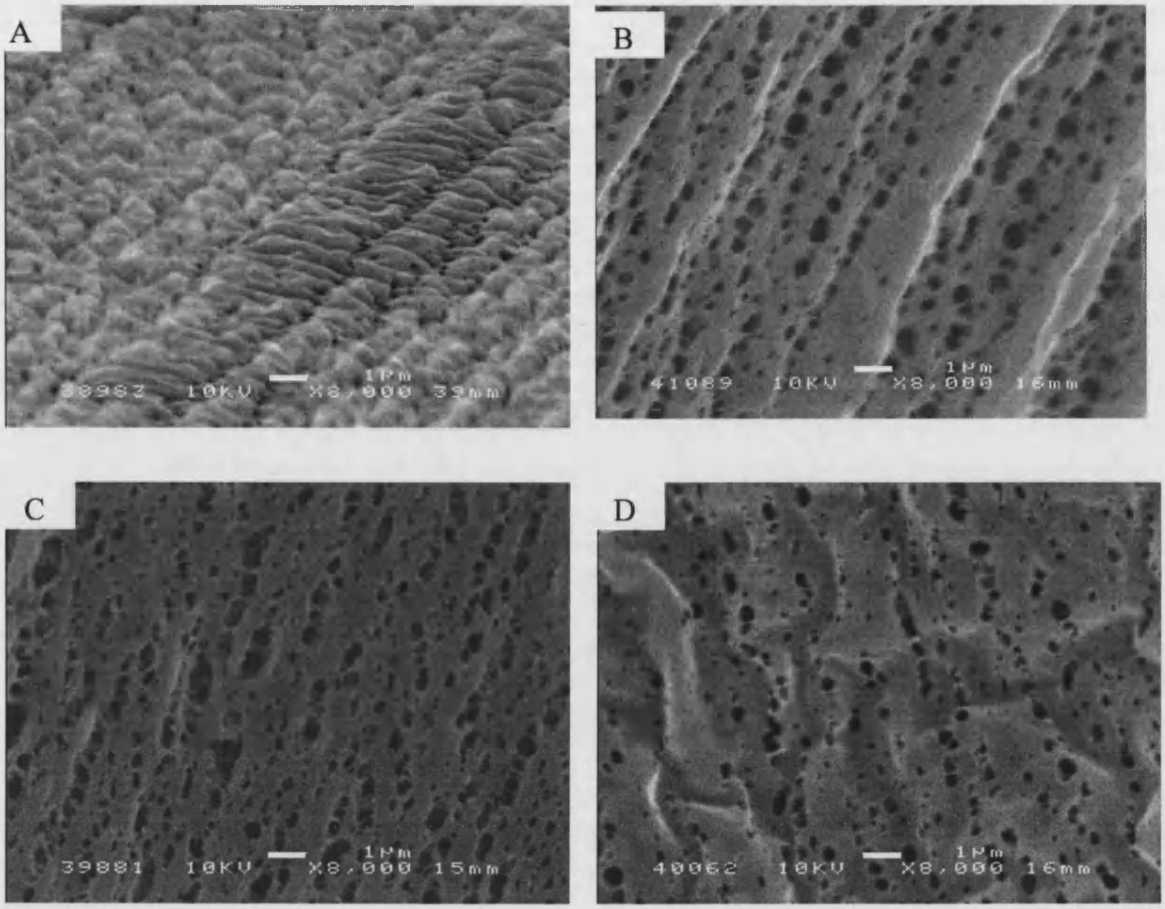

Figure 5.5. Inner surface of hollow fibre membranes at different polymer concentrations.
(A) 25% 50:50, (B) 25% 75:25, (C) 20% 50:50, (D) 20% 75:25. Scale bar 1 μm.

5.2.2 EFFECT OF AIR GAP ON HOLLOW FIBRE STRUCTURE

The dry-wet spinning technique involves the presence of an air gap, whereas no air gap is referred to as wet spinning. Different demixing mechanisms occur when dry-wet or wet spinning are employed (Chung and Hu 1997). The effect of a 30 mm air gap was compared to no air gap, the morphology of the resulting hollow fibres was then analysed.

Cross-sections of the fibres are shown in Figure 5.6. The cross-sections of the 50:50 fibres made with 30 mm air gap (Figure 5.6 A) and 0 mm air gap (Figure 5.6 C) are very similar except for the central section. The central section did not collapse with 0 mm air gap and the finger-like pores penetrating the wall from both edges are themselves nearly connected with only a very thin central section. The cross-section

of the 0 mm air gap 75:25 fibre (Figure 5.6 D) shows the more open pore structure reaching to the surface of the fibre due to fast demixing. The macrovoids seen in the fibre formed with a 30 mm air gap elongated and were more finger-like at 0 mm air gap. 50:50 fibres had a thinner wall than the 75:25 fibres with both air gaps.

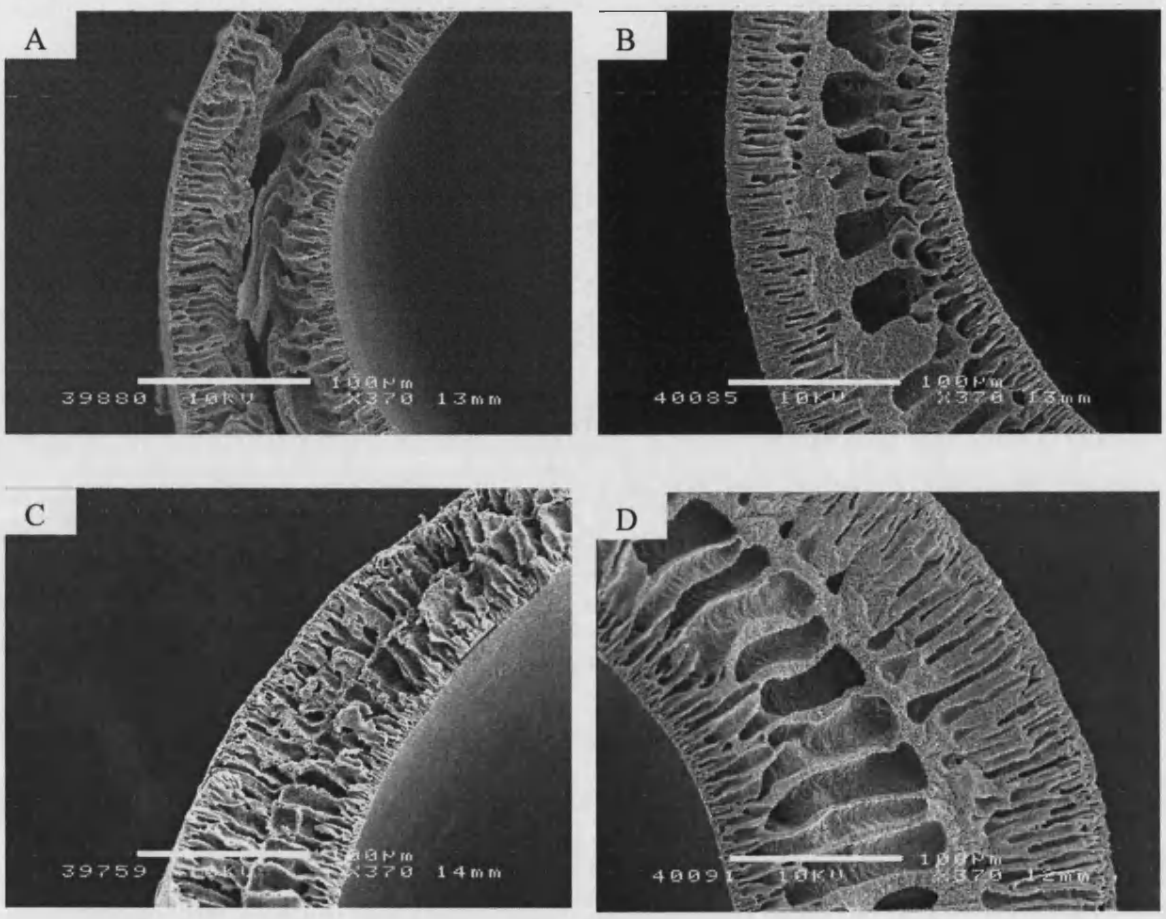

Figure 5.6. Cross-section of hollow fibre membranes at different air gaps.
(A) 30 mm 50:50, (B) 30 mm 75:25, (C) 0 mm 50:50, (D) 0 mm 75:25. Scale bar 100 μm.

Further detail of the finger-like pore structure at the outer and inner edge can be seen in Figures 5.7 and 5.8 respectively. The outer edge of 50:50 was similar with both a 30 mm (Figure 5.7 A) and 0 mm (Figure 5.7 B) air gap, having finger-like pores perpendicular to the porous outer surfaces, up to 15 μm in length. There was a noticeable difference in the structure of the cross-section at the outer edge of the 75:25 fibres. While there is a dense skin of about 5 μm thick at the outer edge with a

30 mm air gap (Figure 5.7 B), with a 0 mm air gap the outer edge had a very thin skin which was 0.5 μm thick long, in contact with open finger-like pores, up to 15μm in length (Figure 5.7 D).

The pores in contact with the inner edges were more finger-like with a 0 mm that a 30 mm air gap for both 50:50 and 75:25 fibres. The 75:25 fibres had longer, finger-like pores than the 50:50 fibres at the respective air gaps. At the inner edge of the 50:50 fibres made with a 30 mm air gap, the pores were less finger-like and more rounded (Figure 5.8 A), approximately 5 μm long while the 75:25 fibres made with a 30 mm air gap had finger-like pores perpendicular to the inner surface up to 10 μm in length for 75:25 (Figure 5.8 B). The 50:50 fibres made with a 0 mm air gap had pores around 7 μm in length (Figure 5.8 C), the 75:25 fibres had pores approximately 15 μm long (Figure 5.8 D).

Both the porosity and the topography differ greatly with air gap, and between the polymers with different PLA content. With a 30 mm air gap, 50:50 has a porous surface structure compared with 75:25 which had a nonporous surface but which was more undulating (Figure 5.9 A & B respectively). The inners surfaces are both highly porous with pores in the size range 0.2 – 1 μm (Figure 5.10 A & B respectively). This pore size is larger than those on the surface of 50:50 which are in the range 0.1 – 0.5 μm.

The observed surface porosity is greater for the 50:50 fibre made with 0 mm air gap (Figure 5.9 A) compared with the surface of the fibre made with 30 mm air gap (Figure 5.9 B). The opposite is seen for the inner surfaces (Figure 5.10 A & B respectively). The nonporous surface is also seen on the 75:25 fibres with a 0 mm air gap (Figure 5.9 D), however the inner surface appears more porous with a 0 mm air gap compared to the 30 mm air gap and also more undulating (Figure 5.10 B & D respectively). The outer and inner surfaces of the 50:50 fibres show a grooved structure aligned in the direction of flow. No such grooved structure is seen with the 75:25 fibres.

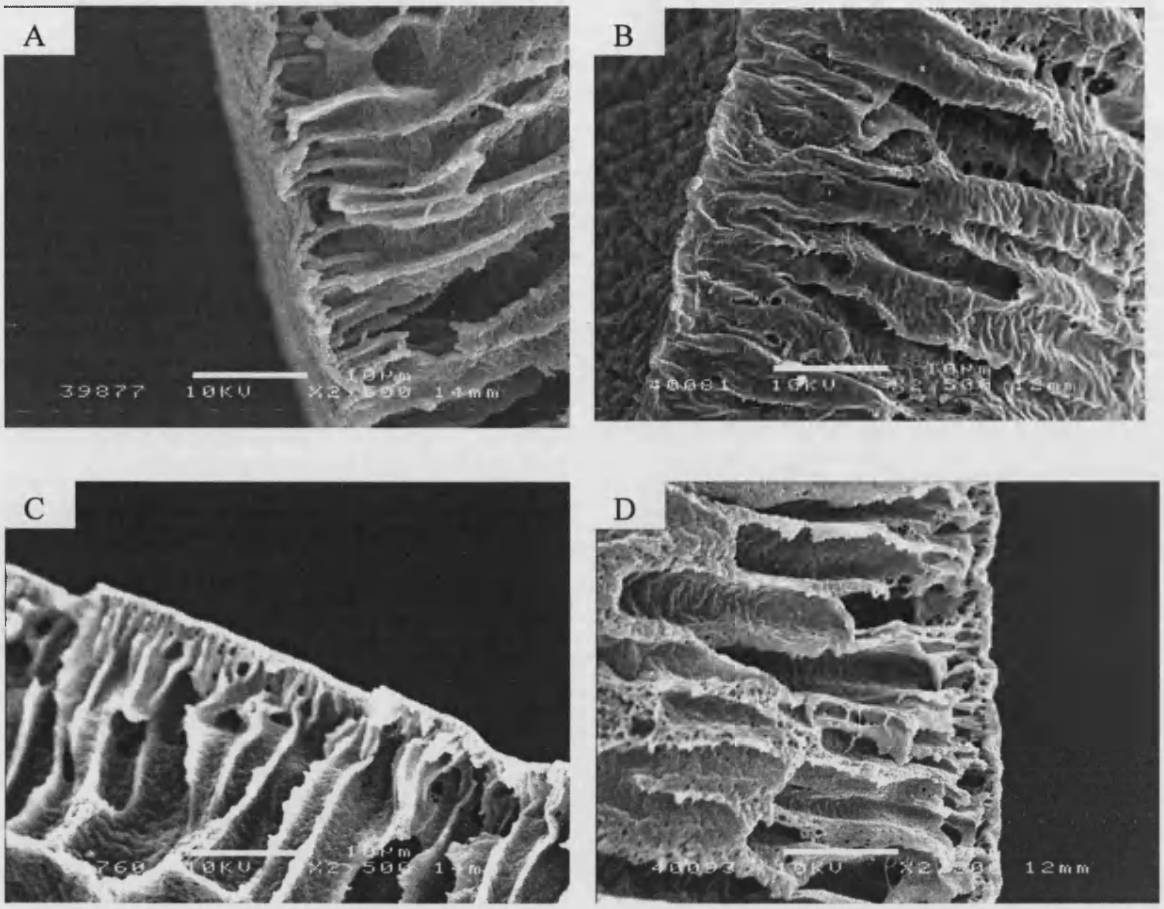

Figure 5.7. Outer edges of the hollow fibre membranes at different air gaps.
(A) 30 mm 50:50, (B) 30 mm 75:25, (C) 0 mm 50:50, (D) 0 mm 75:25. Scale bar 10 μm.

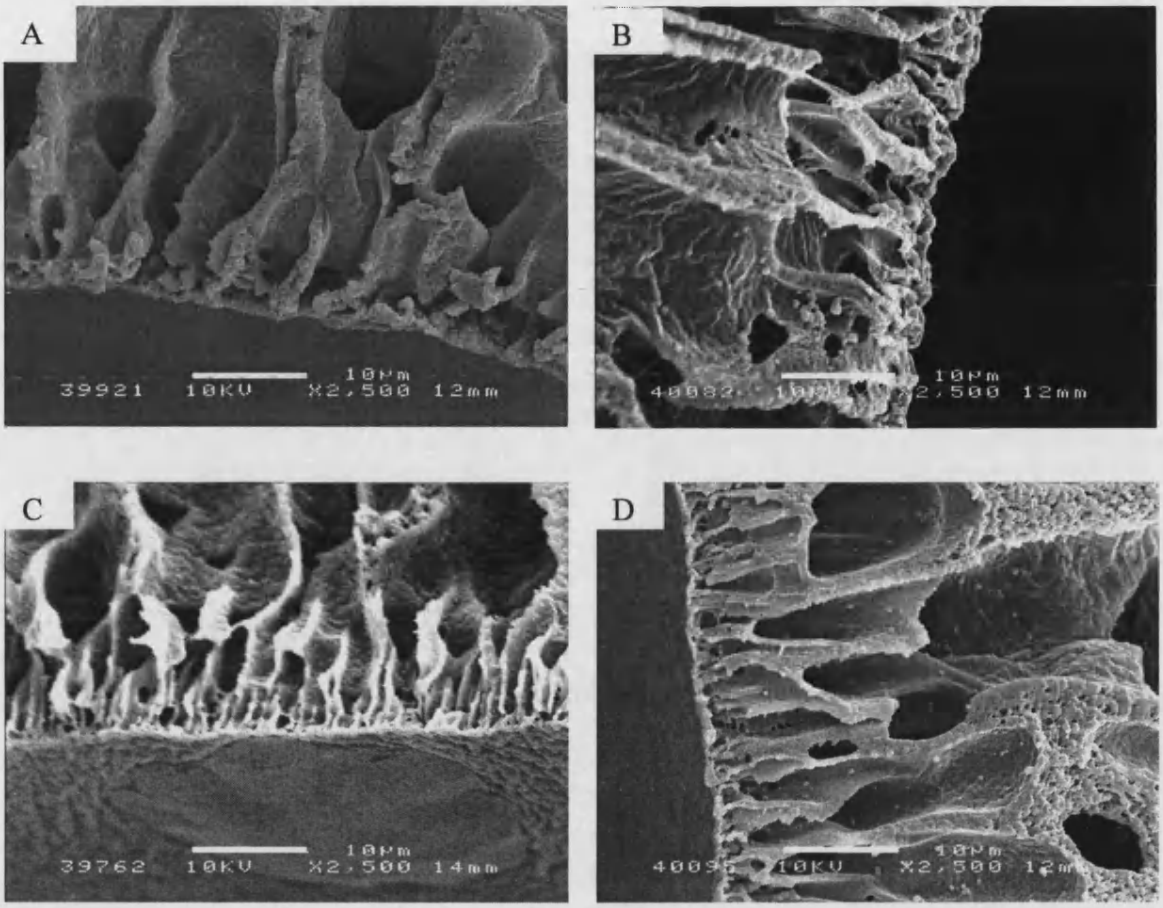

Figure 5.8. Inner edges of the hollow fibre membranes at different air gaps.
(A) 30 mm 50:50, (B) 30 mm 75:25, (C) 0 mm 50:50, (D) 0 mm 75:25. Scale bar 10 μm.

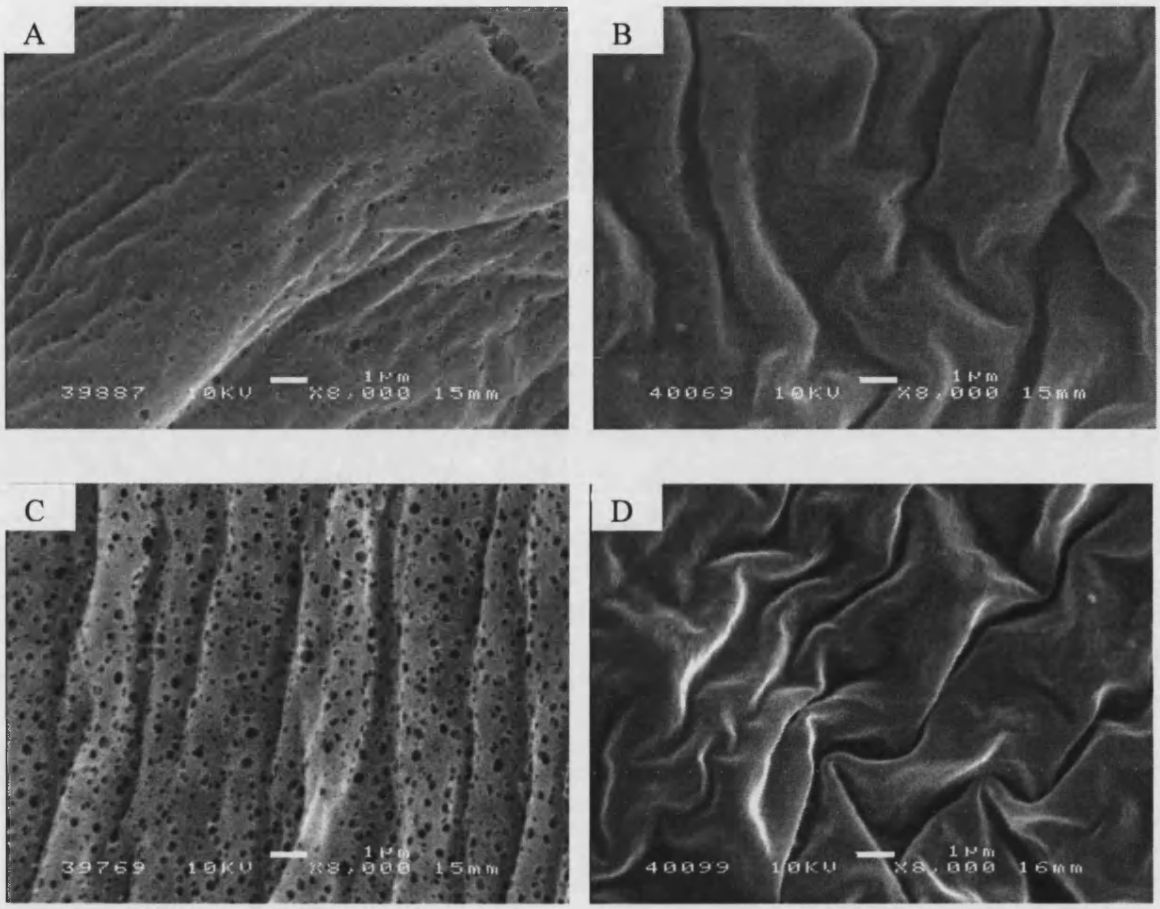

Figure 5.9. Outer surface of hollow fibre membranes at different air gaps.
(A) 30 mm 50:50, (B) 30 mm 75:25, (C) 0 mm 50:50, (D) 0 mm 75:25. Scale bar 1 μm.

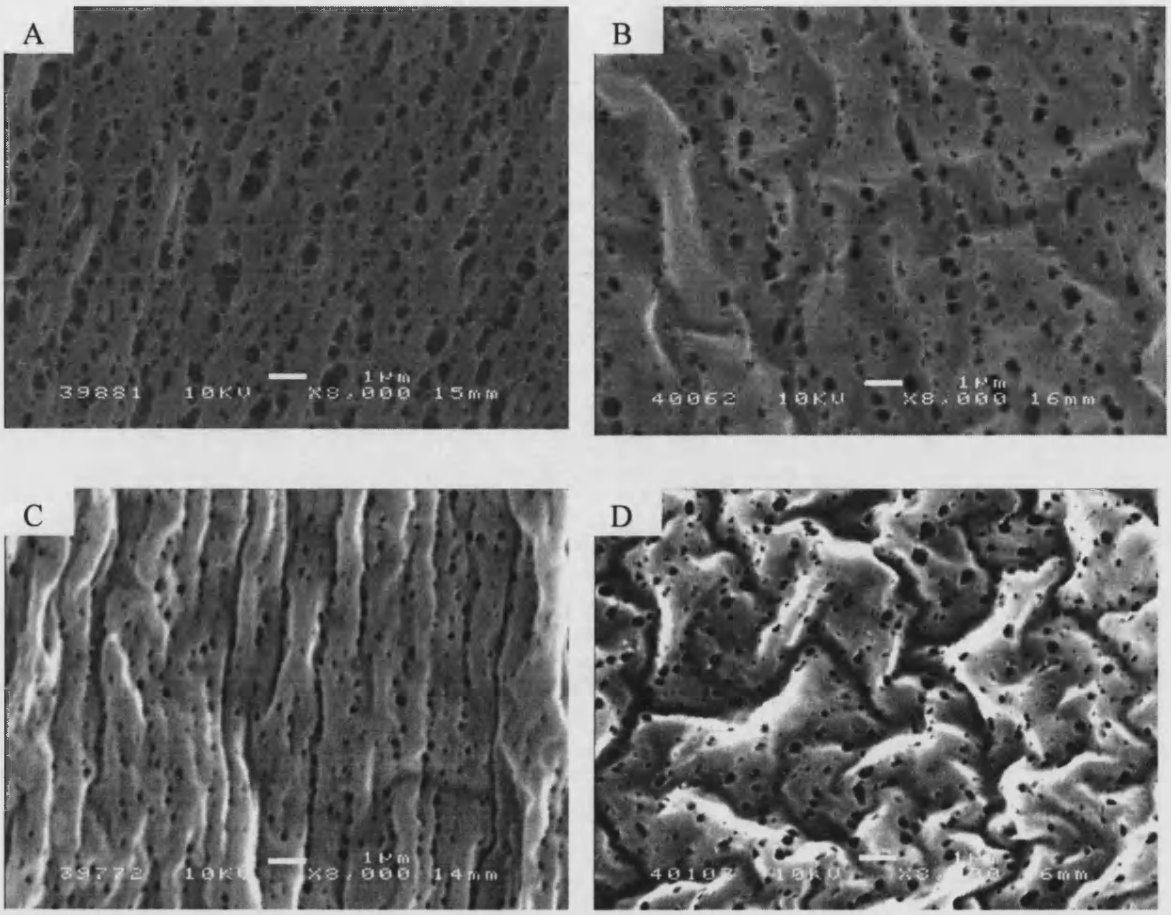

Figure 5.10 Inner surface of hollow fibre membranes at different air gaps.
(A) 30 mm 50:50, (B) 30 mm 75:25, (C) 0 mm 50:50, (D) 0 mm 75:25. Scale bar 1 μm.

5.2.3 EFFECT OF TAKE-UP RATE ON HOLLOW FIBRE STRUCTURE

For this study the take-up rate was set to equal the polymer flow rate so as to prevent drawing. This reduces elongational stress (Qin and Chung 1999) and allows the spinning rate to be considered the same as the take-up rate. Stresses should be due to shear and gravity only, however, by spinning with a 0 mm air gap, the effect of gravity should be largely reduced (Qin and Chung 1999). Bore flow rate was kept constant.

Typical cross-sections at 5.5 m/min and 7.7 m/min for both 50:50 and 75:25 fibres are shown in Figure 5.11. The cross-sections of both 50:50 and 75:25 at 7.7 m/min show pores at right angles to the surfaces (Figure 5.11 C & D), whereas at 5.5 m/min

they appeared slanted (Figure 5.11 A and B). The 50:50 fibre made at 5.5 m/min had very large and slanted macrovoids in the central section. The cross-section of the 50:50 fibre made at 7.7 m/min showed a more regular pore structure, the finger-like pores penetrating the wall from both edges were themselves nearly connected with only a very thin central section. Although the pores are slanted, the pores of the 75:25 fibres prepared at 5.5 m/min were longer and more finger-like compared to the fibres made at 7.7 m/min, which had very large macrovoids.

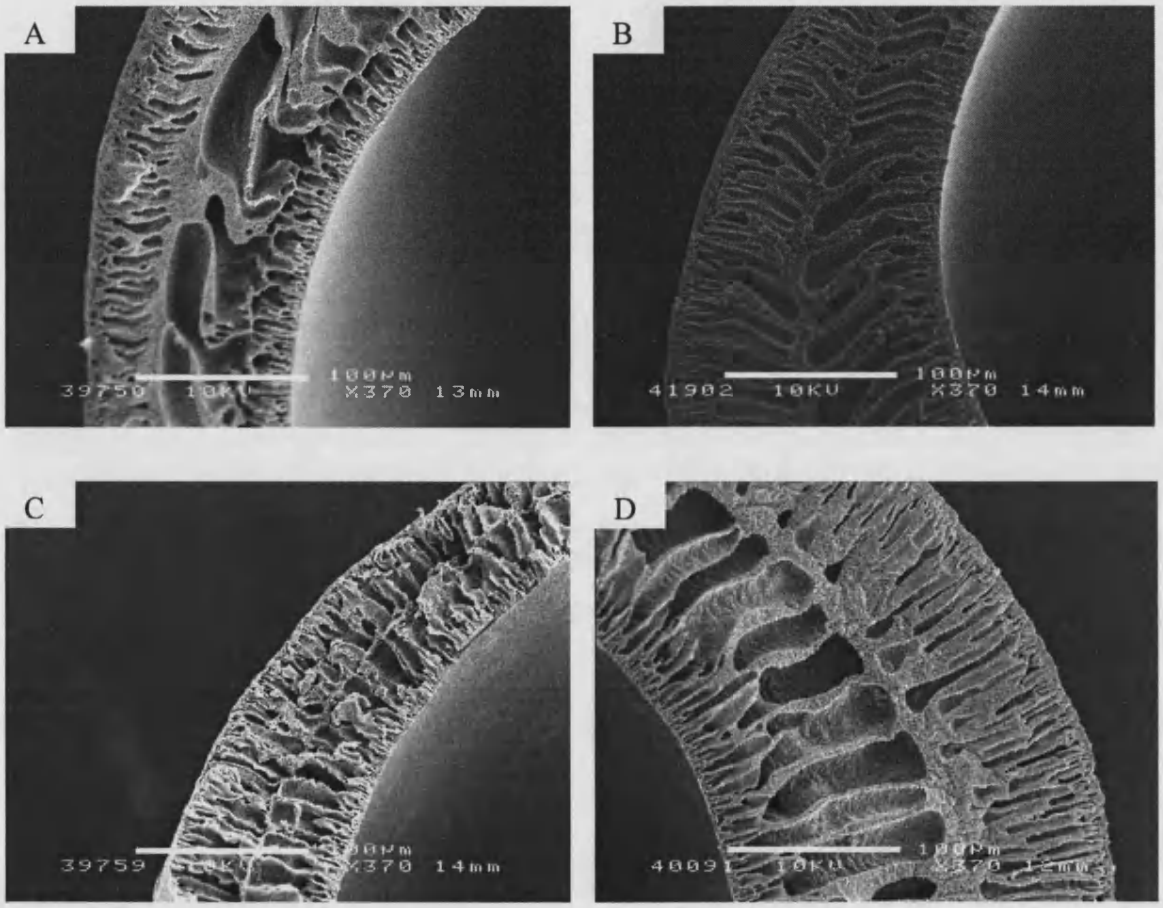

Figure 5.11. Cross-section of hollow fibre membranes at different take-up rates. (A) 5.5 m/min 50:50, (B) 5.5 m/min 75:25, (C) 7.7 m/min 50:50, (D) 7.7 m/min 75:25. Scale bar 100 μm.

Detail of the pores at the outer and inner edges can be seen in Figures 5.12 and 5.13 below. The pores perpendicular to the outer surface of the 50:50 fibres made at 7.7 m/min (Figure 5.12 B) were more finger-like than those of the fibres made at 5.5

m/min (5.12 A). The latter were more round and had thick pore walls, although they were still porous. The pores perpendicular to the outer surfaces of the 75:25 fibres were finger-like for both take-up rates. The pores of the 5.5 m/min fibres (Figure 5.12 B) show better connection to the surface whereas a very thin film could be observed on the surface of the fibres made at 7.7 m/min (Figure 5.12 D).

The inner edges of the 50:50 fibres at both take-up rates had similar morphologies (Figure 5.13 A & C). The pores perpendicular to the inner surface of the 75:25 fibres made at 7.7 m/min (Figure 5.13 D) were longer than those seen in the fibres at 5.5 m/min (Figure 5.13 B).

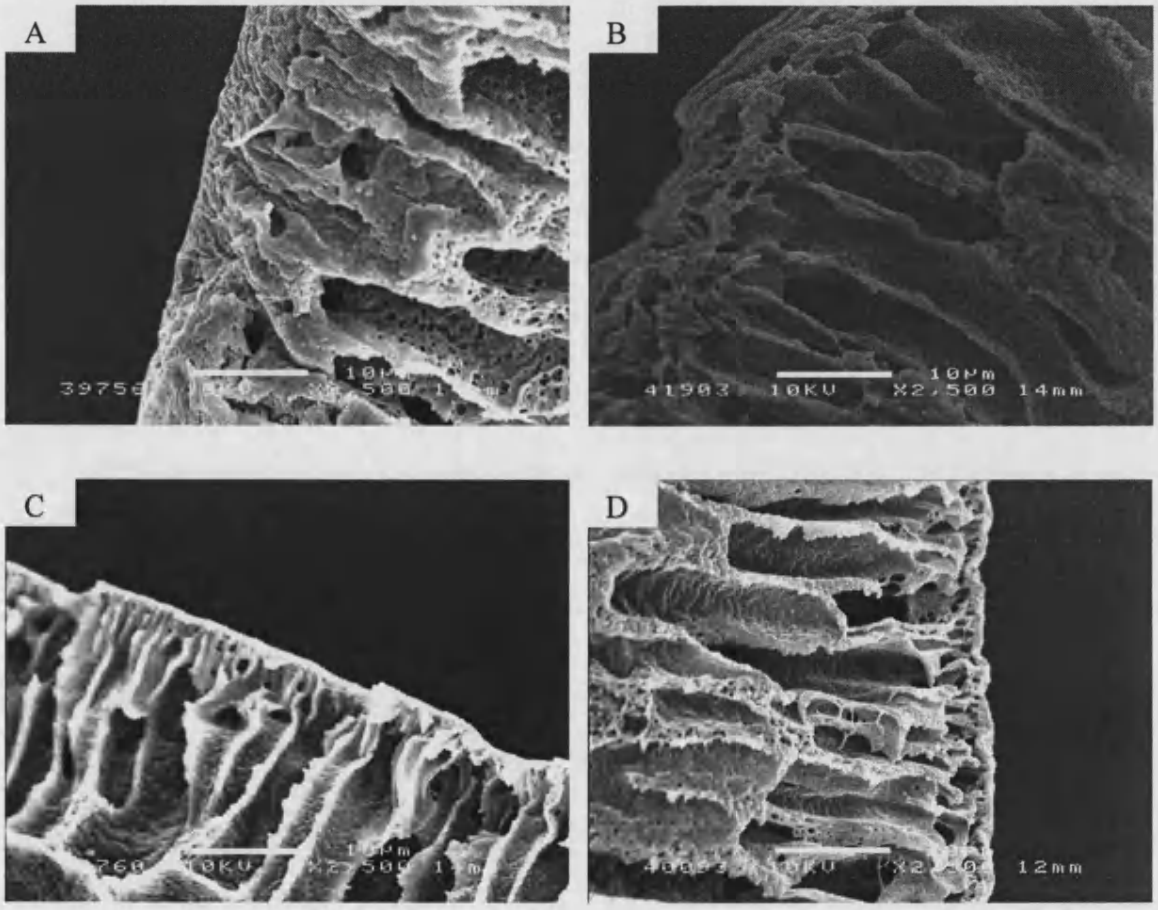

Figure 5.12. Outer edge of cross-section of hollow fibre membranes at different take-up rates.
(A) 5.5 m/min 50:50, (B) 5.5 m/min 75:25, (C) 7.7 m/min 50:50, (D) 7.7 m/min 75:25. Scale bar 10 μm.

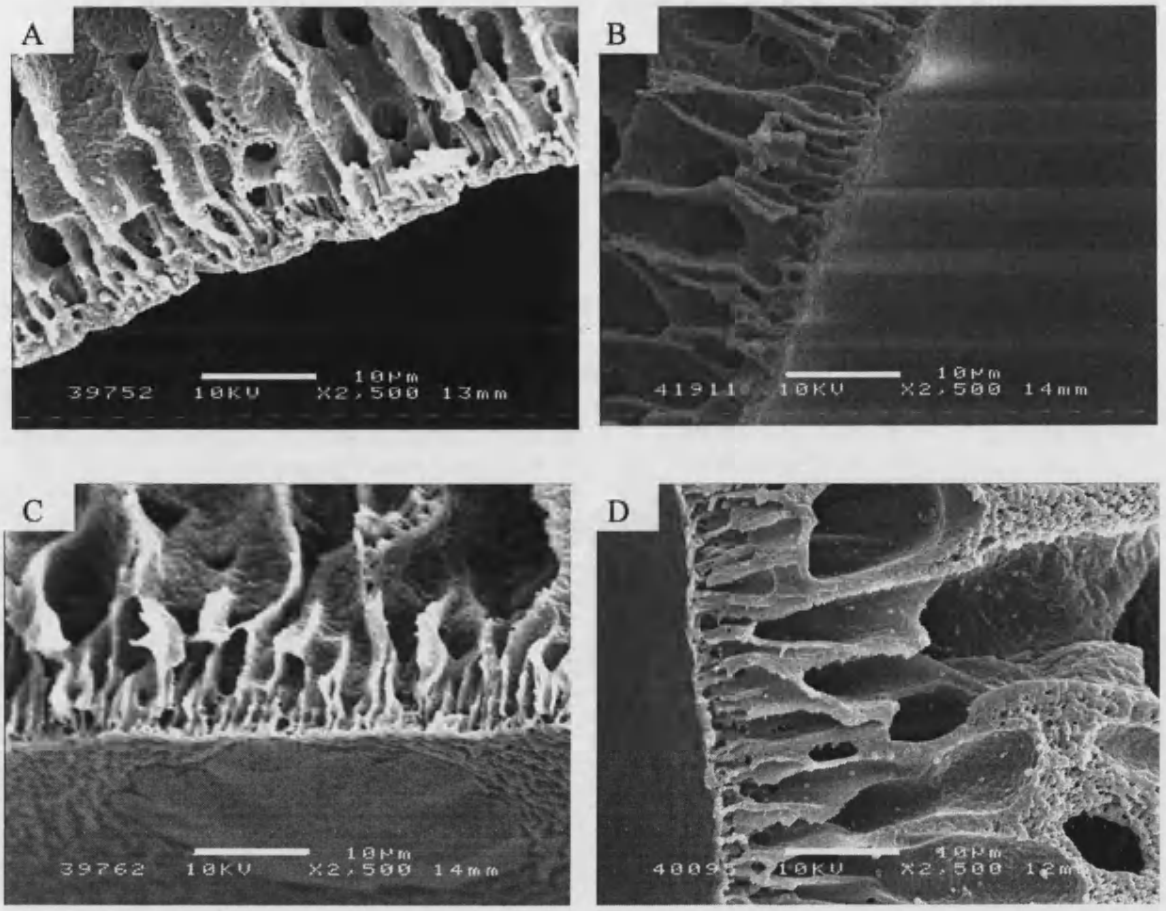

Figure 5.13. Inner edge of cross-section of hollow fibre membranes at different take-up rates.
(A) 5.5 m/min 50:50, (B) 5.5 m/min 75:25, (C) 7.7 m/min 50:50, (D) 7.7 m/min 75:25. Scale bar 10 μm.

The lower take-up rate of 5.5 m/min gave a more porous outer surface for both 50:50 and 75:25 (Figure 5.14 A & B) compared to the fibres resulting from a 7.7 m/min take-up rate (Figure 5.14 C & D). However, at 7.7 m/min, the fibres had a more grooved structure. This is particularly noticeable with the 50:50 fibre which had grooves and pores parallel to the vertical flow of the fibre solution from the spinneret. This orientation is also seen with the 50:50 inner surface at 7.7 m/min (Figure 5.15 C), and can be seen to a lesser extent at 5.5 m/min (Figure 5.15 A). In contrast to the trends seen with the 50:50 fibres made at different take-up rates, the inner surface of the 75:25 fibre made at 7.7 m/min is more porous than that made at 5.5 m/min (Figures 5.15 D & B).

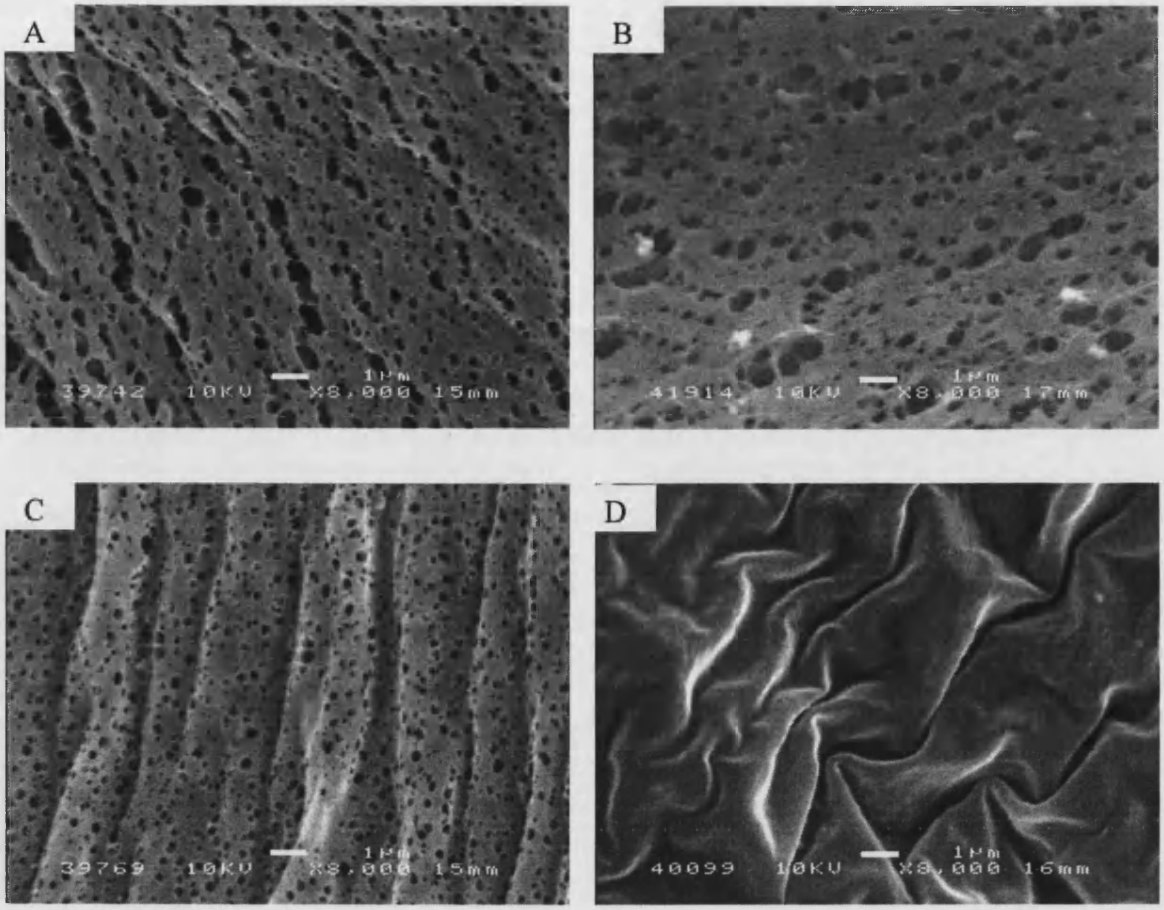

Figure 5.14. Outer surface of hollow fibre membranes at different take-up rates.
(A) 5.5 m/min 50:50, (B) 5.5 m/min 75:25, (C) 7.7 m/min 50:50, (D) 7.7 m/min 75:25. Scale bar 1 μm.

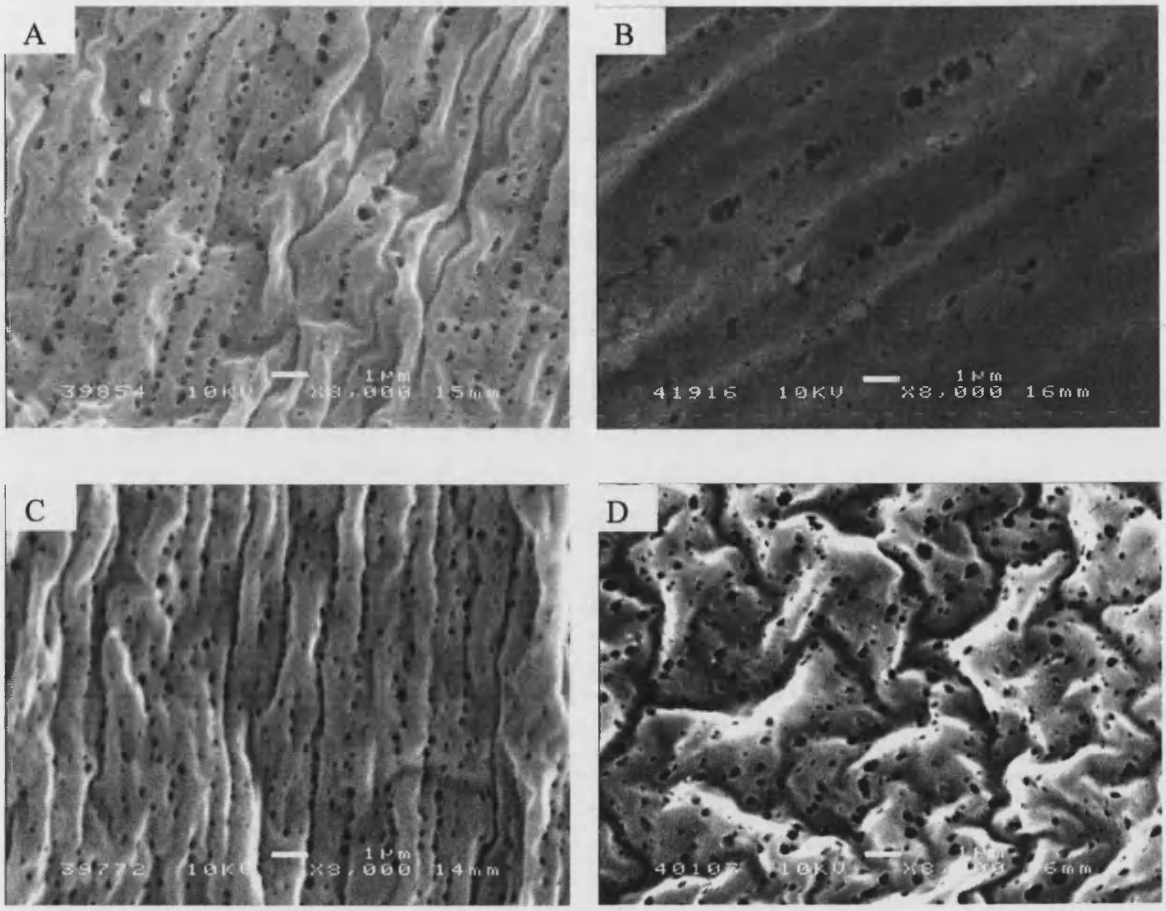

Figure 5.15. Inner surface of hollow fibre membranes at different take-up rates. (A) 5.5 m/min 50:50, (B) 5.5 m/min 75:25, (C) 7.7 m/min 50:50, (D) 7.7 m/min 75:25. Scale bar 1 μm.

5.2.4 HOLLOW FIBRE CHARACTERISATION

A selection of hollow fibres were characterised using gas permeation. The mean pore diameter and effective surface porosity were calculated at a low pressure range of 5 – 40 psig.

The mean pore size for 50:50 was larger than that of the 75:25 fibre at zero air gap, however the opposite was seen with the 30 mm air gap. The effective surface porosity of the 75:25 fibre was over twice that of the 50:50 fibre at zero air gap smaller at 30 mm air gap. For both the 75:25 and 50:50 fibres, there was an increase in mean pores size with the use of a 30 mm air gap. For 75:25, the mean pore diameter nearly doubled when an air gap was introduced, however the effective porosity decreased to around one third. Only a small increase in mean pore diameter

was seen for 50:50 when an air gap was used, and unlike the 75:25 fibres, the effective porosity increased slightly.

Table 5.1. Mean pore diameter and effective surface porosity.

Fibre	Air gap	Mean pore diameter	Effective surface porosity
PLA:PGA	mm	μm	m^{-1}
75:25	0	2.364	5.07×10^{-4}
75:25	30	4.230	1.43×10^{-4}
50:50	0	3.250	2.13×10^{-4}
50:50	30	3.608	2.40×10^{-4}

Hollow fibres were spun from a 20% (w/w) polymer solution at 7.7 m/min.

5.3 DISCUSSION

5.3.1 POLYMER SOLUTION CONCENTRATION

As described in Chapter 4, the concentration at which it is possible to spin with is dependent on viscosity. Both 75:25 and 50:50 have suitable viscosities at 20% and 25% polymer concentration, although 20% 50:50 is at the bottom limit of the ideal spinning viscosity range (Figure 4.3 E). The spinning was carried out at 25°C.

The fibres formed with the lower concentration had a higher free volume and, in the case of 50:50 a higher surface porosity. However, too low a concentration could reduce the mechanical integrity as seen with the 20% 50:50 fibre.

The porosity of the surface of the 50:50 fibres was higher at 20% polymer concentration. The grooves in the surface were also more aligned. This may be beneficial to osteoblast culture as several groups have shown that orientated-grooved surfaces improve cell culture, such as Matsuzaka *et al.* (2000) who showed that microgrooved PLLA effected osteoblast-like rat bone marrow cell behaviour. The grooves in the surface of the 75:25 fibres were also more aligned at the lower concentration, however, the surface was nonporous. This could be due to the air gap (see Section 5.5.2 and below) or delayed demixing. Since pores were seen on the

surface of the 75:25 flat sheets (Chapter 4), the air gap is more likely to be the cause of the dense skin.

The cross-section of the fibres made with the lower concentration showed a more open structure, most noticeably through the central section as expected (Mulder 1992). This was also observed with the pores at the outer and inner edges where the pores were longer, up to 20 μm for 20% compared to 25%. 50:50 had longer and wider pores compared to 75:25, which again would be better as would be less resistant to mass transfer. This would give less resistance to nutrient flow and so would be preferred to a more dense central section. The 50:50 fibre sample showed a near collapsed central section. It is likely that the low viscosity of the spinning dope was below the critical viscosity described by Chung and Hu (1997) to an extent that the central section-the last to coagulate-could not maintain its structure during the demixing process. The macrovoids seen in the 20% 75:25 further suggests instantaneous demixing (Mulder 1992) as opposed to delayed demixing. This supports a dense skin formation due to the air gap.

5.3.2 AIR GAP

The 50:50 and 75:25 fibres spun with no air gap had preferable morphology compared with those spun at 30 mm air gap. The pores were more finger-like, and the dense skin on the outer surface of 75:25 was considerably reduced, from 5 μm to 0.5 μm. The pores on the surface of 50:50 had larger pores and a higher porosity at 0 mm. The surface of 50:50 also had ridges which may be beneficial to osteoblast culture (Matsuzaka *et al.* 2000). The mechanical integrity of the 50:50 fibres was compromised due to a collapsed central section with a 30 mm air gap, but at 0 mm air gap, the central section was in tact.

The outer pores of 50:50 were similar at both air gaps, but at 0 mm, the inner pores were more finger-like. The dense skin on the outer surface of 75:25 was reduced from 5 μm to 0.5 μm. As for 50:50, 0 mm air gap gave more finger-like pores at the inner surface.

The cross-sections were preferable at 0 mm; 50:50 fibres did not have a collapsed central section, and the macrovoids in the 75:25 fibres were more finger-like. These results are in line with the findings of Chung and Hu (1997) who found that by increasing the air gap, the finger-like structure was reduced. An air gap also introduces elongational stresses (Chung and Hu 1997) which could account for the collapsed central section of the 50:50 fibres made with a 30 mm, which was absent in the fibres made with a 0 mm air gap.

The surface of the 50:50 fibres has larger pores and a higher porosity when prepared with a 0 mm air gap as is typically seen (Khayet 2003). Furthermore, Khayet (2003) found that an increasing air gap gave rise to rows of pores and ridges, as would be expected due to elongation stresses, whereas 50:50 showed rows of pores and ridges with 0 mm air gap. The trends seen in the work by Khayet (2003) were at larger air gaps (25-80 mm). The more random distribution of pores and nodules were seen with 1 cm air gap, patterns only starting to appear at 5 cm. Due to the dense skins on the 75:25 outer surface, no pores were visible. No differences in the undulations due to air gap were noticeable from the micrographs.

5.3.3 TAKE-UP RATE

Comparable to similar studies, the lower take-up rate, which is directly proportional to dope flow rate, appeared to induce a lower shear stress in the spinneret. Because the fibres were spun with no air gap, the molecular orientation is maintained when the dope exits the spinneret so influencing the resulting fibre morphology. A lower shear, due to a lower rate, creates less shear so less molecular orientation. At 5.5 m/min, larger pores were seen on the surfaces of both the 50:50 and 75:25 fibres compared to the fibres spun at 7.7 m/min, and in the case of 75:25, the dense skin was eliminated. However, at the higher rate, grooves were seen in the surface which may positively influence osteoblast culture (Matsuzaka *et al.* 2000).

Fibres were spun with no air gap and the take-up rate set to the extrusion rate to reduce elongational forces as much as possible. This means that take-up rate is directly proportional to dope flow rate.

75:25 has a dense skin at 7.7 m/min, but a porous skin when spun with a take-up rate of 5.5 m/min. This agrees with Wang and Chung (2001) and the findings of Qin and Chung (1999) and Chung *et al.* (2000) who concluded that this is due to a higher molecular orientation at a higher dope flow rate which induces greater shear stress within the spinneret. This molecular orientation is maintained because of the absence of an air gap which introduces other (elongational) forces which can change the molecular orientation due to die swell (Qin and Chung 1999; Chung *et al.* 2000).

The pore size of both the 75:25 and 50:50 fibres was larger for the fibres spun at the lower rate, again in agreement with the theories of Qin and Chung (1999) and Chung *et al.* (2000). The formation of grooves on the outer surfaces of both the 75:25 and 50:50 fibres suggest that elongational forces have not been totally eliminated. The grooves have formed in these fibres due to the relatively low viscosities of the spinning dopes causing the solutions to be unable to overcome the, albeit small, elongation forces of the extrusion process.

5.3.4 HOLLOW FIBRE CHARACTERISATION

The mean pore size for all the samples was of the 1μm order of magnitude and all smaller than the maximum allowable pore size of 5μm. The mean pore size tended towards the maximum limit, which would allow the maximum possible mass transfer of nutrients while preventing the cells from migrating into the scaffold. The mean pore size calculated using the gas permeation method was around 10 times greater than the size observed on the micrographs. The effective porosity suggests a very sparse number of pores. This compares to the micrographs for 75:25, which has a dense layer at these spinning conditions, but 50:50 was seen to be highly porous.

5.4 CONCLUSIONS

The results suggest that a low polymer concentration spun without an air gap at lower take-up rates will produce a more suitable structure for a scaffold.

In this study, 50:50 spun from a dope with 20% polymer concentration, no air gap and 5.5 m/min produced the most porous structure with the finger-like pores perpendicular to the inner and outer surfaces separated by only a very thin central section. 75:25 showed a suitably porous surface with a good cross-section when spun from a 20% dope with no air gap at 5.5 m/min.

The greatest differences seen between 50:50 and 75:25 were the surface porosities and the grooved structure. 50:50, which had a lower viscosity relative to 75:25 (Chapter Four) had a porous structure independent of concentration, air gap and take-up rate. 75:25 only showed a porous surface with 0 mm air gap and 5.5 m/min take-up rate. 50:50 had more orientated grooves in both outer and inner surfaces. 75:25 has grooved surfaces but the grooves are less aligned. Both the porosity and orientation of the groove may be attributed to the viscosities of the solutions, but this would need further investigation.

A concentration of 20% for these two polymers is suitable to spin with. Due to the increased free volume, the minimum concentration would be chosen. Fibres spun with no air gap, i.e. wet spinning gave a better morphology, and allowed a fibres to be spun from solutions of lower viscosities as was seen 20% 50:50 which was not possible with a 30 mm gap. A take-up rate between the two tested, which prevented a skin formation but gave rise to grooves would be ideal.

Based on the findings in this chapter, the spinning conditions used to prepare fibres for use in the HFB in Chapter 8 were a polymer concentration of 20% in NMP, zero air gap and a take up rate of 5.5 m/min.

CHAPTER SIX
MEMBRANE SURFACE TREATMENT AND MODIFICATION FOR CELL CULTURE

6.1 INTRODUCTION

PLGA has been shown to form asymmetric membranes suitable for use as a scaffold, in the form of both flat sheet (Chapter 4) and hollow fibre (Chapter 5) membranes. Two steps need to be carried out before cells are added to the membrane scaffolds. These are solvent removal and sterilisation. The degradation of the membranes during cell culture should also be assessed. Once the culture period is complete, the samples then need to be fixed for histological analysis, or a lysing agent added for the quantitative assays used in this project. It is important that the architecture of the membrane is maintained during preparation for cell culture and analytical procedures. The polymer should be inert in the fixing solution so as not to affect the results in any way. This chapter shows the effects of ethanol as a sterilising and fixing agent, 10% Neutral Buffered Formalin (10% NBF) as a fixing agent, and the lysing agent Alkaline buffer solution/ Triton X-100 /MilliQ water (ATM). In addition to testing the effect of these treatments, the hollow fibres were subjected to 'Kokubo's method' (Kokubo *et al.*1998) to investigate the potential of the process to coat them with hydroxyapatite.

6.1.1 SOLVENT REMOVAL FROM SCAFFOLDS

Solvent removal is important to prevent an immune response and potential rejection of the construct in vivo, and any effect, positive or negative on the cell culture analysis in vitro. The removal of solvents from phase inversion cast scaffolds is prerequisite to their use for cell culture. By the very nature of the formation process, this is relatively simple since it is the displacement of the solvent from the polymer-solvent solution that forms the scaffold. Scaffolds formed using volatile solvents such as chloroform can simply be aired dried at room temperature (Gomez *et al.* 2004). By placing the scaffold in a fume cupboard, the safety is improved as is the air flow; this was done at room temperature for 7 days and 40°C for 4 days by Wang

et al. (2004), and 24 hours at 5°C by Santovena *et al.* (2004). The less volatile solvents used in casting by immersion precipitation are either left in the non-solvent, or removed by vacuum drying (Koegler *et al.* 2002). Koegler *et al.* (2002) used liquid CO_2 to remove chloroform from 'dense' PLGA devices in a matter or hours. The residual solvent was 50 ppm after 8 hours at 5000 psi, compared to the significant amount (>1 wt%) left after vacuum drying and the group reported no significant alteration to the architecture. Similarly, Herberger *et al.* (2003) used CO_2 and fund that when used as a gas, residual solvent was decreased to 200 ppm and there was no detrimental effect on the morphology of PLGA microparticles.

6.1.2 DEGRADATION OF PLGA SCAFFOLDS

An important factor to consider when using PLGA as a scaffold is degradation. PLGA is a biodegradable polymer that produces lactic and glycolic acids on hydrolysis of the ester bonds. The ideal time scale of degradation depends on the role of the PLGA construct. Demineralised bone matrix implanted ectopically in animal models showed early angiogenesis and the presence of progenitor cells and chondrocytes after 3 weeks in vivo. Osteoblasts, osteocytes and chondrocytes were seen shortly after along with cartilage and woven bone formation, and by 4 weeks osteoclast and bone remodelling cells are present, duplicating endochondral ossification (Burg *et al.* 2000). Whether the scaffold is seeded prior to implantation and the cell population allowed to expand, or the a cellular scaffold is implanted, this data suggests that the scaffold should maintain its structure and mechanical integrity for a minimum of 4 weeks once placed into a culture environment.

Extensive studies have been carried out on the degradation of PLGA. El-Amin *et al.* (2003) studied the degradation of 50:50 and PLLA over 10 weeks in PBS at 37°C. Mass weight loss and surface changes were examined. PLGA showed a higher degradation rate than PLLA as was also shown previously by Freed *et al.* (1994). The media in which the polymer is placed, and treatment of the scaffold have also been shown to affect the rate of degradation (Kim *et al.* 1998; Catiker *et al.* 2000; Cai *et al.* 2003; Valimaa and Laaksovirta 2004). Catiker *et al.* (2000) showed that there was a greater change in chain length and chain chemical structure of PLGA in the presence of Bovine serum albumin compared to PBS. Cai *et al.* (2003) compared the effect of 4 mg/ml trypsin in PBS and PBS on the degradation of 7030 and 5050

PLGA. It was found that the trypsin solution enhanced weight loss rate, but had little effect on molecular weight or polymer composition. This again suggests that the content of the media affects the degradation process. Kim *et al.* (1998) showed that initial degradation of plasma treated PLLA was faster than the control sample. This was probably due to the improved hyrophilicity of the surface, particularly since the degradation rate was similar after 4 weeks, which may have coincided with the loss of the hydrophilic surface.

6.1.3 STERILISING SCAFFOLDS FOR CELL CULTURE

Many methods of sterilisation have been used for scaffolds. Ethylene oxide and γ-radiation are the most common methods for surgical equipment including both metal and plastic prosthetics and biodegradable pins and sutures (Middleton and Tipton 2000). These methods are hence a good choice for sterilising scaffolds. It has been shown by several groups that both ethylene oxide and γ-radiation affect the crystallinity of PLLA which can in turn affect the degradation properties (Weir *et al.* 2004). Similar results were found by Affatato *et al.* (2002) and Taddei *et al.* (2002) who tested ultra-high molecular weight polyethylene (UHMWPE) as used in the replacement of damaged articulating cartilage for total joint replacement surgery. The tests showed some weight lost and changes in surface crystallinity due to these two methods of sterilization. Other methods include UV (Ishaug *et al.* 1994), β-radiation (Silva *et al.* 2004), γ-radiation (Mooney *et al.* 1996), chemical treatments (Amaechi *et al.* 1998; Lubbe and Henton 1997), autoclaving and elevated temperature treatment (Hofmann *et al.* 2000) and plasma sterilisation (Feichtinger *et al.* 2003; Hofmann *et al.* 2000). Autoclaving and elevated temperature treatments would not be appropriate for PLGA as all have glass transition temperature (T_g) in the range 35-55 °C (Yang *et al.* 2001) and are liable to deform at or above the T_g which could damage the porous structure; chemical treatments can leave harmful residues.

There was shown to be minimal effect on the culture of osteoblasts on cortical bone samples after different sterilising treatments (Hofmann *et al.* 2000); autoclaving, ethylene-oxide sterilisation, demineralized and low-temperature-plasma-sterilisation (DEM-LTP), chemically sterilized (modified Tutoplast(T) method), and 80°C

temperature disinfected were all used. Holy *et al.* (2001) published findings on sterilisation of PLGA and found that ethanol does not affect the morphology of PLGA when in the form of Osteofoam™. No further work has been published on the effect of ethanol on the scaffold despite several groups using ethanol to sterilise and pre-wet the scaffolds.

6.1.4 AFFECT OF FIXATIVES AND LYSING AGENTS ON PLGA SCAFFOLDS

Formalin, an aldehyde works by cross-linking proteins; ethanol leaves proteins in a relatively undenatured state (Bancroft and Gamble 2005) and preserves the enzymatic activity, so is suitable for ALP stains. No reports have been published on the effect of 10% NBF or ATM on the structure of PLGA scaffolds.

6.1.5 SURFACE MODIFICATION OF PLGA MEMBRANE SCAFFOLDS

This chapter also investigates the possibility of surface modification with hydroxyapatite using Kokubo's method. There is currently no scaffold that combines perfect architecture, chemical and physical properties for bone tissue engineering. While it has been shown that PLGA supports bone cell culture (Chapter 7), improvement can be made by the modification of the binding site. PLGA has already been successfully modified by surface treatment using pleiotrophin (an extracellular matrix-associated protein) adsorption (Yang *et al.* 2003), Fibronectin and RGD-peptide adsorption (Yang *et al.* 2001), hydroxyapatite coating (Zhang and Ma 1999; Murphy *et al.* 2000); polymer blends with PVA (Oh *et al.* 2003), hydroxyapatite (Zhang and Ma 1999; Wei and Ma 2004) and beta-tricalcium phosphate (Zhou *et al.* 2004); and encapsulating growth factors such as IGF-I and TGF-beta (Schmidmaier *et al.* 2003) and bone morphogenetic proteins (Saito and Takaoka 2003). Murphy *et al.* (2000) found that a layer of apatite increased the compressive moduli fivefold after 16 days incubation, which would be beneficial in bone tissue engineering. Many more examples on the modification of other polymers and Titanium and its alloys for bone tissue culture can be found in the literature.

6.2 RESULTS

Studies were carried out under conditions used to prepare the membranes for cell culture. Solvent removal, degradation and the effect of the fixatives and lysing agents were tested on flat sheet membranes alone, Hydroxyapatite coating was carried out on hollow fibre membranes alone, while sterilisation was assessed for both flat sheet and hollow fibre membranes.

6.2.1 SOLVENT REMOVAL

While NMP has a low toxicity and has been used in animal models to improve bone growth, generally the removal of solvent is required to prevent the possibility of a negative reaction by the host body. In the case of these tests, removing the solvent removes a variable that could influence the cell culture, positively or negatively.

Solvent removal was carried out using the traditional immersion precipitation of soaking the membrane in the non-solvent for a number of days. The flat sheet membranes were submerged in distilled water for up to seven days at 15°C and 37°C, the water was changed after a sample was taken. Start and end point morphological and roughness values were collected by AFM, along with quantifying the generation of NMP using HPLC.

Morphology

Both the average and maximum roughness of the 75:25 flat sheet membranes was seen to decrease after 7 days in water at 15°C but increase at 37°C (Table 6.1). Topographical changes over time can be seen by comparing Figure 6.1 with Figure 6.2. The images support the roughness values since the surface of the flat sheet membranes appeared smoother after 7 days in water at 15°C, and more undulating after 7 days in water at 37°C.

Table 6.1. Roughness values of 75:25 flat sheet membranes at the start and end point of solvent removal studies.

Time days	Ra (nm) nm	Rmax nm
	15°C	
0	5.05	42.87
7	3.47	39.47
	37°C	
0	5.05	42.87
7	5.35	55.40

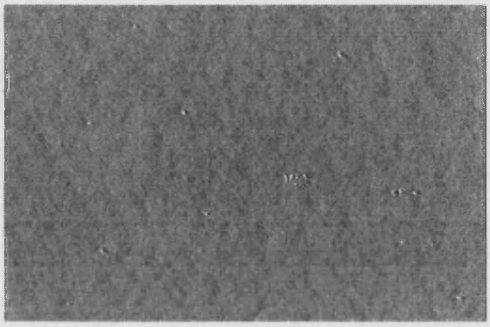

Figure 6.1. 75:25 flat sheet membrane surface immediately after precipitation.
Image is 10 μm wide.

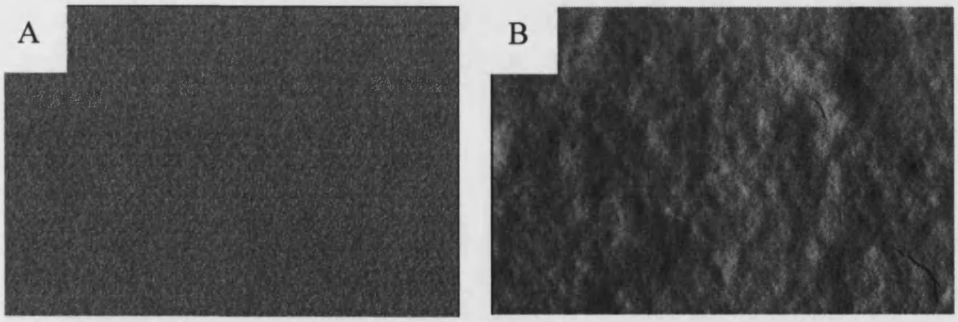

Figure 6.2. 75:25 flat sheet membrane after 1 week in water, post-fabrication.
(A) 15°C, (B) 37°C. Images are 10 μm wide.

Solvent Release

Flat sheet membranes were cast from 75:25 at 15°C. As soon as precipitation had occurred, the membranes were placed into fresh water bath at 15°C or 37°C. The amount of NMP removed from the 75:25 flat sheet membrane was calculated by taking samples from the water bath and analysing using an HPLC. The data is shown in Figure 6.3 as concentration in the water bath over time. The release of NMP was seen to decrease over time; the rate of release over the first data is very rapid. After 1 hour, the membrane at 37°C had released more solvent than that in the 15°C water bath. However, between 6 hours and three days, NMP removal at 37°C was slower that at 15°C when the solvent concentration reached 6 ppm (0.0006 v/v%) and 14 ppm respectively. After this time, the difference in concentration of NMP at both temperatures was less than 4 ppm and the same by day 7.

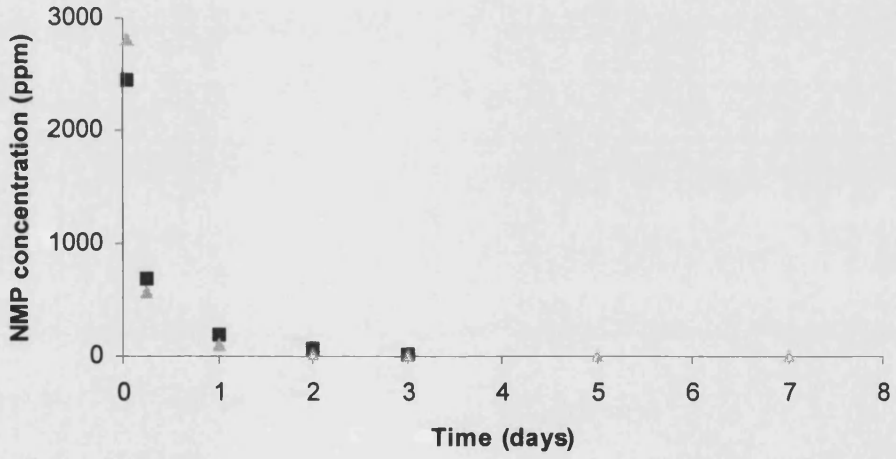

Figure 6.3. NMP removal from the 75:25 flat sheet membrane.
Each data point shows the concentration (ppm) of NMP released since the previous reading. ■ 15°C, ▲37°C.

6.2.2 DEGRADATION OF PLGA MEMBRANES IN CELL CULTURE MEDIA

The degradation of PLGA is one of the key benefits of its use, as once it has served its purpose of assisting in the healing process, it will dissolve to leave no foreign body that the immune system can react to. Both of the acidic by-product are

naturally produced by the body and are remove via normal metabolic pathways (Lu *et al.* 2000).

Degradation studies were carried out over 26 days with 75:25 flat sheet membranes in media at 15°C and 37°C under static conditions. Morphological and roughness analysis was carried out using AFM and degradation was quantified using HPLC to analyse the concentration of lactic and glycolic acid released into the media.

Morphology

By comparing Figure 6.1 above and Figure 6.4 below, changes in topography can by seen. The images in Figure 6.4 A to D show the topography of the membranes maintained in media at 15°C and suggest a total increase in roughness, although the membranes samples at days 12 and 19 appeared smoother than on day 5. The images in Figure 6.4 E to H show the topography of the membranes maintained at 37°C and also show an overall increase in roughness, although the membrane sample on day 19 appeared smoother than the previous sample. The roughness data in Figures 6.5 and 6.6 show a continual increase in roughness. The average roughness profile (Figure 6.5) shows a sharp increase between initial formation and day 5, then a slower increase in roughness up until day 20 when the rate of increasing average roughness increases. Although the trend is the same for both temperatures, the roughness is greater for the samples maintained at 15°C compared to those at 37°C. The profile for maximum roughness (Figure 6.6) shows a similar trend to average roughness although the differences between the two temperatures are not so clearly defined and constant.

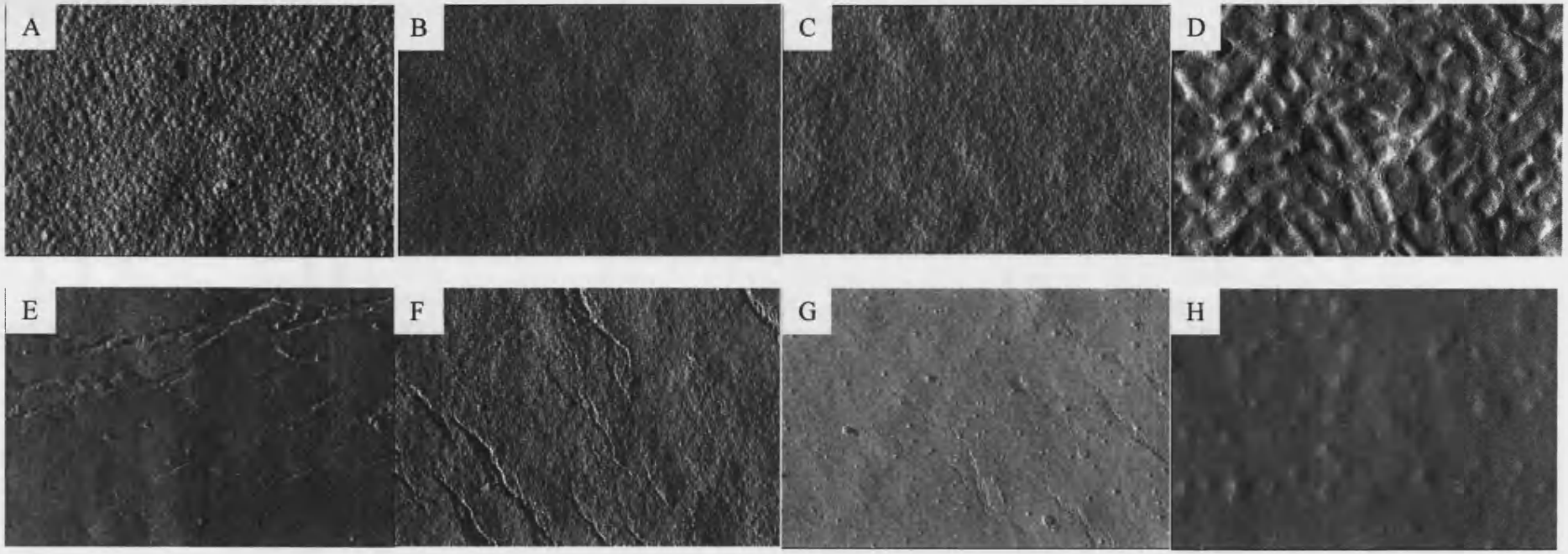

Figure 6.4. Surface images of flat sheet membranes maintained in media at 15°C (A-D) and 37°C (E-H).
(A) 5 days, (B) 12 days, (C) 19 days, (D) 26 days, (E) 5 days, (F) 12 days, (G) 19 days, (H) 26 days. Images are 10 μm wide.

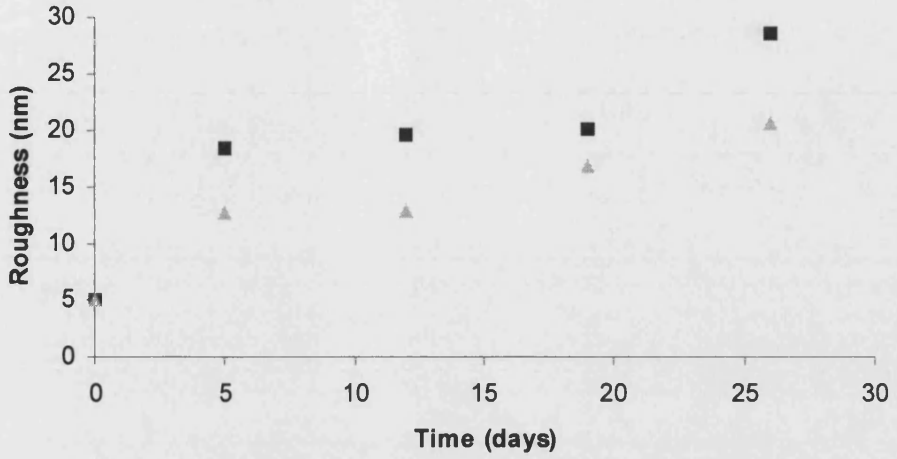

Figure 6.5. Average surface roughness of 75:25 flat sheet membrane maintained in media over 26 days.
■ 15°C, ▲37°C.

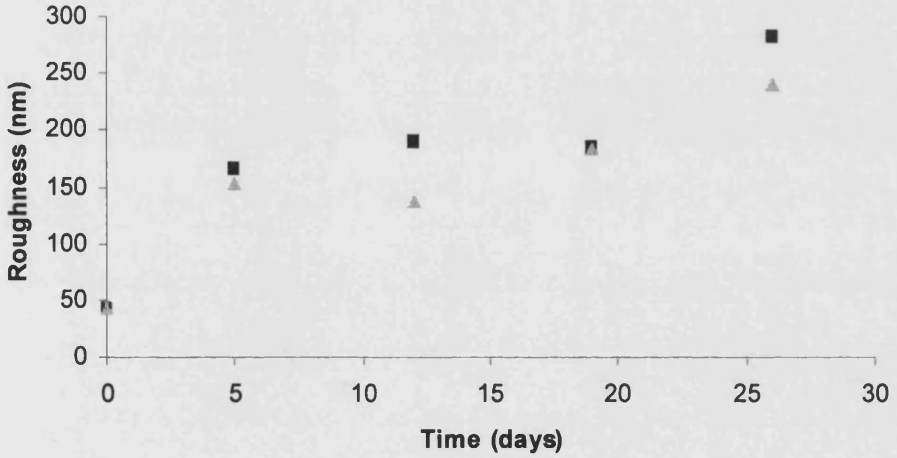

Figure 6.6. Maximum surface roughness of 75:25 flat sheet membrane maintained in media over 26 days.
The maximum roughness is the height between the lowest valley and the highest peak. ■ 15°C, ▲37°C.

Generation of Lactic and Glycolic Acid

The cumulative concentration of the degradation by-products, lactic and glycolic acid, showed a linear increase over the entire 26-day time span of the study. The flat

sheet membrane maintained in media at 15°C showed a greater release of degradation by-products between days 3 and 26 compared to those maintained at 37°C despite the reading on day 1 when there was a higher concentration of acids in the 37°C sample. The effective concentration of degradation by-products in the media on day 26 was 2700 ppm at 15°C and 2500 ppm at 37°C.

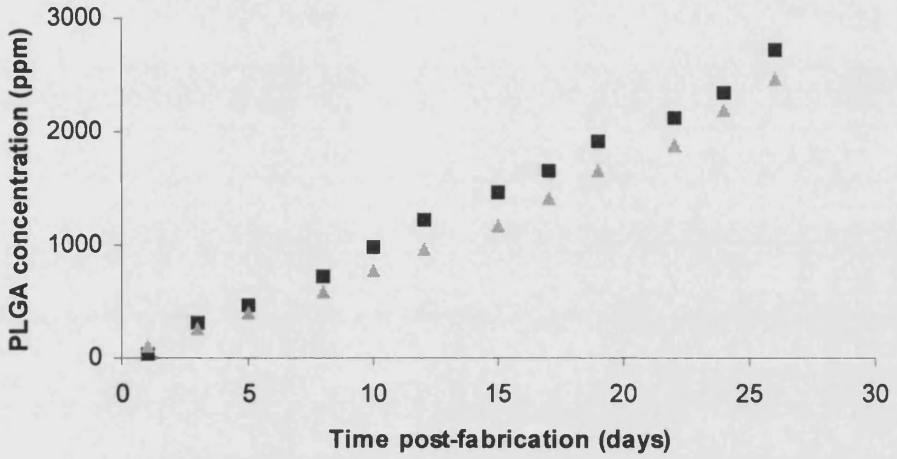

Figure 6.7. Cumulative generation of lactic and glycolic acid in the media in which the 75:25 flat sheet membranes were maintained.
The calibration graph was prepared using samples of lactic and glycolic acid at a ratio of 75:25 mol% so to replicate the hydrolysis of the PLGA hence the term 'PLGA concentration'. ■ 15°C, ▲37°C.

6.2.2 EFFECT OF STERILISATION AGENTS ON PLGA FLAT SHEET AND HOLLOW FIBRE MEMBRANES

It is necessary to sterilise the membranes before their use as a cell culture substrate to prevent any infections occurring. 70v/v% ethanol is a cheap and easily available sterilising agent. Samples were soaked in the ethanol solution for 30 minutes and the effect of the process on membrane morphology was analysed with SEM and 'before and after' measurements of thickness and length of the sample sides.

Morphology of the PLGA Membranes After Treatment with 70% Ethanol

The surfaces of the polymer membranes treated with 70% ethanol are shown in Figures 6.8 and 6.10. The treated membranes had a considerably smoother and flatter top surface (Figure 6.8) between pores compared to the untreated samples (Figure 6.9). The treated membranes also had few, but larger pores on the top surface (Table 6.2). The structure was also more susceptible to the electron beam of the SEM as can be seen from the fractures between pores (examples marked with an arrow). Similar to the top surface morphology, the bottom surfaces that had been treated were smoother and the pores larger compared with untreated samples. The bottom surfaces were particularly susceptible to the electron beam and cracked after only a few seconds exposure (examples marked with an arrow).

The effect of ethanol on the cross section of a PLGA hollow fibre membrane can be seen in Figure 6.11. The untreated hollow fibre shows the typical long and thin finger-like pores extending inwards from both the inner and outer edges, the fibre itself appears quite rigid. The fibres that have been treated with 70% ethanol appear less rigid and the finger-like pores softened to a more rounded structure. Figure 6.11 C shows the effect of the ethanol on fibres that were in contact with each other during the treatment; the fibre walls have bonded. As with the flat sheets the overall dimensions of the fibres were reduced; the outer diameter smaller and the wall thickness thinner.

Table 6.2. Minimum and maximum pore sizes of the top surface of polymer-NMP flat sheet membranes untreated and sterilised in 70% ethanol.

Polymer	Min pore size (μm)		Max pore size (μm)	
	untreated	sterilised	untreated	sterilised
100:0	0.2	0.2	0.5	1.0
75:25	0.2	0.1	0.5	0.8
50:50	0.3	0.1	0.8	0.8
75L:25	0.5	0.1	1.0	1.5

Untreated data from Chapter 4.

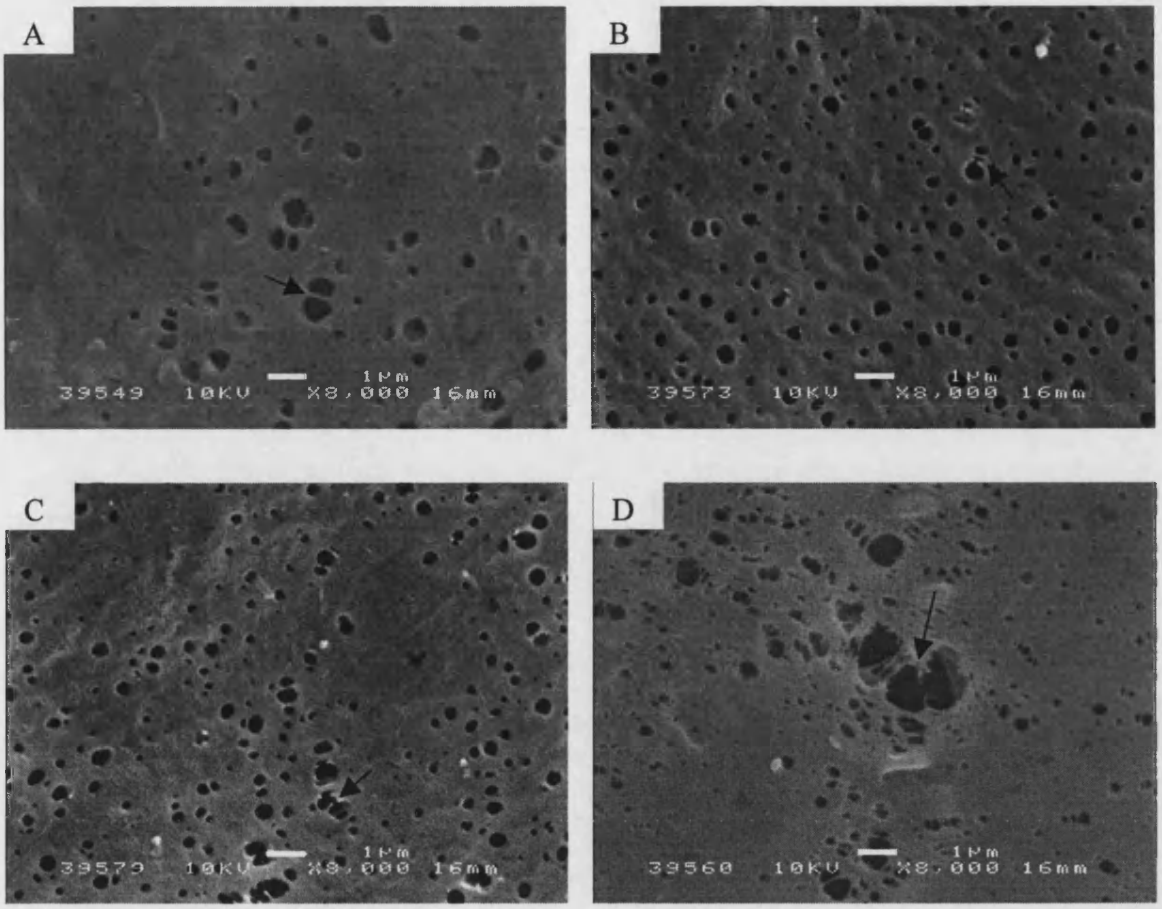

Figure 6.8. Top surface of flat sheet membranes after 30min in 70% ethanol. Membranes were cast from polymer-NMP solutions at 20% polymer concentration, except 75L:25 which was cast at 10% polymer concentration. (A) 100:0, (B) 75:25, (C) 50:50, (D) 75L:25. Cracking is marked with a black arrow. Scale bar 1 μm.

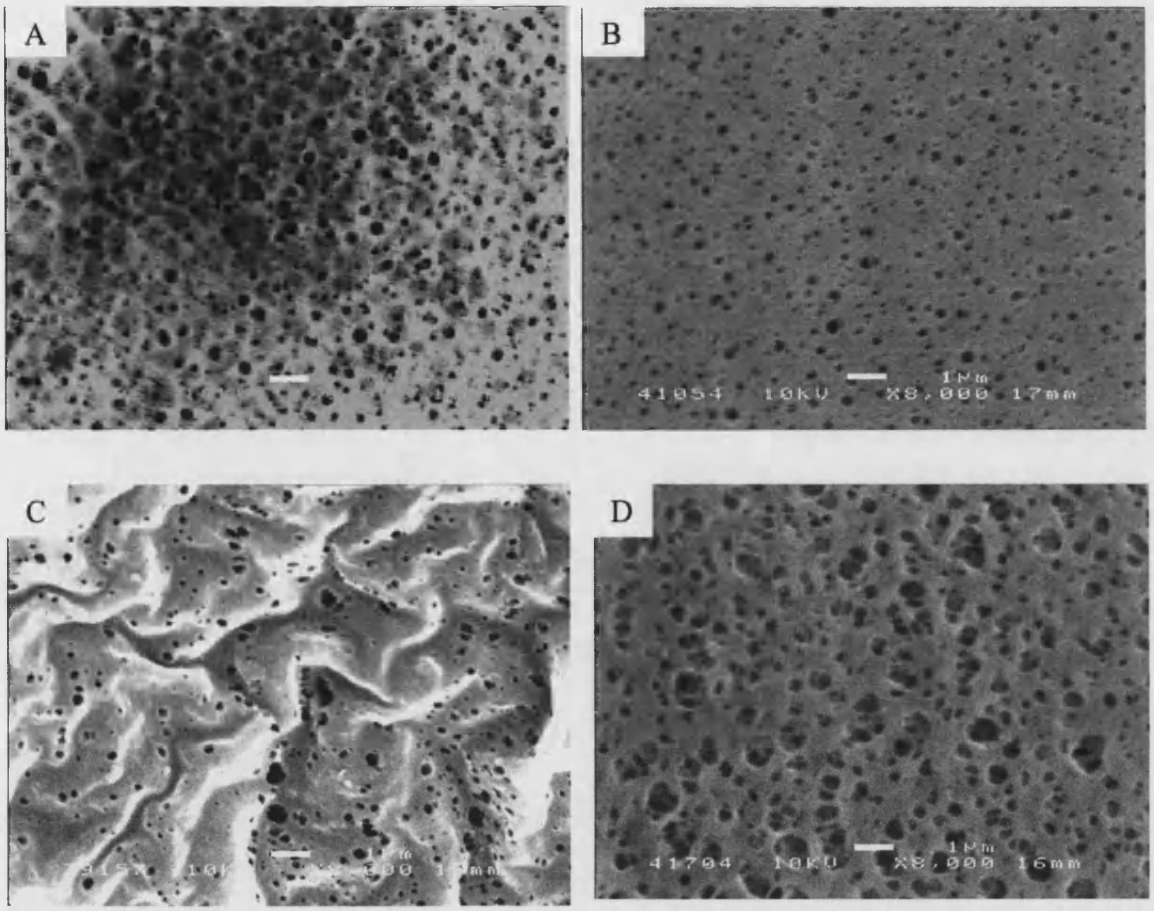

Figure 6.9. Top surface of untreated flat sheet membranes.
Membranes were cast from polymer-NMP solutions at 20 w/w% polymer concentration, except 75L:25 which was cast at 10 w/w% polymer concentration. (A) 100:0, (B) 75:25, (C) 50:50, (D) 75L:25. Scale bar 1 μm.

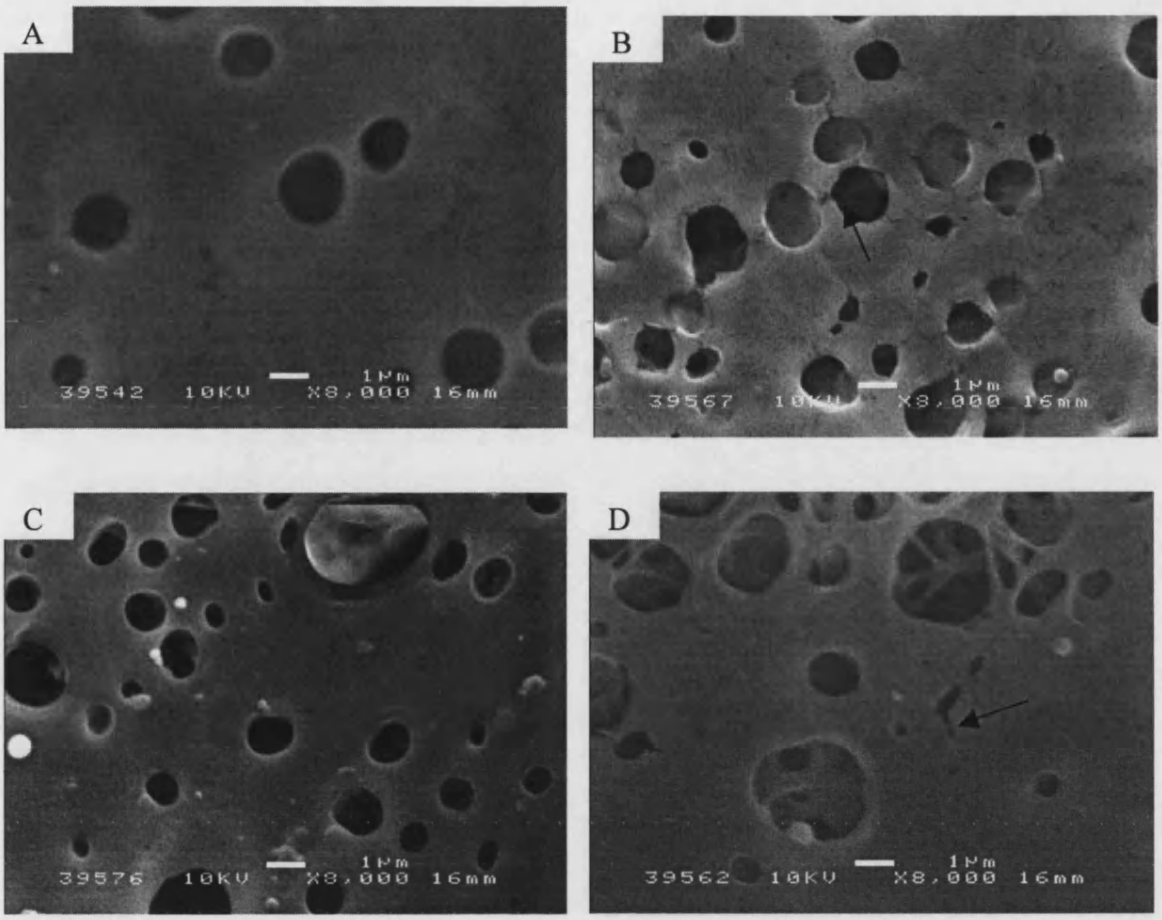

Figure 6.10. Bottom surface of flat sheet membranes after 30min in 70% ethanol. Membranes were cast from polymer-NMP solutions at 20% polymer concentration, except 75L:25 which was cast at 10% polymer concentration. (A) 100:0, (B) 75:25, (C) 50:50, (D) 75L:25. Cracking is marked with a black arrow. Scale bar 1 μm.

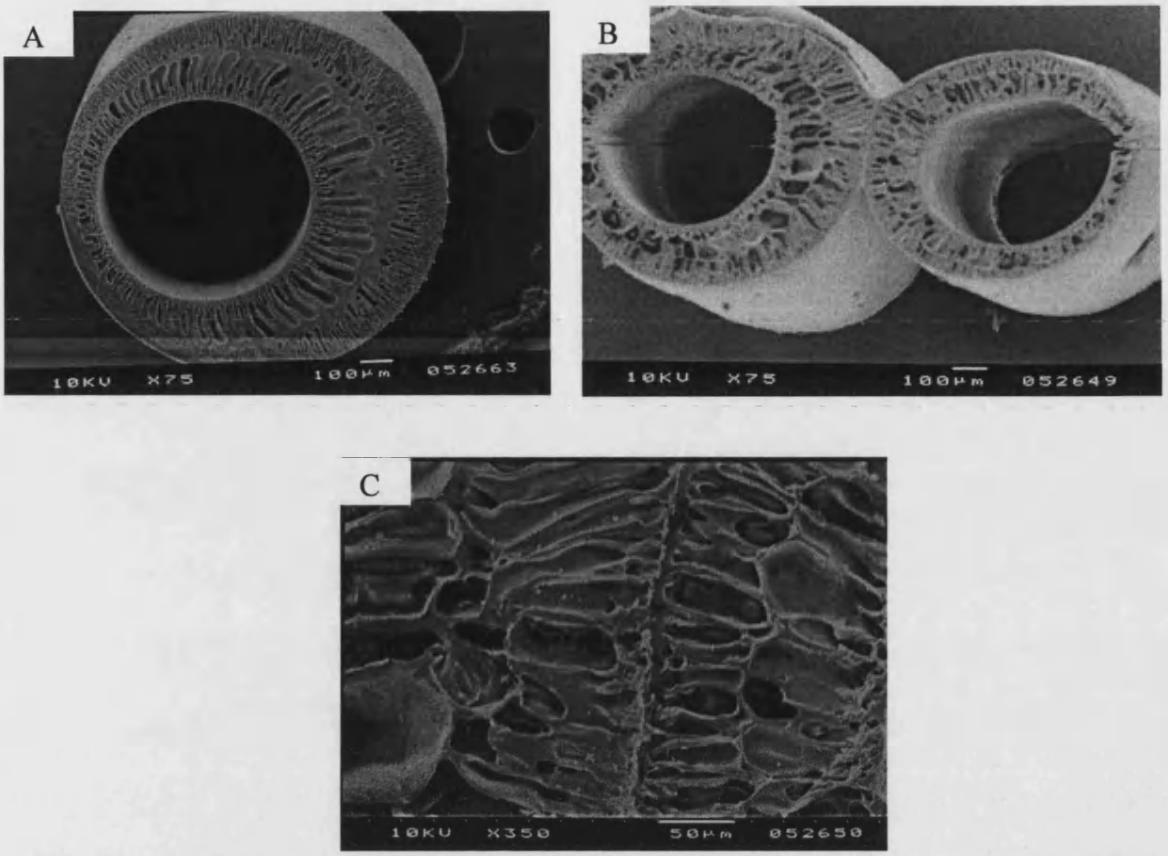

Figure 6.11. Comparison of untreated PLGA hollow fibres and 70% ethanol treated hollow fibres.

(A) Untreated fibre, (B) 70% ethanol treated fibre, (C) Outer edges of two fibres treated with 70% ethanol while in contact. Note different scale bars.

Measurement of Overall Size Change of PLGA Membranes Due to Treatment with 70% Ethanol

Dimension changes are noticeable from observation after treatment, and this is confirmed by the data presented in Figures 6.12 and 6.13.

75:25 showed the largest mean decrease in surface area of 44% after soaking in 70% ethanol. 100:0 showed a mean decrease of 25%, 50:50 decreased by 33%, and 75L:25 by 14%.

The thickness of 100:0 was not noticeably different, however, the other polymer membranes tested did exhibit a decrease in thickness. 50:50 showed the greatest change in thickness, shrinking by 41%, followed by 75:25 which decreased by 23%, and 75L:25 which decreased by 22% (Figure 6.13).

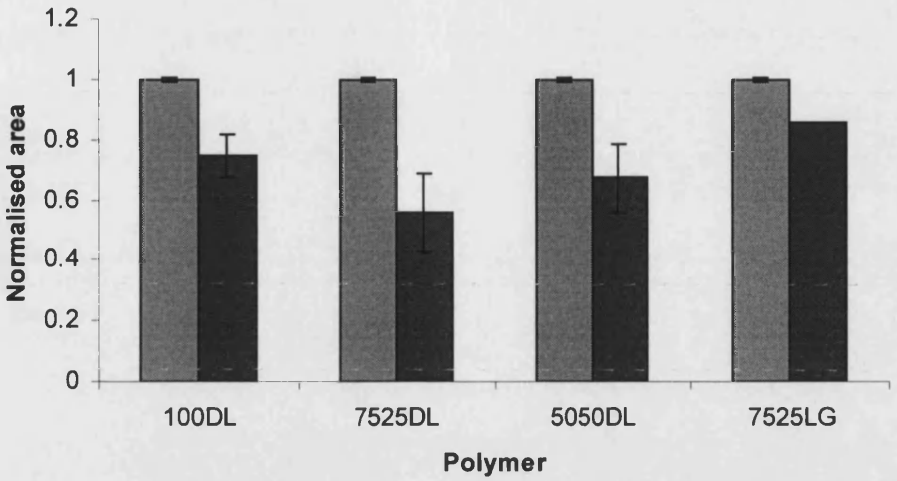

Figure 6.12. Chart showing normalised surface area of PLGA flat sheet membranes after sterilising with ethanol.
■ untreated, ■ 70% ethanol treated. Data presented as mean ±SD, n = 3.

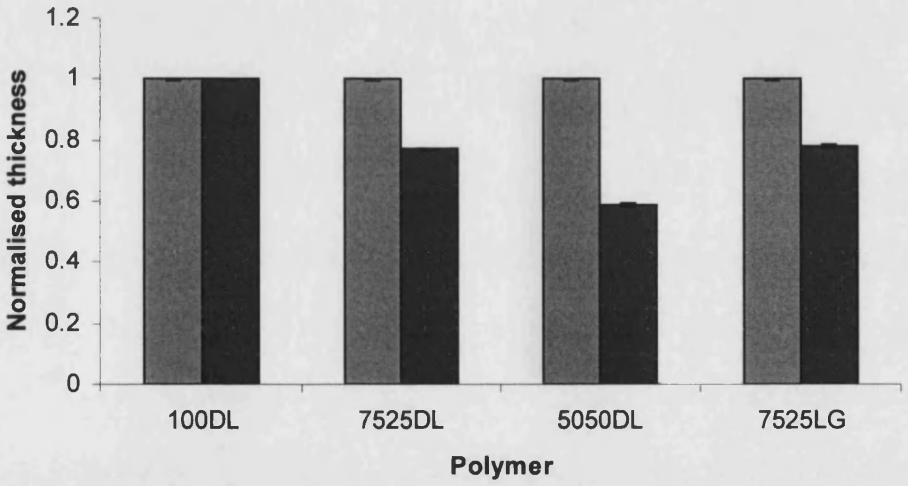

Figure 6.13. Chart showing normalised thickness of PLGA flat sheet membranes after sterilising with ethanol.
■ untreated, ■ 70% ethanol treated. Data presented as mean ±SD, n = 3.

6.2.3 Effect of Fixing and Lysing Agents on PLGA Membranes

Two fixing agents were used; 10% Neutral Buffered Formalin (NBF), commonly used for fixing tissue samples for histology, and 95% ethanol. Samples were soaked

for the times recommended in standard protocols, and analysed for morphological changes.

Morphology of the PLGA Membranes After Treatment with Fixing Agents

For correct analysis of cell cultures on the membranes, the fixing agent should not affect the morphology of the membrane as this would distort the results. SEM was used to investigate the effects of the two fixing agents used, 10% NBF and 90% ethanol, on culture surface of the membranes.

No morphological differences were seen in the membranes soaked in NBF for 15 minutes, either by eye or when photographed using SEM (Figures 6.14 and 6.15). The top surface showed the highly porous and undulating topography as seen with untreated flat sheet membranes (Chapter 4). The bottoms surface also showed topography typical of untreated membranes.

The membranes soaked in 95% ethanol however, were noticeably smaller and transparent in patches (Figures 6.16 and 6.17). The membranes had curled up and were brittle to handle. 75:25 and 50:50 showed the greatest change in membrane structure with the pores size changes (Table 6.3). 100:0 and 75L:25 remained porous on the top surface but the pores were larger than on untreated samples and were distorted in shape. The bottom surfaces of all the membranes were particularly sensitive to the electron beam and burnt very easily.

Table 6.3. Minimum and maximum pore sizes of the top surface of polymer-NMP flat sheet membranes untreated and fixed in 90% ethanol.

Polymer	Min pore size (μm)		Max pore size (μm)	
	untreated	fixed	untreated	fixed
100:0	0.2	0.2	0.5	1.0
75:25	0.2	None visible	0.5	None visible
50:50	0.3	0.1	0.8	0.2
75L:25	0.5	0.1	1.0	0.3

Untreated data from Chapter 4.

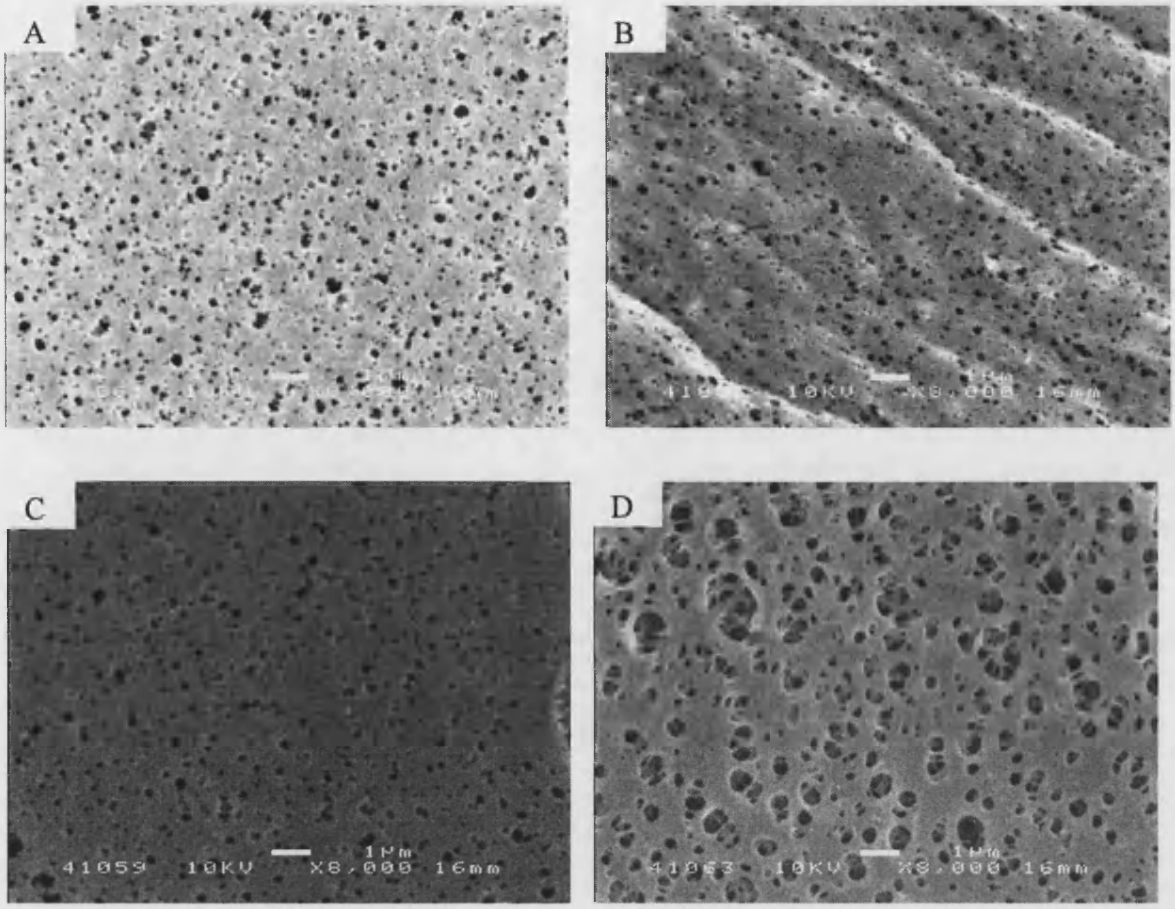

Figure 6.14. Top surface of flat sheet membranes after 15min in NBF. Membranes were cast from polymer-NMP solutions at 20% polymer concentration, except 75L:25 which was cast at 10% polymer concentration. (A) 100:0 (B) 75:25, (C) 50:50, (D) 75L:25. Scale bar 1μm.

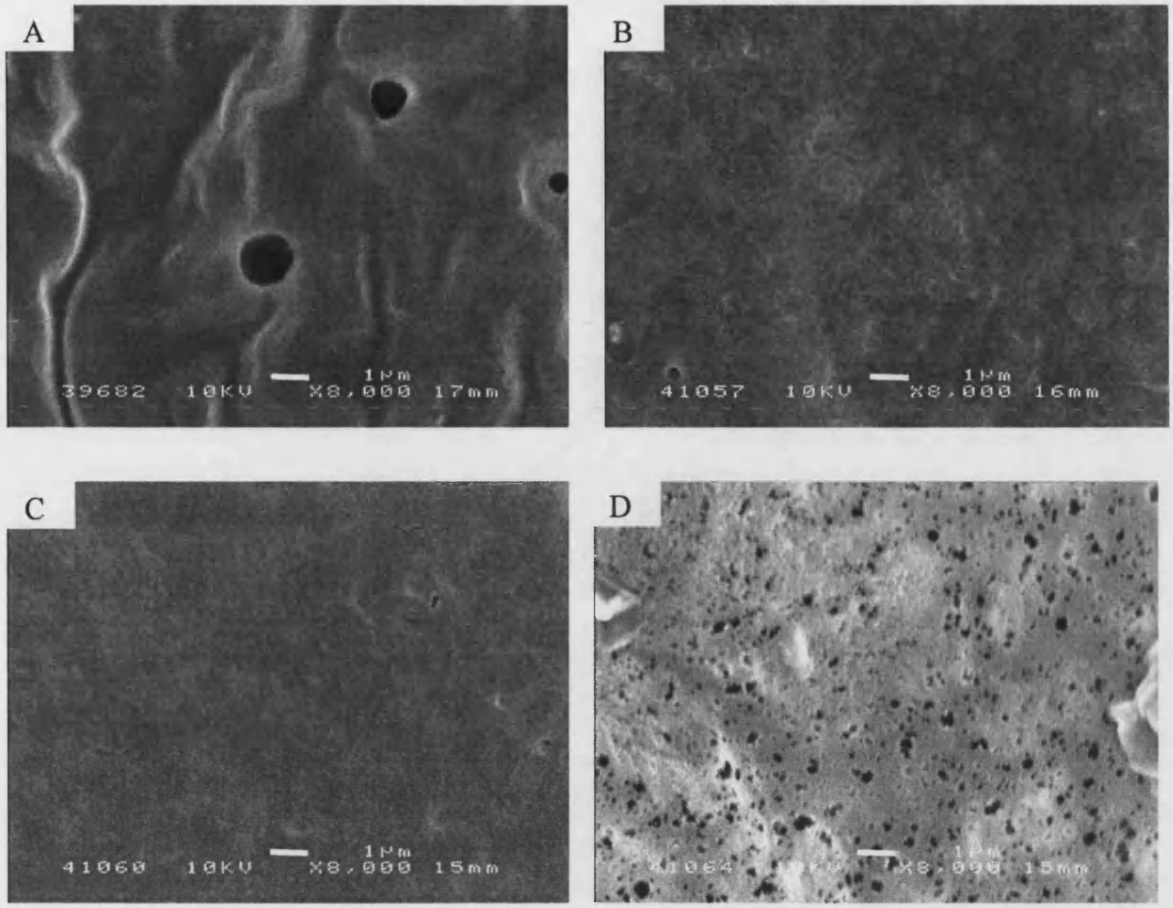

Figure 6.15. Bottom surface of flat sheet membranes after 15min in NBF. Membranes were cast from polymer-NMP solutions at 20% polymer concentration, except 75L:25 which was cast at 10% polymer concentration. (A) 100:0 (B) 75:25, (C) 50:50, (D) 75L:25. Scale bar 1 μm.

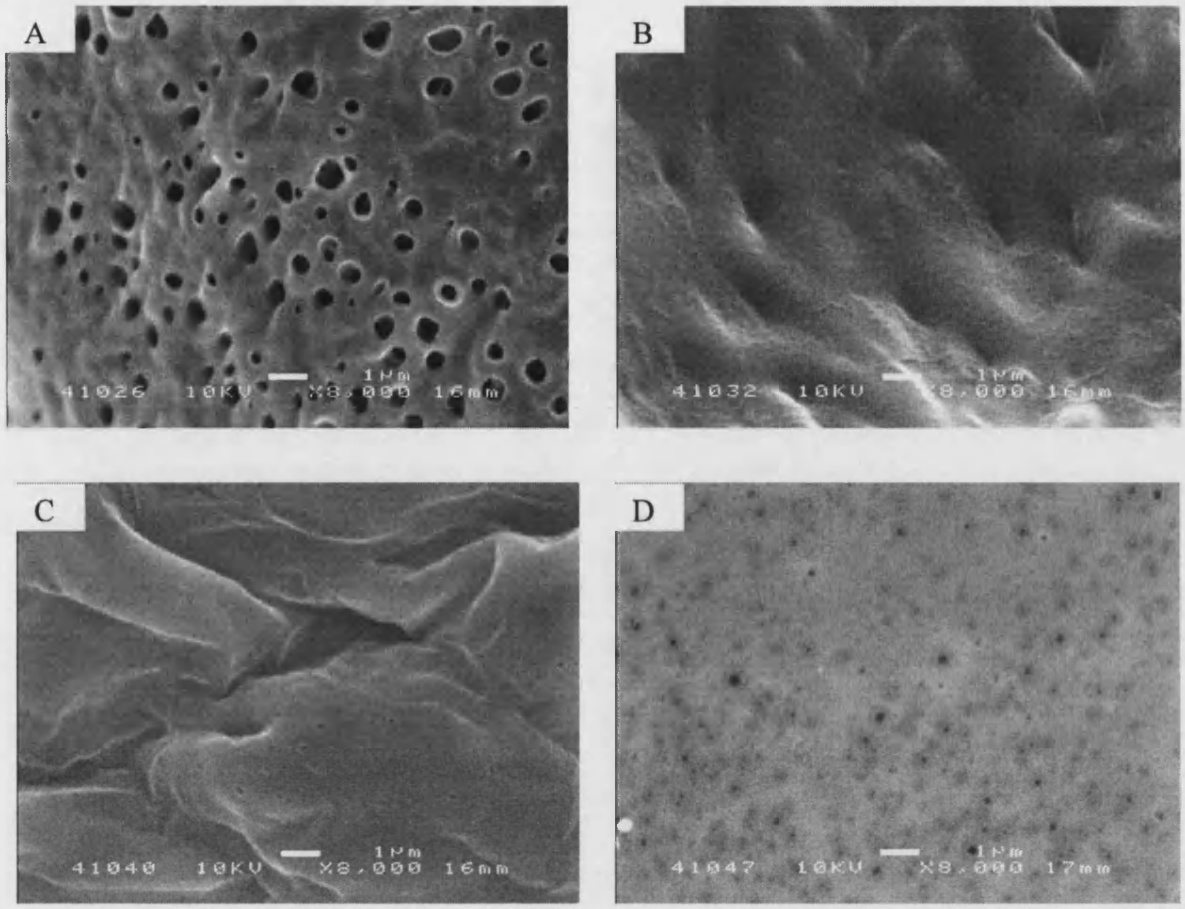

Figure 6.16. Top surface of flat sheet membranes after 10min in 90% ethanol. Membranes were cast from polymer-NMP solutions at 20% polymer concentration, except 75L:25 which was cast at 10% polymer concentration. (A) 100:0 (B) 75:25, (C) 50:50, (D) 75L:25. Scale bar 1 μm.

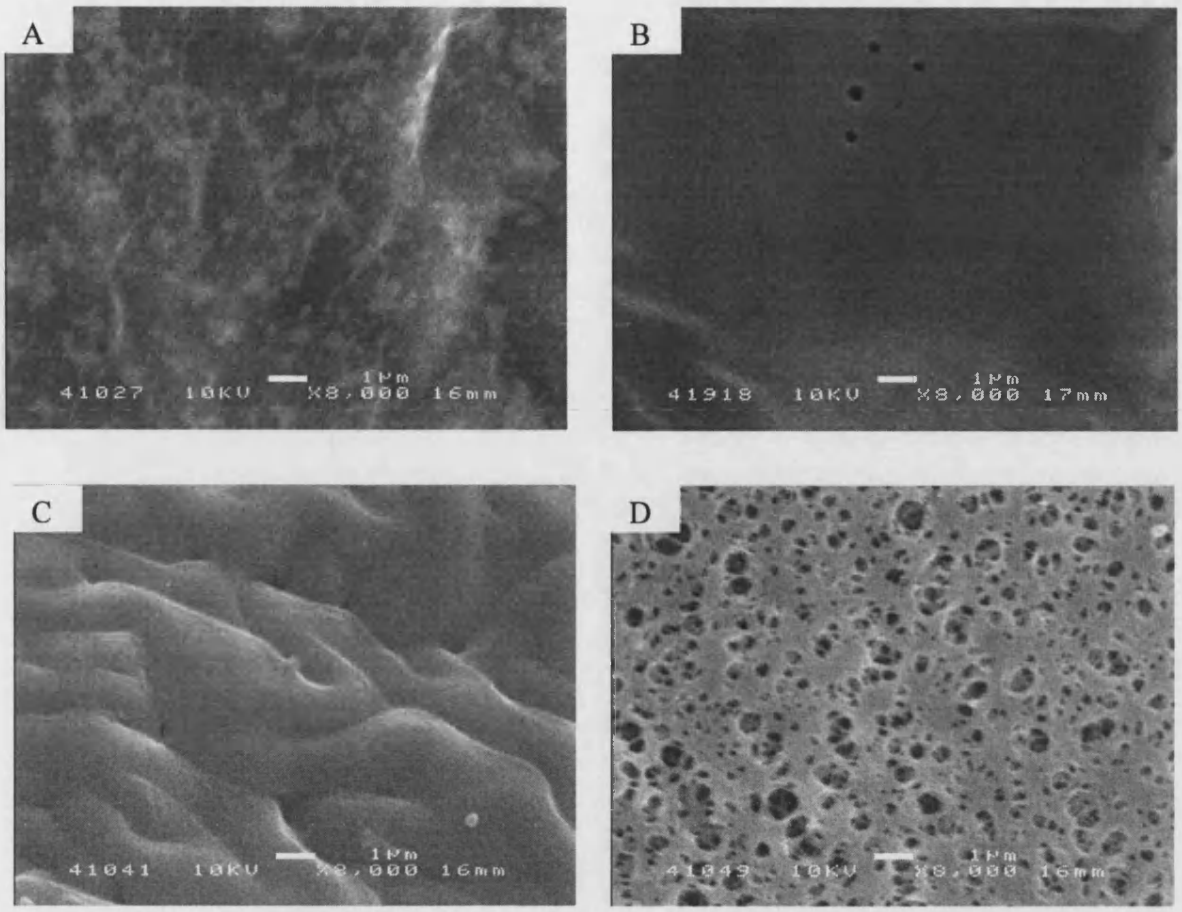

Figure 6.17. Bottom surface of flat sheet membranes after 10min in 90% ethanol. Membranes were cast from polymer-NMP solutions at 20% polymer concentration, except 75L:25 which was cast at 10% polymer concentration. (A) 100:0 (B) 75:25, (C) 50:50, (D) 75L:25. Scale bar 1 µm.

Measurement of Overall Size Change of PLGA Membranes Due to Treatment with Fixing and Lysing Agents

The overall size change of the membranes after treatment with the two fixing agents, 10% NBF and 90% ethanol, showed the extent of shrinkage due to the treatment. NBF treated membranes showed no change in surface area for half the samples and a decrease of 25% for half the samples (Figure 6.18). This was most likely due to experimental error as opposed to differences due to crystalline structure. 100:0 treated with 90% ethanol treatment, showed the greatest mean decrease in surface area with a decrease of 55% (Figure 6.18). 75:25, 50:50 and 75L:25 had mean decreases in surface area of 48%, 33% and 31% respectively.

Membranes soaked in NBF showed no decrease in thickness where as those soaked in 95% ethanol showed 43%, 45%, 36%, 12% decrease in thickness for 100:0, 75:25, 50:50 and 75L:25 (Figure 6.19).

ATM was used to lyse the cells cultured on the PLGA flat sheet membranes for DNA quantification. Although the effect of ATM on the structure will not affect the data collected, the membranes should be inert in the presence of the lysing agent to prevent any interference. While it was seen that the membranes readily absorbed ATM so allowing the samples to be fully wetted and all the cells lysed, it was found that ATM had no effect on the structure of the membrane (results not shown).

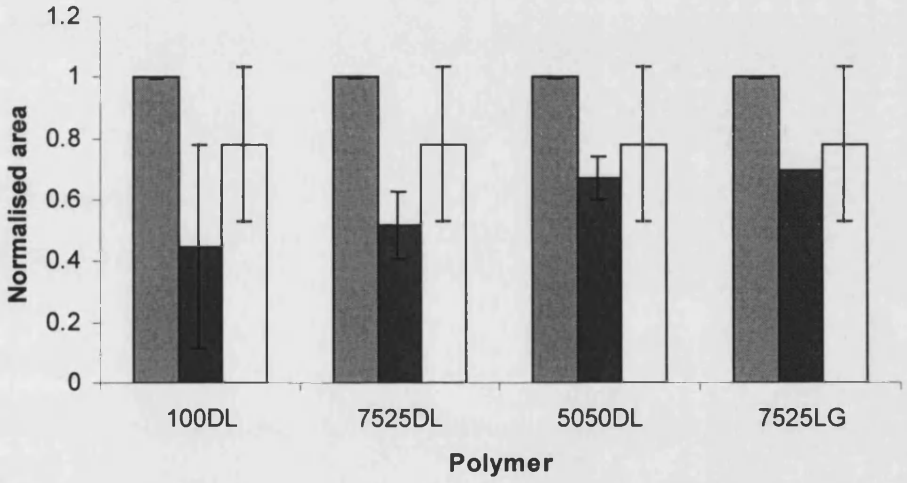

Figure 6.18. Chart showing normalised surface area of PLGA flat sheet membranes after exposure to fixing agents.
■ untreated, ■ 90% ethanol treated, 10% NBF treated. Data presented as mean ±SD, n = 3.

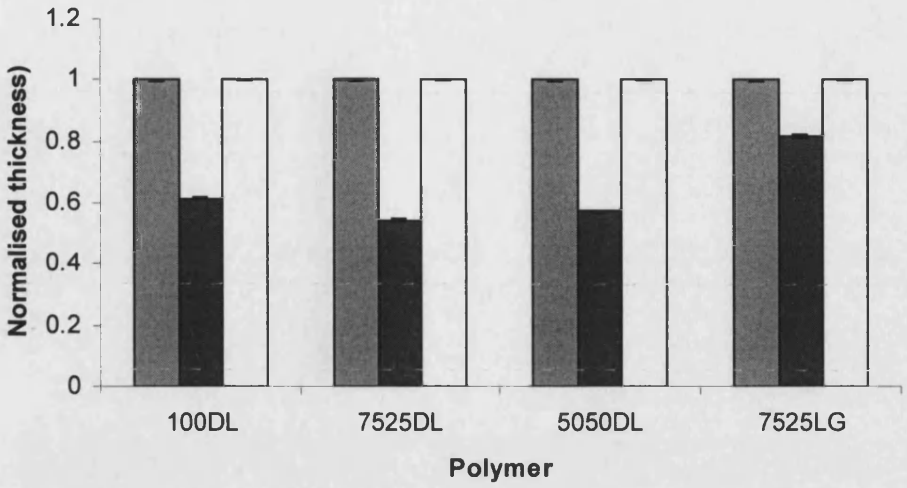

Figure 6.19. Chart showing normalised thickness of PLGA flat sheet membranes after exposure to fixing agents.
■ untreated, ■ 90% ethanol treated, 10% NBF treated. Data presented as mean ±SD, n = 3.

6.2.4 SURFACE MODIFICATION OF PLGA MEMBRANES

Hydroxyapatite coatings were investigated using SEM to view crystal formation as well as EDX and XRD to identify the chemical make up of the crystals. The crystal morphology is dependent on the growth mechanism which is in turn dependent on the material (Kokubo *et al.* 2003b). Hydroxyapatite crystals have high calcium and phosphate peaks in EDX, and an apatite peak in XRD (data not shown).

Hydroxyapatite Coating Using Kokupo's Method

Calcium phosphate crystals were seen from 2 days growth. Individual cone-shaped crystals formed. By day 6 of the growth phase, a greater number of crystals were seen. The morphology had changed from a pointed cone to crystals with rounder tips. This change in morphology can be seen further at day 10 when the crystals had become more dome-like. Figure 6.20 D shows how the density of crystals decreases as distance from the nucleation agent increases.

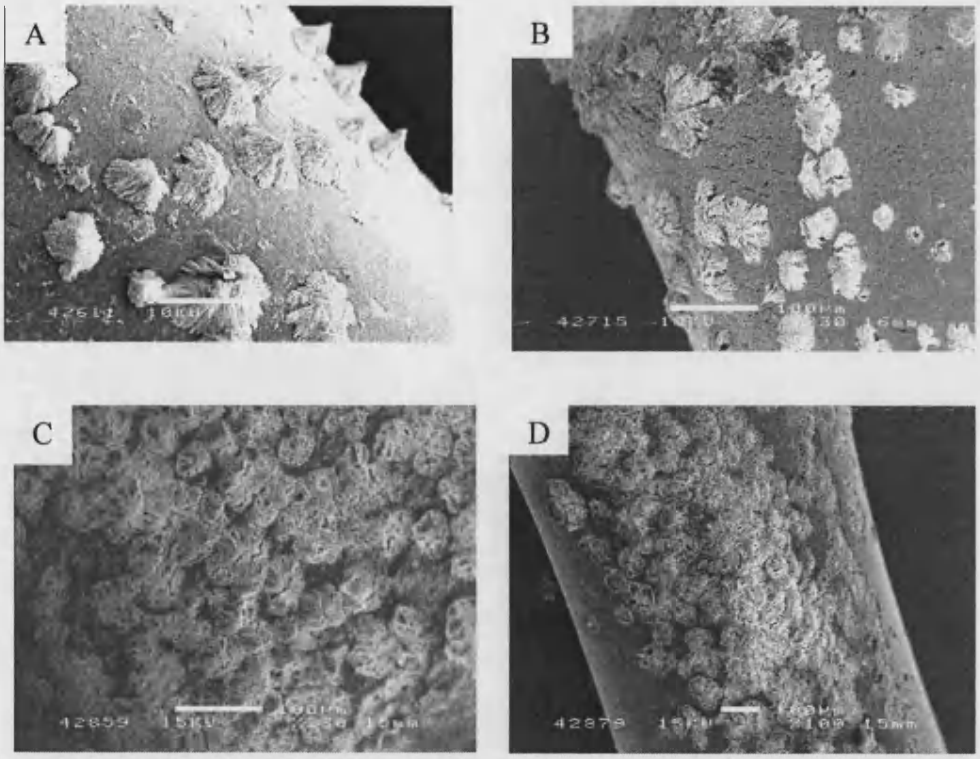

Figure 6.20. Hydroxyapatite coating of 75:25 hollow fibres at different time points during the growth phase.
(A) 2 days, (B) 6 days, (C) 10 days, (D) Fibre surface cross section. Scale bar 100 μm.

6.3 DISCUSSION

An awareness of the effect of scaffold treatments on its structure and properties is essential to understand how this will effect the cell culture development and data obtained from those cultures.

Residual solvent should be removed to reduce the possibility of toxicity and also to maintain the mechanical integrity since NMP will act as a plasticiser. Degradation kinetics of scaffolds are important for tissue regeneration since the scaffold must maintain its structure and mechanical integrity until the body can complete the healing process itself. Sterilisation is an essential part of scaffold preparation for cell culture. An infection would prevent the cell culture from developing and would be harmful, potentially fatal, if an infected construct was implanted in vivo. It is important that the sterilising agent does not affect the scaffold in a way that would

negate its properties as a scaffold. Analysis of the cultures on the scaffold is necessary to assess the suitability for cell culture it is therefore important that the reagents used do not affect the scaffolds in any way that would distort the results. Surface modification with hydroxyapatite, found naturally in the mineralised bone matrix, has the potential to improve the biocompatibility of the PLGA membranes while maintaining the benefits of a PLGA membrane structure.

6.3.1 SOLVENT REMOVAL

The average roughness and the maximum roughness values show that there is some topographical change to the membrane surfaces during solvent removal. These measurements decreased on day 7 for the samples at 15°C and increased at 37°C, change which can be seen in Figure 6.2. It is possible that the increase in temperature may have swelling and deformation hence the larger more rounded peaks. The diffusion model for residual solvent can be obtained based on a dilute solution diffusion across a thin membrane since the concentration of the solvent-the diffusing species-is of the order of parts per million. This would not be the case prior to completion of membrane formation, which is somewhat more complicated since it involved a moving boundary, and high concentrations of the solvent.

The NMP release data showed decay towards an asymptote of zero. Since the solution is dilute and there is no convection, forced or natural, the driving force is the chemical potential, which drops with decreasing solvent concentration (Cussler 1984). It follows then that as solvent diffuses into the water bath, the concentration gradient and so the chemical potential is decreased, so the rate of diffusion decreases. Since the water was fresh for the start of each time point, the accuracy of the apparatus to 10^{-6} v/v% (0.01 ppm) shows that the solvent had been removed from the membrane by day 7. Chemical potential is proportional to temperature so an increase in temperature should increase the rate of diffusion. It was seen that the rate of solvent removal was higher at the lower temperature suggesting that the temperature had an effect on the membrane such that diffusion was inhibited.

6.3.2 DEGRADATION

The topographical changes seen on the membrane surface during the time maintained in media showed that degradation was occurring and affecting the micro-architecture. Cohen *et al.* (1991) reported degradation after 1 day in PBS (pH 7.2 37°C) visible in SEM images of 75:25 microspheres for drug release formed by a modified solvent immersion technique. The microspheres became more porous and by the end of the experiment on day 76 only remnants of the microspheres remained. Panyam *et al.* (2003) also reported pore formation in 50:50 nano- and microparticles made using an emulsion solvent evaporation technique.

The roughness data suggests tri-phasic degradation, however the by-product profile shows linear degradation. The latter data is likely to be more accurate since it is quantitative where as the roughness data is a function of the topography. Reich (1997) report a tri-phasic degradation process with an initial induction period followed by accelerated ester-cleavage 'pre-onset of erosion' and slower ester cleavage 'post-onset of erosion'. Panyam *et al.* (2003) reported that the process PLGA of degradation in PBS (pH 7.4 37°C) was biphasic with an initial fast phase lasting 20-30 days followed by a slower phase, in which the pores were seen to form. PVA (used as part of the oil-in-water emulsion process) and BVA (the model macroprotein) content and molecular weight change were all observed to assess the degradation process. However, PVA improves the hyrophilicity of PLGA, and BVA was also found to increase the degradation rate of PLGA Catiker *et al.* (2000). It is possible that over the 26-day study that the degradation was in the initial stage of a biphasic process, data collected beyond day 30 would be necessary for a comparison to the work by Panyam *et al.* (2003). It is possible that the porous structure, having a large surface to volume ratio would affect degradation as more polymer can be in contact with the media at any time point. Also, as the scaffold degrades and porosity is increased, there is a greater surface area exposed on which degradation can occur. Degradation is dependent on the ratio of PLA:PGA and whether it is the L- or a mixture of D and L-isomers present in PLA (Middleton and Tipton 2000). Lu *et al.* (2000) suggest that faster degradation rate is due to a higher presence of the more hydrophilic glycolic acid. However, the data shown by Yang *et al.* (2001) shows a curve with a minimum at 50:50 having the fastest degradation rate as opposed to a linear relationship between glycolic acid concentration and degradation rate. It is

more likely that degradation rate is more significantly related to crystalinity as reported by Kim *et al.* (1995) for the copolymer PHB/HV. Other factors such as autocatalysis due to the acidic degradation products, temperature, pH and the presence of other chemicals (Hasirci *et al.* 2001) as well as environmental conditions (Lu *et al.* 2000) will affect the degradation rate.

Many factors within the culture system have been found to effect the degradation rate of PLGA such as the contents of the media (Valimaa and Laaksovirta 2004; Catiker *et al.* 2000), temperature and pH (Kimura *et al.* 2002) and pre-treatment of the scaffold (Kim *et al.* 1998). Valimaa and Laaksovirta (2004) compared the effect of PBS and an artificial urine solution (both pH 7.4, at 37°C) on the mechanical properties of 80:20 stents and found significantly greater loss of mechanical integrity and hence degradation in the artificial urine over 6 weeks. Tests by Catiker *et al.* (2000) on 85:15, 75:25 and 50:50 films in PBS (pH 7.4, at 37°C) found faster degradation in the presence of bovine serum albumin. Kimura *et al.* (2002) found degradation of PLA was faster at elevated temperatures. The two temperatures used in this report did not have a significant effect on degradation rate. pH 6 – 8 had little effect on the degradation rate whereas pH 9 increased degradation rate. This is in line with Chu (1982) who found alkaline media increased the rate of degradation of poly α-hydroxy acids.

Pre-treatment of scaffolds should also be taken into consideration. Kim *et al.* (1998) found degradation was accelerated for plasma treated PLLA, concluded to be due to the increased hydrophilicity. The group found that the degradation rate slowed to that of untreated PLLA after 4 weeks, most likely due the loss of the treated surface. Interestingly, Ishaug *et al.* (1994) found that osteoblast morphology was not affected by degradation of PLGA over 14 days.

6.3.3 STERILISATION

In this study, 70% ethanol was shown to alter the structure of the membranes. Surface area decreased by up to 44%. The resulting, smoother surface may also be detrimental to cell attachment, as osteoblasts have been shown to prefer rougher

surfaces (Matsuzaka *et al.* 2000). While the polymer itself shrunk, the pores became enlarged which has the potential to improve mass transfer.

Ishaug-Riley *et al.* (1998) successfully used ethanol to pre-wet and sterilise three-dimensional 75:25 foam scaffolds. The additional action of ethanol to pre-wet the scaffold is an important one. Ethanol easily penetrates the scaffold then on addition of water, with which it has a high affinity, mixes in the liquid phase and so diffuses into the structure via the ethanol solution. This wetting process allows the hydrophobicity of the PLGA scaffold to be overcome.

70% ethanol proved to be a suitable sterilising agent for the work carried out in this project, as proved by the absence of infection after a three-week culture on the ethanol-sterilised membranes (Chapter 7). Holy *et al.* (2001) comment that ethanol is not a suitable sterilizing agent as it does not 'adequately eliminate' hydrophilic viruses and spores. Interestingly, the group report that ethanol does not affect the morphology of PLGA, in the form of Osteofoam™, whereas there is a definite shrinkage of the phase inversion cast membranes in this study. They report that both ethylene oxide and gamma-irradiation cause greater shrinkage, molecular weight loss and increased degradation rates compared to ethanol-sterilised samples. The aim of the paper was to compare RFGD plasma sterilisation, which they found to be the best overall.

70% ethanol is cheap, easily available and was shown to be a suitable sterilizing agent for the in vitro experiments in this project. Cells did attach, proliferate and function on the ethanol sterilised membranes (Chapter 7) so the 70% ethanol was deemed suitable as a sterilising agent for this work.

6.3.4 FIXING AND LYSING

90% ethanol had a major effect on the membranes with up to 55% decrease in surface area (Figure 4.19). The cross section was visibly void of the original porous structure and appeared as a dense sheet. This phenomenon was seen to a greater extent with the more amorphous polymers, 75:25 and 50:50. 75L:25, the most crystalline polymer used retained the most porous structure.

10% NBF had no significant effect on the structure of the membranes and was selected as the fixing agent of choice.

6.3.5 SURFACE MODIFICATION

Kokubo's method (Kokubo *et al.* 1998) was successfully used to modify the surface of the PLGA hollow fibres with calcium phosphate crystals. The use of glass as a nucleation agent limits the coating process to 2D structures as it is necessary to have the scaffold in contact with the nucleating agent. This can be seen from Figure 5.22 (D), which shows the whole fibre with a higher concentration of crystals where it had been in contact with the glass and fewer crystals as the distance from the glass increased. Further studies would be required to assess the effect of the coating on mass transfer. Murphy *et al.* (2000) and Zhang and Ma (1999) successfully coated the inner pore surfaces of a porous PLGA and PLLA foams respectively with apatite using the SBF nucleation and growth method. Ciapetti *et al.* (2003) found that a hydroxyapatite coating formed using SBF improved osteoblast-like cell activity on PCL. Kokubo *et al.* (2003) showed an apatite coating on ethylene vinyl alcohol copolymer after 2 days soaking in SBF (See Section 2.3.3 Figure 2.16). These polymer fibres were pre-treated with glow discharge in O_2 plasma to form polar groups suggesting the surface chemistry has a large effect on the rate, and possibility of apatite coating.

6.5 CONCLUSIONS

A 7-day solvent-removal period in a water bath would minimize the amount of residual solvent. The amount of residual solvent remaining after three days was found to be low enough not to detrimentally effect cell culture (Chapter 7).

Degradation in media was seen to occur with a linear release of acidic by-products over 26 days. Topographical changes were seen from day 5.

70% ethanol was an effective sterilizing agent (Chapter 7) however, it affected the macro- and micro-architecture of the membranes.

10% NMP is a suitable fixing agent since it has little effect on the membrane whereas 90% ethanol is not suitable due to the large amount of shrinkage it causes which would affect the morphological data. ATM did not affect the membrane and was deemed suitable as a lysing agent.

Kokubo's method was successfully used to coat the PLGA hollow fibre membranes, however the uneven coverage would need to be addressed if the method was to be used for surface modification of the fibres or other 3D structures.

The results obtained in this chapter allow the confident use of 70% ethanol as a sterilizing agent, 10%NBF as a fixing agent and ATM as a lysing agent for the analysis in Chapters 7 and 8. Prior to seeding the membranes with cells, soaking in water for between 3 and 7 days will remove the residual NMP solvent.

CHAPTER SEVEN
HUMAN BONE DERIVED CELLS AND CELL LINE CULTURE ON PLGA FLAT SHEET MEMBRANE SCAFFOLDS

7.1 INTRODUCTION

It is a pre-requisite for a scaffold to support both cell culture in vitro, prior to implantation and in vivo, post implantation. The selected material, fabrication method and pre-culture treatment affect the suitability of a scaffold for tissue growth. PLGA is known to be suitable as a scaffold material due to its previous use in sutures and fixation devices; it is US FDA approved and many groups have used PLGA for scaffolds in tissue engineering including orthopaedic applications (Middleton and Tipton 2000).

The use of the phase inversion membrane casting with a PLGA-NMP-water ternary system to prepare a scaffold is a novel scaffold fabrication process. It is therefore necessary to assess the new set of culture parameters presented by the scaffold.

The aim of this chapter is to evaluate the effect the ratio of PLA:PGA in a phase inversion cast flat sheet membrane scaffold on cell attachment, proliferation and differentiation. The osteoblastic cell line 560pZIPv.neo (pZIP) and human bone derived cells (HBDC) were cultured on four different PLGA ratios all of which have been shown to be suitable for spinning hollow fibre membranes (Chapter 4).

7.1.1 CELL ATTACHMENT

Adhesion to the scaffold is the first stage of culture of anchorage-dependent cell types such as the osteoblastic cells used in this study.

Adhesion is important for the processes involved in tissue development such as migration, which is required for cell organisation. Migration is related to the amount of 'adhesivity' cells have with the matrix, and 'cohesivity' to each other (Ryan *et al.* 2000; Lauffenburger and Griffth 2001). Important receptors include integrins (αβ-

heterodimeric transmembrane proteins) that form bonds between the cell and substratum, and cadherins (calcium-dependent trans-membrane proteins) that form bonds between cells (Gumbiner 1996) (Figure 7.1).

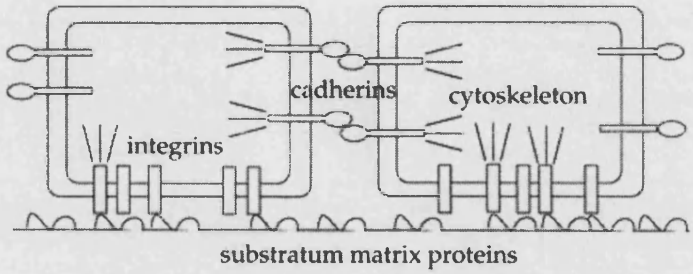

Figure 7.1. Schematic illustration of receptors in the cell plasma membrane that link to the cytoskeleton for force transmission.
Integrins, αβ–heterodimeric transmembrane proteins, bind the extracellular matrix. Cadherins, calcium-dependent transmembrane proteins, bind homotypically to their counterparts on adjacent cells (Lauffenburger and Griffth 2001).

A high cell number attached will lead to better culture development. In relation to osteoblast migration which was shown to be density-dependent, a higher cell concentration lead to enhanced cell migration (Gosiewska *et al.* 2001). Also a minimum cell number is required for a culture to develop to allow the cells to communicate with each other, an essential aspect of tissue function (Francis and Palsson 1997). Similarly the distribution should be even to allow homogeneous monolayer to form over the entire scaffold surface. Good cell-substrate interactions are shown by a high percentage of the seeded cells attaching and a flattened polygonal morphology with protrusions as typically seen in 2D in vitro culture (Beresford and Owen 1998).

7.1.2 CELL PROLIFERATION

If the scaffold can support cell attachment, proliferation, the next stage of culture development, can proceed. Proliferation is the process of increasing the number of equally mature cells. As the population becomes more dense, a healthy osteoblast population will orientate themselves length-ways and parallel to each other (Beresford and Owen 1998) and once confluent a 'whirl' formation can also be seen.

7.1.3 CELL FUNCTION

When an engineered tissue construct is transplanted in vivo, the cells it contained in vitro assist the healing process by maturing to allow new tissue formation. In the case of bone, the cells should be able to undergo mineralisation as mature bone contains a mineralised extra cellular matrix. Matrix mineralisation is an established marker for osteogenic cultures (Beresford and Owen 1998).

Mineralisation studies were carried out to show that the cells were in fact osteoblastic and also that the HBDC could function on the membranes. Dexamethasone and Ascorbic acid were routinely used in the culture media as they are recognised to improve osteoblast differentiation, seen by increased alkaline phosphatase activity, along with the addition of a phosphate reagent to induce mineralisation (Schecroun and Delloye 2003; Atkins *et al.* 2003). Kim *et al.* (2003) found that when porous PLGA scaffolds gave a continuous release of dexamethasone and ascorbate-2-phosphate, mesenchymal stem cells showed a significantly higher amount of mineralsiation compared to the control scaffolds without them. Cultures were run for three weeks in the presence of β-glycerophosphate to confirm cell type and to evaluate whether the scaffold can support normal cell activity based on mineralisation and alkaline phosphatase activity. Alkaline phosphatase is an enzyme which hydrolyses organic phosphate esters, optimally at around pH 9.0 (Bancroft and Gamble 2005). They are found in the cell membranes of osteoblasts along with cells in calcifying cartilage, liver, kidney, placenta and intestine (Pabbruwe 2002). ALP is a suitable as an early marker for osteoblasts as the source of cells is unlikely to be producing any of these other cell types. Mineralisation was used as a full-term marker as this process is unique to bone. On the addition of phosphate, alongside dexamethasone, osteoblasts will mature and differentiate and form mineralised nodules. While there are many markers that can be used to identify bone cell culture, these are both effective and simple to carry out.

7.2 RESULTS

A cell line 560pZIPv.neo (pZIP) tailored for a high proliferation rate and ease of in vitro culture was used initially to assess the potential of the PLGA membranes use as a scaffold. Once it was established that the membranes were suitable for cell culture, HBDC were used to evaluate attachment, proliferation and function of the cells that will be experienced in vivo; this work was carried out on flat sheet membranes.

Attachment over a 6-hour period, and 7 day proliferation was analysed, the resulting cell number and distribution on the membranes as well as morphology were evaluated. Membranes cultures were compared to the TCP control, this being the standard substrate for cell culture. A cell number statistically similar to TCP would suggest that the membrane had suitable attachment properties.

A suspension of cells in media was placed into a specially designed culture chamber (Section 3.3.4) with a PLGA membrane base. The chambers were kept in a humidified environment at 37°C and 5% CO_2 for 6 hours or 7 days. After the culture period, membranes were either fixed with NBF and stained with 0.5% methylene blue for observation of distribution and morphology, or lysed using ATM buffer added and stored at –80°C. On thawing, the DNA content of each membrane culture was calculated using the picogreen DNA quantification assay from which cell number was calculated.

7.2.1 OSTEOBLAST CELL LINE ATTACHMENT AND PROLIFERATION ON PLGA MEMBRANES

Initial attachment and proliferation experiments were conducted using the cell line 560pZIPv.neo (pZIP). pZIP are an sv40 transformed bone marrow stromal cell line generated in Jon Beresford's laboratory, from primary bone marrow stromal cells cultured in osteogenic medium (Beresford 2001). The sv40 gene 'immortalises' the cell and they remain in the proliferation stage of the cell cycle.

Attachment of 560pZIPv.neo to PLGA Membranes After a Six Hour Culture Period

There was no significant difference ($P<0.05$) between the numbers of pZIP attached to TCP and the membranes or between any of membranes (Figure 7.2). While there was statistically no difference between the polymers, based on the mean values, the membranes could be ordered for pZIP attachment, from greatest to least cell number; 75L:25 > 75:25 > TCP > 50:50 > 100:0.

pZIP were evenly distributed on TCP (Figure 7.3). Cells attached to 75:25 were the most evenly distributed, followed by 100:0. 50:50 and 75L:25 had a similar distribution pattern in which clumps of cells were seen in patches with few cells attached individually. The morphology of the cells on 100:0 and 75:25 is flattened with protrusions and some show a leading edge (Figure 7.4). The cells on 75:25 are well flattened but rounded. Cells attached to 50:50 appeared flat with protrusions but leading edges were less distinct than for 100:0 and 75:25. Communication through protrusions can be seen by the cells on all five substrates.

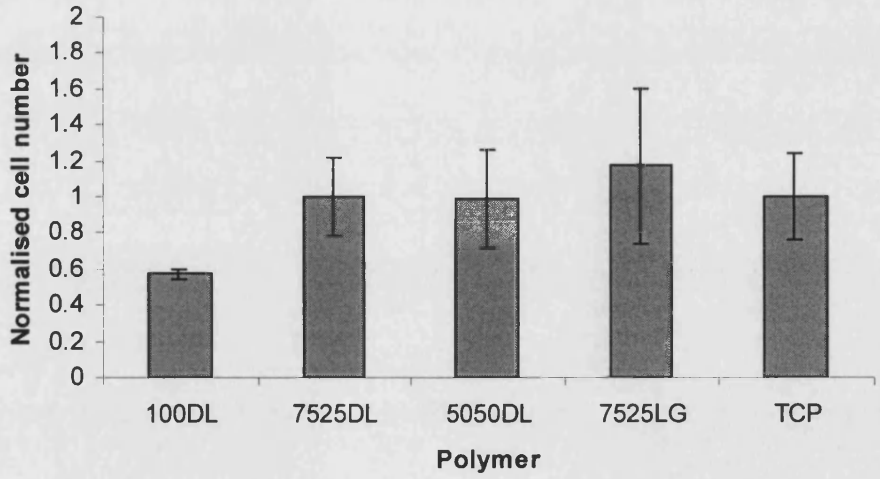

Figure 7.2. Normalised number of 560pZIPv.neo attached to PLGA membranes 6h post-seeding.
TCP is control material. Data presented as mean ±SD, n = 9. Results examined by ANOVA; significant difference at $P<0.05$. *$P<0.05$ compared to TCP.

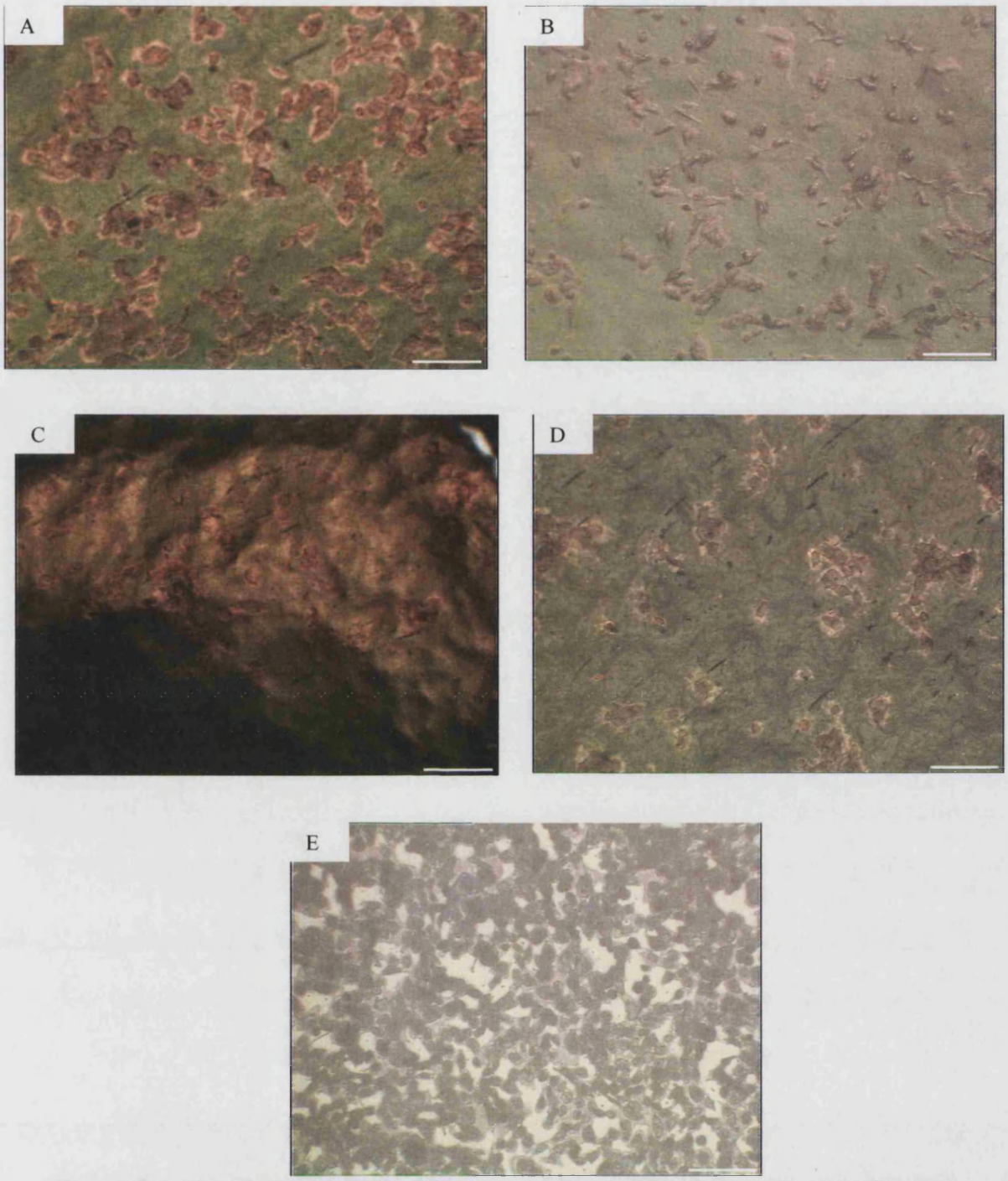

Figure 7.3. Distribution of 560pZIPv.neo attached to PLGA membranes 6h post-seeding.

(A) 100:0, (B) 75:25, (C) 50:50, (D) 75L:25, (E) TCP (control). Scale bar 200 μm.

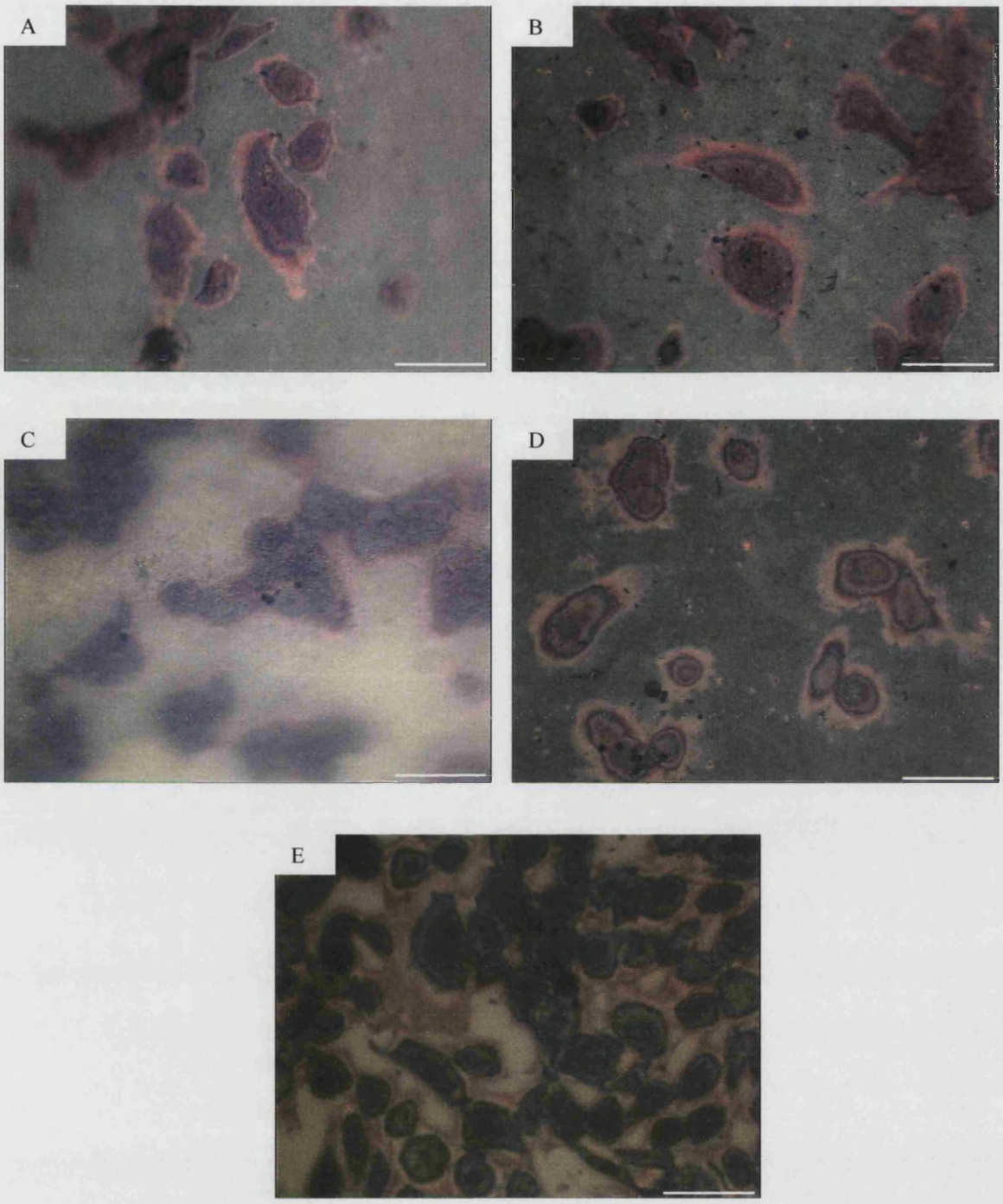

Figure 7.4. Morphology of 560pZIPv.neo attached to PLGA membranes 6h post-seeding.
(A) 100:0, (B) 75:25, (C) 50:50, (D) 75L:25, (E) TCP (control). Scale bar 50 μm.

Proliferation of 560pZIPv.neo on PLGA Membranes After a Seven Day Culture Period

There is no significant difference between the membranes and the TCP for proliferation, or when membranes are compared (Figure 7.5). 75L:25 shows a higher mean cell number after 7 days, although the standard deviation is larger. Based on the mean values, the membranes could be ordered for pZIP proliferation as follows, from greatest to least cell number; 75L:25 > TCP > 50:50 > 100:0 > 75:25.

The images in Figure 7.6 show typical distribution of pZIP on the PLGA membranes after 7 days. Both 75:25 and 75L:25 show confluent cell populations whereas 100:0 and 50:50 show a sparse distribution of cells. Of the membranes, only 75L:25 shows the pZIP organised along an axis. The morphology of the pZIP on both 75:25 and 50:50 show well spread cells which are aligned along an axis (Figure 7.7). Many of the cells show a leading edge suggesting migration across the membrane. The cells on 100:0 are fewer and not orientated, although they are spread and show communication.

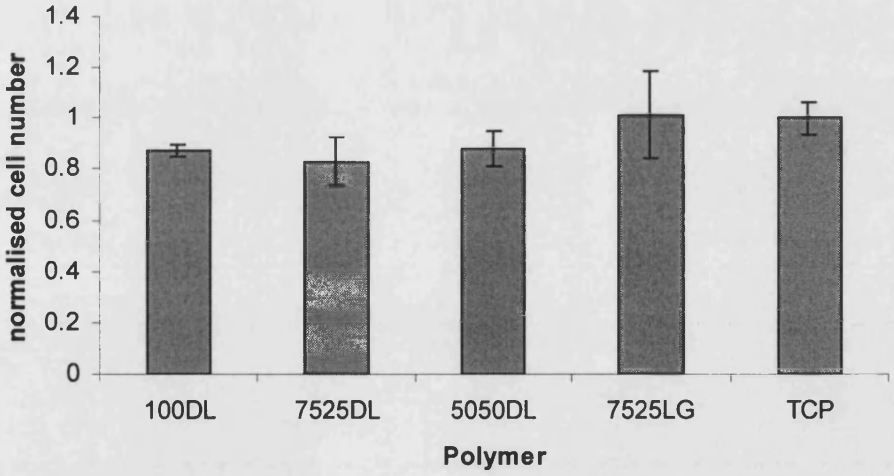

Figure 7.5. Number of 560pZIPv.neo on PLGA membranes 1 week post-seeding.

TCP is control material. Data presented as mean ±SD, n = 9. Results examined by ANOVA; significant difference at $P<0.05$. *$P<0.05$ compared to TCP.

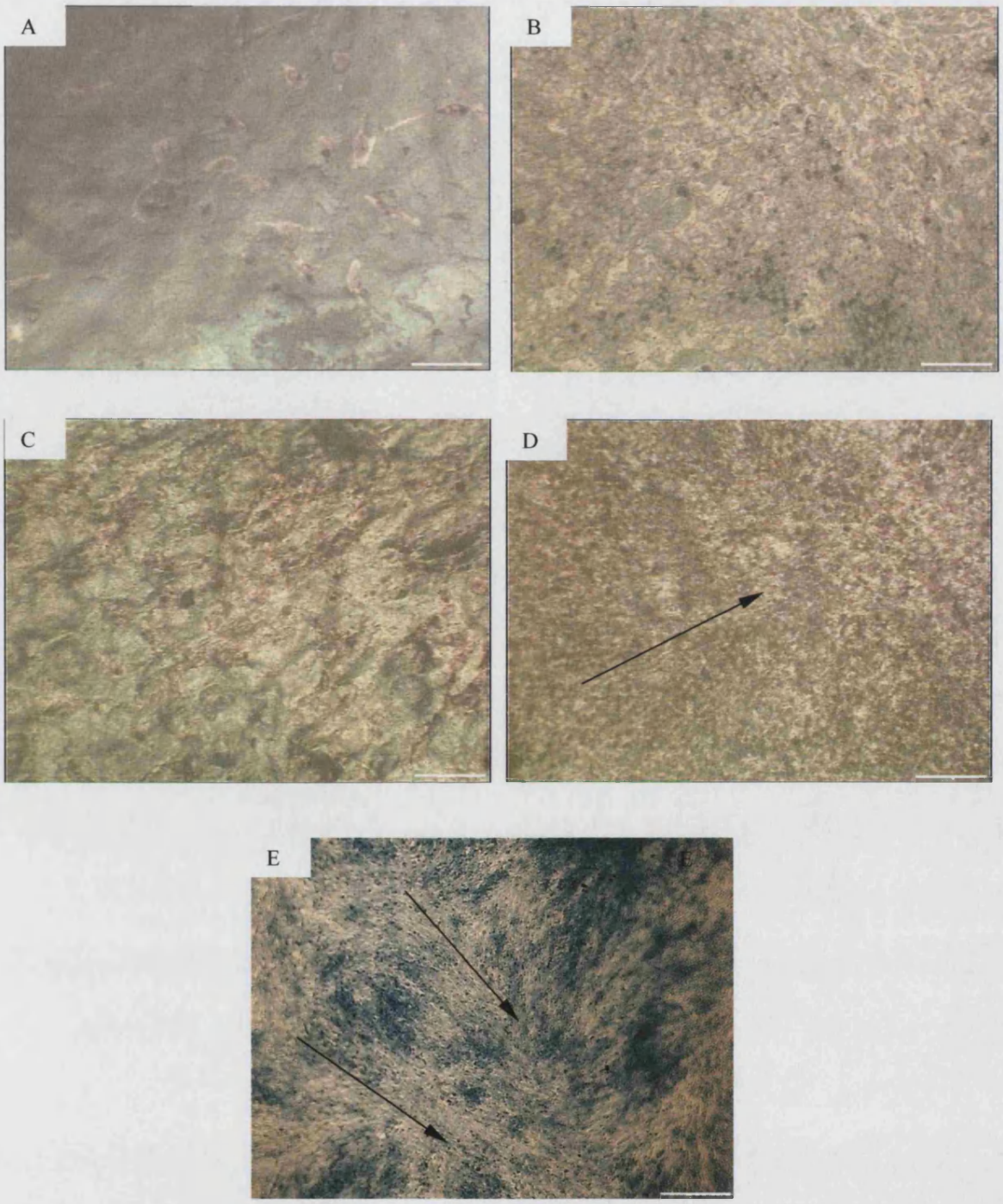

Figure 7.6. Distribution of 560pZIPv.neo cultured on PLGA membranes 1 week post-seeding.
(A) 100:0, (B) 75:25, (C) 50:50, (D) 75L:25, (E) TCP (control). Arrows show direction of alignment of cells. Scale bar 200 μm.

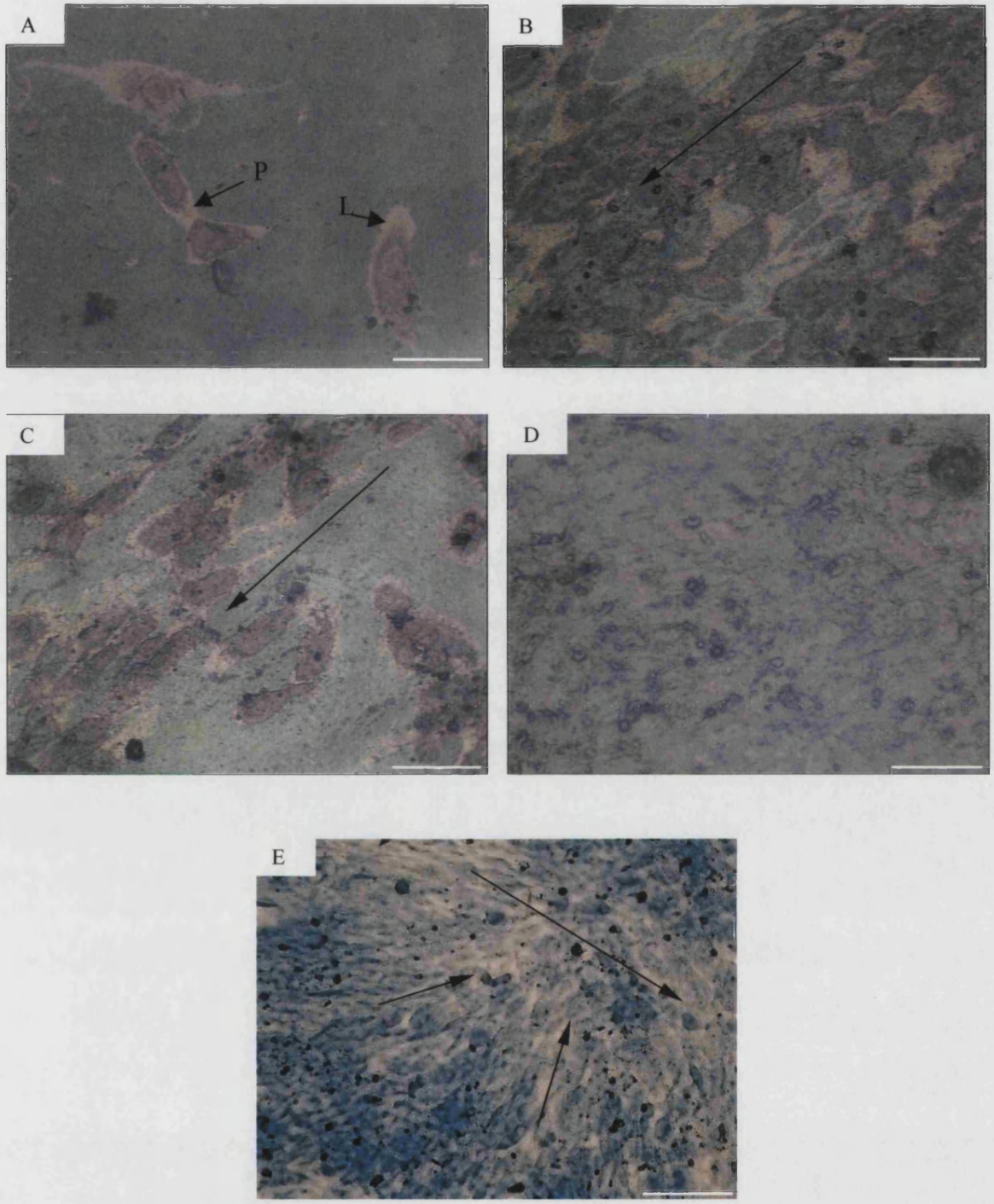

Figure 7.7. Morphology of 560pZIPv.neo cultured on PLGA membranes 1 week post-seeding.

(A) 100:0, (B) 75:25, (C) 50:50, (D) 75L:25, (E) TCP (control). Long-tailed arrows show direction of alignment of cells. L denotes an example of a leading edge, P denotes a example of a protrusion through which the cell can communicate. Scale bar 50 μm.

7.2.2 HBDC ATTACHMENT, PROLIFERATION AND FUNCTION ON PLGA MEMBRANES

Once the membrane scaffolds had been shown to support cell line culture, it was necessary to evaluate the ability of the scaffolds to support HBDC culture, the cells that the membranes will encounter in vivo. HBDC were harvested from bone chips (Section 3.3.1). Attachment over a 6-hour period and 7 day proliferation was analysed, the resulting cell number and distribution on the membranes as well as morphology were evaluated. Osteoblastic differentiation was also assessed.

Attachment of HBDC to PLGA Membranes After a Six Hour Culture Period

The number of cells attached to the membranes is comparable to TCP except 100:0 which showed a significantly lower cell number compared to TCP (Figure 7.8). 100:0 was statistically poorer for HBDC attachment compared with 75:25 and 75L:25 also. 50:50 was not significantly different to any of the other substrates. Taking into account the mean values, the performance for the membranes can be rated for HBDC attachment as follows, from greatest to least cell number: TCP > 75L:25 > 75:25 > 50:50 > 100:0.

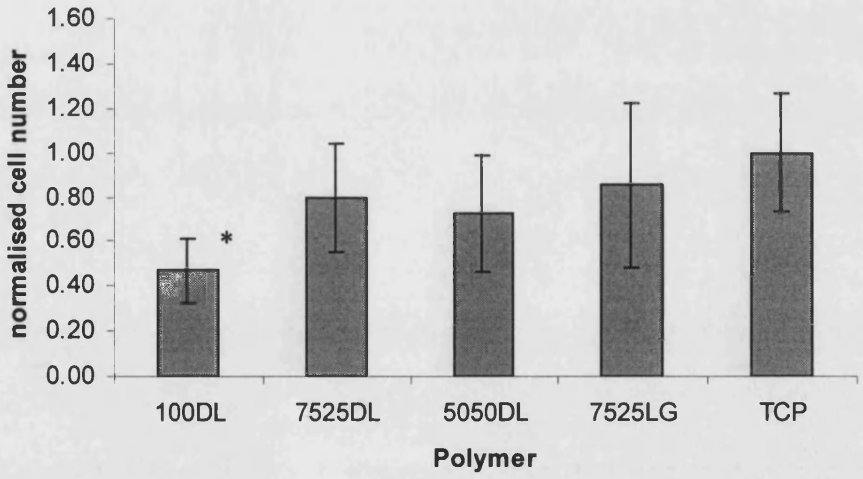

Figure 7.8. Number of HBDC attached to PLGA membranes 6h post-seeding.

TCP is control material. Data presented as mean ±SD, n = 9. Results examined by ANOVA; significant difference at $P<0.05$. *$P<0.05$ compared to TCP.

Figure 7.9 shows typical distribution of HBDC 6 hours post-seeding. The control substrate, TCP showed an even cell distribution and also the greatest number of cells attached. The 50:50, 75:25 and 75L:25 also showed a good distribution with similar cell numbers to each other but lower than TCP. 100:0 had fewer cells and they were not evenly covered across the membrane. The cell morphology 6 hours after attachment is shown in Figure 7.10. The cells attached to 50:50, 75:25 and 75L:25 show similar morphology. The majority of cells on these membranes have flattened out, about half are showing a leading edge. The cells attached to 100:0 show a more rounded morphology.

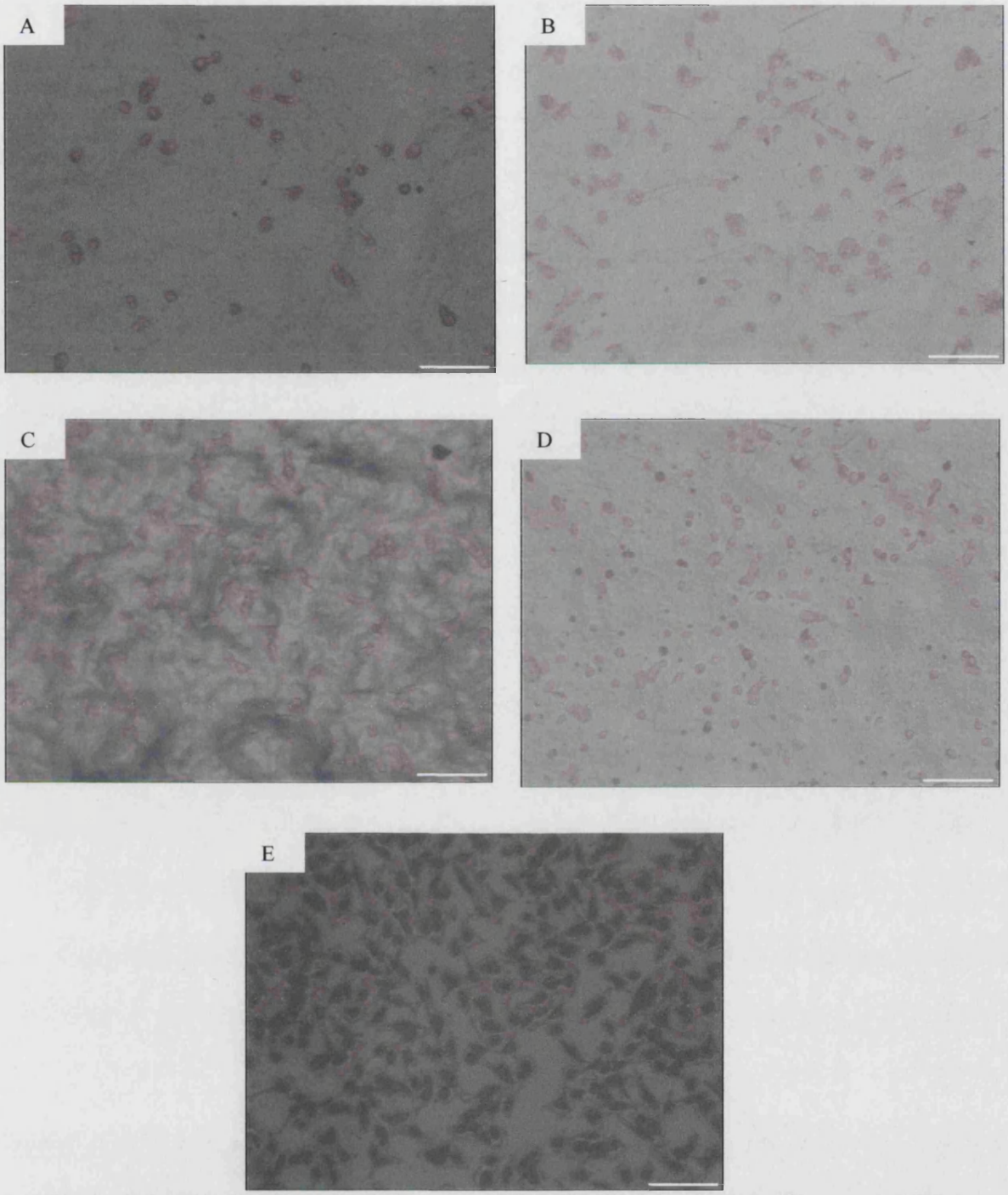

Figure 7.9. Distribution of HBDC attached to PLGA membranes 6h post-seeding.
(A) 100d,l:0, (B) 75:25, (C) 50:50, (D) 75L:25, (E)TCP (control). Scale bar 200 μm.

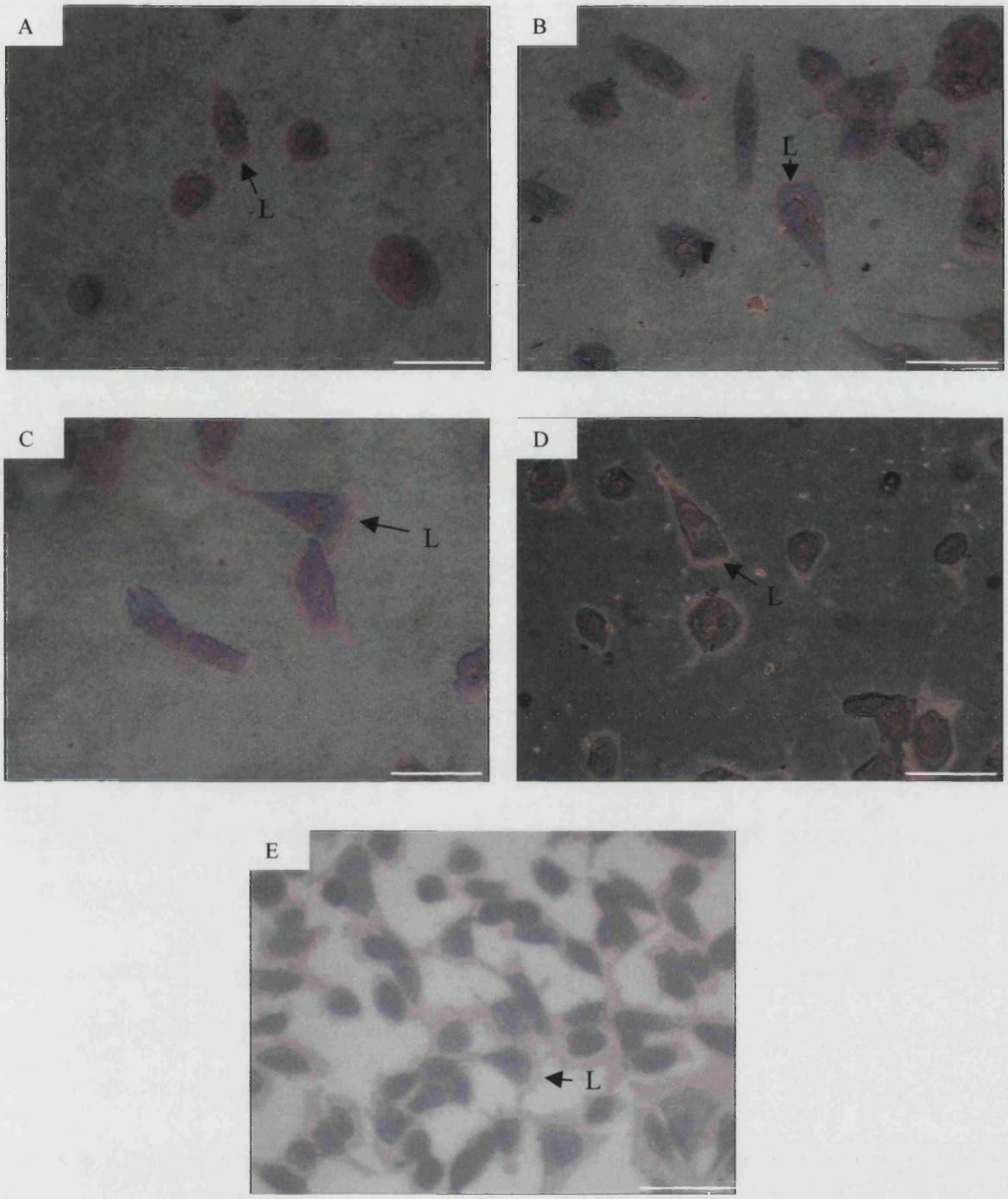

Figure 7.10. Morphology of HBDC attached to PLGA membranes 6h post-seeding. (A) 100:0, (B) 75:25, (C) 50:50, (D) 75L:25, (E) TCP (control). L denotes an example of a leading edge. Scale bar 50 μm.

Proliferation of HBDC on PLGA Membranes After a Seven Day Culture Period

The numbers of cells on 75:25 and 50:50 after 7 days is significantly lower than the TCP control (Figure 7.11). The 100:0 and 75L:25 membranes are comparable to TCP. 75:25 and 50:50 membranes also showed a significantly lower cell number

compared to 75L:25. 100:0 is comparable to all the substrates. Based on the mean cell number, the substrates can be rate for the ability to support proliferation as follows, from greatest to least cell number: TCP > 75L:25 > 100:0 > 75:25 > 50:50.

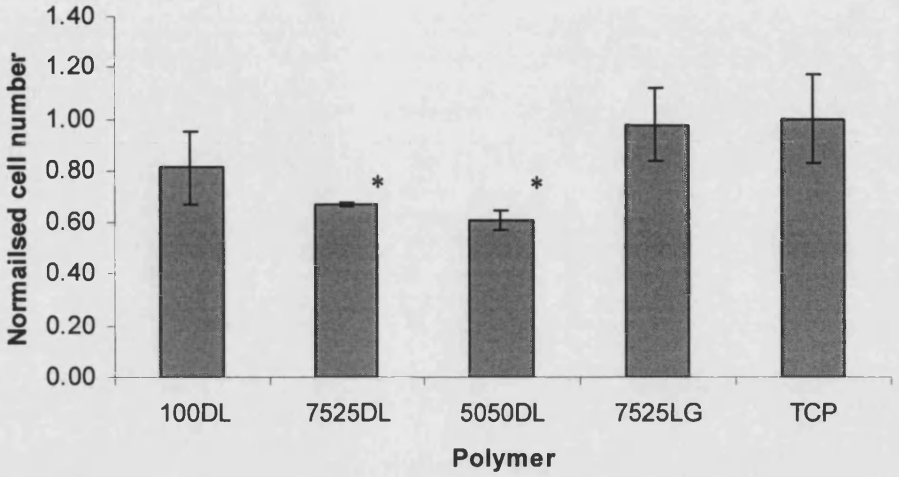

Figure 7.11. Number of HBDC on PLGA membranes 1 week post-seeding. TCP is control material. Data presented as mean ±SD, n = 9. Results examined by ANOVA; significant difference at $P<0.05$. *$P<0.05$ compared to TCP.

The cells cultured on 100:0 and 75L:25 clearly showed an orientated 'whirl' pattern (Figure 7.12). 75:25 has a population that is less ordered and cells on the 50:50 are barely visible. Cell morphology on 100:0, 75:25 and 75L:25 is flattened and polygonal showing some orientation, and comparable to the TCP culture (Figure 7.13). 50:50 shows a culture with cells that have few protrusions compared to those on the other substrates. While connection between cells is good considering the cell number, the cells appear to be less spread.

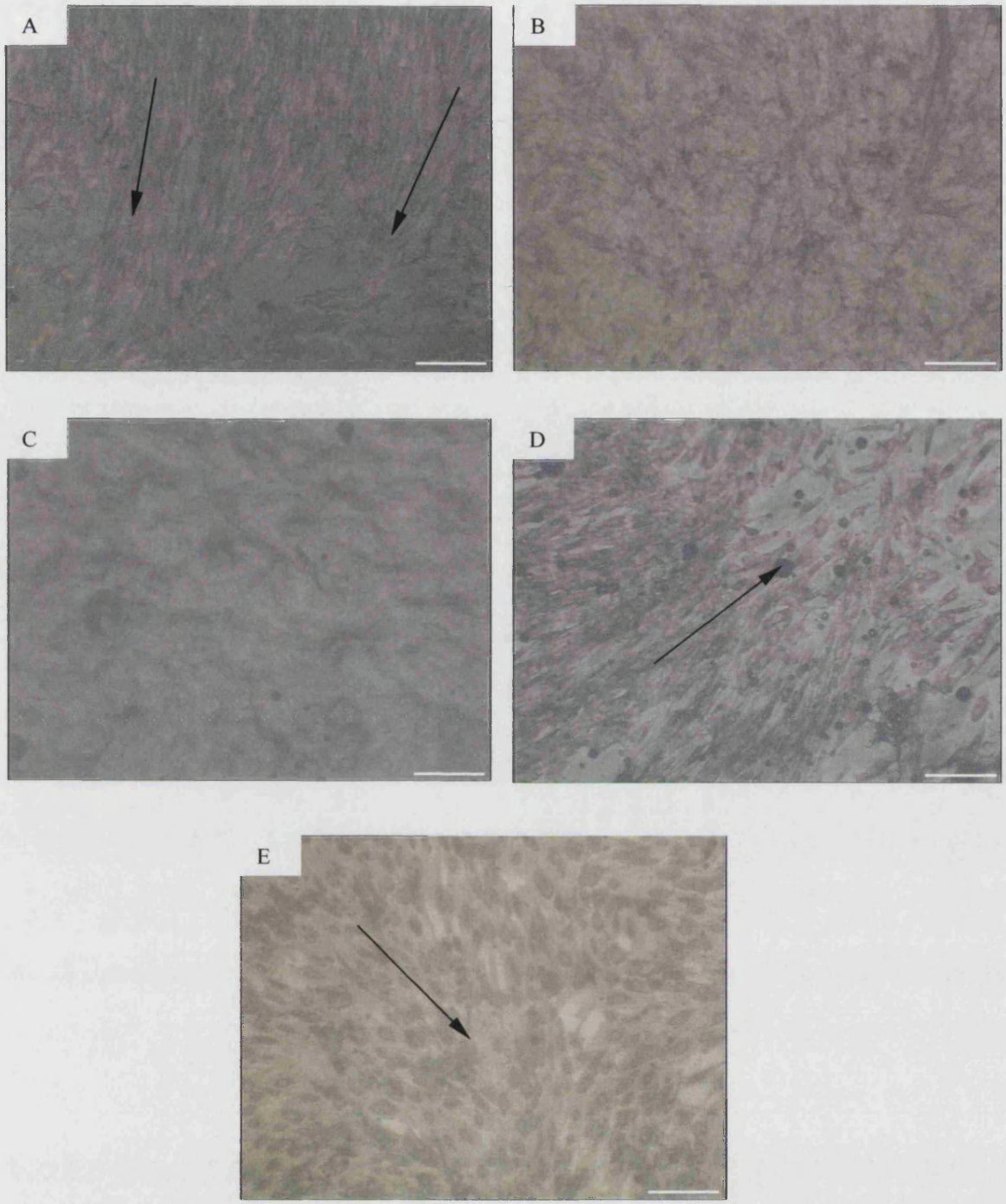

Figure 7.12. Distribution of HBDC cultured on PLGA membranes 1 week post-seeding.

(A) 100:0, (B) 75:25, (C) 50:50, (D) 75L:25, (E)TCP (control). Long-tailed arrows show direction of alignment of cells. Scale bar 200 μm.

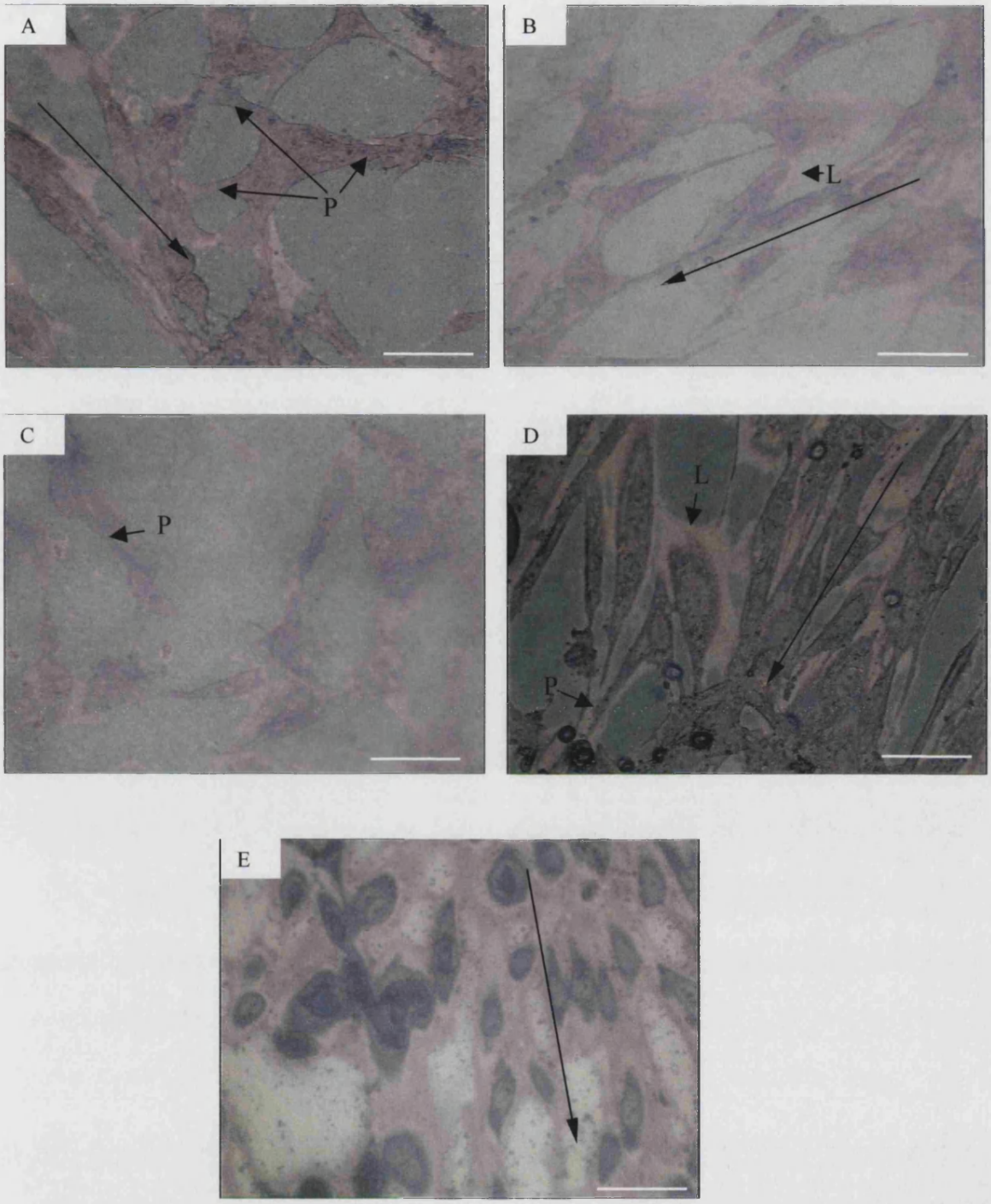

Figure 7.13. Morphology of HBDC cultured on PLGA membranes 1 week post-seeding.

(A) 100:0, (B) 75:25, (C) 50:50, (D) 75L:25, (E) TCP (control). Long-tailed arrows show direction of alignment of cells. L denotes an example of a leading edge, P denotes a example of a protrusion through which the cell can communicate. Scale bar 50 μm.

Osteogenic Function of HBDC on PLGA Membranes

The osteoblastic differentiation of the HBDC was tested over a three-week period by inducing mineralisation by the addition of β-GP from day 7 of the culture period. Von Kossa staining was used to detect the presence of mineralisation, and Fast Red SR stain for alkaline phosphatase activity at 21 days post seeding.

All substrates exhibit a degree of mineralisation but TCP has significantly more than the membranes. The membranes showed distinctive areas of high ALP activity around the nodules. This area was commonly seen to be linear and had drawn the membrane, which had formed a groove (Figure 7.14).

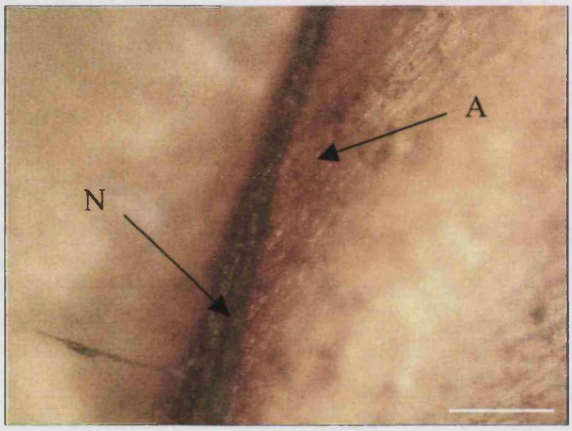

Figure 7.14. Typical morphology of mineralised nodule.
An elongated nodule (N) surrounded by a dense area of cells showing high levels of ALP activity (A) on a 50:50 flat sheet membrane. Scale bar 100 μm.

The control substrate TCP had a mean number of 2.4 nodules evenly spaced across 1 cm^2 of surface, whereas the membranes all had less than 1 nodule in the same area (Figure 7.14). For the membranes, the largest nodules were seen on 100:0, nodules on the other membranes were of similar size. Nodule size on TCP varied but were of similar size or larger than those on the membranes.

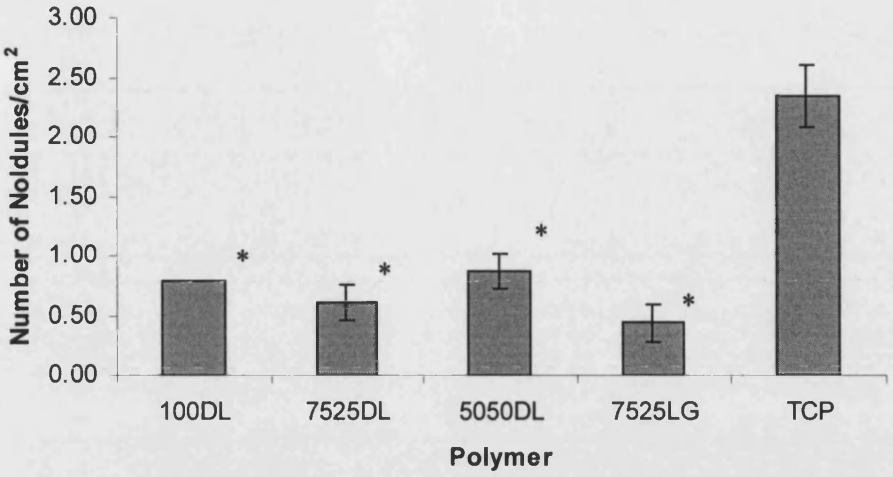

Figure 7.15. Mineralisation of extra cellular matrix laid down by HBDC after 21 days in culture.
Data presented as mean ±SD, n = 9. Results examined by ANOVA; significant difference at $P<0.05$. *$P<0.05$ compared to TCP.

Table 7.1 summarises the extent of alkaline phosphatase activity. 100:0, 75:25 and 50:50 showed similar levels of ALP activity. While 75L:25 showed some mineralisation (Figure 7.15), ALP activity was not visible; the membrane appeared silver-coloured throughout.

Table 7.1. Alkaline phosphatase activity shown by extent of fast red staining.

100:0	75:25	50:50	75L:25	TCP
+	+	+	-	+++

+ = 0.1 cm^2/ cm^2 of surface, - = no staining observed.

7.3 DISCUSSION

The results in this chapter can be used along side those in Chapters 4 and 5 to select the optimal phase inversion cast PLGA membrane scaffold, specifically the best ratio of PLA:PGA for bone cell culture.

Attachment is essential for bone tissue development as the cells involved in the process are anchorage-dependent and so the cell-substrate interaction will influence proliferation and differentiation on the scaffold. Osteoblasts attach to proteins absorbed on the substrate surface, (Puleo and Bizios 1992; Bagambisa *et al.* 1994) and the adhesive proteins used by the cells may depend on both the material chemistry and the adsorbed protein (Steele *et al.* 1993; Sinha and Tuan 1996; Cooper *et al.* 1998). Once the cells have attached, they are able to spread. After these initial stages, proliferation can begin. Proliferation is necessary for a population to develop on the material. The cells divide and increase the population with cells of the same maturity. A faster rate of proliferation is preferential for tissue engineered constructs to produce new tissue quickly. Once confluent, the cells can differentiate to produce mature tissue. Mature bone contains a mineralised matrix, which is essential for mechanical strength.

7.3.1 ATTACHMENT

Both the cell line (Section 7.2.1) and the HBDC (Section 7.2.2) showed a good distribution on the membranes after 6 hours. This shows that the seeding method used (Section 3.3.4) is appropriate for good distribution.

For both the cell line and HBDC, 100:0 showed the lowest number of attached cells at 6 hours, but the value was only significant for the HBDC. Based on the mean values, the substrates can be rated for attachment as follows, from greatest to least cell number:

pZIP	75L:25 > 75:25 > TCP > 50:50 > 100:0
HBDC	TCP > 75L:25 > 75:25 > 50:50 > 100:0

No significant difference was seen between any substrates for the cell line. 100:0 was statistically poorer for attachment of HBDC compared with TCP, 75:25 and 75L:25.

The morphology of the cell line on all substrates was comparable to that on TCP supporting the quantitative data that the pZIP attach similarly on the membranes and the control. The cells were well spread on all membranes. 75L:25 cultures look the

most similar to the cells on TCP. The majority of HBDC have flattened out, about half are showing a leading edge suggesting they are migrating across the membrane. The cells attached to 100:0 show a more rounded morphology which suggests the cells-substrate interaction are not as good for this PLA:PGA ratio polymer (Beresford and Owen 1998).

Ishaug *et al.* (1994) carried out extensive (rat) osteoblast culture on PLGA films during the 1990's. In a study comparing PLLA, 75:25, 50:50, PGA plus TCP as control, rat osteoblasts attached equally well to the polymer films compared with the TCP control after 8 hours. While there was no significant difference ($P<0.05$) between the substrates and TCP for attachment, there was a significant difference between PLLA and 50:50. The cells attached at 52% (±5%)of original seeded cell number to TCP, and 66% (±3%) to 50:50. Osteoblasts on 50:50 and 75:25 were reported as having spread and formed a monolayer after 1 day. A more recent study by El-Amin *et al.* (2003) to investigate the effect of polymer composition used scaffolds formed using methylene chloride solvent casting. 50:50 and PLLA were compared for attachment of human osteoblasts at 3, 6, and 12 hours with TCP as the control. They found that adhesion was greater on 50:50 than PLLA, and comparable to TCP, and that the cells seeded onto 50:50 also produced higher levels of extra cellular matrix proteins. They concluded that the composition of PLGA polymers does affect cell behaviour, although recommended further studies.

The data in the project is in agreement with the work of both these groups in that PLA, albeit different isomers, is the poorest for attachment and 50:50 was comparable to TCP. The similarities in these three sets of work point towards a polymer composition effect on attachment, not a fabrication method effect.

The attachment data shows that the membranes have the potential to support bone cell culture. 75L:25 supported the greatest cell number after 6 hours with both pZIP and HBDC. 100:0 showed the lowest attachment, significantly lower for HBDC culture. 75L:25 and 100:0 are the two most crystalline polymers so this initial data suggests that crystalinity does not affect cell attachment.

7.3.2 PROLIFERATION

After a period of seven days, the cell population should be confluent and the substrate covered by a layer of cells. The number of cells attached to the membranes was compared to the TCP control, this being the standard substrate for cell culture. A cell number statistically similar to TCP would suggest that the membrane had suitable proliferation properties. Some orientation would also be expected; the cells should be aligned and seen to form 'whirls'.

There is some discrepancy between the distribution of the cells and the cell number for the cell line (Section 7.2.1). Both 100:0 and 50:50 appeared to have few cells, however, quantitatively they are comparable to TCP, as well as 75:25 and 75L:25 which showed confluent populations.

The cells should be well spread and orientated along the same axis as its neighbours. This shows that the substrate allows interaction and organisation desirable for tissue formation (Beresford and Owen 1998). Confluent cultures with a 'whirl' appearance were seen on 75L:25 for both the cell line (Section 7.2.1) and the HBDC (Section 7.2.2). This same distribution was seen on 75:25 with pZIP and 100:0 with HBDC. 50:50 showed a sparse population with both cell types as did 75:25 for HBDC and 100:0 for pZIP.

Based on the mean values, the substrates can be rated for proliferation as follows, from greatest to least cell number:

pZIP 75L:25 > TCP > 50:50 > 100:0 > 75:25

HBDC TCP > 75L:25 > 100:0 > 75:25 > 50:50

Similar to attachment, 75L:25 had the highest cell number, significantly higher than 50:50 and 75:25 for HBDC culture. The number of cells on all four of the membranes cultured with pZIP was comparable with TCP and there were no significant differences between any of the substrates. 7527DL and 50:50 both supported a significantly smaller HBDC culture compared to TCP.

The results reported by Ishaug *et al.* (1994) showed 50:50 having the highest mean cell number of all the polymer membranes. Despite PLLA having significantly fewer cells at 1 day, the proliferation was comparable on all substrates between day 4 and 14. If one substrate had to be chosen from the study, 50:50 appeared to have the best proliferation rate, although like the other substrates, mean cell number did not show the incremental increase over the culture period but rather tended to oscillate. If this oscillation was also occurring in the study carried out for this work then the HBDC are behaving in a similar manor to these earlier studies. The significantly lower proliferation results for PLLA in the study by Ishaug *et al.* (1994) and PDLLA in this study, along with the fact that 75L:25 was statistically similar to TCP suggest that the composition as opposed to the crystalinity is the important factor. A later study by the same researcher (Ishaug *et al.* 1996) used 75:25 and 85:15 PLGA films for up to 14 days and found no significant difference between the rate at which cells migrated and proliferated to cover the substrates. This led them to conclude that in fact the composition does not affect these phenomena. However, the small difference in PLA and PGA content in the study may not be significant in comparison to PLA alone or the presence of PGA.

A further possible factor effecting both attachment and proliferation is the polymer content of the membranes. The membranes were all prepared with the minimum amount of polymer to give a viscosity with which hollow fibres could be spun. This was 20% for 50:50, 75:25 and 100:0, and 10% for 75L:25. The 75L:25 membranes were shown to have larger pores a higher surface porosity (Chapter 4). It is also a possibility that the surface chemistry of the 75L:25 allowed better protein absorption. Further experiments to quantify these effects need to be carried out.

7.3.3 HBDC FUNCTION

Mineralisation was seen on all polymer membranes with HBDC cultures after three weeks (Section 7.2.2). However, the number of nodules was significantly lower for all membranes compared with TCP. Holy *et al.* (2000) used a seeding density of 0.5 - 10 x10^6 cells/cm^3 on 75:25 sponges, and reported 'scattered (von kossa) staining on edges of scaffold' at 3 weeks and 'strong (von kossa) labelling throughout entire scaffold' at 6 weeks.

All polymers showed ALP activity after 3 weeks, however all showed significantly less activity compared to TCP. Earlier studies (Ishaug *et al.* 1994) showed that 75:25 and PGA had similar ALP activity to TCP at 7 days. 75:25 was still similar to TCP at 14 days but levels of ALP activity did not increase between 7 days and 14 days on PGA. PLLA and 50:50 showed significantly lower ALP activity at 7 days and 14 days compared to TCP; ALP activity on 50:50 did not increase between 7 days and 14 days. The silver staining of the entire 75L:25 membrane may have been due to the high porosity which saw greater diffusion of the von Kossa stain into the membrane. This prevented any ALP staining from being visible, but the fact that the mean mineralisation was the lowest for 75L:25 coupled with the higher cell numbers in the proliferation studies could suggest that *l*-isomer of PLA induces greater proliferation as opposed to differentiation.

The low amount of both mineralisation and ALP activity may be a function of the low cell number. Although this work by Ishaug *et al.* (1994) showed no significant difference between proliferation on TCP and the polymer membranes, a much higher seeding density (0.5 - 6.0 x 10^6cells/cm^2) was used, compared to 20,000 cells/cm^2 in this study, and consequently 3 week cell number.

7.4 CONCLUSIONS

The PLA:PGA ratio 75:25, with both the *d*- and *l*-isomers and the *l*-isomer alone, showed more successful attachment results compared to 50:50 or PLA alone. There was no statistical difference between the polymers and TCP for pZIP culture, however PLA was significantly poorer compared with all substrates except 50:50 for attachment of HBDC. The results were more mixed for proliferation. Again, 75L:25 was the polymer showing the greatest cell number for both pZIP and HDBC. As with attachment, there was no significant difference between substrates for pZIP culture. The HBDC number on 50:50 and 75:25 was significantly lower compared with 75L:25 and TCP. Osteogenic function of HBDC was significantly lower on all polymer membranes compared to TCP, and none was seen on 75L:25.

The attachment and proliferation studies carried out on the polymer membranes suggest that the polymer composition does effect cell culture and that neither crystallinity or fabrication method does not since similar trends were found in this study as well as previous studies using PLGA scaffolds made prepared with different fabrication methods.

While attachment is a prerequisite to proliferation, the long term cell number and function are important for a clinically useful scaffold. ALP activity along with mineralisation not only serves to show that the HBDC are osteogenic, but that the PLGA membranes can support differentiation and the resulting function. The results obtained in this chapter, and previous studies by other groups, imply that any PLA:PGA ratio can support bone regeneration in vitro, and regardless of the presence or absence of the *d*-isomer of PLA. The most important aspect of this chapter is the proof that a membrane cast using immersion precipitation is suitable as a scaffold for bone tissue engineering. Since the scaffold properties are essentially the same for flat sheets and hollow fibres, except for the curvature of the fibres, cell culture studies can be carried out using hollow fibre membranes with confidence that they are able to support the culture.

CHAPTER EIGHT
CELL CULTURE IN A PLGA HOLLOW FIBRE BIOREACTOR

8.1 INTRODUCTION

The choice of bioreactor is dependent on the tissue to be regenerated and the choice of scaffold (Ellis *et al.* 2005). Hollow fibre phase inversion cast membranes were selected as the scaffold structure because of the structural similarities with cortical bone (Section 2.2.1). As described in Chapter 2, cortical bone consists of osteons, each supplied with nutrients via the Haversian canal. Nutrients pass from the blood supply in the Haversian canals, into the interstitial fluid in the canniculi and lacuna that house the osteocytes and supply the cells surrounding the osteon. Once the construct is implanted, the lumen of the fibres can act as guides for angiogenesis and are proposed to function in a similar role to the Haversian canal until remodelling occurs and the scaffold is replaced with mature bone. The major benefit of a hollow fibre bioreactor configuration is a large surface area to volume ratio beneficial for obtaining large cell numbers (Scragg 1991).

Previous chapters have described the development of PLGA hollow fibres and have shown that PLGA flat sheet membranes can support attachment and proliferation of both pZIP and HBDC in a static 2D environment (Chapter 7). This chapter will describe the seeding of pZIP onto the hollow fibre membranes in a 3D environment and the effect of a continuous flow bioreactor system on proliferation.

8.1.1 THE RATIONALE OF SELECTING A HOLLOW FIBRE MEMBRANE BIOREACTOR CONFIGURATION FOR BONE TISSUE ENGINEERING

It has been shown by several other groups (Koller and Palsson 1993; Goldstein *et al.* 2001) that perfusion systems result in greater culture densities (cells/cm^2), and that constructs of a few mm thick can be made due to the enhanced mass transfer properties of a perfusion system. However, such bioreactors still encounter mass transfer limitations due to the use of packed bed type scaffolds. Typically, scaffolds are PLGA sponges, fibrin gels or microspheres (Section 2.3.3). Nutrients pass

through the larger pores due to the pressure gradients created by the continuous flow of media, however, small pores on an axis from the bulk flow of the liquid rely on the diffusion of nutrients into the pores to feed the cells, and also remove waste products. Nutrients are used by the cells closest to the pore entrance so creating a concentration gradient which, at some point deeper within the pore is too low for the cells' needs and the cells become necrotic. The benefit of a membrane bioreactor is that the bulk flow of the media on one side of the membrane feeds the cells on the other side by both convection and diffusion. The membrane not only provides a scaffold for the cells but also a protective barrier from the shear forces of the bulk flow of the media. This allows the media flow rate to be high so increasing the rate of nutrient mass transfer. Since the bulk flow is considerably greater than the rate of diffusion across the membrane wall, the cells receive the same concentration along the length of the membrane. Not only does a hollow fibre bioreactor configuration have a similar structure to the Haversian canal system of bone, it has a very high surface area:volume ratio. It is these two factors that distinguish the PLGA hollow fibre membrane bioreactor from current systems.

8.1.2 SEEDING METHODS OF HOLLOW FIBRE BIOREACTORS

Efficient seeding of the bioreactor is essential for the development of a tissue engineered construct. As described in Section 7.1.1, osteoblasts migration and communication, required for cell organisation, is density-dependent so a high seeding density will result in an organised culture developing sooner. The down-side of a high seeding density is the requirement of a large number of cells to start with; this is not always possible so a seeding method that allows near one hundred percent of the seeding population would give the culture the best chance to develop.

Seeding can be carried out in situ in a number of ways, namely settling where the cell solution is added and allow to settle through the construct, perfusion where the cells are pumped through the construct and rotation where the cell solution is added and the cells kept in suspension around the fibre by gently rotating the bioreactor. Allowing the cell solution to simply settle will be the least efficient as there is only one opportunity for a particular part of the scaffold to come into contact with the cells. The cell solution is continually passed through the scaffold during both perfusion and rotation. The pump should be carefully chosen for perfusion as the

cells can be easily damaged. An oscillatory pump as described by (Wendt *et al.* 2003) would allow cells to be pumped through the construct without actually passing through the pump. Rotation does not involve the cells passing into and out of the bioreactor. The movement of the bioreactor itself causes the cells to stay in suspension around the construct (Lappa 2003).

8.1.3 CELL NUMBERS IN HOLLOW FIBRE BIOREACTORS COMPARED TO TRADITIONAL SYSTEMS

The theoretical cell number that can be obtained using a hollow fibre bioreactor is the greatest with cell numbers of around 2 x 10^8 cell/ml compared to 5 x 10^5 cell/ml for a stirred tank and 2.5 x 10^5 cell/ml for a packed bed (Scragg 1991) (see also Table 2.6). It is generally accepted throughout the field of tissue engineering that a perfusion system is considerably more beneficial to tissue regeneration in vitro due to the reduction of concentration gradients and the stimulating effects of fluid shear (Sikavitsas *et al.* 2001).

8.2 PLGA HOLLOW FIBRE BIOREACTOR DESIGN AND OPERATION

8.2.1 MODULE DESIGN AND PREPARATION

Two main factors were considered when designing the module; ease of potting and removal of the fibres to prevent damage, and transparent material to allow observation of the culture, primarily to check for infection.

Prior to module assembly, the entire bioreactor system was sterilised in an autoclave at 121°C for 20 min. The fibres were soaked in a penicillin/streptomycin (P/S) solution for 6 hours at 4°C. The module was then assembled in a laminar flow hood.

Two different potting gasket designs were used that either held the fibres individually in separate holes, or held the fibres as a bunch and the apoxy resin was used to separate the fibres (Figure 8.1). The latter method had a less damaging effect on the fibres and was found to be easier to prepare so many more fibres could be used. This method was selected and 10 fibres were potted into each module.

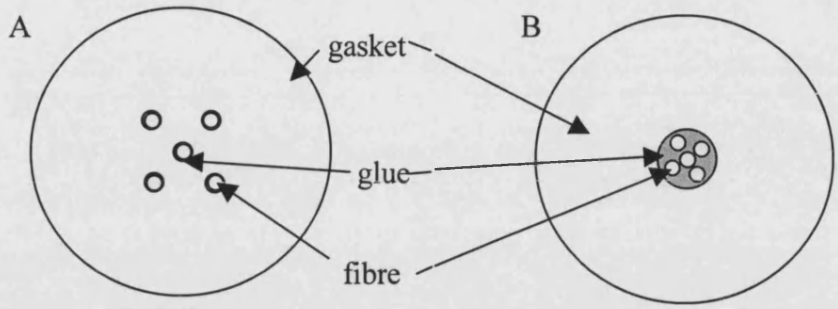

Figure 8.1. Schematic diagram of different potting-gaskets used.
(A) individually potted fibres, (B) bundle potted fibres.

Once the fibres had been glued into the potting-gaskets, which were then glued onto the module ends, it was left to dry in the hood for a minimum of 3 hours containing P/S solution. The P/S solution was removed via a side port and DMEM used to rinse the module by syringing the solution through one side-port and allowing it to flow out the other. pZIP media was then added for 1.5 hours before the cell solution was added (Section 8.3.1).

8.2.2 BIOREACTOR SYSTEM DESIGN

The use of silicon gaskets to hold the tube connectors in place, and silicon tubing, acted as seals without the need for a sealing system such as ferrules, which were not suitable with the glass module that was designed. The use of PTFE tape and tubing ties was required to prevent leaks. While it was not ideal for a sterile, repeatable system and a different module design would be beneficial, this set up was adequate for these preliminary experiments.

Media was fed through the lumen and side-ports using a counter current set up to maximise the likelihood of mass transfer across the membrane wall. The ablumenal stream was set to the lowest flow rate possible of 0.17 ml/min to minimise the fluid shear experienced by the cells, while the lumen stream was maintained at 1.7 ml/min. The system was operated as shown in the schematic in Section 3.4.2 (Figure

3.4). The media fed through the lumen and to the ablumen side was recirculated over the entire week period from separate feed bottles each containing 50 ml of media.

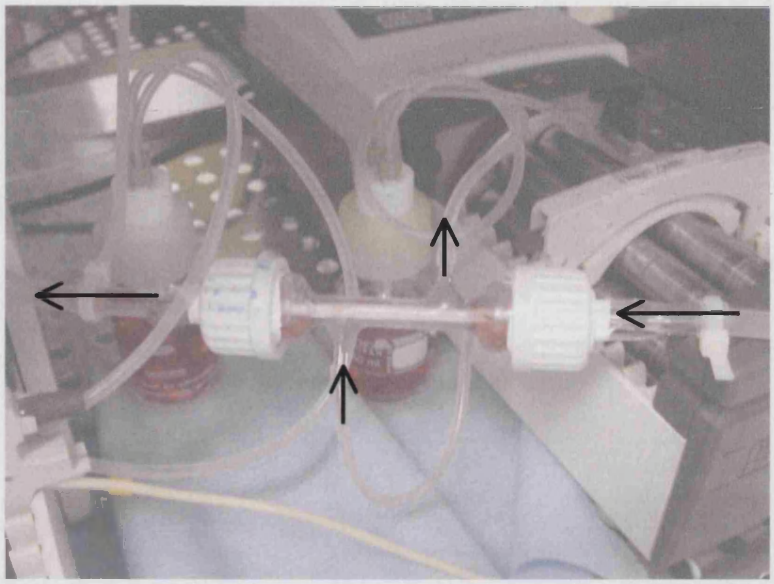

Figure 8.2. Hollow fibre bioreactor set up for the proliferation of 560pZIPsv.neo on PLGA hollow fibre membranes.
Arrows show direction of media flow.

8.3 RESULTS

8.3.1 SEEDING AND SIX-HOUR ATTACHMENT OF 560PZIPV.NEO TO PLGA HOLLOW FIBRE MEMBRANES IN THE HOLLOW FIBRE BIOREACTOR

Seeding Method

During attachment, the bioreactor was attached to a rotary mixer (Figure 8.3) and rotated at 6.6 rpm for 6 hours.

The rotating mixer was used to make use of centrifugal force to aid mixing; this avoids the use for stirring vanes (Lappa 2003). By calculating the instantaneous velocity, u_i, and the terminal velocity, u_o, of the cells a simplified proof of the effectiveness of rotational seeding can be shown. At the low rate of rotation u_i, towards the wall of the bioreactor, tends towards zero which implies the cells are maintained at the starting distance, r_0, from the axis of rotation, r, for any time, t, i.e.

$r_t = r_0$ (Equation 8.1). However, since gravity still acts on the cells and, by comparing u_o and u_i, it can be seen that the resulting terminal velocity is greater than the instantaneous velocity. Settling will occur but since the bioreactor is rotating, the suspension will be well mixed and settling can occur towards the fibres.

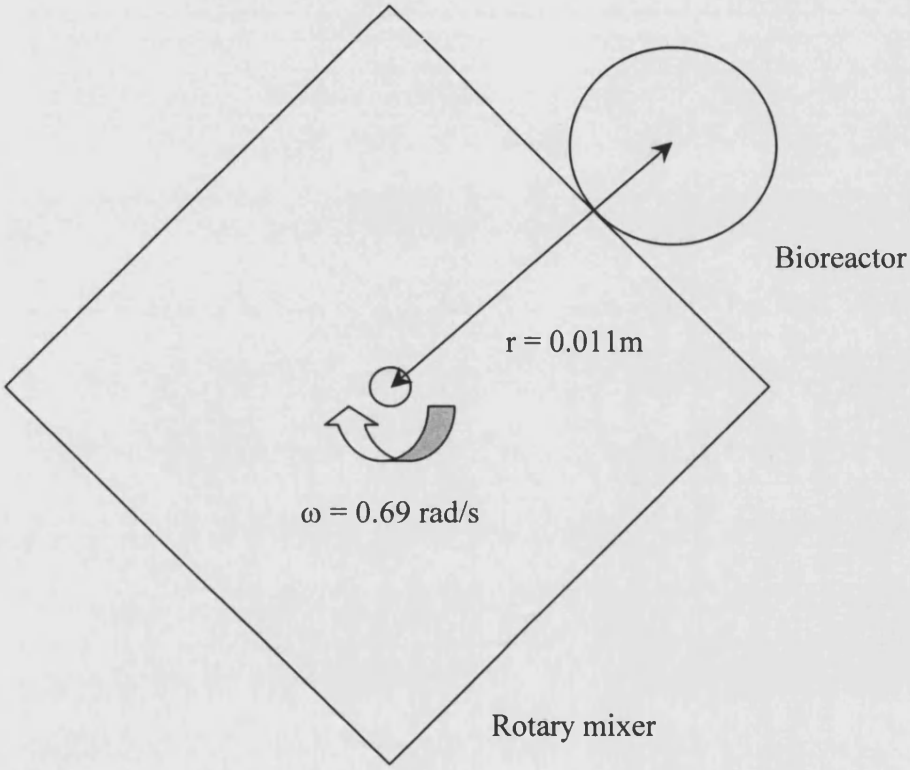

Figure 8.3. Schematic of the method used to seed the PLGA hollow fibre membrane bioreactor

$$u_i = \frac{dr}{dt} = \frac{d^2(\rho_s - \rho_f)r\omega^2}{18\mu}$$ Equation 8.1 (Coulson *et al.* 1996)

$$u_o = \frac{d^2(\rho_s - \rho_f)g}{18\mu}$$ Equation 8.2 (Coulson *et al.* 1996)

When the solid, s, is a mammalian cell and the fluid, f, is an aqueous medium; $d = 10\ \mu m$, $\rho_s = 1100\ kg/m^3$, $\rho_f = 1000\ kg/m^3$, $\mu = 10^{-3}\ Ns/m^2$, and $g = 9.81\ m/s^2$.

so,

$u_i = 2.91 \times 10^{-19}$ m/s

$u_o = 5.45 \times 10^{-10}$ m/s

Attachment of 560pZIP'sv.neo on the PLGA Hollow Fibre Membranes After Six Hours in the Hollow Fibre Bioreactor

A suspension of pZIP in media was placed into the bioreactor through one of the side ports onto 10 fibres with a total surface area of 25 cm^2. The bioreactor was placed on a rotary mixer, which was then placed in a humidified environment at 37 ºC and 5% CO_2 for 6 hours. After the six hour period, membranes were either fixed with 10%NBF to allow staining and observation of distribution of the cells and their morphology, or lysed using ATM buffer and stored at –80 ºC. On thawing, the DNA content of each membrane culture was calculated using the picogreen DNA quantification assay from which cell number was calculated. The supernatant from the bioreactor was collected and the cell number counted using a haemocytometer. The number of cells attached to the membranes was compared to the TCP control. The standard static seeding method was used for the TCP control; a dilute cell suspension in complete media was added to each well, the plate was then placed into a humidified environment at 37 ºC and 5% CO_2 for 6 hours.

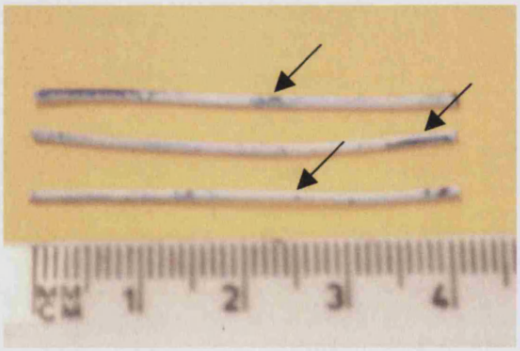

Figure 8.4. 560pZIPsv.neo attached to PLGA membranes 6h post-seeding.
Arrows show examples of areas of attached cells.

The distribution of the cells on the PLGA membranes was observed using a 0.5% methylene blue stain. Distribution was patchy with greater attachment at the ends of the samples, although cells were seen across the entire fibre length (Figure 8.4). A cell number significantly lower ($P<0.05$) than that seen on the TCP control was seen after 6 hours. The number of cells remaining in the bioreactor supernatant after 6 hours was 220,000 cells, which suggests a 65% seeding efficiency (Table 8.1).

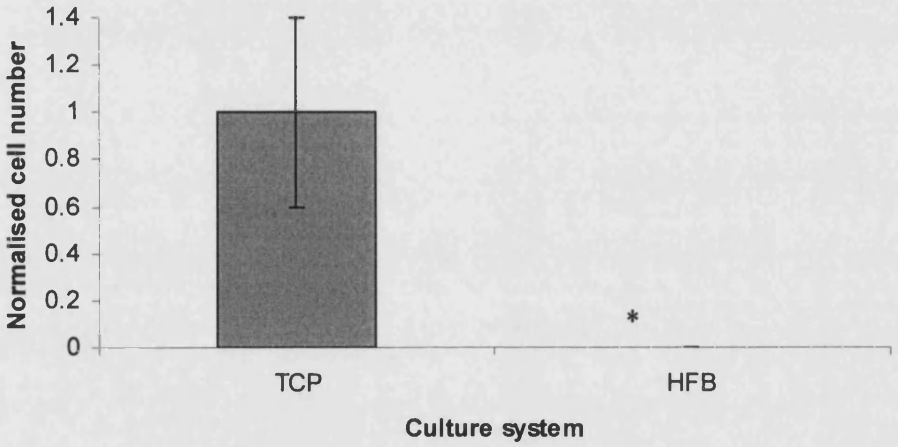

Figure 8.5. Normalised number of 560pZIPsv.neo attached to PLGA hollow fibre membranes 6h post-seeding in the hollow fibre bioreactor.
TCP is control material. Data presented as mean ±SD, n=10. Results examined by ANOVA; significant difference at $P<0.05$. *$P<0.05$ compared to TCP.

Table 8.1. Number of cells added to the bioreactor at t = 0 h and the number of cells removed from the bioreactor at t = 6 h.

Time (h)	Cell number in bioreactor
0	625,000 added
6	220,000 in supernatant

8.3.2 PROLIFERATION OF 560PZIPV.NEO ON PLGA HOLLOW FIBRE MEMBRANES IN THE HOLLOW FIBRE BIOREACTOR

Proliferation of 560pZIP'sv.neo on the PLGA Hollow Fibre Membranes After One Week in the Hollow Fibre Bioreactor

After the hollow fibres had been seeded as described in Section 8.2.1, the bioreactor was filled with fresh media before being placed into the hollow fibre bioreactor system shown in Figure 8.2. The bioreactor was kept in a humidified environment at 37 °C and 5% CO_2 for the seven-day culture period. After the seven day period, as for the 6-hour attachment analysis, membranes were either fixed with NBF to allow staining and observation of distribution of the cells and their morphology, or lysed using ATM buffer added and stored at –80 °C. On thawing, the DNA content of each membrane culture was calculated using the picogreen DNA quantification assay from which cell number was calculated.

The number of pZIP on the hollow fibre membranes was significantly less ($P<0.05$) compared to the TCP after the 7-day culture period (Figure 8.6). The fibres had 0.15 the number of cells found on the TCP control. It can be seen that, while the number of cells per cm^2 is 1.5% for the HBF compared to the TCP, the cell number per unit volume of the HFB is 12% of that seen with the TCP flask (Table 8.2).

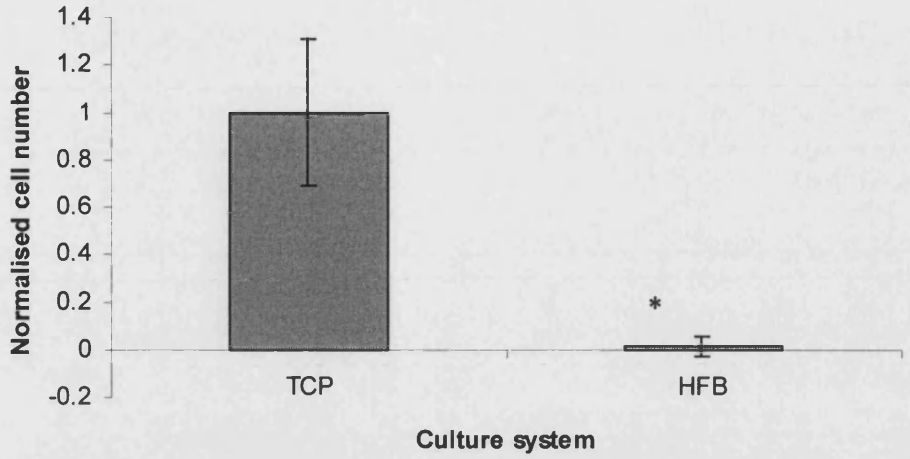

Figure 8.6. Normalised number of 560pZIPsv.neo attached to PLGA hollow fibre membranes 7 days post-seeding in the hollow fibre bioreactor.
TCP is control material. Data presented as mean ±SD, n = 10. Results examined by ANOVA; significant difference at $P<0.05$. *$P<0.05$ compared to TCP.

Table 8.2. Cell concentrations in the PLGA hollow fibre membrane bioreactor after a 7-day culture period.

Vessel	Cell/cm^2	Cell/ml
T75 Cell Culture Flask	36,530	13,700
HFB	530	1,330

8.4 DISCUSSION

A tissue engineering bioreactor can be deemed successful if it allows the culture of a cell population with no interference during the culture period so reducing the chance of infecting and culture disruption, the entire construct is supplied with media, cell attachment and proliferation can be supported in the module and there should be evidence that the increased surface area:volume ratio has been utilised. The seeding method should be efficient to utilise all the cells added to the bioreactor, which will give the greatest chance of culture expansion.

8.4.1 SEEDING

Three-dimensional scaffolds can be seeded and cultured in traditional static systems (Borden *et al.* 2003; Ma and Zhang 2001; Ishaug *et al.* 1997). Scaffolds for use in perfusion systems are still often seeded in separate systems using either static drop-wise seeding (Goldstein *et al.* 2001) and left overnight, or the scaffold suspended in a stirrer-tank bioreactors. Sun and Zhang (2003) seeded Chinese hamster ovary cells into a Fibra-cell polyester scaffold in situ. Perfusion was begun when the glucose level in the packed-bed bioreactor dropped to 6 x 10^{-3} M, after 72 hours.

The aim of the seeding method described in Section 8.2.1 was to utilise an in situ seeding method for the hollow fibre bioreactor. The number of cells attached to the fibres was significantly less than on the TCP after 6 hours showing a seeding efficiency of close to zero, however, by considering the cell number in the supernatant, the seeding efficiency was 65%. It is highly likely that the processing of the bioreactor caused cell loss, which was reflected in the subsequent analysis. A 65% seeding efficiency after 6 hours is comparable to the efficiency of static seeding method used by Ishaug *et al.* (1997), calculated after 24 hours, suggesting the mixing method was 4 times faster. Ishaug *et al.* (1997) seeded rat stromal osteoblastic cells onto porous PLGA foams (1.9 mm thick and 7 mm diameter) by adding concentrated cell suspensions (849,000 or 263,000 cells/foam, equivalent to 22.1 x 10^5 and 6.83 x 10^5 cells/cm^2) onto the top of the foams, leaving undisturbed for three hours before adding a further 1 ml of media. It was found that the seeding efficiency was 53% and 68% after 24 hours for the high- and low-density seeded scaffold, however the respective cell numbers were 11.8 x 10^5 cells/cm^2 and 4.63 x 10^5 cell/cm^2. The similar method employed by (Goldstein *et al.* 2001) found the drop-wise method gave a 72% loading efficiency after 24 hours. Saini and Wick (2003) found that the seeding efficiency of bovine chondrocytes was 95% after 24 hours in the concentric cylinder bioreactor (based on a concentric cylinder viscometer), further evidence that agitation assists seeding.

8.4.2 PROLIFERATION

The aim of Section 8.3.2 was to investigate whether PLGA hollow fibre bioreactor could support the expansion of an osteoblastic cell-line.

The hollow fibre bioreactor used in this study was not fully packed but still had a 25 cm^2 surface area in a 10 ml total volume. This is compared to the TCP, which had a 75 cm^2 surface area in a 200 ml total volume. This allowed the volumetric cell density to be around 10 times greater than the area cell density relative to the TCP. As with the seeding analysis, it is likely that cells were lost during processing. Assuming this to be the case, and there was a 1.8 cell number increase for the HBF as for the TCP, the concentration of cells in the HFB would have been 18,000 cells/cm^2 or 45,000 cell/ml, which is some way below the saturation density of cells derived from trabecular bone, of 1-3 x 10^5 cells/cm^2 (Beresford 2003). Takeshita *et al.* (1995) achieved a very high cell density in a HFB seeded with hepatocytes which were entrapped in a collagen gel. After 14 days a density of 2 x 10^7 cell/ml was obtained while maintaining the secretion of albumin and ureogenesis at the same level as the monolayer control. Although a different cell microenvironment (discussed in Section 2.4.4), the use of cell entrapment in a gel, was employed, such a high density is proof of the efficiency of a HFB and is a target to aim towards.

A perfusion system acts to stimulate the cells in culture (Goldstein *et al.* 2001; Sikavitsas *et al.* 2001), reduce concentration gradients and improve mass transfer, due to the flow of media. Goldstein *et al.* (2001) employed a packed-bed system (set up can be seen in Figure 2.22) into which PLGA foams pre-seeded with rat osteoblastic marrow stromal cells and maintained for 14 days. Media was fed at a rate of 0.03 ml/s/foam, which equated to a mean velocity of 0.3 cm/s. The system was compared to a spinner flask, rotary vessel (Figure 2.20 C) and static culture. After 7 days, the cell density was statistically higher for the spinner flask compared to the other systems which all had comparable cell numbers. After 14 days there was no significant difference between any of the culture systems. However, cell distribution was uniformly distributed throughout the foams cultured in the flow system and rotary bioreactor. An enhanced ALP activity was also seen in the flow system suggesting that the fluid flow enhanced osteoblastic function (Goldstein *et al.* 2001). It was concluded from the study that while the cell density over the 14 day time period was similar, a more uniform distribution was obtained in the flow system and rotary vessel and the convective currents have stimulatory effects on the function of the cells.

To obtain the large cell number increases and the increased osteogenic function seen in these studies, further work is required with the PLGA hollow fibre membrane bioreactor (Section 9.3). On optimisation of the system, the PLGA hollow fibre bioreactor is predicted show results that are an improvement of those carried out in the packed beds due to the reduction of high shear required at higher cell densities (Millward *et al.* 1996) and the larger surface area that is available per unit volume.

Sun and Zhang (2003) used a packed-bed bioreactor system. The study was to investigate the use potential use of lactate production rate to estimate cell density in a bioreactor. The scaffold was a Fibra-cell disc made of non-woven polyester. The system was perfused to maintain a glucose concentration of 5×10^{-3} M and stopped after 246 hours (10 ¼ days). The seeding density was 2×10^{8} cells/l and the final seeding density was 1.3×10^{10} cell/l. The use of this lactate quantification method to calculate cell number could be used with the PLGA HFB. This method would avoid destruction of the module so preventing the cell loss that was most probably encountered in this study. Future module design incorporating a more robust sealing system between the module and tubing would improve the sterility of the system as well as making the handling easier which would further reduce the disruption seen during processing.

8.5 CONCLUSIONS

The in situ, rotational seeding of the PLGA HFB was successful and more efficient than simple settling methods. While the cell numbers achieved after a 7-day culture were low in comparison with the TCP static control, optimisation of the bioreactor is likely to lead to the benefits of a HFB being utilised for the development of a bone tissue engineering construct with a high cell density being achieved due to the reduction of mass transfer limitations found in traditional perfusion bioreactors.

CHAPTER NINE
CONCLUSIONS AND FUTURE WORK

9.1 INTRODUCTION

The results in this thesis have shown that PLGA can be used to spin porous hollow fibre membranes suitable for use as a scaffold for bone tissue engineering. The main findings of the work are summarised in Section 9.2, by research chapter. Section 9.3 considers the findings as a whole and their implications for the field of bone tissue engineering. The final section, Section 9.4 outlines the future work that could lead to a fully developed clinically useful product.

9.2 CONCLUSIONS

Design of PLGA Membrane Scaffold: Flat Sheets (Chapter 4)

NMP was selected as the solvent for use in the phase inversion spin c asting processes to fabricate the membrane scaffolds. This was based primarily on the macrostructure of the resulting membrane, and also on the wide range of polymer concentrations with viscosities suitable for spinning, and the relatively low toxicity and volatility compared to dioxane.

- While the PLGA polymers containing the *d-* and *l-* isomers of PLA dissolved in both NMP and dioxane for the 10-30% (w/w) polymer concentrations, 75L:25 dissolved at 10% but appeared to gel at 20% and 30% and 100L:0 did not dissolve at any of the conditions in either solvent. PGA did not dissolve in either solvent.

- The viscosities of the PLGA polymers dissolved in NMP and dioxane showed that both solvents were suitable for spinning. The viscosity of the PLGA-dioxane solutions was relatively higher than the equivalent PLGA-NMP solution due to the solvent-polymer interactions. The viscosity of

75L:25 was relatively higher than 75:25 due to the higher crystallinity of the 75L:25 compared to 75:25. Suitable polymer concentrations in NMP ranged from 19%-30% at 25°C.

- PLGA-NMP membranes had an interconnected asymmetric finger-like pore structure with top surface pores ranging from 0.2-1.0 μm for the four PLA:PGA ratios tested. PLGA-dioxane membranes had a sponge like cross-section, the pores were not interconnected but had a dense film surrounding each one. The top surface pore size range was 0.2-2 μm. Both the PLGA-NMP and PLGA-dioxane membranes would retain cells on the top surface since the pores were smaller than 5 μm, however, only the interconnected porous macrostructure of the PLGA-NMP membrane would allow the transfer of nutrients and waste products which have a molecular mass of around 150 kDa.

Design of PLGA membrane scaffolds: Hollow Fibres (Chapter 5)

Low polymer concentration, zero air gap and a low take-up rate produced the most suitable hollow fibre membrane for use as a scaffold using the PLGA-NMP-Water ternary system. At such conditions, the hollow fibre membranes made using both 50:50 and 75:25 were observed to have more pores on the surface and a higher free volume, both factors would allow a greater mass transfer of nutrients and waste products.

- The hollow fibre membrane spun using a polymer concentration of 20% (w/w) had a more suitable structure compared to 25% for both 50:50 and 75:25. The lower concentration led to a higher free volume and also reduced the non-finger-like pores in the centre of the fibre cross-section. The top surfaces were more porous at the lower concentration, with grooves that were more aligned.

- The reduction of the air gap from 30 mm to 0 mm resulted in hollow fibre membranes with preferable morphologies. The pores were more finger-like and the outer skin was less dense; the top surface porosity was also increased in the case of 50:50. The 50:50 solution, which was on the lower limit of the ideal

spinning viscosity range, showed a complete cross section without an air gap, whereas the air gap lead to a collapsed central section.

- The reduction of the take-up rate from 7.7 m/min to 5.5 m/min, equivalent to the spinning rate (see Appendix C.1.1), resulted in the 75:25 surface changing from a dense outer skin to a porous skin, the outer skin pore size being larger for both 50:50 and 75:25 at the lower take-up rate.

Membrane Surface Treatment and Modification for Cell Culture (Chapter 6)

The PLGA membranes can be free from NMP in one week, successfully sterilised using 70% ethanol and were seen to be unaffected by the fixing agent 10%NBF and the lysing agent ATM, however, the use of 90% ethanol for fixing was found to be detrimental to the membrane morphology. Degradation occurred on submerging the membranes in media. It was possible to modify the surface of the hollow fibre membranes with hydroxyapatite.

- Soaking the flat sheet membrane in the nonsolvent, water, reduced the residual solvent to a level of 4 ppm after 7 days.

- Placing the flat sheet membranes into culture media led to the linear release of PLA and PGA into solution suggesting bulk degradation. The roughness of the membrane surface was seen to increase during the 26-day time period.

- While 70% ethanol was an effective sterilising agent, it was seen to affect the morphology of the flat sheet and hollow fibre membranes; the overall membrane dimension decreased, the roughness of the surfaces was also reduced while the pore size increased.

- 10%NBF and ATM had no significant effect on the flat sheet membranes and were selected as the fixing and lysing agents for the analysis of cell cultures on the membranes.

- Kokubo's method (Kokubo *et al.* 1998) of surface modification with hydroxyapatite using SBF was partially successful; while crystals were seen to

form on the part of the hollow fibre membrane that had been in contact with the nucleating agent, none were seen in other areas.

Cell Culture on PLGA Flat Sheet Membrane Scaffolds (Chapter 7)

From the results obtained in this study and by comparison with previous research, it is suggested to be the polymer composition that affects cell culture as opposed to the scaffold fabrication method or the crystallinity per se.

- There was no significant difference between the PLGA membranes and TCP for the attachment of pZIP, however 100:0 was comparatively poorer for the attachment of HBDC. 75L:25 showed the greatest number of both cell types attached although not by a significant amount.

- There was no significant difference between the PLGA membranes and TCP for the proliferation of pZIP. 50:50 and 75:25 had significantly lower cell numbers after the 7-day period compared to 75L:25 and TCP. As for attachment, 75L:25 supported the greatest number of both cell types at the end of the culture period.

- Osteoblastic function of the HBDC was present but significantly lower compared to the TCP control. Cells showing high ALP activity surrounded the mineralised areas on the membranes. These areas of the membranes had been drawn into a long groove.

Cell Culture in a PLGA Hollow Fibre Membrane Bioreactor (Chapter 8)

The rotational seeding of the hollow fibre membrane bioreactor (HFB) was four times more efficient than traditional settling methods. The proliferation of the pZIP in the HFB was significantly lower compared to TCP although it is likely the processing of the HFB caused cells to be sheared off the hollow fibre surface. Despite this, the benefit of the HFB with respect to a higher surface area:volume ratio was demonstrated.

- The rotational seeding method used for the HFB allowed in situ seeding of the hollow fibre scaffolds as well as a 65% seeding efficiency after 6 hours; this is comparable to settling methods carried out over 24 hours.

- The final cell density after the 7-day culture period was significantly less for the HFB compared to the TCP control. The number of cells per cm^2 in the HFB was 1.5% of the number for TCP. However, on a volume basis, the number of cells per ml in the HFB was 12% of the number for TCP showing the advantage of the high surface area:volume ratio of the HBF configuration.

9.3 IMPLICATIONS OF THE FINDINGS ON BONE TISSUE ENGINEERING

The ultimate aim of bone tissue engineering is to aid the regeneration of tissue that would otherwise not heal. Tissues that are essentially 2D such as skin and cornea have been successfully regenerated in humans, as has cartilage, which despite being 3D is notably small compared to other 3D tissues and is non-vascularised. The highly vascularised 3D structure of bone has proved to be a major challenge since traditional tissue engineering scaffolds were designed with a large surface area but without mass transfer in mind. The use of membranes as a scaffold structure presents a novel approach to 3D tissue engineering and hollow fibre membranes are particularly suited to bone tissue, the benefits being summarised below:

- The lumen of the fibre acts as the Haversian canal supplying the cells surrounding it with nutrients and removing waste products.
- The cells are retained on the outer surface while nutrients and waste products can move freely across the membrane.
- The membrane barrier between the cells and the nutrient stream allows high flow rates of media through the lumen without damaging the cells with fluid shear.
- Once in an HFB, different media can be supplied through the lumen and through the side-ports to the shell-side, at different flow rates so allowing control of fluid shear.
- By controlling the distance between fibres, a 3D cell population can grow on and between the fibres without necrosis due to lack of nutrients.

The use of autografts is the current preferred method for bone grafts. However, taking an autograft can result in problems including donor site morbidity and deformity, and there is a limited supply per patient (Kokubo *et al.* 2003). The autograft donor site can take longer to heal than the injury site (Eddy 2004) and the grafted injury site may suffer from an inadequate blood supply, particularly for larger defects (Burg *et al.* 2000: Peter *et al.* 1998).

The PLGA hollow fibre membrane scaffold presented in this thesis has the potential to eliminate the problems associated with the donor site, and significantly reduce the mass transfer limitations to allow the regeneration of bone defects which would otherwise not heal satisfactorily. Chapters 4 and 5 showed the development of the novel PLGA hollow fibre membrane scaffold, and its partial optimisation. While several solvents would be suitable for phase inversion spin casting, NMP was found to be the best all-round solvent and the PLGA-NMP-Water system formed the necessary interconnected finger-like pore structure conducive to mass transfer of molecules in the size range of the nutrients and waste products. The range of viscosities were suitable for spinning and by assessing the effect of altering spinning conditions the results in Chapter 5 go some way to optimise the hollow fibre membrane manufacturing process.

Once the PLGA hollow fibre membrane structure had been successfully obtained, it was necessary to assess the effects of the culture environment and processing methods that it would encounter during in vitro use. The results in Chapter 6 show that the hollow fibre membranes are robust with the selected analysis reagents, although morphological changes were seen with the otherwise successful sterilising method of 70% ethanol soaking. The degradation results are not surprising since PLGA is known to undergo hydrolysis in aqueous media. The ability of surface modification with hydroxyapatite, while in need of refinement, shows the potential for improving the properties of the membrane scaffolds.

It is inherent that a scaffold must support a population of cells, ideally to a level equal to or better than traditional substrates. The results in Chapter 7 show that the hollow fibre membrane scaffolds can support attachment, proliferation and osteoblastic function at levels similar to TCP. Since these results were comparable to

other studies using PLGA scaffolds, the data shows that the PLGA phase inversion cast membranes are a suitable scaffold structure.

The results in Chapter 7 were obtained on flat sheets in a static environment, which are representative of the hollow fibres. However, the culture of bone cells in a HFB would produce a 3D construct in a compact, low labour-intensive set up. Chapter 8 introduces the culture of osteoblast-like cells on PLGA hollow fibre membrane scaffolds in a HFB. Firstly the seeding method combined in situ seeding with mixing, thus eliminating the need to transfer the scaffold into the bioreactor. This decreases the chance of damage and infection. The efficiency of the rotation also decreases the time needed for seeding. Despite the low number of cells found on the fibres after the 7-day proliferation study, the results demonstrated the potential for the PLGA hollow fibre membrane bioreactor to support more long term bone cell cultures.

9.4 FUTURE WORK

For the further development of the PLGA hollow fibre membranes and their use in a HFB several steps need to be taken. Section 9.4.1 details initial work to be carried out to further characterise and optimise the PLGA hollow fibre membrane bioreactor and Section 9.4.2 details work required for clinical application of the system.

9.4.1 SHORT TERM

Hollow Fibre Membrane Manufacture

The spinning conditions can be altered to reduce the outer skin of the hollow fibres, however it may be useful to utilize the use of sodium hydroxide to remove the dense skin and which also improves hydrophilicity (Shakesheff 2005). This would allow a greater range of spinning conditions to be used that may otherwise have had to be eliminated. For instance, increasing the spinning rate would increase the overall fibre dimensions; the fibre dimensions will need optimising to meet the needs of a bone tissue construct and give the most efficient culture dimensions in the HFB, but the spinning conditions for the ideal fibre size may not give the ideal pore size and porosity. The mechanical integrity of the fibres is reduced at 37°C since this

temperature approaches the glass transition temperature (T_g) of PLGA. Either a PLA:PGA ratio could be selected with a higher T_g, a thicker walled fibre could be produced, or the fibres could be combined with a ceramic such as hydroxyapatite. The effects of a thicker wall and the addition of a ceramic on mass transfer and cell culture would need to be tested and the benefits weighed up.

Cell Culture and Analysis

The cell culture work in this thesis has shown that PLGA membranes can support both an osteoblastic cell line and HBDC. There is a vast array of future studies that would further quantify the success of the membranes as a scaffold. Immunochemistry techniques used to detect bone markers such as collagen type I and cbfa-1, and osteocalcin, and total collagen using Sirius red histochemistry would show the presence or otherwise of functional bone tissue on the membranes in vitro and in vivo (Yang *et al.* 2003).

Hollow Fibre Membrane Bioreactor

A unique feature of a hollow fibre membrane bioreactor is the variety of operating set ups that can be used. Investigation of these conditions will lead to optimised media recipes, flow rates and mass transfer, and fluid dynamics and shear stresses. It is possible to have two separate feed streams; one through the lumen and one through a side port. The flow can be counter-current or co-current and the two media streams can contain different growth factors. Since the two streams can be supplied at different flow rates it should be possible to use the shell-side stream to stimulate the cells using fluid shear. It has been reported that the typical critical shear stress is 0.6 Pa (Curran 2005), and this value can be used as a basis for optimising the shear stresses in the extracapillary space of the HFB.

Additional optimisation of the HFB will involve calculation of the optimal number of fibres and the development of methods to construct the HFB with consistent and reproducible fibre spacing. In situ analysis methods would also be beneficial for the in vitro studies to prevent damage to the cultures.

9.4.2 LONG TERM

The ultimate test for the hollow fibre membrane scaffold is its function in vivo. For this to be fully successful, further work in vitro is required as well as consideration for the transfer from bioreactor to patient.

As the construct develops in vitro, in line analysis would allow the progress of the culture to be remotely assessed so preventing the risk of infection and disruption by handling, along with minimising the labour required. The data collected could initially be used to develop mathematical models for the expansion and function of the construct and its effect on the mass transfer of nutrients and waste products. Similarly, the effect of the fluid dynamics on the culture could be modelled. These models could be coupled with the data collected and used to assess the maturity of the construct to determine when it is ready for implantation.

There are various stages at which the construct could be implanted, from non-seeded to just seeded and undifferentiated osteoblasts, differentiated functional osteoblasts with a simple collagenised matrix or a mineralised matrix, or the use of stem cells at similar stages of maturity. The length of time the construct remains in vitro will affect the degree of degradation of the PLGA membrane. By combining data from in vitro and in vivo studies, the optimal culture time in vitro prior to implantation can be determined. In addition to this, a method for the removal of the construct from the bioreactor must be developed to prevent damage such as that reported in Chapter 8.

While in vitro culture and degradation studies provide useful base-data for the construct, the in vivo environment will affect the construct differently. The degradation rate and tissue development rate need to be quantified in conjunction with each other to decide the useful life of the construct before the healing process can support itself. This may have an effect on the choice of the ratio of PLA:PGA since this effects degradation rate, the length of time the construct is mainlined in vitro and the maturity it reaches will also contribute to this aspect of the bone tissue regeneration. The effectiveness of the construct as a synthetic bone graft should be at least equal to, but ideally better than, current methods of filling bone defects. The results should be compared to the those obtained from previous studies using

autografts and synthetic constructs such as that using PLGA on gelatin sponges (Kokubo *et al.* 2003).

To take the results presented in the thesis towards becoming a useful clinical product will involve an iterative process of analysis in vitro, in vivo and by considering the transplantation between the two. This process of future work is summarised in Figure 9.1.

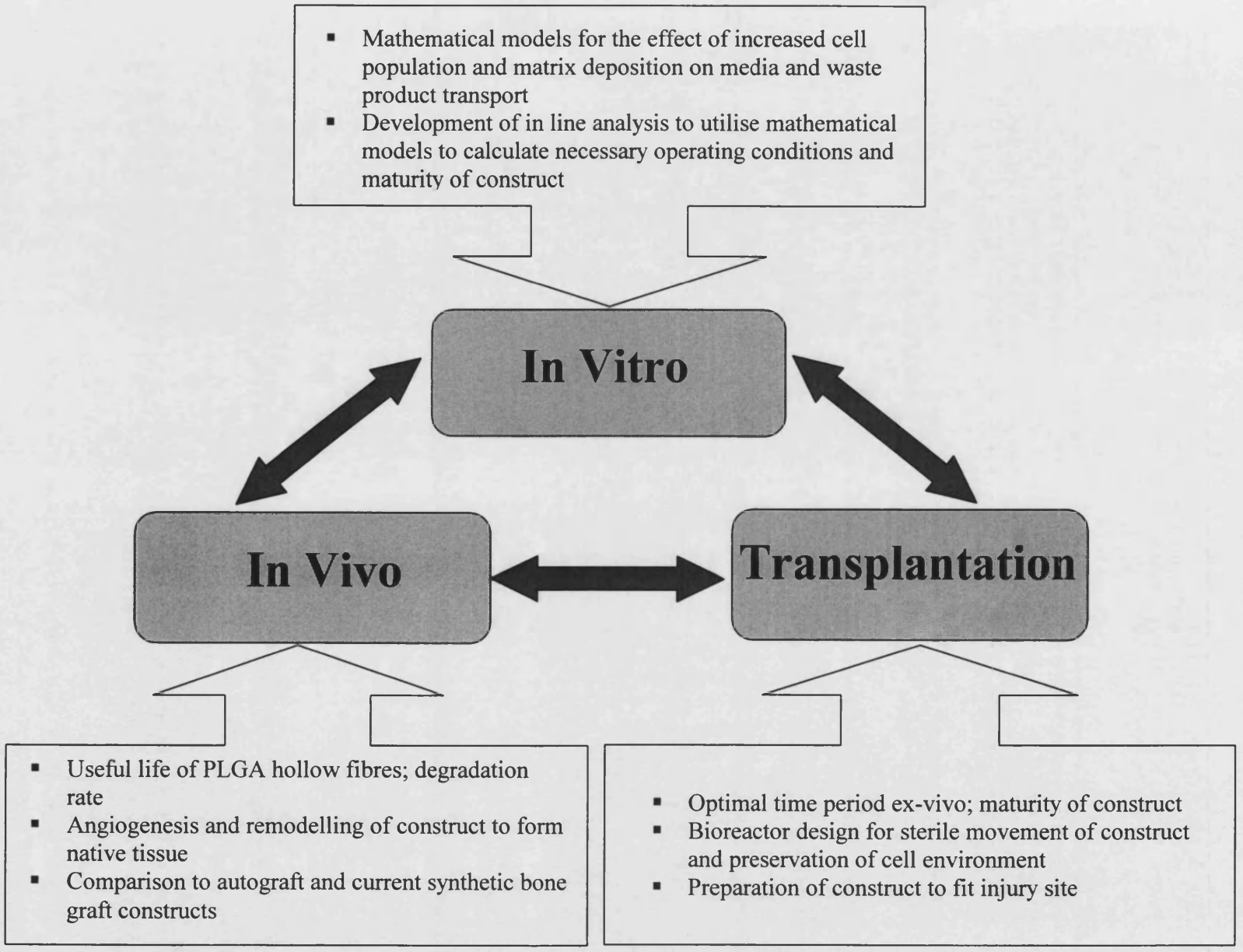

Figure 9.1. Future Work model for the clinical application of the PLGA hollow fibre membrane bioreactor system.

REFERENCES

Abbott, A. (2003). "Cell culture: Biology's new dimension." Nature 424(6951): 870-872.

Affatato, S., B. Bordini, C. Fagnano, P. Taddei, A. Tinti and A. Toni (2002). "Effects of the sterilisation method on the wear of UHMWPE acetabular cups tested in a hip joint simulator." Biomaterials 23(6): 1439-1446.

Ajubi, N. E., P. J. Klein-Nulend, P. J. Nijweide, T. Vrijheid-Lammers, M. J. Alblas and E. H. Burger (1996). "Pulsating fluid flow increases prostaglandin production by cultured chicken osteocytes - a cytoskeleton dependent process." Biochemical and Biophysical Research Communications 225: 62-68.

Alsberg, E., K. W. Anderson, A. Albeiruti, R. T. Franceschi and D. J. Mooney (2001). "Cell-interactive alginate hydrogels for bone tissue engineering." Journal of Dental Research 80(11): 2025-2029.

Amaechi, B. T., S. M. Higham and W. M. Edgar (1998). "Efficacy of sterilisation methods and their effect on enamel demineralisation." Caries Research 32(6): 441-446.

Ambrosio, A. M. A., J. S. Sahota, Y. Khan and C. T. Laurencin (2001). "A novel amorphous calcium phosphate polymer ceramic for bone repair: 1. Synthesis and characterization." Journal of Biomedical Materials Research 58(3): 295-301.

Arnaud, S. B., D. J. Sherrard, N. Maloney, R. T. Whalen and P. Fung (1992). "Effects of 1-week head-down tilt bed rest on bone formation and the calcium endocrine system." Aviation Space and Environmental Medicine Jan: 14-20.

Atkins, G. J., P. Kostakis, B. Q. Pan, A. Farrugia, S. Gronthos, A. Evdokiou, K. Harrison, D. M. Findlay and A. C. W. Zannettino (2003). "RANKL expression is

related to the differentiation state of human osteoblasts." Journal of Bone and Mineral Research 18(6): 1088-1098.

Aubin, J. E. (1996). The osteoblast lineage. Principles of Bone Biology. J. P. Bilezikian, L. G. Raisz and G. A. Rodan. San Diego, Academic Press: 51-68.

Aunins, J. G., B. Bader, A. Caola, J. Griffiths, M. Katz, P. Licari, K. Ram, C. S. Ranucci and W. Zhou (2003). "Fluid mechanics, cell distribution, and environment in CellCube bioreactors." Biotechnology Progress 19: 2-8.

Bader, A., E. Knop, N. Fruhauf, O. Crome, K. Boker, U. Christians, K. Oldhafer, B. Ringe, R. Pichlmayr and K. F. Sewing (1995). "Reconstruction of Liver-Tissue in-Vitro - Geometry of Characteristic Flat Bed, Hollow-Fiber, and Spouted Bed Bioreactors with Reference to the in-Vivo Liver." Artificial Organs 19(9): 941-950.

Bagambisa, F. B., H. F. Kappert and W. Schilli (1994). "Cellular and Molecular Biological Events at the Implant Interface." Journal of Cranio-Maxillofacial Surgery 22(1): 12-17.

Bancroft, G. N., V. I. Sikavitsas and A. G. Mikos (2003). "Design of a flow perfusion bioreactor system for bone tissue- engineering applications." Tissue Engineering 9(3): 549-554.

Bancroft, J. D. and M. Gamble, Eds. (2005). Theory and practice of histological teqhniques. Oxford, Churchill Livingstone.

Banes, A., G. W. Link, J. Gilbert, R. T. S. Tay and O. Monbureau (1990). "Culturing cells in a mechanically active environment." American Biotechnology Lab 8: 12-22.

Basset, C. A. L. (1966). Electro-mechanical factors regulating bone architecture. Third European Symposium on calcified tissues. H. Fleisch, H. J. J. Blackwood and M. Owen. Berlin, Springer-Verlag: 78-89.

Basso, N. and J. Heersche (2002). "Review: Characteristics of In Vitro Osteoblastic Cell Loading Models." Bone 30(2): 347-351.

Beresford, J. (2001). Origin of the cell line 560pZIPv.neo. M. Ellis. Bath.

Beresford, J. (2002). Maximum pore size to prevent cell migration into pores. M. Ellis.

Beresford, J. (2003). Trabecular cell saturation density. M. J. Ellis. Bath.

Beresford, J. N. (1984). Volume I: Studies in the Metabolism of Human Bone Cells In Vitro. Department of Human Metabolism and Clinical Biochemistry. Sheffield, Sheffield: 115.

Beresford, J. N. and M. E. Owen, Eds. (1998). Marrow stromal cell culture. Cambridge, Cambridge University Press.

Bilezikian, J. P., L. G. Raisz and G. A. Rodan, Eds. (1996). Principles of Bone Biology. San Diego, Academic Press.

Blumenstein, R., M. Dias, I. H. Russo, Q. Tahin and J. Russo (2002). "DNA content and cell number determination in microdissected samples of breast carcinoma in situ." International Journal of Oncology 21(2): 447-450.

Borden, m., S. F. El-Amin, M. Attawia and C. T. Laurencin (2003). "Structural and human cellular assessment of a novel microsphere-based tissue engineered scaffold for bone repair." Biomaterials 24: 597-609.

Borkenhagen, M., R. C. Stoll, P. Neuenschwander, U. W. Suter and P. Aebischer (1998). "In vivo performance of a new biodegradable polyester urethane system used as a nerve guidance channel." Biomaterials 19(23): 2155-2165.

Botchwey, E. A., S. R. Pollack, E. M. Levine and C. T. Laurencin (2001). "Bone tissue engineering in a rotating bioreactor using a microcarrier matrix system." Journal of Biomedical Materials Research 55(2): 242-253.

Boyan, B. D., T. W. Hummert, D. D. Dean and Z. Schwartz (1996). "Role of material surfaces in regulating bone and cartilage cell response." Biomaterials 17(2): 137-146.

Brighton, C. T. and W. P. McCluskey (1986). "Cellular response and mechanisms of action of electrically induced osteogenesis." Bone Mineral Research 4: 213-254.

Brotherton, J. D. and P. C. Chau (1996). "Review: Modeling of Axial-Flow Hollow Fiber Cell Culture Bioreactors." Biotechnology Progress 12: 575-590.

Buckwalter, A., M. J. Glimcher, R. R. Cooper and R. Recker (1996). "Bone Biology." Journal of Bone Joint Surgery 77A: 1256-1289.

Burdick, J. A. and K. S. Anseth (2002). "Photoencapsulation of osteoblasts in injectable RGD-modified PEG hydrogels for bone tissue engineering." Biomaterials 23(22): 4315-4323.

Burdick, J. A., D. Frankel, W. S. Dernell and K. S. Anseth (2003). "An initial investigation of photocurable there-dimensional lactic acid based scaffolds in a critical-sized cranial defect." Biomaterials 24: 1613-1620.

Burg, K. J. L., S. Porter and J. F. Kellam (2000). "Biomaterial developments for bone tissue engineering." Biomaterials 21(23): 2347-2359.

Burger, E. H. and J. Klein-Nulend (1999). "Mechanotransduction in bone - role of the lacuno-canalicular network." FASEB Journal 13S: S101-S112.

Cabasso, I. (1980). Hollow Fibre Membranes. Kirk-Othmer, Encyclopedia of Chemical Technology. New York, Wiley. 12: 492-517.

Cabasso, I., E. Klein and J. K. Smith (1977). "Polysulfone hollow fibres. II. Morphology." Journal of Applied Polymer Science 21: 165-180.

Cai, Q., G. Shi, J. Bei and S. Wang (2003). "Enzymatic degradation behaviour and mechanism of poly(lactide-co-glycolide) foams by trypsin." Biomaterials 24: 629-638.

Calvert, J. W., K. G. Marra, L. Cook, P. N. Kumta, P. A. DiMilla and L. E. Weiss (2000). "Characterization of osteoblast-like behavior of cultured bone marrow stromal cells on various polymer surfaces." Journal of Biomedical Materials Research 52(2): 279-284.

Caplan, A. and B. Boyan (1994). Endochondral bone formation: the lineage cascade. Bone. B. Hall. London, CRC Press. 8: 1-46.

Caplan, A. I. and S. P. Bruder (1997). Cell and Molecular Engineering of Bone regeneration. Principles of Tissue Engineering. R. Lanza, R. Langer, William and Chick. 1: 603-618.

Catiker, E., M. Gumusderelioglu and A. Guner (2000). "Degradation of PLA, PLGA homo- and copolymers in the presence of serum albumin: a spectroscopic investigation." Polymer International 49(7): 728-734.

Chu, C. C. (1982). "A Comparison of the Effect of PH on the Biodegradation of 2 Synthetic Absorbable Sutures." Annals of Surgery 195(1): 55-59.

Chung, T. S. and X. D. Hu (1997). "Effect of air-gap distance on the morphology and thermal properties of polyethersulfone hollow fibers." Journal of Applied Polymer Science 66(6): 1067-1077.

Chung, T. S. and X. D. Hu (1997). "Effect of air-gap distance on the morphology and thermal properties of polyethersulfone hollow fibers." Journal of Applied Polymer Science 66(6): 1067-1077.

Chung, T. S., J. J. Qin and J. Gu (2000). "Effect of shear rate within the spinneret on morphology, separation performance and mechanical properties of ultrafiltration polyethersulfone hollow fiber membranes." Chemical Engineering Science 55(6): 1077-1091.

Chung, T. S., S. K. Teoh, W. W. Y. Lau and M. P. Srinivasan (1998). "Effect of shear stress within the spinneret on hollow fiber membrane morphology and separation performance." Industrial & Engineering Chemistry Research 37(10): 3930-3938.

Ciapetti, G., L. Ambrosio, L. Savarino, D. Granchi, E. Cenni, N. Baldini, S. Pagani, S. Guizzardi, F. Causa and A. Giunti (2003). "Osteoblast growth and function in porous poly epsilon- caprolactone matrices for bone repair: a preliminary study." Biomaterials 24(21): 3815-3824.

Cohen, S., T. Yoshioka, M. Lucarelli, L. H. Hwang and R. Langer (1991). "Controlled Delivery Systems for Proteins Based on Poly(Lactic Glycolic Acid) Microspheres." Pharmaceutical Research 8(6): 713-720.

Collins, P. C., W. M. Miller and E. T. Papoutsakis (1998). "Stirred culture of peripheral and cord blood hematopoietic cells offers advantages over traditional static systems for clinically relevant applications." Biotechnology and Bioengineering 59(5): 534-543.

Colton, C. K. (1995). "Implantable biohybrid artificial organs." Cell Transplantation 4(4): 415-436.

Cooper, L. F., T. Masuda, P. K. Yliheikkila and D. A. Felton (1998). "Generalizations regarding the process and phenomenon of osseointegration. Part II. In vitro studies." International Journal of Oral & Maxillofacial Implants 13(2): 163-174.

Costantini, A., G. Luciani, F. Branda, L. Ambrosio, G. Mattogno and L. Pandolfi (2002). "Hydroxyapatite coating of titanium by biomimetic method." Journal of Materials Science-Materials in Medicine 13(9): 891-894.

Coulson, J. M., J. F. Richardson, J. R. Backhurst and J. Harker (1997). Coulson & Richardson's Chemical Engineering: Fluid Flow, Heat Transfer and Mass Transfer. Oxford, Butterworth-Heinemann Ltd.

Coulson, J. M., J. F. Richardson, J. R. Bankhiurst and J. H. Harker (1996). Coulson & Richardson's Chemical Engineering: Particle Technology and Separation Processes. Oxford, Butterworth-Heinemann Ltd.

Cowin, S. C., L. Moss-Salentijn and M. L. Moss (1991). "Candidates for the mechanosensory system in bone." Journal of Biomechancal Engineering 113: 191-197.

Cowin, S. C., S. Weinbaum and Y. Zeng (1995). "A case for bone canaliculi as the anatomical site of strain-generated potentials." Journal of Biomechanics 28: 1281-1296.

Curran, S. (2005). Bioreactors to engineering living tissue. Seminars in the Department of Chemical Engineering, University of Bath.

Currey, J. (1984). The mechanical properties of materials and the structure of bone. The mechanical adaptations of bones. Princeton, Princeton University Press: 3-37.

Cussler, E. L. (1984). Diffusion: Mass trasnfer in fluid systems. Cambridge, Cambridge University Press.

Dalby, M. J., L. D. Silvio, G. W. Davies and W. Bonfield (2000). "Surface topography and HA filler volume effect on primary human osteoblasts in vitro." Journal of Materials Science-Materials in Medicine 11(12): 805-810.

Dalby, M. J., M. V. Kayser, W. Bonfield and L. D. Silvio (2002). "Initial attachment of osteoblasts to an optimised HAPEX topography." Biomaterials 23: 681-690.

Damsky, C. H., A. Moursi, Y. Zhou, S. J. Fisher and R. K. Globus (1997). "The solid state environment orchestrates embryonic development and tissue remodeling." Kidney International 51: 1427-1433.

De Oliveira, J. F., P. F. De Aguiar, A. M. Rossi and G. A. Soares (2003). "Effect of process parameters on the characteristics of porous calcium phosphate ceramics for bone tissue scaffolds." Artificial Organs 27(5): 406-411.

Den Dunnen, W. F. A., M. F. Meek, P. H. Robinson and J. M. Schakernraad (1998). "Peripheral n erve r egeneration t hrough P (DLLA-epsilon-CL) nerve guides." Journal of Materials Science-Materials in Medicine 9(12): 811-814.

Dillaman, R., R. Roer and D. Gay (1991). "Fluid movement in bone: Theoretical and imperial." Journal of Biomechanics 24: 163-177.

Donaldson, C. L., S. B. Hulley, J. M. Vogel, R. S. Hattner, J. H. Bayers and D. E. McMillan (1970). "Effect of prolinged bed rest on bone mineral." Metabolism 19: 1071-1084.

Eddy, K. (2004). Effect of bone graft donor site morbidity on the rehabilitation of an elite rugby player. M. J. Ellis. Bath.

Eenink, M. J. D. and J. Feijen (1987). "Biodegradable hollow fibres for the controlled release of hormones." Journal of Controlled Release 6: 225-247.

Einhorn, T. A. (1996). Biomechanics of Bone. Principles of Bone Biology. J. P. Bilezikian, L. G. Raisz and G. A. Rodan. London, Academic Press Limited: 25-38.

El-Amin, S. F., H. H. Lu, Y. Khan, J. Burems, J. Mitchell, R. S. Tuan and C. T. Laurencin (2003). "Extracellular martix production by human osteoblasts cultured on biodegradable polmers applicable for tissue engineering." Biomaterials 24: 1213-1221.

Elias, K. L., R. L. Price and T. J. Webster (2002). "Enhanced functions of osteoblasts on nanometer diameter carbon fibres." Biomaterials 23: 3279-3287.

Ellis, M., M. Jarman-Smith and J. B. Chaudhuri (2005). Bioreactor systems for tissue engineering: a four dimensional challenge. Bioreactors for tissue engineering. J. B. Chaudhuri and M. Al-Rubeai. Amsterdam, Kluwer Academic Publishers: 1-18.

Evans, G. R. D., K. Brandt, M. S. Widmer, L. Lu, R. K. Meszlenyi, P. K. Gupta, A. G. Mikos, J. Hodges, J. Williams, A. Gurlek, A. Nabawi, R. Lohman and C. W. Patrick (1999). "In vivo evaluation of poly(L-lactic acid) porous conduits for peripheral nerve regeneration." Biomaterials 20(12): 1109-1115.

Evans, G. R. D., K. Brandt, S. Katz, P. Chauvin, L. Otto, M. Bogle, B. Wang, R. K. Meszlenyi, L. C. Lu, A. G. Mikos and C. W. Patrick (2002). "Bioactive poly(L-lactic acid) conduits seeded with Schwann cells for peripheral nerve regeneration." Biomaterials 23(3): 841-848.

Eyre, D. R. (1996). Biochemical basis of collagen metabolites as bone turnover markers. Principles of Bone Biology. J. P. Bilezikian, L. G. Raisz and G. A. Rodan. San Diego, Academic Press: 143-154.

Feichtinger, J., A. Schulz, M. Walker and U. Schumacher (2003). "Sterilisation with low-pressure microwave plasmas." Surface & Coatings Technology 174: 564-569.

Ferrier, J., S. M. Ross, J. Kanehisa and J. E. Aubin (1986). "Osteoclasts and osteoblasts migrate in opposite directions in response to a constant electrical field." Journal of Cell Physiology 129: 283-288.

Francis, K. and B. O. Palsson (1997). "Effective intercellular communication distances are determined by the relative time constants for cyto/chemokine secretion and diffusion." Proceedings of the National Academy of Sciences of the United States of America 94(23): 12258-12262.

Freed, L. E., G. Vunjaknovakovic, R. J. Biron, D. B. Eagles, D. C. Lesnoy, S. K. Barlow and R. Langer (1994). "Biodegradable Polymer Scaffolds for Tissue Engineering." Bio-Technology 12(7): 689-693.

Fukuda, J., H. Mizumoto, K. Nakazawa, T. Kajiwara and K. Funatsu (2004). "Hepatocyte organoid culture in elliptic hollow fibers to develop a hybrid artificial liver." International Journal of Artificial Organs 27(12): 1091-1099.

Gibson, L. J. (2003). "Cellular solids." Mrs Bulletin 28(4): 270-271.

Goldstein, A. S., T. M. Juarez, C. D. Helmke, M. C. Gustin and A. G. Mikos (2001). "Effect of convection on osteoblastic cell growth and function in biodegradable polymer foam scaffolds." Biomaterials 22: 1279-1288.

Goldstein, A. S., T. M. Juarez, C. D. Helmke, M. C. Gustin and A. G. Mikos (2001). "Effect of convection on osteoblastic cell growth and function in biodegradable polymer foam scaffolds." Biomaterials 22: 1279-1288.

Gomes, M. E., J. S. Godinho, D. Tchalamov, A. M. Cunha and R. L. Reis (2002). "Alternative tissue engineering scaffolds based on starch: processing methodologies, morphology, degradation and mechanical properties." Materials Science & Engineering C-Biomimetic and Supramolecular Systems 20(1-2): 19-26.

Gomes, M. E., R. L. Reis, A. M. Cunha, C. A. Blitterswijk and J. D. de Bruijn (2001). "Cytocompatibility and response of osteoblastic-like cells to starch-based polymers: effect of several additives and processing conditions." Biomaterials 22(13): 1911-1917.

Gomez, C., M. D. Blanco, M. V. Bernardo, R. Olmo, E. Muniz and J. M. Teijon (2004). "Cytarabine release from comatrices of albumin microspheres in a poly(lactide-co-glycolide) film: in vitro and in vivo studies." European Journal of Pharmaceutics and Biopharmaceutics 57(2): 225-233.

Gosiewska, A., A. Reziania, S. Dhanaraj, M. Vyakarnam, J. Zhou, D. Burtis, L. Brown, W. Kong, M. Zimmerman and J. C. Geesin (2001). "Development of a Three-Dimensional Transmigration Assay for Testing Cell-Polymer Interactions for Tissue Engineering Applications." Tissue Engineering 7(3): 267-277.

Granet, C., N. Laroche, L. Vico, C. Alexandre and M. H. Lafage-Proust (1998). "Rotating-wall vessels, promising bioreactors for osteoblastic cell culture: comparison with other 3D conditions." Medical & Biological Engineering & Computing 36(4): 513-519.

Gray, C., A. Boyde and S. Jones (1996). "Topographically Induced Bone Formation In Vitro: Implications for Bone Implants and Bone Grafts." Bone 18(2): 115-123.

Green, D., D. Walsh, S. Mann and R. O. C. Oreffo (2002). "The Potential of Biomemesis in Bone Tissue Engineering: Lessons From The Design and Synthesis of Invertebrate Skeletons." Bone 30(6): 810-815.

Gugala, Z. and S. Gogolewski (1999). "Regeneration of segmental diaphyseal defects in sheep tibiae using resorbable polymeric membranes: A preliminary study." Journal of Orthopaedic Trauma 13(3): 187-195.

Gumbiner, B. M. (1996). "Cell adhesion: The molecular basis of tissue architecture and morphogenesis." Cell 84(3): 345-357.

Hacker, M., J. Tessmar, M. Neubauer, A. Blaimer, T. Blunk, A. Gopferich and M. B. Schulz (2003). "Towards biomimetic scaffolds: Anhydrous scaffold fabrication from biodegradable amine-reactive diblock copolymers." Biomaterials 24(24): 4459-4473.

Hadlock, T., C. Sundback, D. Hunter, M. Cheney and J. P. Vacanti (2000). "A polymer foam conduit seeded with Schwann cells promotes guided peripheral nerve regeneration." Tissue Engineering 6(2): 119-127.

Hartgerink, J. D., E. Beniash and S. I. Stupp (2001). "Self-assembly and mineralization of peptide-amphiphile nanofibers." Science 294(5547): 1684-1688.

Hasirci, V., K. Lewandrowski, J. D. Gresser, D. L. Wise and D. J. Trantolo (2001). "Versatility of biodegradable biopolymers: degradability and an in vivo application." Journal of Biotechnology 86(2): 135-150.

Herberger, J., K. Murphy, L. Munyakazi, J. Cordia and E. Westhaus (2003). "Carbon dioxide extraction of residual solvents in poly(lactide- co-glycolide) microparticles." Journal of Controlled Release 90(2): 181-195.

Hillsey, M. and J. Frangos (1994). "Review: Bone Tissue Engineering: The Role of Interstitial Fluid Flow." Biotechnology and Bioengineering 43: 573-581.

Hofmann, A., C. Hofmann and L. Gotzen (2000). "The influence of different desinfection and sterilisation procedures on osteoblastic function. A comparative in-vitro study." Unfallchirurg 103(5): 380-388.

Hollinger, J. O., S. Winn and J. Bonadio (2000). "Options for tissue engineering to address challenges of the aging skeleton." Tissue Engineering 6(4): 341-350.

Holy, C. E. and R. Yakubovich (2000). "Processing cell-seeded polyester scaffolds for histology." Journal of Biomedical Materials Research 50(2): 276-279.

Holy, C. E., C. Cheng, J. E. Davies and M. S. Shoichet (2001). "Optimizing the sterilization of PLGA scaffolds for use in tissue engineering." Biomaterials 22(1): 25-31.

Holy, C. E., M. S. Shoichet and J. E. Davies (2000). "Engineering three-dimensional bone tissue in vitro using biodegradable scaffolds: Investigating initial cell-seeding density and culture period." Journal of Biomedical Materials Research 51(3): 376-382.

Hong, J. Y., Y. J. Kim, H. W. Lee, W. K. Lee, J. S. Ko and H. M. Kim (2003). "Osteoblastic cell response to thin film of poorly crystalline calcium phosphate apatite formed at low temperatures." Biomaterials 24(18): 2977-2984.

Hu, Y. H., D. W. Grainger, S. R. Winn and J. O. Hollinger (2002). "Fabrication of poly(alpha-hydroxy acid) foam scaffolds using multiple solvent systems." Journal of Biomedical Materials Research 59(3): 563-572.

Hulbert, S. F., F. A. Young, R. S. Mathews, J. J. Klawitter, C. D. Talbert and F. H. Stelling (1970). "The potential of ceramic materials as permanently implantable skeletal prostheses." Journal of Biomedical Materials Research 4: 433-456.

Ishaug, S. L., G. M. Crane, M. J. Miller, A. W. Yasko, M. J. Yaszemski and A. G. Mikos (1997). "Bone formation by three-dimensional stromal osteoblast culture in biodegradable polymer scaffolds." Journal of Biomedical Materials Research 36(1): 17-28.

Ishaug, S. L., M. J. Yaszemski, R. Bizios and A. G. Mikos (1994). "Osteoblast Function on Synthetic Biodegradable Polymers." Journal of Biomedical Materials Research 28(12): 1445-1453.

Ishaug, S. L., R. G. Payne, M. J. Yaszemski, T. B. Aufdemorte, R. Bizios and A. G. Mikos (1996). "Osteoblast migration on poly(alpha-hydroxy esters)." Biotechnology and Bioengineering 50(4): 443-451.

IshaugRiley, S. L., G. M. Crane, A. Gurlek, M. J. Miller, A. W. Yasko, M. J. Yaszemski and A. G. Mikos (1997). "Ectopic bone formation by marrow stromal osteoblast transplantation using poly(DL-lactic-co-glycolic acid) foams implanted into the rat mesentery." Journal of Biomedical Materials Research 36(1): 1-8.

Ishaug-Riley, S. L., G. M. Crane-Kruger, M. J. Yaszemski and A. G. Mikos (1998). "Three-dimensional culture of rat calvarial osteoblasts in porous biodegradable polymers." Biomaterials 19(15): 1405-1412.

Ismail, A. F., B. C. Ng and W. Rahman (2003). "Effects of shear rate and forced convection residence time on asymmetric polysulfone membranes structure and gas separation performance." Separation and Purification Technology 33(3): 255-272.

Jeong, B., Y. H. Bae and S. W. Kim (2000). "In situ gelation of PEG-PLGA-PEG triblock copolymer aqueous solutions and degradation thereof." Journal of Biomedical Materials Research 50(2): 171-177.

Jeong, J. H., Y. Byun and T. G. Park (2003). "Synthesis and characterization of poly(L-lysine)-g-poly(D,L- lactic-co-glycolic acid) biodegradable micelles." Journal of Biomaterials Science-Polymer Edition 14(1): 1-11.

Jin, Q.-M., H. Takita, T. Kohgo, K. Atsumi, H. Itoh and Y. Kuboki (2000). "Effects of geometry of hydroxyapatite as a cell substratum in BMP-induced ectopic bone formation." Journal of Biomedical Materials 52: 491-499.

Karp, J. M., M. S. Shoichet and J. E. Davies (2002). "bone formation on two-dimensional poly(L-lactide-co-glycolide) (PLGA) films and three-dimensional PLGA tissue engineering scaffolds in vitro." Journal of Biomedical Materials Research 64A: 388-396.

Kempen, D. H. R., L. C. Lu, X. Zhu, C. Kim, E. Jabbari, W. J. A. Dhert, B. L. Currier and M. J. Yaszemski (2004). "Development of biodegradable poly(propylene fumarate)/poly(lactic-co-glycolic acid) blend microspheres. I. Preparation and characterization." Journal of Biomedical Materials Research Part A 70A(2): 283-292.

Khayet, M. (2003). "The effects of air gap length on the internal and external morphology of hollow fiber membranes." Chemical Engineering Science 58(14): 3091-3104.

Kim, H. W., J. C. Knowles and H. E. Kim (2004). "Development of hydroxyapatite bone scaffold for controlled drug release via poly(epsilon-caprolactone) and hydroxyapatite hybrid coatings." Journal of Biomedical Materials Research Part B-Applied Biomaterials 70B(2): 240-249.

Kim, H. W., S. S. Kim and J. M. Kim (1998). "Behavior of hydrolysis of plasma-treated poly(L-lactic acid)." Polymer-Korea 22(3): 455-460.

Kim, H., H. W. Kim and H. Suh (2003). "Sustained release of ascorbate-2-phosphate and dexamethasone from porous PLGA scaffolds for bone tissue engineering using mesenchymal stem cells." Biomaterials 24(25): 4671-4679.

Kim, I. B., M. C. Lee, I. S. Seo and P. K. Shin (1995). "The effects of properties on the biodegradation of biodegradable polymers." Polymer-Korea 19(6): 727-733.

Kim, S. S., C. A. Sundback, S. Kaihara, M. S. Benvenuto, B. S. Kim, D. J. Mooney and J. P. Vacanti (2000). "Dynamic seeding and in vitro culture of hepatocytes in a flow perfusion system." Tissue Engineering 6(1): 39-44.

Kimura, T., N. Ihara, Y. Ishida, Y. Saito and N. Shimizu (2002). "Hydrolysis characteristics of biodegradable plastic (Poly Lactic Acid)." Journal of the Japanese Society for Food Science and Technology-Nippon Shokuhin Kagaku Kogaku Kaishi 49(9): 598-604.

Kivalo, M., V. Siren, C. Raitta and I. Immonen (1999). "Biodegradable tube implants in experimental glaucoma surgery in the rabbit." Journal of Materials Science-Materials in Medicine 10(1): 53-58.

Klawitter, J. J. and S. F. Hulbert (1971). "Application of porous ceramics for the attachment of load-bearing internal orthopedic applications." Journal of Biomedical Materials Research Symp 2: 161.

Klee, D., Z. Ademovic, A. Bosserhoff, H. Hoecker, G. Maziolis and H. J. Erli (2003). "Surface modification of poly(vinylidenefluoride) to improve the osteoblast adhesion." Biomaterials 24(21): 3663-3670.

Klein-Nulend, J., A. V. d. Plas, C. M. Semeins, N. E. Ajubi, J. A. Frangos, P. J. Nijweide and E. H. Burger (1995). "Sensitivity of osteocytes to biomechanical stress in vitro." FASEB Journal 9: 441-445.

Knothe-Tate, M. L., U. Knothe and P. Niederer (1998). "Experimental elucidation of mechanical load-induced fluid flow and its potential role in bone metabolism and functional adaptation." American Journal of Medical Science 316: 189-195.

Koegler, W. S. and L. G. Griffith (2004). "Osteoblast response to PLGA tissue engineering scaffolds with PEO modified surface chemistries and demonstration of patterned cell response." Biomaterials 25(14): 2819-2830.

Koegler, W. S., C. Patrick, M. J. Cima and L. G. Griffith (2002). "Carbon dioxide extraction of residual chloroform from biodegradable polymers." Journal of Biomedical Materials Research 63(5): 567-576.

Kokubo, S., R. Fujimoto, S. Yokota, S. Fukushima, K. Nozaki, K. Takahashi and K. Miyata (2003a). "Bone regenreation by recombinant human bone morphogenic protein-2 and a novel biodegradable carrier in a rabbit ulnar defect model." Biomaterials 24: 1643-1651.

Kokubo, T., H. M. Kim and M. Kawashita (2003b). "Novel bioactive materials with different mechanical properties." Biomaterials 24(13): 2161-2175.

Kokubo, T. (1998). "Apatite formation on surfaces of ceramics, metals and polymers in body environment." Acta Materialia 46(7): 2519-2527.

Koller, M. and B. Palsson (1993). "Tissue Engineering: Reconstitution of Human Hematopoiesis Ex Vivo." Biotechnology and Bioengineering 42(8): 909-930.

Kuznetsov, S. A., P. H. Krebsbach, K. Satomura, J. Kerr, M. Riminucci, D. Benayahu and P. G. Robey (1997). "Single-Colony Derived Strains of Human Marrow Stromal Fibroblasts Form Bone After Transplantation In Vivo." Journal Of Bone And Mineral Research 12(9): 1335-1347.

Langer, R. and J. P. Vacanti (1993). "Tissue Engineering." Science 260(5110): 920-926.

Lappa, M. (2003). "Organic tissues in rotating bioreactors: Fluid-mechanical aspects, dynamic growth models, and morphological evolution." Biotechnology and Bioengineering 84(5): 518-532.

Lauffenburger, D. A. and L. G. Griffth (2001). "Who's got pull around here? Cell organisation in development and tissue engineering." PNAS 98(8): 4282-4284.

Lavos-Valereto, I. D., M. C. Z. Deboni, N. Azambuja and M. M. Marques (2002). "Evaluation of the titanium Ti-6Al-7Nb alloy with and without plasma-sprayed hydroxyapatite coating on growth and viability of cultured osteoblast-like cells." Journal of Periodontology 73(8): 900-905.

Lee, K. Y., E. Alsberg and D. J. Mooney (2001). "Degradable and injectable poly(aldehyde guluronate) hydrogels for bone tissue engineering." Journal of Biomedical Materials Research 56(2): 228-233.

Lee, Y.-J., S.-J. Park, W.-K. Lee, J. S. Ko and H.-M. Kim (2003). "MG63 osteoblastic cell adhesion to the hydrophobic surface precoated with recombinant osteopontin fragments." Biomaterials 24: 1059-1066.

Li, D. F., T. S. Chung, J. Z. Ren and R. Wang (2004). "Thickness dependence of macrovoid evolution in wet phase- inversion asymmetric membranes." Industrial & Engineering Chemistry Research 43(6): 1553-1556.

Li, W. J., C. T. Laurencin, E. J. Caterson, R. S. Tuan and F. K. Ko (2002). "Electrospun nanofibrous structure: A novel scaffold for tissue engineering." Journal of Biomedical Materials Research 60(4): 613-621.

Li, K., J. F. Kong, D. L. Wang and W. K. Teo (1999). "Tailor-made asymmetric PVDF hollow fibers for soluble gas removal." Aiche Journal 45(6): 1211-1219.

Lu, L., S. J. Peter, M. D. Lyman, H.-H. Lai, S. M. Leite, J. A. Tamada, S. Uyama, J. P. Vacanti, R. langer and A. G. Mikos (2000). "In vitro and in vivo degradation of porous poly(DL-lactic-co-glycolic acid) foams." Biomaterials 21: 1837-1845.

Lubbe, A. M. and M. M. Henton (1997). "Sterilisation of surgical instruments with formaldehyde gas." Veterinary Record 140(17): 450-453.

Luciano, R. M., C. A. d. C. Zavaglia and E. A. d. R. Duek (2000). "Preparation of bioadsorbable nerve guide tubes." Artifical Organs 24(3): 206-208.

Ma, P. X. and R. Y. Zhang (2001). "Microtubular architecture of biodegradable polymer scaffolds." Journal of Biomedical Materials Research 56(4): 469-477.

MacDonald, J. M., S. P. Wolfe, I. Roy-Chowdhury, H. Kubota and L. M. Reid (2001). Effect of flow configuration and membrane characteristics on membrane fouling in a novel multicoaxial hollow-fiber bioartificial liver. Bioartificial Organs Iii: Tissue Sourcing, Immunoisolation, and Clinical Trials. New York, NEW YORK ACAD SCIENCES. 944: 334-343.

Mankani, M. H., S. A. Kuznetsov, B. Fowler, A. Kingman and P. G. Robey (2000). "In Vivo Bone Formation by Human Bone Marrow Stromal Cells: Effect of Carrier particle Size and Shape." Biotechnology & Bioengineering 72: 96-107.

Marks, S. C. and D. C. Hermey (1996). The structure and development of bone. Principles of Bone Biology. J. P. Bilezikian, L. G. Raisz and G. A. Rodan. San Diago, Academic Press.

Marler, J. J., J. Upton, R. langer and J. P. Vacanti (1998). "Transplantation of cells in matrices for tissue regeneration." Advanced Drug Delivery Reviews 33(1-2): 165-182.

Martson, M., J. Viljanto, T. Hurme and P. Saukko (1998). "Biocompatibility of cellulose sponge with bone." European Surgical Research 30(6): 426-432.

Matsuzaka, K., F. Walboomers, A. de Ruijter and J. A. Jansen (2000). "Effect of microgrooved poly-l-lactic (PLA) surfaces on proliferation, cytoskeletal organization,

and mineralized matrix formation of rat bone marrow cells." Clinical Oral Implants Research 11(4): 325-333.

McAllister, T. and J. Frangos (1999). "Steady and transient fluid shear stress stimulate NO release in osteoblasts through distinct biochemical pathways." Journal of Bone and Mineral Research 14: 930-936.

Mercier-Bonin, M., I. Daubert, D. Leonard, C. Maranges, C. Fonade and C. Lafforgue (2001). "How unsteady filtration conditions can improve the process efficiency during cell cultures in membrane bioreactors." Separation and Purification Technology 22-3(1-3): 601-615.

Merolli, A., A. Moroni, C. Faldini, P. T. Leali and S. Giannini (2003). "Histomorphological study of bone response to hydroxyapatite coating on stainless steel." Journal of Materials Science-Materials in Medicine 14(4): 327-333.

Middleton, J. C. and A. J. Tipton (2000). "Synthetic biodegradable polymers as orthopedic devices." Biomaterials 21: 2335-2346.

Millward, H. R., B. J. Bellhouse and I. J. Sobey (1996). "The vortex wave membrane bioreactor: Hydrodynamics and mass transfer." Chemical Engineering Journal and the Biochemical Engineering Journal 62(3): 175-181.

Mooney, D. J., C. L. Mazzoni, C. Breuer, K. McNamara, D. Hern, J. P. Vacanti and R. Langer (1996). "Sabilized polyglycolic acid fibre-based tubes for tissue engineering." Biomaterials 17: 115-124.

Moussy, Y. (2003). "Convective flow through a hollow fiber bioartificial liver." Artificial Organs 27(11): 1041-1049.

Mulder, M. (1992). Basic principles of membrane technology. Netherlands, Kluwer Academic Publishers Group.

Murphy, W. L., D. H. Kohn and D. J. Mooney (2000). "Growth of continuous bonelike mineral within porous poly(lactide-co-glycolide) scaffolds in vitro." Journal of Biomedical Materials Research 50(1): 50-58.

Miyaji, F., H. M. Kim, S. Handa, T. Kokubo and T. Nakamura (1999). "Bonelike apatite coating on organic polymers: novel nucleation process using sodium silicate solution." Biomaterials 20(10): 913-919.

Nillson, B. E. and N. E. Westlin (1971). "Bone density in athletes." Clinical Orthopaedics and Related Research 77: 179-182.

Nyberg, S. L., R. A. Shatford, M. V. Peshwa, J. G. White, F. B. Cerra and W. S. Hu (1993). "Evaluation of a Hepatocyte-Entrapment Hollow Fiber Bioreactor - a Potential Bioartificial Liver." Biotechnology and Bioengineering 41(2): 194-203.

Oh, S. H., S. G. Kang, E. S. Kim, S. H. Cho and J. H. Lee (2003). "Fabrication and characterization of hydrophilic poly(lactic-co- glycolic acid)/poly(vinyl alcohol) blend cell scaffolds by melt-molding particulate-leaching method." Biomaterials 24(22): 4011-4021.

Oudega, M., S. E. Gautier, P. Chapon, M. Fragoso, M. L. Bates, J. M. Parel and M. B. Bunge (2001). "Axonal regeneration into Schwann cell grafts within resorbable poly(alpha-hydroxyacid) guidance channels in the adult rat spinal cord." Biomaterials 22(10): 1125-1136.

Owen, M. and R. A. Melick (1973). Albumin in bone. In Hard tissue growth, repair and remineralisation. Amsterdam, Elsevier-Excerpta Medica, Associated Science Publishers.

Pabbruwe, M. B. (2002). Effect of Bioceramic chemistry on cellular behaviour in vitro and bone formation in vivo. Materials Science and Engineering. Sydney, University of New South Wales: 319.

Palsson, B. (2000). Tissue Engineering. In Introduction to Biomedical Engineering. J. D. Enderle, S. M. Blanchard and J. D. Bronzino. San Diego, Academic Press: 579-655.

Panyam, J., M. A. Dali, S. K. Sahoo, W. X. Ma, S. S. Chakravarthi, G. L. Amidon, R. J. Levy and V. Labhasetwar (2003). "Polymer degradation and in vitro release of a model protein from poly(D,L-lactide-co-glycolide) nano- and microparticles." Journal of Controlled Release 92(1-2): 173-187.

Park, H. C., Y. P. Kim, H. Y. Kim and Y. S. Kang (1999). "Membrane formation by water vapor induced phase inversion." Journal of Membrane Science 156(2): 169-178.

Partridge, K., X. B. Yang, N. M. P. Clarke, Y. Okubo, K. Bessho, W. Sebald, S. M. Howdle, K. M. Shakesheff and R. O. C. Oreffo (2002). "Adenoviral BMP-2 gene transfer in mesenchymal stem cells: In vitro and in vivo bone formation on biodegradable polymer scaffolds." Biochemical and Biophysical Research Communications 292(1): 144-152.

Peter, S., M. Miller, A. Yasko, M. Yaszemski and A. Mikos (1998). "Polymer Concepts in Tissue Engineering." Journal of Biomedical Materials Research 43: 422-427.

Petite, H., V. Viateau, W. Bensaid, A. Meunier, C. de Pollak, M. Bourguignon, K. Oudina, L. Sedel and G. Guillemin (2000). "Tissue-engineered bone regeneration." Nature Biotechnology 18(9): 959-963.

Planchamp, C., T. L. Vu, J. M. Mayer, M. Reist and B. Testa (2003). "Hepatocyte hollow-fibre bioreactors: design, set-up, validation and applications." Journal of Pharmacy and Pharmacology 55(9): 1181-1198.

Porter, B. D., J. B. Oldham, S.-L. He, M. E. Zobitz, R. G. Payne, K. N. An, B. L. Currier, A. G. Mikos and M. J. Yaszemski (2000). "Mechanical Properties of a Biodegradable Bone Regeneration Scaffold." Journal of Biomechanical Engineering 122: 286-288.

Puleo, D. A. and R. Bizios (1992). "Formation of Focal Contacts by Osteoblasts Cultured on Orthopedic Biomaterials." Journal of Biomedical Materials Research 26(3): 291-301.

Qi, H. N., C. T. Goudar, J. D. Michaels, H. J. Henzler, G. N. Jovanovic and K. B. Konstantinov (2003). "Experimental and theoretical analysis of tubular membrane aeration for mammalian cell bioreactors." Biotechnology Progress 19(4): 1183-1189.

Qin, J. J., J. Gu and T. S. Chung (2001). "Effect of wet and dry-jet wet spinning on the sheer-induced orientation during the formation of ultrafiltration hollow fiber membranes." Journal of Membrane Science 182(1-2): 57-75.

Qin, J. J. and T. S. Chung (1999). "Effect of dope flow rate on the morphology, separation performance, thermal and mechanical properties of ultrafiltration h ollow fibre membranes." Journal of Membrane Science 157(1): 35-51.

Qin, L., A. Mak, C. Cheng, L. Hung and K. Chan (1999). "Histomorphological study on pattern of fluid movement in cortical bone in goats." Anatomical Record 255: 380-387.

Reich, G. (1997). "Use of DSC to study the degradation behavior of PLA and PLGA microparticles." Drug Development and Industrial Pharmacy 23(12): 1177-1189.

Rocha, L. B., G. Goissis and M. A. Rossi (2002). "Biocompatibility of anionic collagen matrix as scaffol for bone healing." Biomaterials 23: 449-456.

Roer, R. D. and R. M. Dillaman (1990). "Bone growth and calcium balance during simulated weightlessness in the rat." Journal of Applied Physiology 68: 13-20.

Rose, F. R. A. J. and R. O. C. Oreffo (2002). "BREAKTHROUGHS AND VIEWS; Bone Tissue Engineering: Hope vs Hype." Biochemical and Biophysical Communications 292: 1-7.

Rosen, V. and R. S. Thies (1995). Adult skeletal repair. The cellular and molecular basis of bone formation and repair. New York, Springer: 97-142.

Russell, R. G. G., T. M. Skerry and U. Kollenkirchen, Eds. (1998). Novel approaches to treatment of osteoporosis. Ernst Schering Research Foundation Workshop. Berlin, Springer-Verlag.

Ryan, P. L., R. A. Foty, J. Kohn and M. S. Steinberg (2000). "Tissue spreading on implantable substrates is a competative outcome of cell-cell vs. cell-substratum adhesivity." PNAS 98(8): 4323-4327.

Sadek, P. C. The HPLC solvent guide, Wiley-Interscience.

Saini, S. and T. M. Wick (2003). "Concentric cylinder bioreactor for production of tissue engineered cartilage: Effect of seeding density and hydrodynamic loading on construct development." Biotechnology Progress 19(2): 510-521.

Saito, N. and K. Takaoka (2003). "New synthetic biodegradable polymers as BMP carriers for bone tissue engineering." Biomaterials 24(13): 2287-2293.

Salem, A. K., F. Rose, R. O. C. Oreffo, X. B. Yang, M. C. Davies, J. R. Mitchell, C. J. Roberts, S. Stolnik-Trenkic, S. J. B. Tendler, P. M. Williams and K. M. Shakesheff (2003). "Porous polymer and cell composites that self-assemble in situ." Advanced Materials 15(3): 210-+.

Santovena, A., C. Alvarez-Lorenzo, A. Concheiro, M. Llabres and J. B. Farina (2004). "Rheological properties of PLGA film-based implants: correlation with polymer degradation and SPf66 antimalaric synthetic peptide release." Biomaterials 25(5): 925-931.

Schecroun, N. and C. Delloye (2003). "Bone-like nodules formed by human bone marrow stromal cells: comparative study and characterization." Bone 32(3): 252-260.

Schiller, C. and M. Epple (2003). "Carbonated calcium phosphates are suitable pH-stabilising fillers for biodegradable polyesters." Biomaterials 24: 2037-2043.

Schirrmacher, K., I. Schmitz, E. Winterhager, O. Traub, F. Brummer, D. Jones and D. Bingmann (1992). "Characterization of gap junctions between osteoblast-like cells in culture." Calcified Tissue International 51: 285-290.

Schmidmaier, G., B. Wildemann, M. Lubberstedt, N. P. Haas and M. Raschke (2003). "IGF-I and TGF-beta 1 incorporated in a poly(D,L-lactide) implant coating stimulates osteoblast differentiation and collagen-1 production but reduces osteoblast proliferation in cell culture." Journal of Biomedical Materials Research Part B-Applied Biomaterials 65B(1): 157-162.

Schneider, V. S. and J. McDonald (1984). "Skeletal calcium homeostasis and countermeasures to prevent disuse osteoporosis." Calcified Tissue International 51: 285-290.

Schwartz, Z., C. H. Lohmann, J. Oefinger, L. F. Bonewald, D. D. Dean and B. D. Boyan (1999). "Implant surface characteristics modulate differentiation behaviour of cells in the osteoblastic lineage." Advanced Dental Research 13: 38-48.

Scragg, A. H., Ed. (1991). Bioreactors in biotechnology: A practical approach. Ellis Horwood Series in Biochemistry and Biotechnology. Chichester, West Sussex, Ellis Horwood Limited. September 12-16, 2004.

Shakesheff, K. (2005). Use of sodium hydroxide to remove the dense outer skin from PLGA scaffolds. J. Chaudhuri. Bath.

Shi, S., S. Gronthos, S. Chen, A. Reddi, C. M. Counter, P. G. Robey and C.-Y. Wang (2002). "Bone formation by human postnatal bone marrow stromal cells is enhanced by telomerase expression." Nature Biotechnology 20: 587-591.

Shieh, M. (2000). "Control of Bone Cell Functions on Three-Dimensional Tissue Engineering Scaffolds." b.u.g.? 3: 194-204.

Sikavitsas, V. I., G. N. Bancroft and A. G. Mikos (2002). "Formation of three-dimensional cell/polymer constructs for bone tissue engineering in a spinner flask and a rotating wall vessel bioreactor." Journal of Biomedical Materials Research 62(1): 136-148.

Sikavitsas, V., J. Temenoff and A. Mikos (2001). "Review: Biomaterials and bone mechanotransduction." Biomaterials 22: 2581-2593.

Silva, R. M., C. Elvira, J. F. Mano, J. San Roman and R. L. Reis (2004). "Influence of beta-radiation sterilisation in properties of new chitosan/soybean protein isolate membranes for guided bone regeneration." Journal of Materials Science-Materials in Medicine 15(4): 523-528.

Silvio, L. D., M. J. Dalby and W. Bonfield (2002). "Osteoblast behaviour on HA/PE composite surfaces with different HA volumes." Biomaterials 23(1): 101-107.

Simosen, J. L., C. Rosada, N. Serakinci, J. Justesen, K. Stenderup, S. I. S. Rattan, T. G. Jensen and M. Kassem (2002). "Telomerase expression extends the proliferative life-span and maintains the osteogenic potential of human bone marrow stromal cells." Nature Biotechnology 20: 592-595.

Sinha, R. K. and R. S. Tuan (1996). "Regulation of human osteoblast integrin expression by orthopedic implant materials." Bone 18(5): 451-457.

Sinnott, R. K. (1998). Coulson & Richardson's Chemical Engineering: Chemical Engineering Design. Oxford, Butterworth-Heinemann Ltd.

Spencer, P. (2003). PLGA ratio availability from Alkermes. M. Ellis. Bath.

Steele, J. G., C. McFarland, B. A. Dalton, G. Johnson, M. D. M. Evans, C. R. Howlett and P. A. Underwood (1993). "Attachment of Human Bone-Cells to Tissue-Culture Polystyrene and to Unmodified Polystyrene - the Effect of Surface-Chemistry Upon

Initial Cell Attachment." Journal of Biomaterials Science-Polymer Edition 5(3): 245-257.

Stephansson, S. N., B. A. Byers and A. J. Garcia (2002). "Enhanced expression of the osteoblastic phenotype on substrates that modulate fibronectin conformation and integrin receptor binding." Biomaterials 23: 2527-2534.

Sun, X. M. and Y. X. Zhang (2003). "Estimation of Chinese hamster ovary cell density in packed-bed bioreactor by lactate production rate." Biotechnology Letters 25(11): 853-857.

Sundback, C., T. Hadlock, M. Cheney and J. Vacanti (2003). "Manufacture of porous nerve conduits by a novel low-pressure injection molding process." Biomaterials 24: 819-830.

Tabata, Y. (2001). "Recent progress in tissue engineering." Drug Discovery Today 6(1): 483-487.

Taddei, P., S. Affatato, C. Fagnano, B. Bordini, A. Tinti and A. Toni (2002). "Vibrational spectroscopy of ultra-high molecular weight polyethylene hip prostheses: influence of the sterilisation method on crystallinity and surface oxidation." Journal of Molecular Structure 613(1-3): 121-129.

Tai, C. C., S. P. Perrera and B. D. Crittenden (2005). Development of adsorbent hollow fibres. 7th World Congress of Chemical Engineering, Glasgow.

Takeshita, K., H. Ishibashi, M. Suzuki, T. Yamamoto, T. Akaike and M. Kodama (1995). "High Cell-Density Culture System of Hepatocytes Entrapped in a 3-Dimensional Hollow-Fiber Module with Collagen Gel." Artificial Organs 19(2): 191-193.

Terai, H., D. Hannouche, E. Ochoa, Y. Yamano and J. P. Vacanti (2002). "In vitro engineering of bone using a rotational oxygen- permeable bioreactor system."

Materials S cience & E ngineering C -Biomimetic and Supramolecular Systems 20(1-2): 3-8.

Tessmar, J., A. Mikos and A. Gopferich (2003). "The use of poly(ethylene glycol)-block-poly(lactic acid) derived copolymers for the rapid creation of biomimetic surfaces." Biomaterials 24(24): 4475-4486.

Tjandrawwinata, R., V. Vincent and M. Hughes-Fulford (1997). "Vibrational force alters mRNA expression in osteoblasts." FASEB Journal 11: 493-497.

Torrestiana-Sanchez, B., R. I. Ortiz-Basurto and E. Brito-De La Fuente (1999). "Effect of nonsolvents on properties of spinning solutions and polyethersulfone hollow fiber ultrafiltration membranes." Journal of Membrane Science 152(1): 19-28.

Triffitt, J. T. and M. Owen (1973). "Studies on bone matrix glycoproteins. Incorporation of (1-14C) glucosamine and plasma (14C) glycoprotein into rabbit cortical bone." Biochemistry Journal 136: 125-34.

Vaananen, K. (1996). Osteoclast function: biology and mechanisms. Principles of Bone Biology. J. P. Bilezikian, L. G. Raisz and G. A. Rodan. San Diego, Academic Press: 103-114.

Valimaa, T. and S. Laaksovirta (2004). "Degradation behaviour of self-reinforced 80L/20G PLGA devices in vitro." Biomaterials 25(7-8): 1225-1232.

Vaughan, J. M. (1975). The Physiololgy of Bone. Oxford, Oxford University Press.

Vehof, J., J. Fisher, D. Dean, J.-P. v. d. Waerden, P. Spauwen, A. Mikos and J. Jansen (2002). "Bone formation in transforming growth factor Beta-1-coated porous poly(propylene fumerate) scaffolds." Journal of Biomedical Materials Research 60(2): 241-251.

Wake, M. C., P. D. Gerecht, L. Lu and A. Mikos (1998). "Effects of biodegradable polymer particles on rat marrow-derived stromal o steoblasts i n v itro." B iomaterials 19: 1255-1268.

Wan, A. C. A., H. Q. Mao, S. Wang, K. W. Leong, L. Ong and H. Yu (2001). "Fabrication of poly(phosphoester) nerve guides by immersion precipitation and the control of porosity." Biomaterials 22(10): 1147-1156.

Wan, Y. Q., J. Yang, J. L. Yang, J. Z. Bei and S. G. Wang (2003). "Cell adhesion on gaseous plasma modified poly-(L-lactide) surface under shear stress field." Biomaterials 24(21): 3757-3764.

Wan, Y. Q., Y. Wang, Z. M. Liu, X. Qu, B. X. Han, J. Z. Bei and S. G. Wang (2005). "Adhesion and proliferation of OCT-1 osteoblast-like cells on micro- and nano-scale topography structured pply(L-lactide)." Biomaterials 26(21): 4453-4459.

Wang, R. and T. S. Chung (2001). "Determination of pore sizes and surface porosity and the effect of shear stress within a spinneret on asymmetric hollow fiber membranes." Journal of Membrane Science 188(1): 29-37.

Wang, S., A. C. A. Wan, X. Y. Xu, S. J. Gao, H. Q. Mao, K. W. Leong and H. Yu (2001). "A new nerve guide conduit material composed of a biodegradable poly(phosphoester)." Biomaterials 22(10): 1157-1169.

Wang, Y., P. Challa, D. L. Epstein and F. Yuan (2004). "Controlled release of ethacrynic acid from poly(lactide-co- glycolide) films for glaucoma treatment." Biomaterials 25(18): 4279-4285.

Wang, D. L., K. Li and W. K. Teo (1996). "Polyethersulfone hollow fiber gas separation membranes prepared from NMP/alcohol solvent systems." Journal of Membrane Science 115(1): 85-108.

Webb, K., V. Hlady and P. A. Tresco (2000). "Relationships among cell attachment, spreading, cytoskeletal organization, and migration rate for anchorage-dependent cells on model surfaces." Journal of Biomedical Materials Research 49: 362-368.

Weber, F. E., H. G. Schmökel, R. J. Blanca San Miguel, E. Pirhonen and K. W. Grätz (2004a). "The bioactivity of a novel guided bone regeneration membrane depends on BMP." 5th International Conference on Bone Morphogenetic Proteins, 2004, Nagoya, JAPAN

Weber, F., B. S. Miguel, H. Schmoekel, E. Pirhonen, R. Jung and K. Graetz (2004b). "A NOVEL BIOACTIVE AND DEGRADABLE MEMBRANE FOR GUIDED BONE REGENERATION." An oral presentation at the IADR 2004 in Hawaii, June 2004:.

Weber, W., E. Weber, S. Geisse and K. Memmert (2002). "Optimisation of protein expression and establishment of the Wave Bioreactor for Baculovirus/insect cell culture." Cytotechnology 38(1-2): 77-85.

Wei, G. B. and P. X. Ma (2004). "Structure and properties of nano-hydroxyapatite/polymer composite scaffolds for bone tissue engineering." Biomaterials 25(19): 4749-4757.

Weinbaum, S., S. C. Cowin and Y. Zheng (1994). "A model for the excitation of osteocytes by mechanical loading-induced bone fluid shear stresses." Journal of Biomechanics 27: 339-360.

Weir, N. A., F. J. Buchanan, J. F. Orr, D. F. Farrar and A. Boyd (2004). "Processing, annealing and sterilisation of poly-L-lactide." Biomaterials 25(18): 3939-3949.

Wendt, D., A. Marsano, M. Jakob, M. Heberer and I. Martin (2003). "Oscillating perfusion of cell suspensions through three- dimensional scaffolds enhances cell seeding efficiency and uniformity." Biotechnology and Bioengineering 84(2): 205-214.

Whang, K., K. E. Healy, D. R. Elenz, E. K. Nam, D. C. Tsai, C. H. Thomas, G. W. Nuber, F. H. Glorieux, R. Travers and S. M. Sprague (1999). "Engineering bone regeneration with bioabsorbable scaffolds with novel microarchitecture." Tissue Engineering 5(1): 35-51.

Whedon, G. D. (1984). "Disuse osteoporosis: physiological aspects." Calcified Tissue International 36: S146-S150.

Widmer, M. S., P. K. Gupta, L. Lu, R. K. Meszlenyi, G. R. D. Evans, K. Brandt, T. Savel, A. Gurlek, C. W. P. Jr and A. G. Mikos (1998). "Manufacture of porous biodegradable polymer conduits by an extrusion process for guided tissue regeneration." Biomaterials 19: 1945-1955.

Williamson, M. R. and A. G. A. Coombes (2004). "Gravity spinning of polycaprolactone fibres for applications in tissue engineering." Biomaterials 25(3): 459-465.

Xu, Z. L. and F. A. Qusay (2004). "Polyethersulfone (PES) hollow fiber ultrafiltration membranes prepared by PES/non-solvent/NMP solution." Journal of Membrane Science 233(1-2): 101-111.

Xu, Q. X., X. T. Sun, Y. D. Qiu, H. Y. Zhang and Y. T. Ding (2004b). "The optimal hepatocyte density for a hollow-fiber bioartificial liver." Annals of Clinical and Laboratory Science 34(1): 87-93.

Yang, S., K.-F. Leong, Z. Du and C.-K. Chua (2001). "Review: The Design of Scaffolds for Use in Tissue Engineering. Part I. Traditional Factors." Tissue Engineering 7(6): 679-689.

Yang, X. B., H. I. Roach, N. M. P. Clarke, S. M. Howdle, R. Quirk, K. M. Shakesheff and R. O. C. Oreffo (2001). "Human osteoprogenitor growth and differentiation on synthetic biodegradable structures after surface modification." Bone 29(6): 523-531.

Yang, X. B., R. S. Tare, K. A. Partridge, H. I. Roach, N. M. Clarke, S. M. Howdle, K. M. Shakesheff and R. O. Oreffo (2003). "Induction of human osteoprogenitor chemotaxis, proliferation, differentiation, and bone formation by osteoblast stimulating factor-1/pleiotrophin: Osteoconductive biomimetic scaffolds for tissue engineering." Journal of Bone and Mineral Research 18(1): 47-57.

Yang, Y., J. Magnay, L. Cooling and A. E. Haj (2002). "Development of a mechano-active scaffold for tissue engineering." Biomaterials 23: 2119-2126.

Yoshimoto, H., Y. M. Shin, H. Terai and J. P. Vacanti (2003). "A biodegradable nanofiber scaffold by electrospinning and its potential for bone tissue engineering." Biomaterials 24: 2077-2082.

Zhang, R. Y. and P. X. Ma (1999). "Poly(alpha-hydroxyl acids) hydroxyapatite porous composites for bone-tissue engineering. I. Preparation and morphology." Journal of Biomedical Materials Research 44(4): 446-455.

Zhang, Y. M., T. Fu, Y. Han, Q. T. Wang, Y. M. Zhao and K. W. Xu (2002). "In vitro and in vivo tests of hydrothermally synthesised hydroxyapatite coating." Biomolecular Engineering 19(2-6): 57-61.

Zhou, D. L., W. Z. Yang, G. F. Yin, C. Q. Zheng, Y. Zhang, H. Q. Chen and R. Chen (2004). "In vitro characterizations of PLLA/beta-TCP porous matrix materials and RMSC-PLLA-beta-TCP composite scaffolds." Journal of Materials Science & Technology 20(3): 248-252.

APPENDIX A
REAGENT PREPARATION

A.1 MEDIA REAGENTS

Reagent	***DMEM***
Full Name	Dulbecco's Modified Eagles Medium
Role	Basal media; supplies nutrients inc. glucose and additives
Usage concentration	1x
Storage concentration	1x, 500ml as purchased
Storage method	Fridge. 1mth once opened
Preparation method	Use as purchased

Reagent	***SP***
Full Name	Sodium Pyruvate
Role	Metabolite
Usage concentration	1mM (1ml/100ml)
Storage concentration	100mM
Storage method	Fridge. 100ml bottles as purchased
Preparation method	Use as purchased

Reagent	***NEAA***
Full Name	non-essential amino acids
Role	Supply non-essential amino acids
Usage concentration	1x (1ml/100ml)
Storage concentration	100x
Storage method	Fridge. 100ml bottles as purchased
Preparation method	Use as purchased

Reagent	***P/S***
Full Name	penicillin/streptomycin
Role	antibiotic
Usage concentration	1x (1ml/100ml)
Storage concentration	5ml aliquots, as purchased
Storage method	Freezer. 1-2days in fridge once thawed
Preparation method	Filter then aliquot 5ml in sterile conditions into bijoux

Reagent	***FCS***
Full Name	fetal calf serum
Role	protein source
Usage concentration	10%
Storage concentration	50ml aliquots H.I.
Storage method	Freezer. 1week in fridge once thawed
Preparation method	Heat inactivation 1. Thaw out a bottle of FCS 2. Heat water bath to 58°C 3. Label 50ml falcon tubes "HI FCS" 4. Dispense 50ml into each falcon tube 5. Tighten lid and seal with parafilm tape 6. Fill a spare tube with water and place in same rack 7. Place the rack of tubes in the water bath 8. Put a thermometer in the tube of water. When this reached 58°C time the incubation for a further 30min 9. Freeze aliquots upright at -20°C

Reagent	***BSA***
Full Name	linoleic acid-bovine serum albumin
Role	adhesion protein
Usage concentration	1mg/ml
Storage concentration	10mg/ml
Storage method	Freezer. 30days in fridge once thawed
Preparation method	1. Add 50ml DMEM to 500mg bottle 2. Swirl to mix and dissolve for apporx 30sec 3. Set out 1.5ml microfuge tubes 4. Swirled to mix for approx 5sec 5. Aliquoted 1.5ml solution into microfuge tubes 6. Mark microfuge tubes 'BSA' and store in fridge

Reagent	***A2P***
Full Name	Ascorbate-2-phosphate
Role	Stimulates proliferation and differentiation (Beresford and Owen 1998)
Usage concentration	100μM
Storage concentration	10mM
Storage method	Freezer. 1mth in fridge once thawed
Preparation method	1. Dissolve A2P in sterile PBS (289mg/100ml). It may need to go into an incubator to get it all to dissolve 2. Filter sterilise the solution 3. Dispense into bijoux in 5ml aliquots

Reagent	***G418***
Full Name	Geneticin
Role	Antibiotic
Usage concentration	50μg/ml
Storage concentration	100mg/ml DMEM
Storage method	Freezer. 1mth in fridge once thawed. Stock bottle can be stored in fridge for up to one year before preparation
Preparation method	1. Dissolve G418 in sterile DMEM (100mg/ml) 2. Filter sterilise the solution 3. Dispense into 1ml microfuge tubes in 500μl aliquots

Reagent	***$ZnSO_4$***
Full Name	Zinc Sulphate
Role	Induces proliferation
Usage concentration	1M
Storage concentration	200μM (20μl/100ml)
Storage method	Freezer. 1month in fridge once thawed
Preparation method	1. Dissolve $ZnSO_4$ in sterile PBS (288mg/ml) 2. Filter sterilise the solution 3. Dispense into microfuge tubes in 1ml aliquots

Reagent	***$CdSO_4$***
Full Name	Cadmium Sulphate
Role	Induces proliferation
Usage concentration	1μM (10μl/100ml)
Storage concentration	10mM. 7.70mg/ml in PBS
Storage method	Freezer. 1month in fridge once thawed
Preparation method	1. Dissolve $CdSO_4$ in sterile PBS (7.70mg/ml) 2. Filter sterilise the solution 3. Dispense into microfuge tubes in 1ml aliquots

Reagent	***Dx***
Full Name	Dexamethasone
Role	Stimulates osteogenic function
Usage concentration	1x 10^{-8}M (20µl/100ml)
Storage concentration	5x10^{-5}M in DMEM
Storage method	Freezer. 1week in fridge once thawed
Preparation method	1. Dissolve 10mg in 1ml absolute ethanol. Rotate to dissolve 2. Add 100µl to 49ml DMEM. Disguard the rest 3. Filter sterilise with syringe filter into 50ml falcon tube 4. Dispense into microfuge tubes in 1ml aliquots

Reagent	***β-GP***
Full Name	β-Glycerophosphate
Role	phosphate mineralisation
Usage concentration	10mM (20µl/100ml)
Storage concentration	1M in DMEM
Storage method	Freezer. 1month in fridge once thawed
Preparation method	1. weigh out 10.8g β-GP. Add to falcon 2. add 50ml DMEM and shake to dissolve 3. filter sterilise 4. dispense into bijou in 5ml aliquots

A.2 PASSAGING REAGENTS

Reagent	***Collagenase***
Full Name	Collagenase Type VII
Role	dissociation of cells from culture surface
Usage concentration	0.025units/ml (50µl/5ml)
Storage concentration	2500units/ml
Storage method	freezer. 1 month in fridge once thawed
Preparation method	1. Dissolve collagenase in DMEM (2500units/ml) 2. Filter sterilise the solution 3. Dispense into microfuge tubes in 1ml aliquots

Reagent	***DNase***
Full Name	Deoxyribonuclease I
Role	Inhibits trypsin activity
Usage concentration	1µg/ml
Storage concentration	100µg/ml
Storage method	Freezer. 1month in fridge once thawed
Preparation method	1. add 10ml DMEM to one vial (contains 1mg as stated in Sigma catalogue) 2. gently shake to dissolve 3. filter sterilise 4. aliquot into 1.5ml microfuge tubes

Reagent	***$CaCl_2$***
Full Name	Calcium chloride
Role	Additive for collagenase solution
Usage concentration	0.002M (10ul/5ml)
Storage concentration	1M
Storage method	fridge
Preparation method	1. dissolve 2.22 mg in 20ml 2. filter sterilise 3. keep in universal bottle

Reagent	***Trypsin***
Full Name	Trypsin-EDTA solution
Role	Dissociation of cell-cell bonds
Usage concentration	1x
Storage concentration	1x
Storage method	freezer. 1month in fridge once thawed
Preparation method	1. thaw bottle as purchased 2. Purchased solution is 10x so dilute 1:10 to 1x. Aliquot 5ml trypsin to a falcon tube 3. add 45ml PBS 4. mark tubes 'TE' and store in freezer

A.3 ANALYSIS REAGENTS

Reagent	***10%NBF***
Full Name	10% Neutral Buffered Formalin
Role	fixing agent
Usage concentration	as storage
Storage concentration	10% v/v formalin
Storage method	fridge
Preparation method	1. add 100ml formalin to 1L duran 2. add 16g Na_2HPO_4 to 1L duran 3. add 4g $NaH_2PO_4.H_20$ to 1L duran 4. make up to 1L with 900ml deionised water 5. store in fridge marked '10% NBF'

Reagent	***ATM buffer***
Full Name	Alkaline buffer solution/ Triton X-100 /MilliQ water
Role	lysing agent
Usage concentration	as storage
Storage concentration	0.5M alkaline buffer solution
Storage method	fridge
Preparation method	To make up 100ml ATM 1. add 33.3ml AMP to duran (so 0.5M) 2. add 0.5ml TX-100 (so 0.5%) 3. add 66.2ml milliQ water to make up to 100ml

Reagent	***FR***
Full Name	Fast Red
Role	Alkaline phosphatase stain
Usage concentration	1% w/v fast red
Storage concentration	NA
Storage method	make up as needed, do not store
Preparation method	To make up 10ml 1. weigh out 2mg Napthol AS-MX and add to a glass container 2. add 200ul DMF to the glass container 3. make up to 10ml with 9.8ml tris buffer 4. weigh out and add 10mg fast red TR salt just before use 5. shake to mix 6. filter sterilise

Reagent	***Tris buffer***
Full Name	Tris buffer
Role	solubilise fast red
Usage concentration	as storage
Storage concentration	0.1M
Storage method	Freezer. 2weeks in fridge once thawed
Preparation method	To make up 1L 1. weigh out 15.8g Trizma-HCl 2. make up to 1L with MilliQ H_2O 3. adjust pH to 9.2 4. aliquot into 50ml flacon tubes

Reagent	***Von Kossa***
Full Name	2.5% silver nitrate in distilled water
Role	mineralisation (phosphate) stain
Usage concentration	1x
Storage concentration	1x
Storage method	fridge. Keep wrapped in foil
Preparation method	

Reagent	***Borate Buffer***
Full Name	Borate Buffer
Role	solubilise methylene blue
Usage concentration	as storage
Storage concentration	0.01M
Storage method	fridge
Preparation method	To make up 1L 1. weigh out 0.62g boric acid and add to 1L duran 2. add 5ml 1N sodium hydroxide to duran 3. Add DH_2O to 1L. shake to mix 4. adjust pH to 8.5

Reagent	***MB***
Full Name	1% Methylene Blue
Role	cell membrane stain
Usage concentration	as storage
Storage concentration	1% w/v
Storage method	room temp
Preparation method	To make up 100ml 1. weigh out 1g methylene blue powder 2. measure 100ml borate buffer 3. mix and store in 100ml duran

Reagent	***MTT***
Full Name	Thiazol blue (3-[4,5-dimethyl-2-yl]-2,5-diphenyltetrazolium bromide)
Role	live cell stain
Usage concentration	0.05mg/ml (1ml/100ml)
Storage concentration	5mg/ml
Storage method	Freezer. Keep wrapped in foil. 2weeks fridge once opened
Preparation method	To make up 200ml 1. weigh out 1g MTT powder 2. dissolve in 200ml DMEM 3. filter sterlise 4. aliquot into 5ml bijou, wrap in foil and freeze

Reagent	***Haematoxylin***
Full Name	Haematoxylin Harris
Role	cell membrane stain
Usage concentration	as storage
Storage concentration	1% v/v
Storage method	room temperature
Preparation method	To make up 20ml
	1. add 200ul Haematoxylin solution to universal
	2. add 19.8ml MilliQ H_2O to make up to 20ml
	3. filter sterilise

Reagent	***Acidified Alcohol***
Full Name	Acidified Alcohol
Role	elution of MB
Usage concentration	as storage
Storage concentration	1% v/v
Storage method	room temperature
Preparation method	To make up 20ml
	1. add 200ul 1M HCl to universal
	2. add 19.8ml ethanol to make up to 20ml
	3. filter sterilise

Reagent	***3N NaOH***
Full Name	3N sodium hydroxide
Role	histology
Usage concentration	as storage
Storage concentration	3N
Storage method	room temperature
Preparation method	For NaOH (and HCl), 1N ≡1M
	To make up 100ml
	1. weigh out 12g NaOH pellets
	2. add 100ml DH_2O

A.4 MEDIA PREPARATION

Table A.1. Preparation of 100 ml human bone derived cell media.

Reagent	Volume
1x NEAA	1 ml
1x pen/strep	1 ml
1x sodium pyruvate	1 ml
A2P	1 ml
DMEM	86 ml
FCS	10 ml

Reagents are shown in alphabetical order. The volumes are based on addition of stock solution concentrations (see Section A.1).

Table A.2. Preparation of 100 ml 560PMT1 media.

Reagent	Volume
1x NEAA	1 ml
1x pen/strep	1 ml
1x sodium pyruvate	1 ml
A2P	1 ml
$CdSO_4$	10 µl
DMEM	85.9 ml
Dx	20 µl
FCS	10 ml
G418	50 µl
$ZnSO_4$	20 µl

Reagents are shown in alphabetical order. The volumes are based on addition of stock solution concentrations (see Section A.1).

Table A.3. Preparation of 100 ml 560PzipU19 media.

Reagent	Volume
1x NEAA	1 ml
1x pen/strep	1 ml
1x sodium pyruvate	1 ml
A2P	1ml
DMEM	85.9 ml
Dx	20 µl
FCS	10 ml

Reagents are shown in alphabetical order. The volumes are based on addition of stock solution concentrations (see Section A.1).

A.5 SIMULATED BODY FLUID PREPARATION

Table A.4. Preparation of '1SBF' for the apatite coating nucleation phase.

Reagent	NaCl	$NaHCO_3$	KCl	$K_2HPO_4.3H_2O$	$MgCl_2.6H_2O$	$CaCl_2.2H_2O$	Na_2SO_4
Molecular weight	58.44	84.01	74.55	228.23	203.30	147.00	142.04
Concentration (mM)	137	4.2	3	1	1.5	2.5	0.5
Weight (g)	0.4003	0.0180	0.0110	0.0114	0.0150	0.0180	0.0035

Weights are listed as required to prepared 50 ml in distilled water.

Table A.5. Preparation of '1.5SBF' for the apatite coating growth phase.

Reagent	NaCl	$NaHCO_3$	KCl	$K_2HPO_4.3H_2O$	$MgCl_2.6H_2O$	$CaCl_2.2H_2O$	Na_2SO_4
Molecular weight	58.44	84.01	74.55	228.23	203.30	147.00	142.04
Concentration (mM)	205.5	6.30	4.5	1.5	2.3	3.8	0.75
Weight (g)	6.0000	0.2600	0.1700	0.1711	0.2300	0.2800	0.0532

Weights are listed as required to prepared 500 ml in distilled water.

APPENDIX B

EQUIPMENT AND CONSUMABLES

Table B.1. Consumables used during project

Item	Supplier	Catalogue number
Asparator tips	Beckton Dickinson	357558
Bijou 7ml	Bibby Sterilin	129A
Biodyne B transfer membrane	Pall	BNBZF3RT
Cryotubes	Nalgene	5000-1020
Disposable scapel	Fisher	SCA-310-150A
Duran bottles (50 ml)	Fisher	BTF-682-050B
Duran bottles (100 ml)	Fisher	BTF-682-071Q
Eppendorf multipipette tips, Combitips®	Fisher	PMP-117-519E
Falcon tube 50ml	Triple Red	2141100
Falcon tubes 15ml	Triple Red	2141300
Filters, nylon 13mm, 0.2um pore	Fisher	FDC-890-120P
Glass coverslips 18 x 18 mm	Fisher	MNJ-450-010C
Glass coverslips 22x26 mm	Fisher	MNJ-400-050C
Microcentrifuge tubes 0.5 ml	Triple Red	900117
Microcentrifuge tubes 1.5 ml	Fisher	TUL-150-150N
Microplates 12-well NUNC	Fisher	TKT-190-070N
Microplates 24-well NUNC	Fisher	TKT-190-010Y
Microplates 24-well untreated Iwaki	SLS	TIS 5220
Microplates 4-well NUNC	Fisher	TKT-190-130V
Microplates 96-well NUNC	Fisher	TKT-190-070U
Needle BD Microlance ® 3 1.5" 20guage 0.9mm x 40mm	Fisher	SZR-175-550L
Parafilm with paper 75m length 50mm width	Fisher	SEL-400-030P

Pipette tips Finntip 1000 rack	Thermo Life Sciences	9401 110
Pipette tips Finntip 250 refil	Thermo Life Sciences	9400267
Pippettor tips, graduated, 10ml	Triple Red	PN10E1
Pippettor tips, graduated, 25ml	Triple Red	PN25E1
Pippettor tips, graduated, 50ml	Triple Red	PN50E1
Polycarbonate sheet, thickness 25mm	Goodfellow	593-123-92
Polycarbonate sheet, thickness 5mm	Goodfellow	972-237-77
Pots-metal flow sealed cap 150ml	Bibby Sterilin	165A
Reagent Packs	Nova Biomedical	36281
Silicone Elastomer, thickness 1.0mm	Goodfellow	947-690-83
Steribag heat seal 140mm x 75mm x 250mm pack of 1000	Fisher	AUY-100-040P
Steribag heat seal 190mm x 65mm x 330mm pack of 500	Fisher	AUY-100-080D
Steribag heat seal 90mm x 50 x 125mm pack of 2000	Fisher	AUY-100-010B
Syringe 10ml	Fisher	SZR-150-041H
Syringe 5 ml	Fisher	SZR-150-031K
Technovit 7100 kit	Taab	T218
Tissue culture flasks T75 vented	Triple Red	2020200
Universal tube 30ml	Bibby Sterilin	128A

Table B.2. Equipment used in project

Item	Supplier and model
Adjustable pipette	Bibby
Aparator pump	Charles Austen Pumps Capex L2C
Asparator bottle	Pyrex 4L
Centrifuge	Jouan BR4i
Class II Laminar Flow Cabinet	Heraeus HS12
Distilled water reservoir	Vivendi Water Systems, Purelab Option Elga Reservoir 40L
Eppindorf multipipette dispensing pipette	Fisher
Fluorospectometer	Fluoroscan
Forceps	Fisher DKC-551-S
Freezer	Scandinova SFF-7054
Fridge-freezer	Scandinova FF6-9236W
HPLC	Gilson
Incubator	Jencon
Microscope	Nikon Eclipse TS100
Microscope camera	Nikon COOLPIX995
Pipettors	Finnpippette
Polypor H 220x4.6 mm Column	Whatman
Reflective light microscope	Nikon Eclipse E400
Reflective light microscope camera	JVC KY-F30B
Rheometer	Bohlin Rheometer CS
Roller mixer	Stuart Scientific SRT2
Rotary mixer	Stuart Scientific Rotator Drive STR4
Scales-cell culture ±0.001g	Mettler PB303-S
Scales-chemical ±0.0001g	Precisa 125A
Scales-chemical ±0.1g	Mettler PM3000
Scanning electron microscope (SEM)	JEOL JSM6310
Scanning probe microscope	Digital Instruments Nanoscope III

(AFM)	
Sputter coater	Edwards Sputter Coater S310B
Synerg I 4u Polar-RP 80A Column	Whatman
Water bath	Grant OLS 200

APPENDIX C
DEVELOPMENT OF CELL CULTURE AND ANALYSIS METHODS

C.1 PICOGREEN ASSAY BUFFER SELECTION

While TE is the traditional buffer for the picogreen assay, it was decided the universal buffer ATM would be preferable to allow multi-analysis of the cell culture samples, specifically its use for ALP activity assays. The DNA standard solutions were prepared in both buffers and read using the fluorospectrometer (see Section 3.5.1) using the standard excitation and emission filters of 485nm and 538nm respectively.

The comparison of the calibration curves can be seen in Figure C.1 below. While the gradient of the TE curve is approximately twice that of the ATM curve, the slope of the ATM curve was steep enough to be practical.

The ATM was considered a suitable buffer for the picogreen assay based on the slope obtained with the DNA standards and along side the multi-purpose benefits.

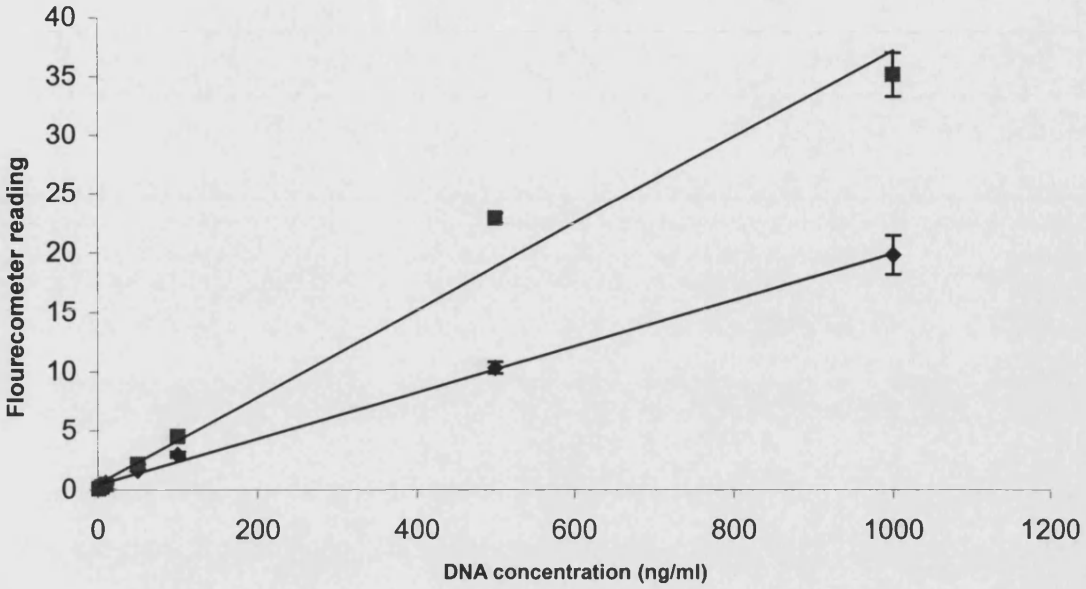

Figure C.1. Comparison of buffers for the picogreen assay.
■ TE (y = 0.0367x + 0.4943), ◆ATM (y = 0.0195x + 0.4363).

C.2 QUANTITATIVE CELL NUMBER ASSAY SELECTION

There are many cell number quantification methods available. The picogreen, MTT and MB assays were compared to find the most appropriate assay for use with the PLGA membranes. Cells were seeded onto TCP and after 6 hours (see Section C.3 for choice of attachment time) the number of cells attached to the surface was calculated using one of three methods as detailed in Section 3.5.1. 50:50 membrane was also analysed using the same method to assess the 'background noise' of the method that could be expected when cell culture analysis was carried out on the membranes.

It can clearly be seen that the picogreen assay could be used for low cell numbers, down to approximately 3000 cells/cm^2, the MTT assay would be suitable only for high cell numbers above approximately 40,000 cells/cm^2, and MB would not be a suitable cell quantification assay for use with the membranes since the background noise was considerably greater than the actual readings taken (Figure C.2).

The picogreen assay was chosen as the cell number quantification method for this thesis since the background noise would not effect readings for cell numbers over 3000 cells/cm^2.

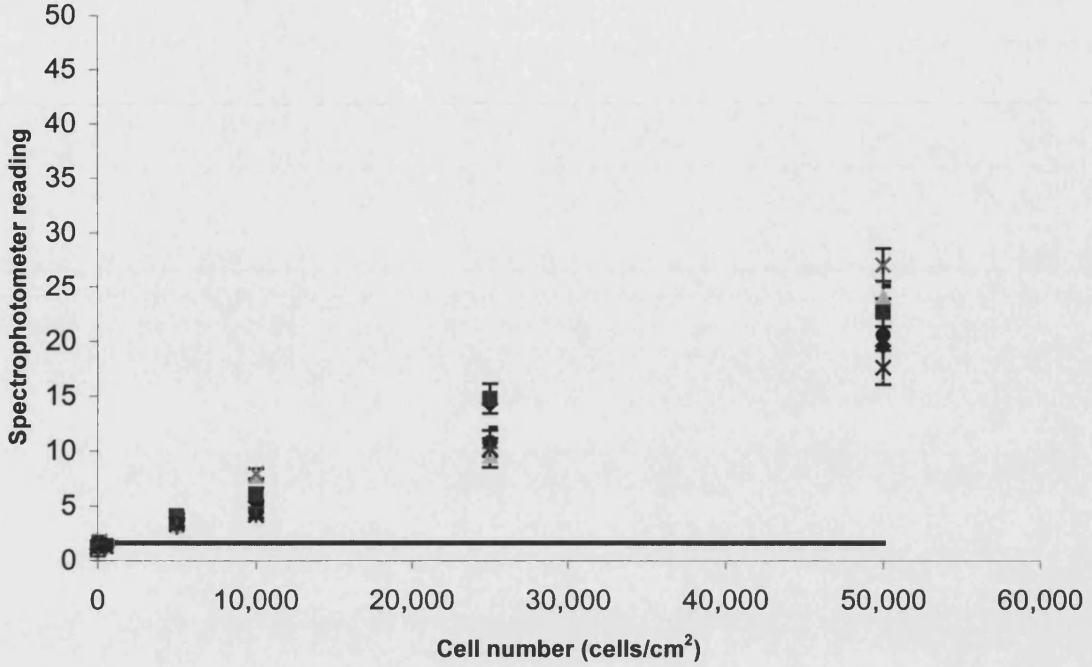
Spectrophotometer reading
50
45
40
35
30
25
20
15
10
5
0
0
10,000
20,000
30,000
40,000
50,000
60,000
Cell number (cells/cm²)

A

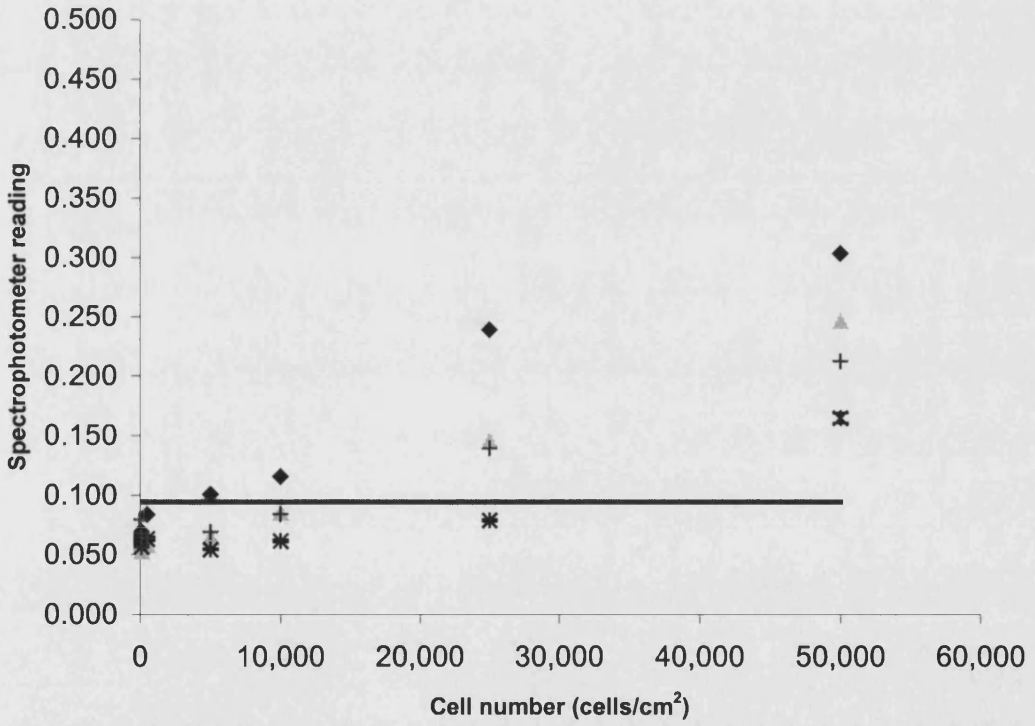
Spectrophotometer reading
0.500
0.450
0.400
0.350
0.300
0.250
0.200
0.150
0.100
0.050
0.000
0
10,000
20,000
30,000
40,000
50,000
60,000
Cell number (cells/cm²)

B

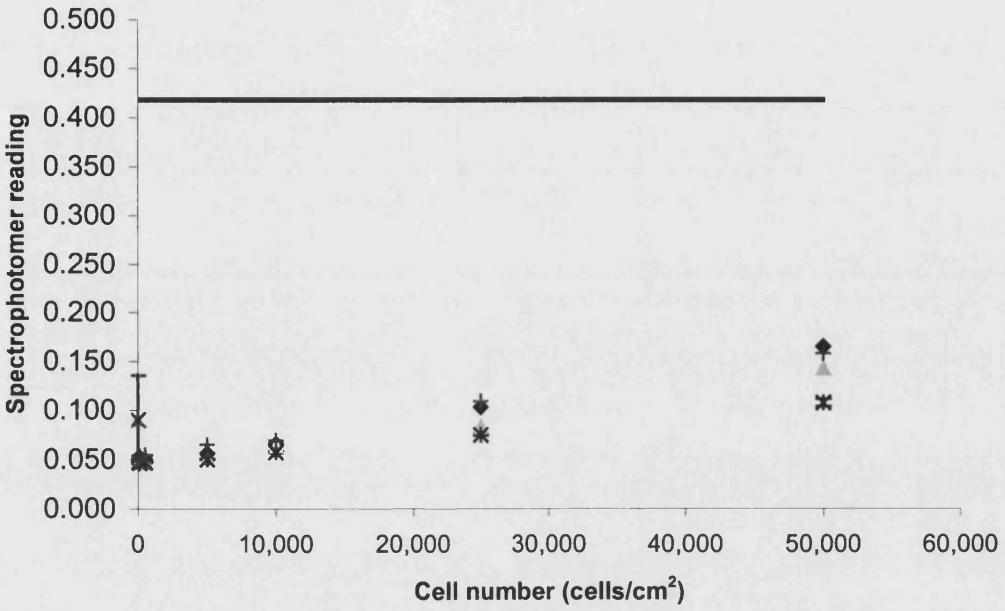

C

Figure C.2. Comparison of cell number quantitative assays.
(A) Picogreen, (B), MTT, (C) Methylene Blue. — 50:50 membrane reading. Each data set represents the mean readings for repeat experiments.

C.3 ATTACHMENT KINETICS

To establish a suitable time to allow attachment to take place, a media solution containing the cell line 560pMT1 was added to TCP well plates. The wells were seeded at 25,000 cell/cm^2 and the number of cells attached to the surface was calculated using the picogreen assay at various time points up to 24 hours.

During the first half hour, 8,000 cells/cm^2 had attached to TCP whereas 2,500 cell/cm^2 had attached to NTCP (Figure C.3). This trend of TCP having more cells attached than NTCP continued for the entire time range. After three hours, the number of cells attached to the TCP levelled out at a mean density of 24,000 cells/cm^2, 96% of the initial seeding density, and remained close to this density for the remaining 21 hours. The mean cell density on the NTCP dropped between 3- and 6 hours but was constant thereafter.

It was concluded that a minimum attachment time of 6 hours would allow a reasonable representation of attachment to the PLGA membranes since, like NTCP, they are not specifically treated for cell culture.

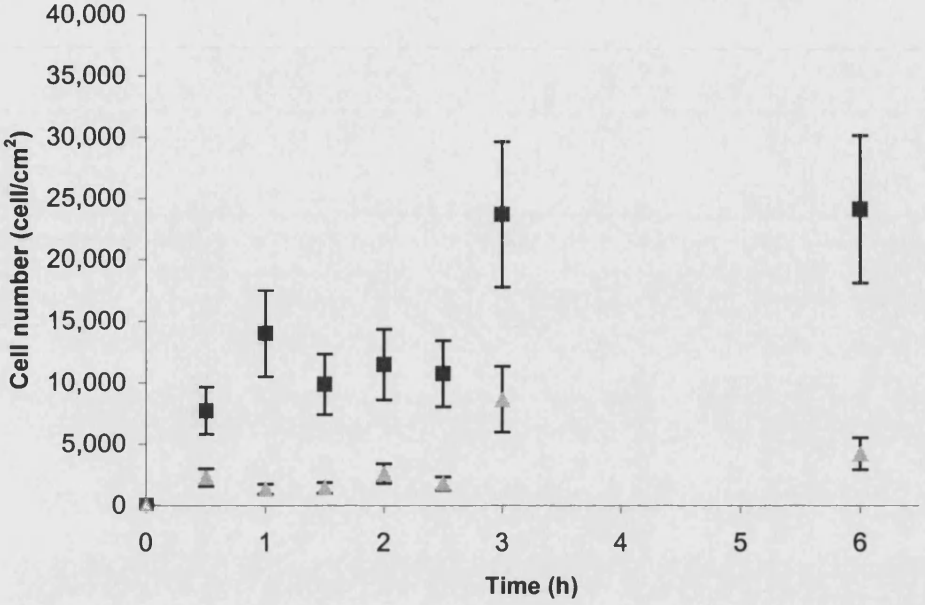

A

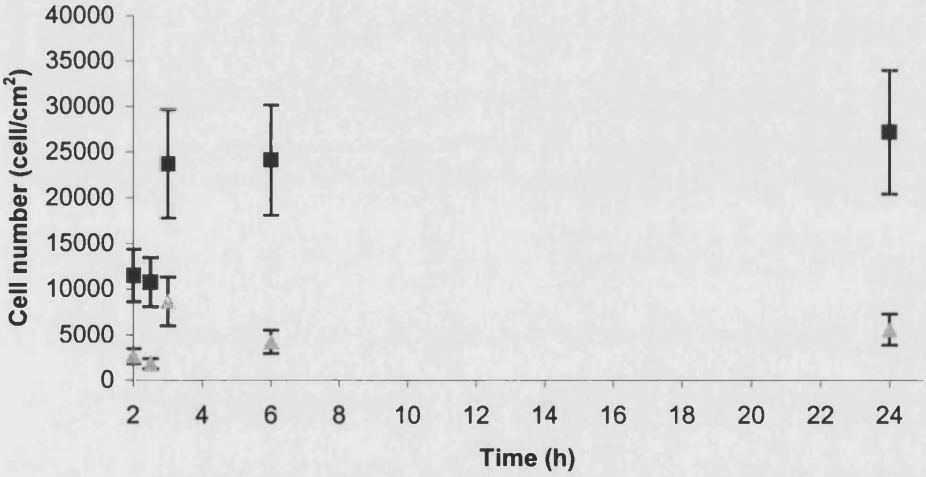

B

Figure C.3. Attachment kinetics of the osteoblast cell line 560pMT1.
(A) attachment kinetics over a 6 hour period, (B) attachment kinetics over a 25 hour period. ■ TCP, ▲NTCP

C.4 CELL MORPHOLOGY STAIN SELECTION

To analyse the morphology of the cells attached to the membranes a suitable stain needed to be selected. Cultures on TCP and 75L:25 were fixed with 10%NBF were stained with MB and Haematoxylin Harris for 10 min and 30 min respectively, and viewed under a reflective light microscope.

It can be seen from Figure C.4 that the cultures stained with MB were more visible on the membranes and more detail could be seen of the protrusions, than those stained with Haematoxylin Harris.

MB was selected as the stain for morphological assessment due to the clarity fo the cells on the membranes.

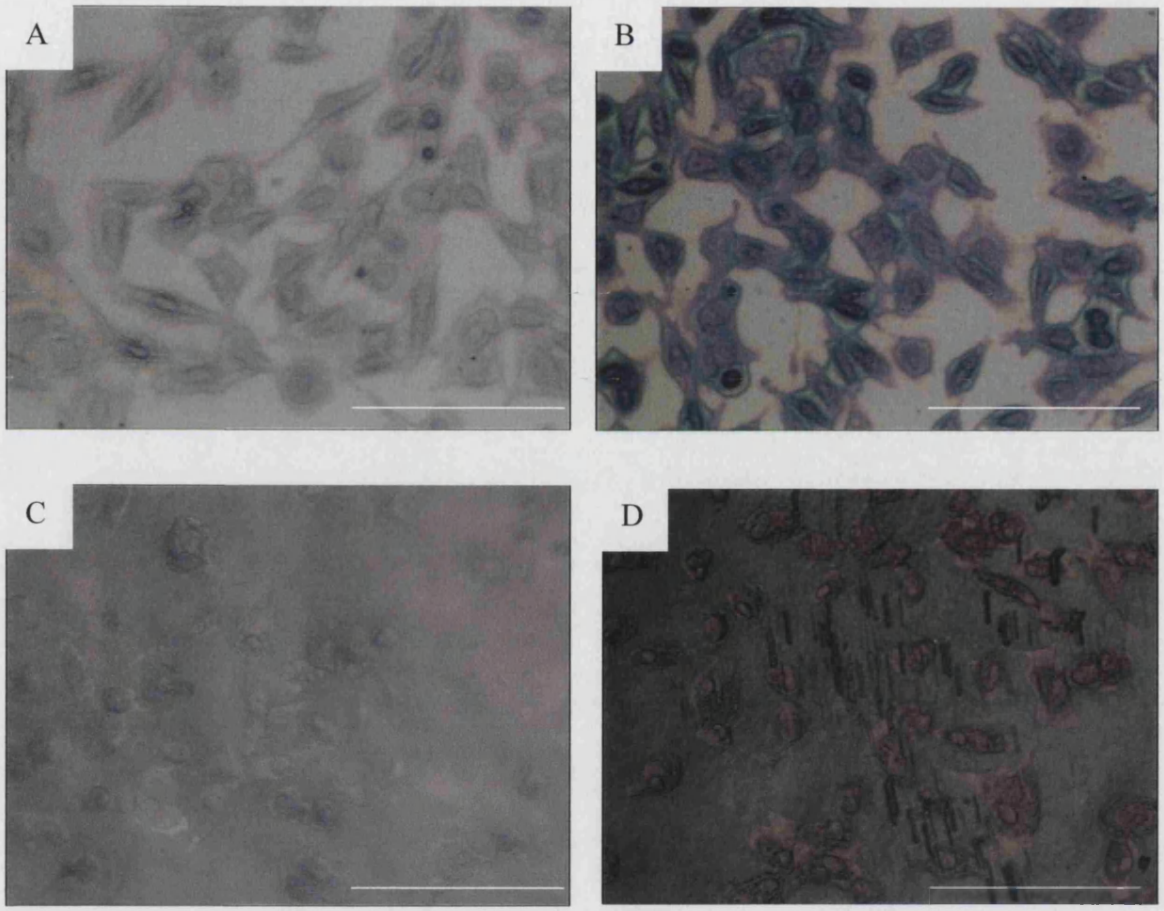

Figure C.4. Comparison of haematoxylin and methylene blue stains for morphology visualisation.

Primary osteoblasts at 6h post-seeding; (A) haematoxylin stained cells on TCP (B) methylene blue stained cells on TCP, (C) haematoxylin stained cells on 75L:25 (D) methylene blue stained cells on 75L:25. Scale bar 50 μm.

APPENDIX D
PHYSICAL PROPERTIES OF POLYMERS AND SOLVENTS

D.1 SOLVENT PROPERTIES

Table D.1. Physical properties of selected solvents.

Property	NMP	1,4-Dioxane	Chloroform
Structure	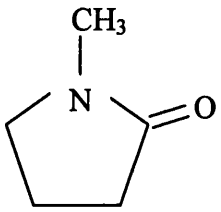	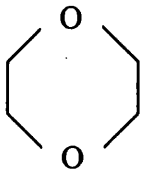	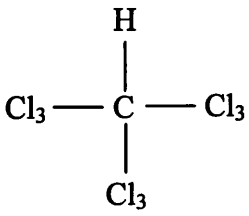
Molecular formula	C_5H_9NO	$C_4H_8O_2$	$CHCl_3$
Mw (g/mol)	99.13	88.11	119.38
Melting point (°C)	-23	11.8	63
Boiling point (°C)	202	100 - 120	61
Vapour density (relative to air)	NONVOLATILE at STP	3	4.1
Vapour pressure (mm Hg at 20 °C)	0.29	27	159
Density (g cm^{-3})	1.026	1.034	1.48
Specific gravity	1.033	/	/
pH	8-9.5	/	/
Flash point (°C)	95	12	/
Explosion limits	1.3 - 9.5 %	2% - 22%	/
Autoignition temperature (°C)	346	180	/
Water solubility	miscible	miscible	immiscible
EVAPORATION RATE BuAc=1:	0.03	/	/

VOC	806 Gm/L	/	/
ODP	0.00	/	/
Toxicology	Skin, eye and respiratory irritant. Typical OES-LTEL 25 ppm.	Probable carcinogen. Toxic. Harmful by inhalation, ingestion and through skin contact. Irritant.	This material causes cancer in laboratory animals, and is IARC listed as a probable human carcinogen. Inhalation and ingestion are harmful and may be fatal. May cause reproductive damage. Irritant. Exposure to alcohol may increase toxic effects. Prolonged or repeated skin contact may cause dermatitis. Typical TLV 50 ppm.

Data from Oxford University MSDS
/ Data not available

D.2 POLYMER PROPERTIES

The tables below summarise the properties of the PLGA as purchases (Table D.2) and the suitable polymer concentrations in the spinning dopes (Table D.3 and D.4). The data in Table D.3 and D.4 has been extrapolated in some instances where the concentrations tested are within the viscosity range. This assumes that no gelling occurs at the higher polymer concentrations.

Table D.2. Polymers and their specifications used in this work.

Polymer	IV dL/g	Tg	Mw kD	Mn kD	polydispersity
100:0	0.71	49.44	109	63	1.761
100L:0	1.6				
85:15	0.76	50.8	123.6	80.4	1.54
75L:25	1.4		246		
75:25	0.77	50.6	123	74	1.68
65:35	0.76	47.2	114	65	1.7
50:50	0.75	48.40	74	45	1.65
45:55	0.15	37.6	11.8		1.8

Data from alkermes certificate of analysis sheets.

Table D.3. PLGA-NMP solution concentration ranges suitable for spinning at various temperatures.

NMP		Concentration (w/w%)					
	Temperature	20°C		25°C		30°C	
	Viscosity	1 Pas	10 Pas	1 Pas	10 Pas	1 Pas	10 Pas
Polymer	100:0	21	32	22	35	23	37
	85:15	19	30	20	32	22	34
	75:25	18	28	19	30	20	32
	65:35	18	27	19	28	20	29
	50:50	21	36	22	30	23	38
	45:55	-	-	-	-	-	-
	751:25	10	18	11	19	12	21

The concentrations shown are for the minimum ideal spinning viscosity, 1 Pas and the maximum ideal spinning viscosity, 10 Pas.

Table D.4. PLGA-dioxane solution concentration ranges suitable for spinning at various temperatures.

Dioxane		Concentration (w/w%)					
	Temperature	20°C		25°C		30°C	
	Viscosity	1 Pas	10 Pas	1 Pas	10 Pas	1 Pas	10 Pas
Polymer	100:0	12	27	20	25	18	24
	85:15	8	25	9	21	12	23
	75:25	12	25	20	27	18	26
	65:35	12	25	15	26	16	27
	50:50	19	27	21	32	20	28
	45:55	-	-	-	-	-	-
	751:25	6	13	7	14	7	14

The concentrations shown are for the minimum ideal spinning viscosity, 1 Pas and the maximum ideal spinning viscosity, 10 Pas.

APPENDIX E
CALIBRATION DATA

E.1 CALIBRATIONS FOR HOLLOW FIBRE SPINNING

E.1.1 TAKE-UP RATE

The rotational speed of the take-up reel used for hollow fibre spinning can be converted into a linear speed as follows.

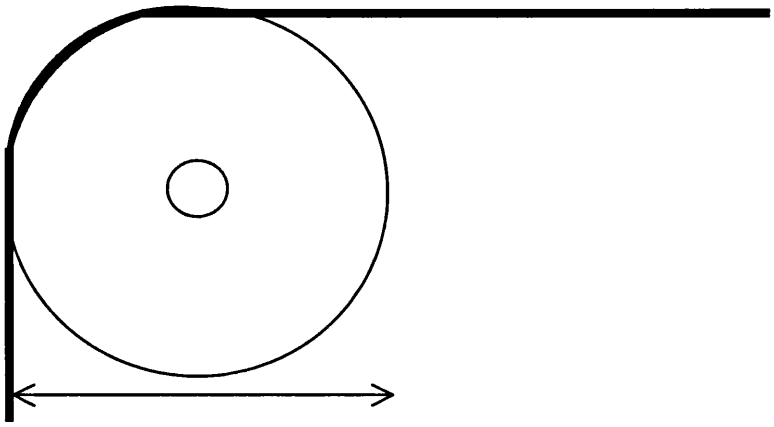

Figure E.1. Schematic of the take up reel showing the diameter (d_r).

Circumference of take up reel = Πd_r

= 3.14... x 7.7

= 24.19 cm 2d.p.

So

Linear take-up rate (m/min) = [(rotational take-up rate rpm) x (circumference of take-up reel cm)] / (100 cm/m)

Example

Linear take-up rate = (22.5 x 34.56)/100

= 5.44 m/min

Table E.1. Rotational take-up rate and corresponding linear take-up rate.

Rotational take-up rate	Linear take-up rate
(rpm)	(m/min)
0	0
10	2.42
15	3.63
20	4.84
22.5	5.44
25	6.05
30	7.26
32	7.74
35	8.47
35	8.47
40	9.68
45	10.89
50	12.10

Since the take-up rate was matched to the rate of hollow fibre formation, the linear take-up rate is hereafter referred to as the spinning rate.

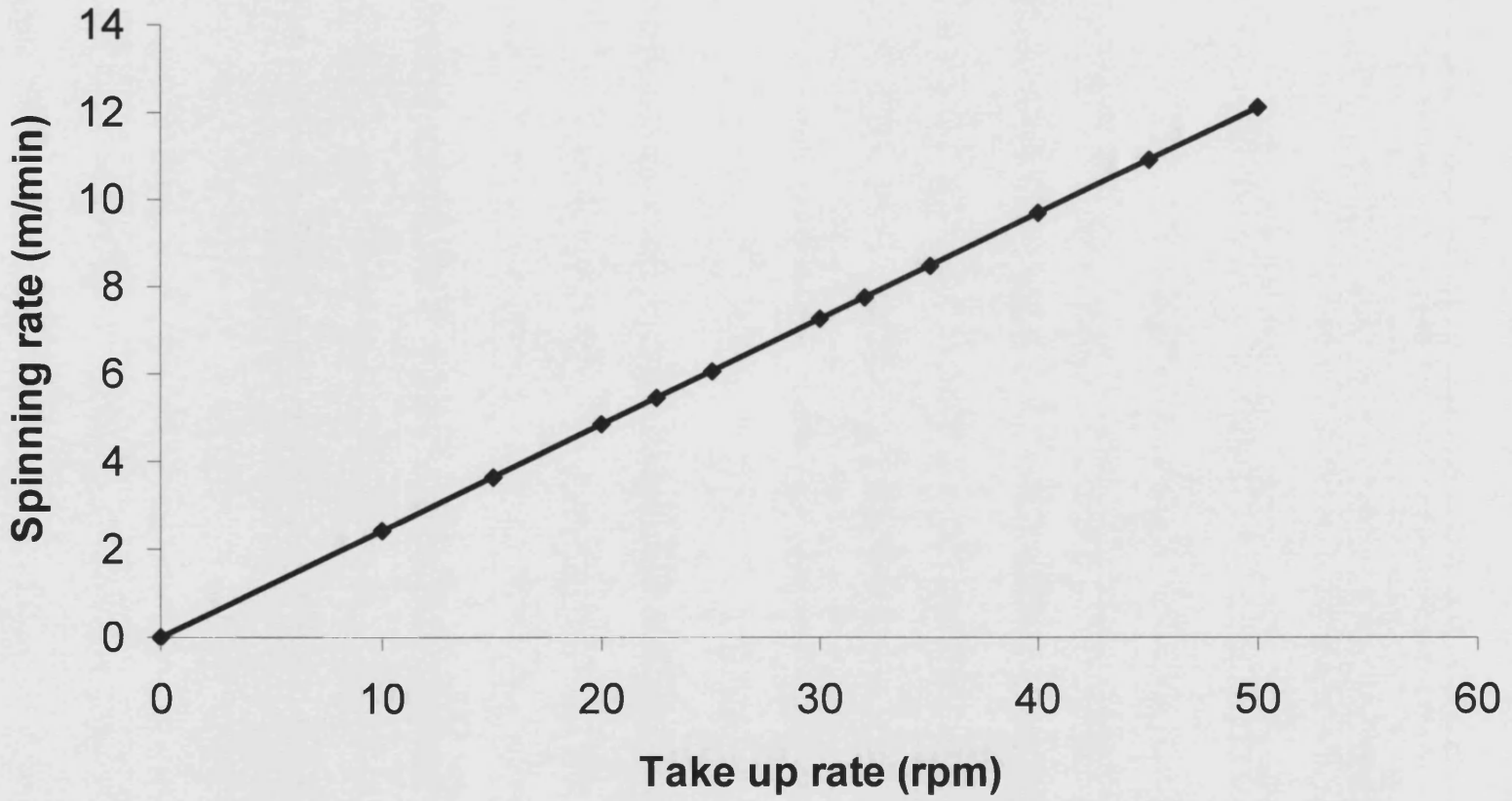

Figure E.2. Calibration graph for spinning rate based on take up rate. y = 0.2419x.

E.1.2 POLYMER SOLUTION FLOW RATE

Since the flow rate was set to the spin rate for the hollow fibre spinning, the volumetric flow rate of the polymer solution can be calculated as follows.

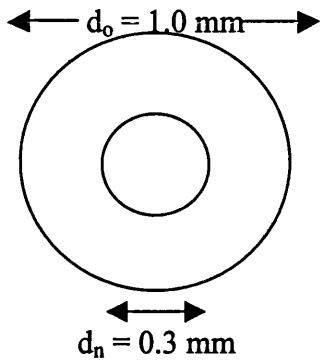

Figure E.3. Schematic of spinneret showing dimensions of diameter of exit port (d_o)and bore needle (d_n).

Volumetric flow rate = velocity x area of annular space

i.e.

Volumetric flow rate = (spin rate m/min) x (area of annular space cm) x (100 cm/m)

Area of annular space = area of outer diameter – area of needle diameter

$= \Pi d_o^2/4 - \Pi d_n^2/4$

$= \Pi(0.01)^2/4 - \Pi(0.003)^2/4$

$= 7.85 \times 10^{-5} - 7.07 \times 10^{-6}$

$= 7.15 \times 10^{-5}$ cm^2

Example for a take up rate of 22.5 rpm

Volumetric flow rate $= 5.44 \times (7.15 \times 10^{-5}) \times 100$

$= 0.039$ cm^3/min

Table E.2 Polymer solution flow rate as a function of take-up a rate and spinning rate.

Take-up rate	Spinning rate	Flow rate
(rpm)	(m/min)	(ml/min)
0	0	0.000
10	2.42	0.017
15	3.63	0.026
20	4.84	0.035
22.5	5.44	0.039
25	6.05	0.043
30	7.26	0.052
32	7.74	0.055
35	8.47	0.061
35	8.47	0.061
40	9.68	0.069
45	10.89	0.078
50	12.10	0.086

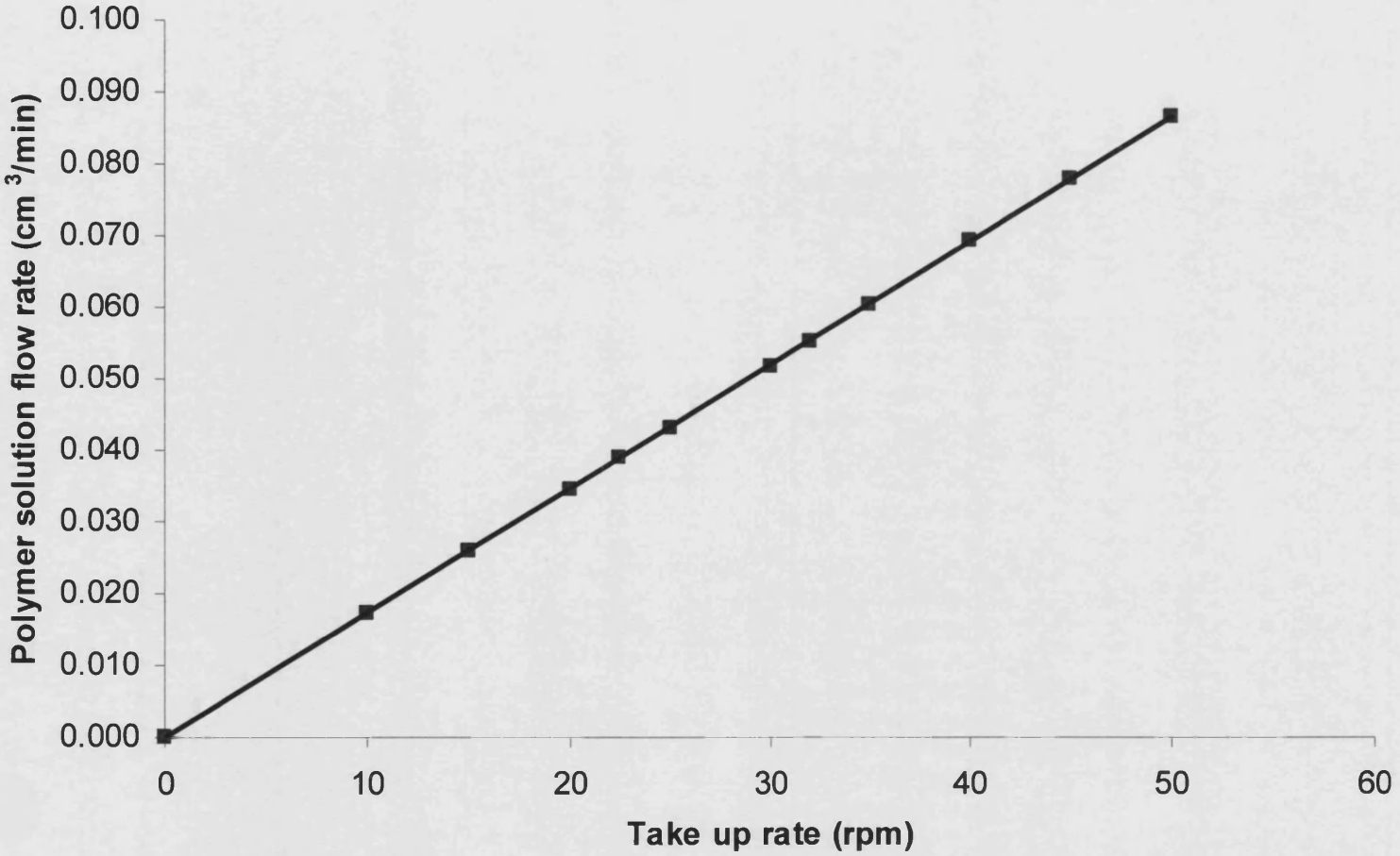

Figure E.4 Calibration graph for polymer flow rate based on take up rate. $y = 0.0017x$.

E.1.3 BORE FLOW RATE

The bore flow rate was calculated by measuring the time taken to collect 10 ml of the nonsolvent (water) then working out the volume collected in one minute. The calibration graph is shown in Figure E.5.

Table E.3. Bore liquid pump settings and corresponding bore flow rates for water.

Pump setting	Time/10ml (s)	ml/s	ml/min
2	260	0.04	2.31
3	190	0.05	3.16
5	112	0.09	5.36

E.1.4 AIR GAP RESIDENCE TIME

The air gap residence time is a function of air gap size and spinning rate. The calibration graph is shown in Figure E.6.

Air gap residence time (s) = (air gap cm)/[(spinning rate m/min) x (60 s/min) / (100cm/m)]

Example with 22.5 rpm take up rate, ie 5.44 m/min spinning rate and 3 cm air gap

Air gap residence time = 3 / (5.44 x 60 / 100)
= 0.643 s 3dp

Table E.4. Air gap residence times as a function of spinning rates at a selection of different air gaps.

Take up rate	Spinning rate		Air gap residence time (s)					
(rpm)	(m/min)	(cm/s)	0 cm	1cm	2cm	3cm	4cm	5cm
0	0.00	0.00	/	/	/	/	/	/
10	2.42	1.45	0.000	0.689	1.378	2.067	2.756	3.445
15	3.63	2.18	0.000	0.459	0.919	1.378	1.837	2.297
20	4.84	2.90	0.000	0.344	0.689	1.033	1.378	1.722
22.5	5.44	3.27	0.000	0.306	0.612	0.919	1.225	1.531
25	6.05	3.63	0.000	0.276	0.551	0.827	1.102	1.378
30	7.26	4.35	0.000	0.230	0.459	0.689	0.919	1.148
32	7.74	4.64	0.000	0.215	0.431	0.646	0.861	1.077
35	8.47	5.08	0.000	0.197	0.394	0.591	0.787	0.984
35	8.47	5.08	0.000	0.197	0.394	0.591	0.787	0.984
40	9.68	5.81	0.000	0.172	0.344	0.517	0.689	0.861
45	10.89	6.53	0.000	0.153	0.306	0.459	0.612	0.766
50	12.10	7.26	0.000	0.138	0.276	0.413	0.551	0.689

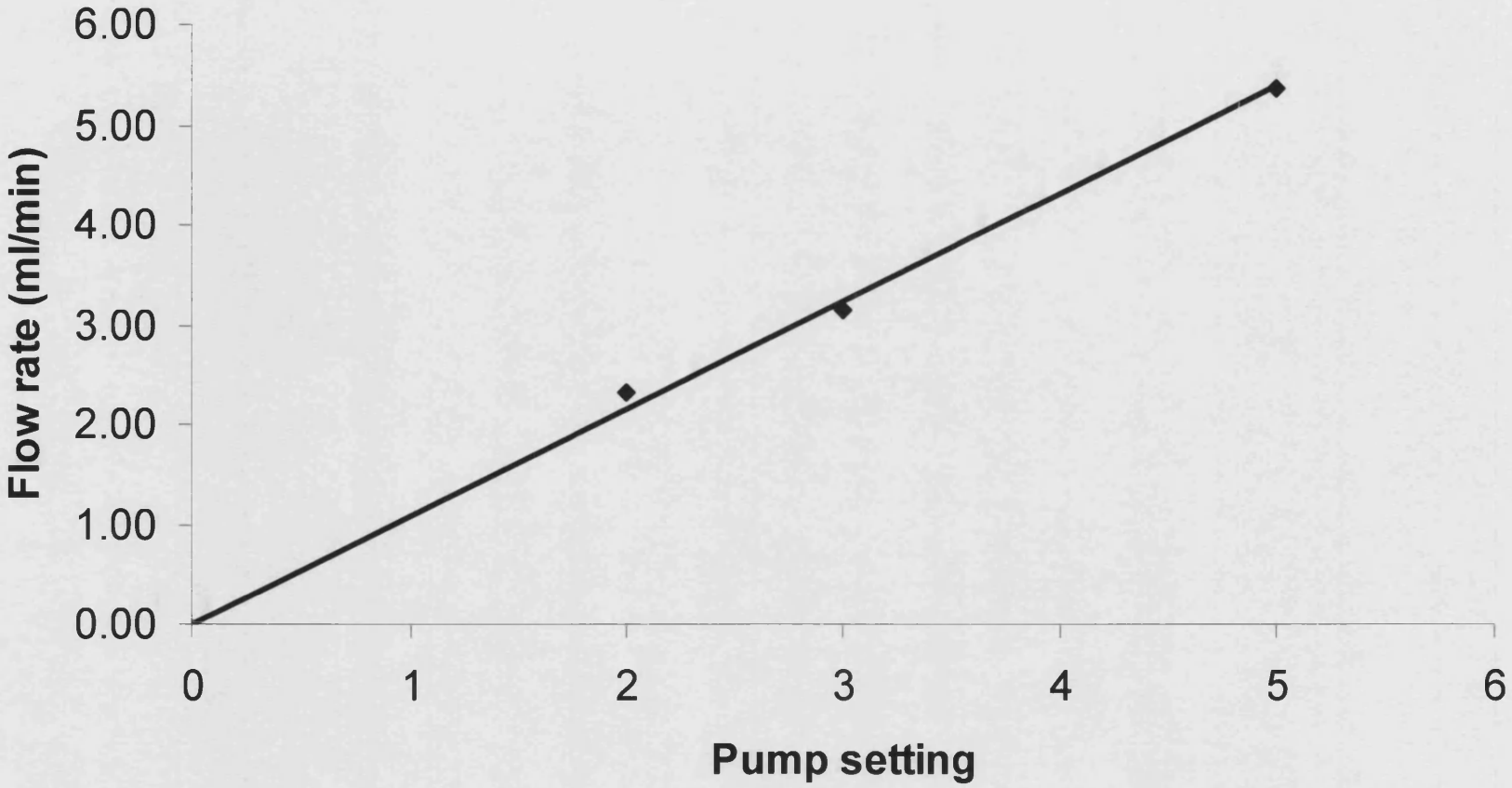

Figure E.5. Calibration graph for bore flow rate of water as a function of bore setting.

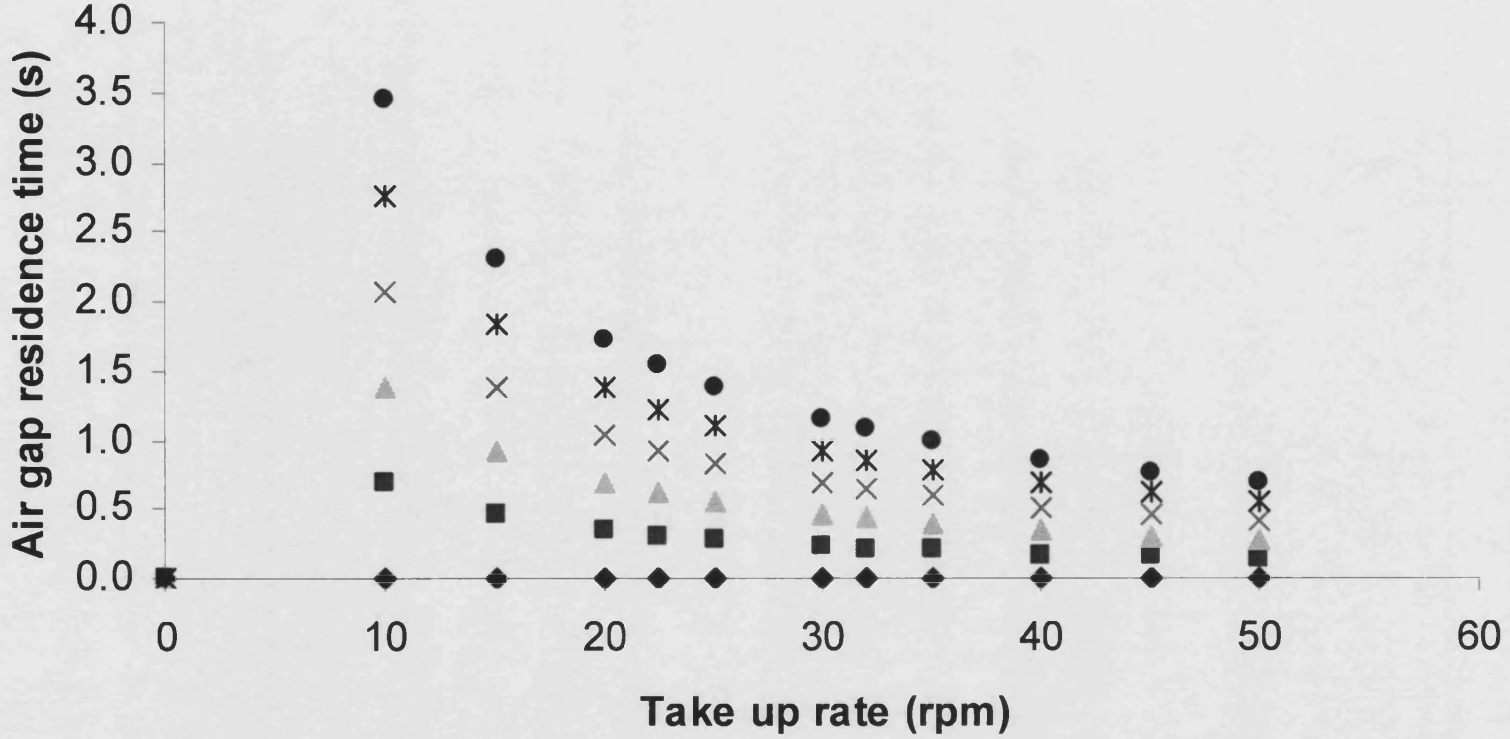

Figure E.6. Calibration graph for air gap residence time as a function of take up rate.
● 5 cm, ✳ 4 cm, × 3 cm, ▲2 cm ■ 1cm, ◆ 0 cm.

E.2 OTHER CALIBRATIONS

The following section shows the calibration charts for the peristaltic pumps used in the hollow fibre bioreactor set up in Chapter 8 (Figure E.7), the HPLC used in Chapter 6 (Figures E.8 and E.9) and the picogreen assay used in Chapters 7 and 8 (Figure E.10).

Table E.5. Calibration data for peristaltic pumps.

Pump setting (RPM)	Flow rate (ml/min)
2	0.16
4	0.34
6	0.53
8	0.67
10	0.86
15	1.27
20	1.74
25	2.14

Table E.6. Calibration data for HPLC degradation readings.

Concentration (w/v%)	HPLC reading (units of area)
0.02	393,904
0.04	484,861
0.08	1,006,007

Table E.7. Calibration data for HPLC NMP release readings.

Concentration (w/v%)	HPLC reading (units of area)
0.0001	744
0.0010	8496
0.0050	44779
0.0100	89177
0.1000	473608

Table E.8. Calibration data for picogreen assay.

DNA conc.	Fluorospectrometer reading										
(ng/ml)	Reading 1			Reading 2			Reading 3			Mean	SD
0	0.325	0.317	0.164	0.453	0.428	0.433	0.453	0.428	0.433	0.381	0.096
0.5	0.309	0.333	0.332	0.448	0.468	0.443	0.448	0.468	0.443	0.410	0.065
1	0.277	0.342	0.425	0.531	0.400	0.407	0.531	0.400	0.407	0.413	0.080
5	0.461	0.646	0.484	0.848	0.785	0.861	0.848	0.785	0.861	0.731	0.161
10	0.756	0.737	0.767	0.823	0.935	0.760	0.823	0.935	0.760	0.811	0.076
50	2.191	2.253	2.240	2.218	1.957	1.944	2.218	1.957	1.944	2.102	0.145
100	4.356	4.347	3.624	3.763	3.669	2.660	3.763	3.669	2.660	3.612	0.608
500	17.460	13.290	15.990	15.060	15.620	12.500	15.060	15.620	12.500	14.789	1.689
1000	25.270	25.080	31.630	24.000	31.840	29.360	24.000	31.840	29.360	28.042	3.434

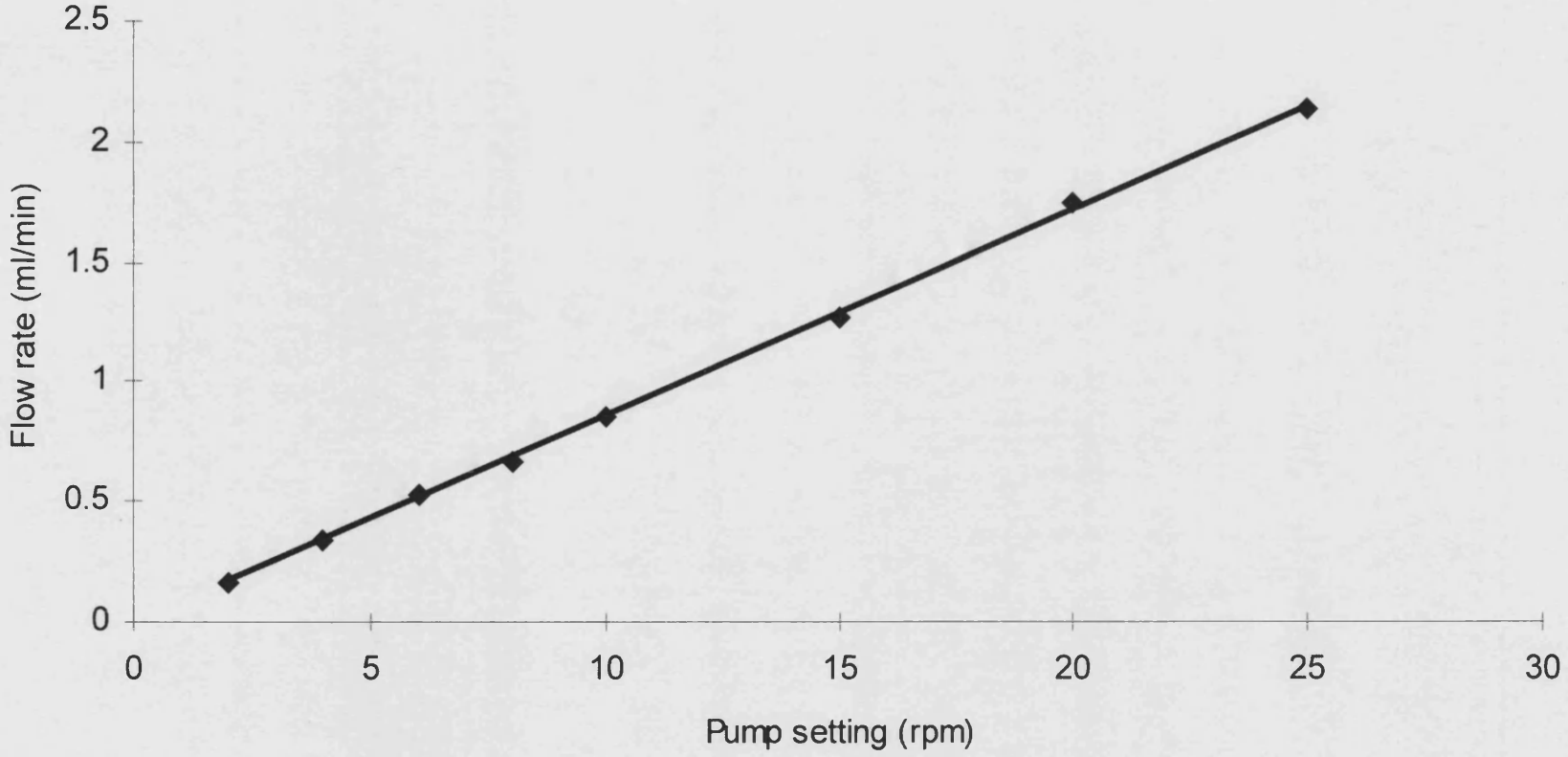

Figure E.7. Calibration chart for peristaltic pump used in the bioreactor system. $y = 0.0858x$

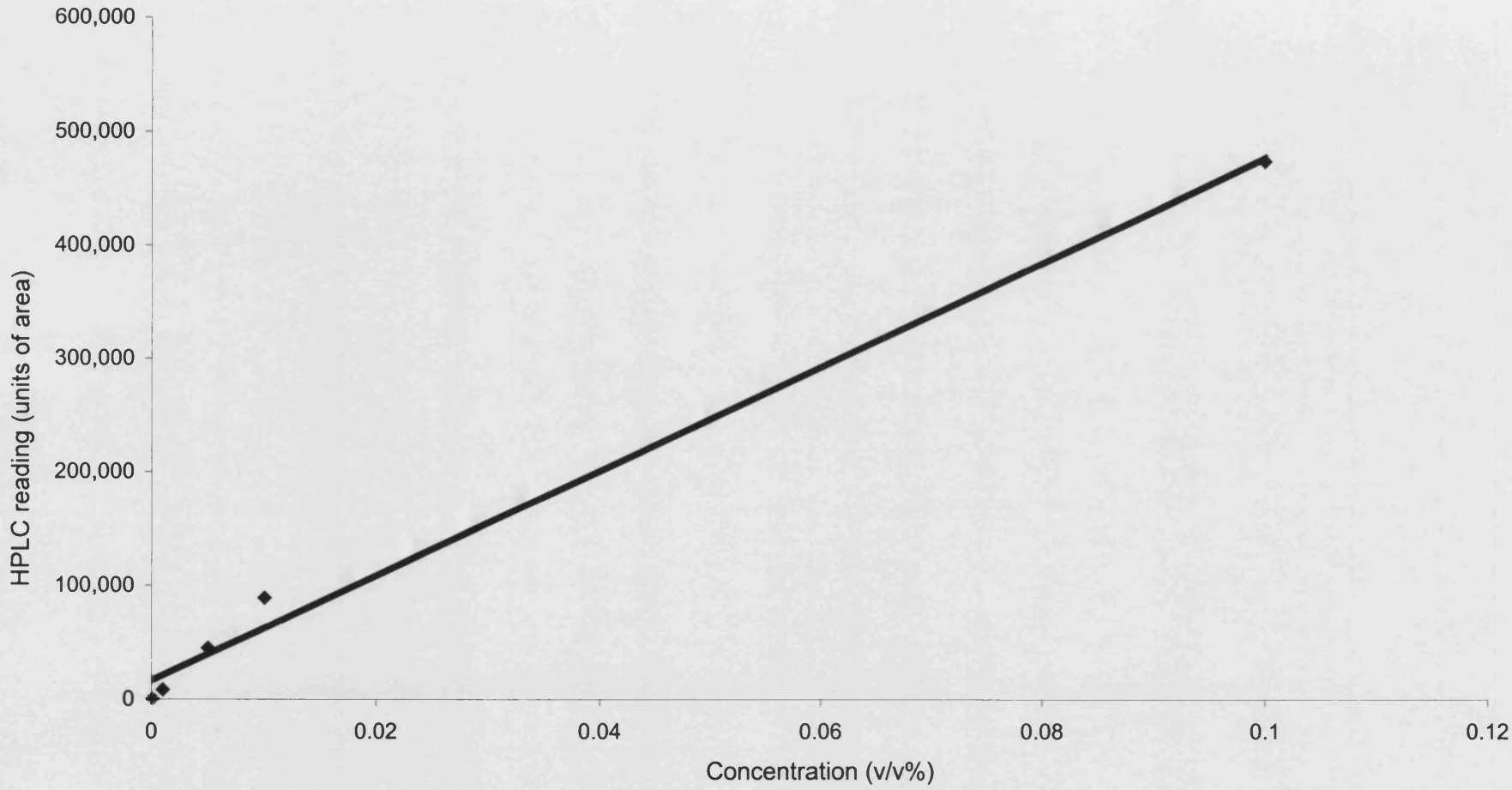

Figure E.8. Calibration chart for HPLC for NMP concentration. $y = 5 \times 10^{6}x + 16599$

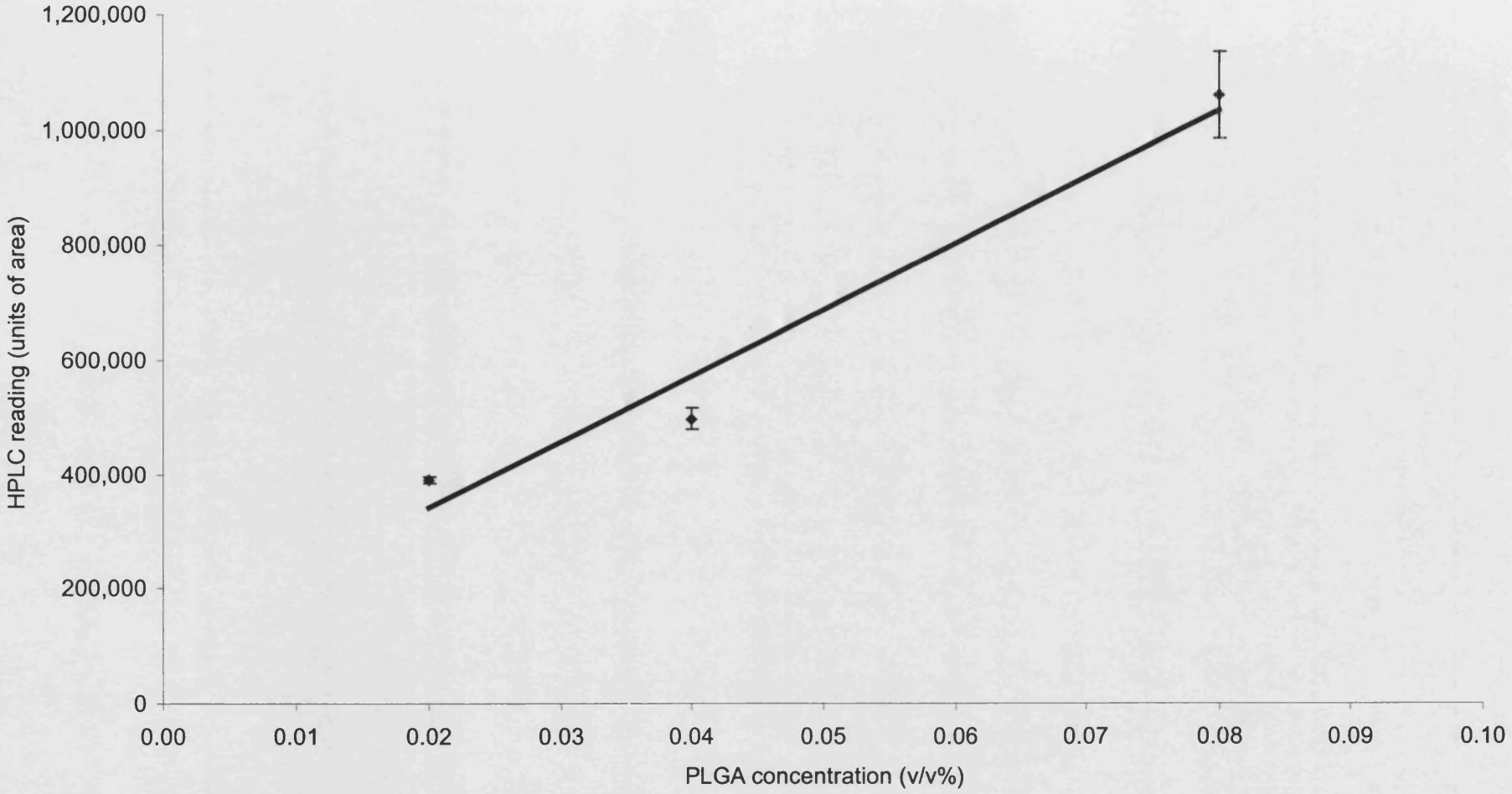

Figure E.9. Calibration chart for HPLC for the degradation of 75:25 in media. $y = 1 \times 10^{7}x + 110116$

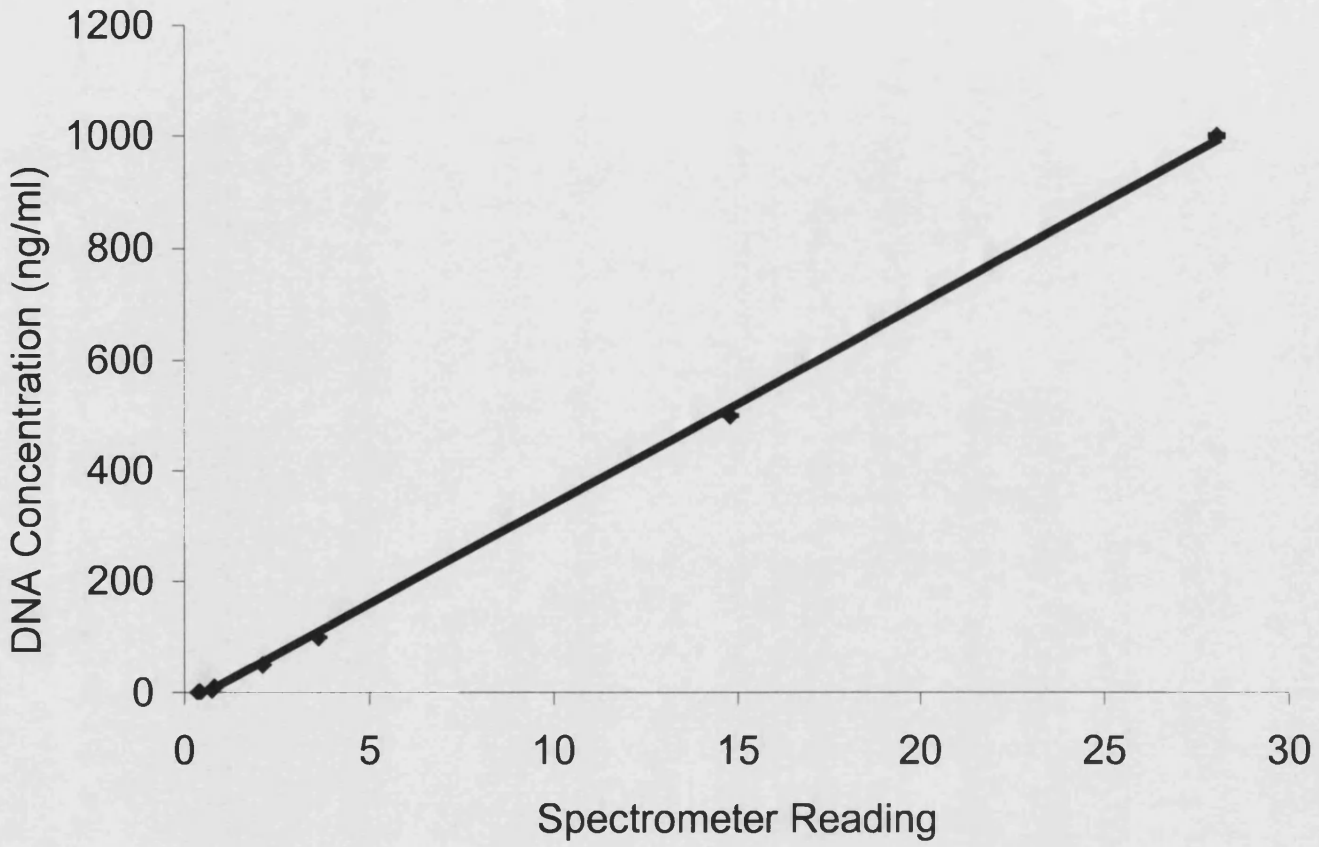

Figure E.10. Calibration chart for Picogreen assay using ATM buffer. y= 36.095x - 20.544

APPENDIX F

SAMPLE RAW DATA AND RELATED CALCULATIONS

F.1 EXAMPLE OF VISCOSITY RAW DATA

The viscosity is taken as the asymptote value at which the readings tend towards (Figure F.1).

Table F.1. Raw data for 20% 75:25 in NMP.

		Temperature (°C)		
		20	25	30
Shear no.	Shear stress (Pa)	Viscosity (Pas)		
2	0.07892	0.08513	0.07204	0.06144
4	0.1373	0.0927	0.07725	0.06667
6	0.2389	0.09348	0.08096	0.06936
8	0.4162	0.09584	0.08324	0.07196
10	0.724	0.09751	0.08515	0.07284
12	1.261	0.09882	0.0861	0.07423
14	2.195	0.09945	0.08677	0.07483
16	3.829	0.1001	0.08726	0.07526
18	6.662	0.1004	0.08755	0.07541
20	11.59	0.1006	0.08791	0.07582
22	20.19	0.1009	0.08795	
24	35.2		0.08811	
26	61.25			
Viscosity of solution (Pas)		**0.101**	**0.088**	**0.076**

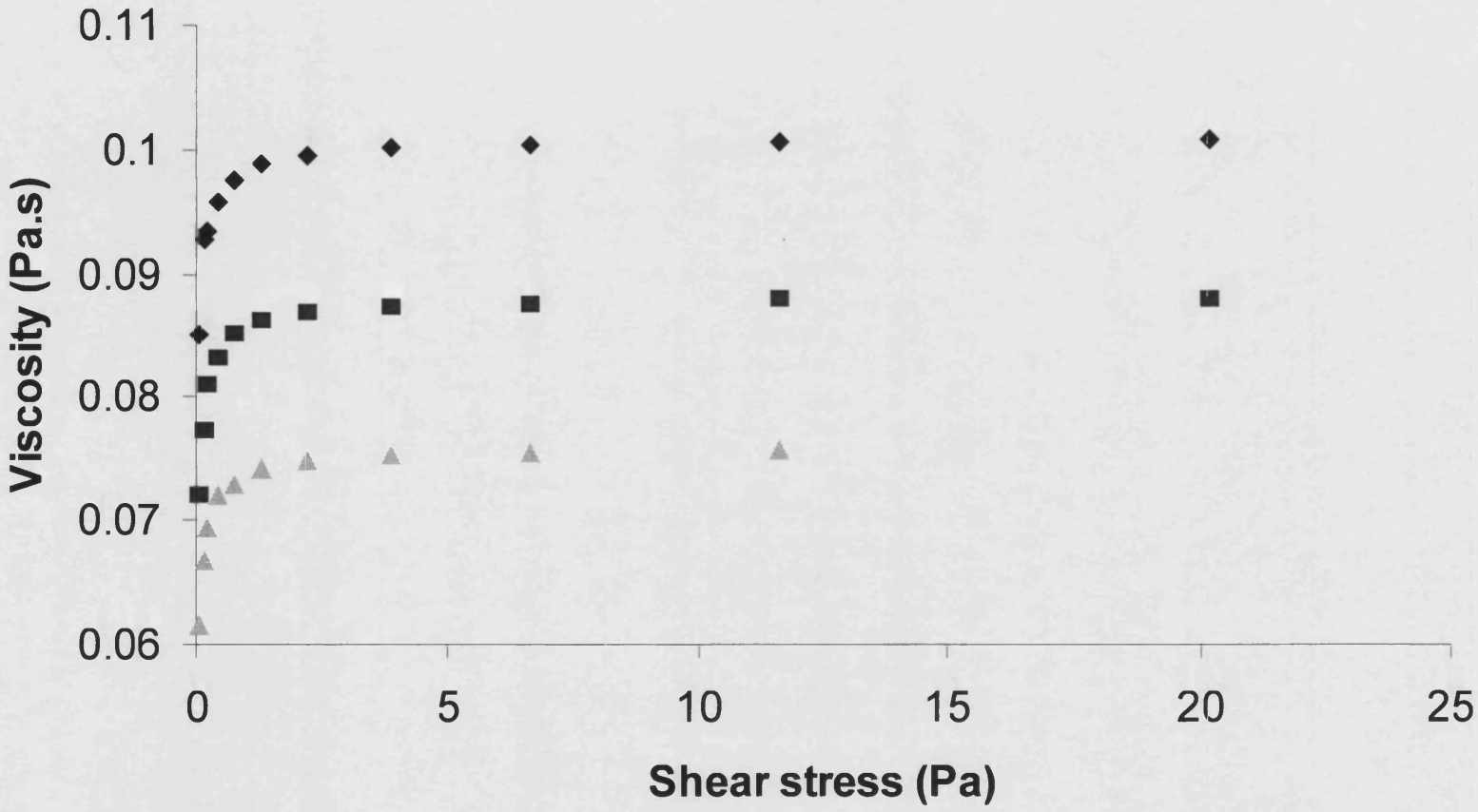

Figure F.1. Rheometer readings for 10% 7525DL in NMP.
◆ = 20 °C, ■ = 25 °C, ▲ = 30 °C

F.2 SAMPLE CALCULATION FOR THE PICOGREEN ASSAY

The picogreen assay was carried out as detailed in Section 3.5.1. The raw data for HBDC 6 hour attachment is shown in Tables F.2 and F.3.

Table F.2. Fluorospectrometer readings for the seeded membranes.

seeded material	fluorospectrometer reading											
100DL	17.72	16.23	21.37	20.22	17.08	15.86	29.71	14.08	11.53	11.91	11.50	12.56
7525DL	24.72	25.53	21.13	32.53	49.60	28.56	15.62	17.82	31.66	29.97	31.40	24.82
5050DL	25.43	43.20	33.91	25.42	38.87	20.01	18.08	13.33	28.56	17.98	18.55	18.81
7525LG	47.60	27.20	45.68	31.58	23.75	20.96	47.06	22.19	14.90	15.08		
TCP	26.97	54.83	27.05	34.43	38.40	38.80	30.64	33.23	22.93			

Table F.3. Fluorospectrometer readings for the unseeded membranes.

unseeded material	fluorospectrometer reading						mean
100DL	0.45	0.45	0.63	0.58	0.39	0.56	0.51
7525DL	1.61	1.22	0.82	0.60	0.51	0.44	0.86
5050DL	0.59	0.61	0.44	0.42	0.41	0.43	0.48
7525LG	0.61	0.53	0.98	0.71	0.73	0.62	0.70
TCP	0.48	0.38	0.41	0.45	0.27	0.42	0.40

To eliminate background noise, the mean unseeded reading for each susbtrate was taken away from each seeded reading (Table F.4).

Table F.4. Fluorospectrometer readings for the unseeded membranes.

Material	Actual fluorospectrometer reading (seeded reading-unseeded reading)												Mean	SD
100DL	17.21	15.72	20.86	19.71	16.57	15.35	29.20	13.57	11.02	11.40	10.99	12.05	16.14	5.28
7525DL	23.86	24.67	20.27	31.67	48.74	27.70	14.76	16.96	30.80	29.11	30.54	23.96	26.92	8.77
5050DL	24.95	42.72	33.43	24.94	38.39	19.53	17.60	12.85	28.08	17.50	18.07	18.33	24.70	9.31
7525LG	46.90	26.50	44.98	30.88	23.05	20.26	46.36	21.49	14.20	14.38	/	/	28.90	12.86
TCP	26.57	54.43	26.65	34.03	38.00	38.40	30.24	32.83	22.53	/	/	/	33.74	9.41

Using the calibration curve for the fluorospectrometer (Appendix E), the concentration of DNA and subsequent cell numbers was calculated as follows.

Calibration curve equation;

$y = 36.095x - 20.544$

where y is the DNA concentration (ng/ml) and x is the fluorospectrometer reading.

Since each sample contained 0.5ml ATM, the DNA conc (ng/ml) is twice that of the total DNA content per sample, to calculate total (DNA per sample) = [DNA conc (ng/ml)] x 0.5ml.
By dividing the (DNA per sample) by the surface area of the sample, the amount of DNA, and hence cell number, can be calculated per unit area.
Each cell contains 5.5×10^{-12} g DNA, ie 5.5pg DNA (Blumenstein *et al.* 2002).

Table F.5. Cell number calculations.

	spec reading		**DNA conc (ng/ml)**		**DNA/sample (ng)**		**DNA conc (ng/cm^2)**		**cell number ($cell/cm^2$)**			**normalised cell number ($cells/cm^2$)**		
Material	Mean	SD	Mean (y)	SD	Mean (y)	SD	Mean	SD	Mean	SD	SE	Mean	SD	SE
100DL	16.1	5.3	562	169.9	280.9	85.0	73.4	22.2	13,337	4,033	1,164	0.47	0.14	0.04
7525DL	26.9	8.8	951	296.1	475.5	148.1	124.1	38.7	22,572	7,029	2,029	0.79	0.25	0.07
5050DL	24.7	9.3	871	315.6	435.5	157.8	113.7	41.2	20,673	7,490	2,497	0.73	0.26	0.09
7525LG	28.9	12.9	1,023	443.5	511.4	221.8	133.5	57.9	24,275	10,528	3,329	0.85	0.37	0.12
TCP	33.7	9.4	1,197	319.1	598.6	159.6	156.3	41.7	28,419	7,575	2,187	1.00	0.27	0.08

The data was then plotted as shown in Figure F.2.

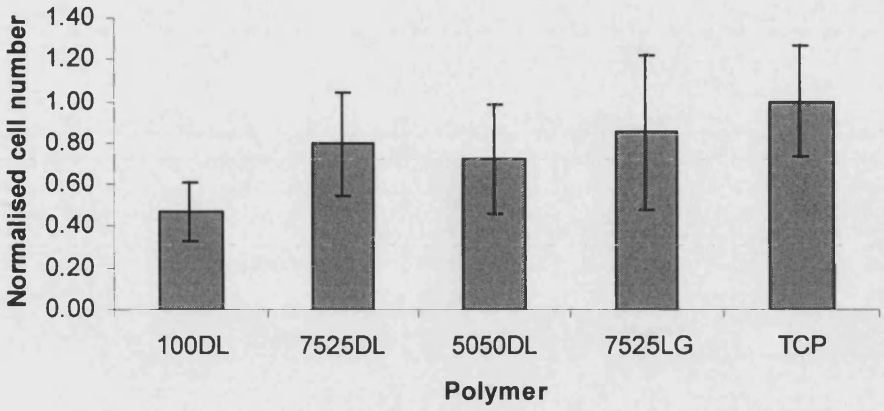

Figure F.2. Graph of normalised HBDC cell number for different polymers.

F.3 EXAMPLE STATISTICS

The statistics was carried out using SPPS. Data for Figure 6.8 Number of HBDC's attached to PLGA membranes 6h post-seeding is shown as an example.

Table F.6. Descriptives for the normalized cell numbers.

	N	Mean	Std. Deviation	Std. Error	95% Confidence Interval for Mean		Minimum value	Maximum value
					Lower Bound	Upper Bound		
TCP	9	33.7402	9.4104	3.1368	26.5068	40.9737	22.53	54.43
50:50	12	24.6982	9.3119	2.6881	18.7817	30.6147	12.85	42.72
75:25	12	26.9160	8.7735	2.5327	21.3416	32.4904	14.76	48.74
75L:25	10	28.9030	12.8573	4.0658	19.7054	38.1006	14.20	46.90
100:0	12	16.1365	5.2765	1.5232	12.7840	19.4890	10.99	29.20
Total	55	25.5582	10.6403	1.4347	22.6817	28.4347	10.99	54.43

Table F.7. Multiple Comparisons for the Dependent Variable, the normalised cell number using Tukey post hoc tests.

		Mean Difference (I-J)	Std. Error	Sig.	95% Confidence Interval	
(I) Substrate	(J) Substrate				Lower Bound	Upper Bound
TCP	5050	9.0421	4.0907	.193	-2.5340	20.6181
	7525	6.8242	4.0907	.462	-4.7519	18.4003
	7525LG	4.8372	4.2624	.787	-7.2248	16.8992
	100	17.6037*	4.0907	.001	6.0276	29.1798
5050	TCP	-9.0421	4.0907	.193	-20.6181	2.5340
	7525	-2.2178	3.7873	.977	-12.9352	8.4995
	7525LG	-4.2048	3.9721	.827	-15.4453	7.0356
	100	8.5617	3.7873	.175	-2.1557	19.2790
7525	TCP	-6.8242	4.0907	.462	-18.4003	4.7519
	5050	2.2178	3.7873	.977	-8.4995	12.9352
	7525LG	-1.9870	3.9721	.987	-13.2275	9.2535
	100	10.7795*	3.7873	.048	6.214E-02	21.4969
7525LG	TCP	-4.8372	4.2624	.787	-16.8992	7.2248
	5050	4.2048	3.9721	.827	-7.0356	15.4453
	7525	1.9870	3.9721	.987	-9.2535	13.2275
	100	12.7665*	3.9721	.019	1.5260	24.0070
100	TCP	-17.6037*	4.0907	.001	-29.1798	-6.0276
	5050	-8.5617	3.7873	.175	-19.2790	2.1557
	7525	-10.7795*	3.7873	.048	-21.4969	-6.2137E-02
	7525LG	-12.7665*	3.9721	.019	-24.0070	-1.5260

* The mean difference is significant at the .05 level.

F.4 MEAN PORE SIZE CALCULATION METHOD

Below is the set of equations used to calculate mean pore size by gas permeation analysis, the results of which are shown in Chapter 5. The example given is for 75:25-NMP-water spun from a 20% polymer concentration dope, at 7.7 m/min with a zero air gap.

Table F.8. Conversions and constants used in the calculation of the mean pore size and effective surface porosity.

Conversions				Constants		
1	psi	6894.74483	Pa	R	8.3145	$J K^{-1} mol^{-1}$
1	atm	14.5038	psi	μ_{N2}	1.80E-02	g/m s
18	°C	291.15	K	M_{N2}	28	g/mol
1	cm^3	1.00E-06	m^3			

1] Calculate mean volumetric gas flow rate

(mean volume of gas measured in time t) cm^3 = (sum of volume of gas measured in time t) cm^3 / (number of readings)

(mean gas flow rate) cm^3/s = (mean volume of gas measured in time t) cm^3 /(time t) s

Table F.9. Raw data and mean volumetric gas flow rate.

Pressure	Time						volume	gas flow rate
psig	sec					mean	cm^3	cm^3/s
5	17.00	18.00	17.00	17.00		17.25	1	0.058
6	13.00	13.00	13.00	13.00		13.00	1	0.077
8	9.00	9.00	9.00	9.00		9.00	1	0.111
10	14.53	14.59	14.45	14.29		14.47	2	0.138
12	11.63	11.48	11.38	11.37	11.47	11.47	2	0.174
14	9.93	9.78	9.76	9.57		9.76	2	0.205
16	8.35	8.32	8.28	8.37		8.33	2	0.240
18	11.17	11.11	11.14	11.17		11.15	3	0.269
20	9.69	9.80	9.69	6.69		8.97	3	0.335
25	10.18	10.11	10.13	10.07		10.12	4	0.395
30	8.17	8.19	8.08	8.13		8.14	4	0.491
35	6.88	6.71	6.81	6.8		6.80	4	0.588
40	5.84	5.87	5.78	5.9		5.85	4	0.684

2] Calculate mean molar gas flow rate

First, convert pressure readings from psig to Pa

(pressure) Pa = (gauge pressure reading + 14.5038) psig x 6894.74483 Pa/psi

Then, convert mean volumetric flow rates from cm^3 to m^3

(volume) m^3 = (volume) cm^3 x 10^{-6} m^3/cm^3

Use ideal gas law $P_AV = nRT$ where P_A = absolute pressure in bubble column Pa,

V = volume m^3, n= number of moles, R = universal gas constant J K^{-1} mol^{-1},

T = temperature K

If V is volumetric flow rate, n will be molar flow rate

so,

$n = P_AV/RT$

(molar gas flow rate) mol/s = {(absolute pressure) Pa x (volumetric flow rate) m^3/s} / {(universal gas constant) J K^{-1} mol^{-1} x (temperature) K}

Table F.10. Mean molar flow rate.

Pressure		mean molar flow rate
psig	P_A (Pa)	(mol/s)
5	134,474	2.39E-11
6	141,368	3.18E-11
8	155,158	4.59E-11
10	168,947	5.71E-11
12	182,737	7.21E-11
14	196,526	8.47E-11
16	210,316	9.92E-11
18	224,105	1.11E-10
20	237,895	1.38E-10
25	272,369	1.63E-10
30	306,842	2.03E-10
35	341,316	2.43E-10
40	375,790	2.83E-10

3] Calculate surface area for gas permeation

Use area of a cylinder A = πdL where A = surface area, d = diameter of cylinder, L = length of cylinder

(surface area for gas permeation) m^2 = π x (inside diameter of fibre) m x length of fibre m

Table F.11. Surface area for permeation.

Fibre length (m)	0.03
ID (m)	0.003
Surface area (m^2)	2.83E-04

4] Calculate gas permeability

J = nA/P {Li, 1999 #581} where J = gas permeability mol m^{-2} Pa^{-1} s^{-1}, n = mean molar flow rate mol/s, A = surface area of fibre m^2,
P = gauge pressure reading Pa

Table F.12. Gas permeability.

Pressure		Gas permeability
psig	P_A (Pa)	(mol m^{-2} Pa^{-1} s^{-1})
5	134,474	2.46E-12
6	141,368	2.72E-12
8	155,158	2.94E-12
10	168,947	2.93E-12
12	182,737	3.08E-12
14	196,526	3.10E-12
16	210,316	3.18E-12
18	224,105	3.17E-12
20	237,895	3.54E-12
25	272,369	3.35E-12
30	306,842	3.47E-12
35	341,316	3.56E-12
40	375,790	3.62E-12

5] Calculate mean pressure

$P_m = (P + 2P_A) / 2$ where P_m = mean pressure Pa, P = gauge pressure reading Pa, P_A = absolute pressure Pa

Table F.13. Mean pressure.

Pressure			
P (psig)	P (Pag)	P_A (Pa)	P_m (Pa)
5	34,474	134,474	1.69E+05
6	41,368	141,368	1.83E+05
8	55,158	155,158	2.10E+05
10	68,947	168,947	2.38E+05
12	82,737	182,737	2.65E+05
14	96,526	196,526	2.93E+05
16	110,316	210,316	3.21E+05
18	124,105	224,105	3.48E+05
20	137,895	237,895	3.76E+05
25	172,369	272,369	4.45E+05
30	206,842	306,842	5.14E+05
35	241,316	341,316	5.83E+05
40	275,790	375,790	6.52E+05

6] Plot gas permeability against mean pressure

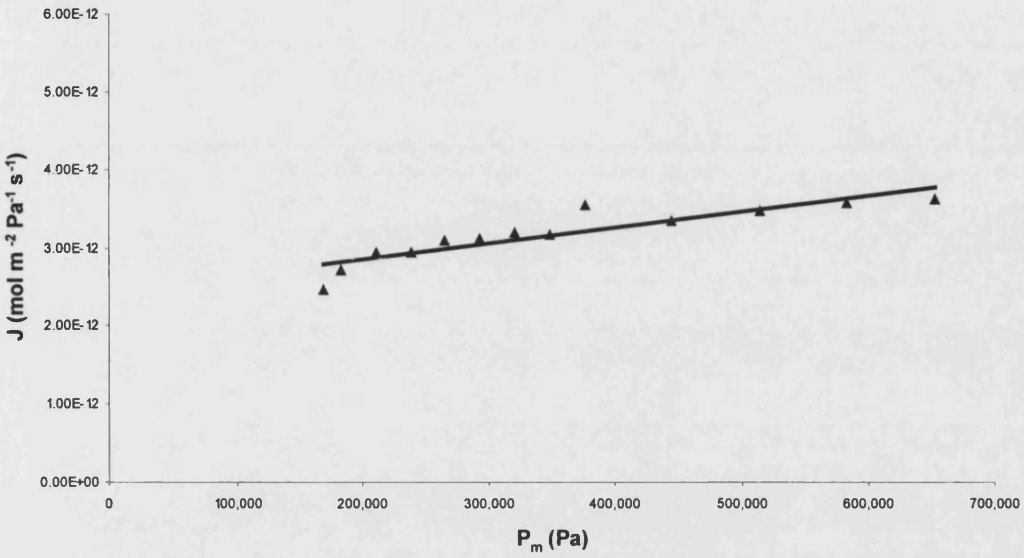

Figure F.3. Plot of gas permeability versus mean pressure.

7] Calculate intercept and gradient for each fibre

Use the graph to calculate the gradient P_0 and the intercept K_0 for each fibre.

Table F.14. The gradient and intercept.

Gradient P_0	Intercept K_0	P_0/K_0
(mol m^{-2} s^{-1})	(mol m^{-2} Pa^{-1} s^{-1})	
2.03E-18	2.45E-12	8.29E-07

8] Calculate mean pore diameter

Use $r = 16/3 \times (P_0/K_0) \times (8RT/\pi M_{N2})0.5$ m {Li, 1999 #581}

where r = radius of pore m, M_{N2} = molecular mass of the gas g/mol,
μ = viscosity of the gas g/m s

(mean pore diameter) cm = 2 x {(mean pore radius) m * 100 cm/m}

Table F.15. Mean pore diameter of fibre.

r_m	d_m	d_m
m	cm	μm
1.18E-06	2.36E-04	2.364

9] Calculate effective surface porosity

Use $\varepsilon/L_p = 8\mu RTP_0/r^2$ m^{-1} {Li, 1999 #581}

Where ε is the porosity, and L_p is the effective pore length m

Table F.16. Effective porosity of fibre.

r_m	ε/L_p
m	m^{-1}
1.18E-06	5.07E-04